UNIVERSITAT AUTÒNOMA DE BARCELONA

FACULTAT DE CIÈNCIES

DEPARTAMENT DE QUÍMICA

COMBINATION OF ADVANCED OXIDATION PROCESSES AND BIOLOGICAL TREATMENTS FOR COMMERCIAL REACTIVE AZO DYES REMOVAL

JULIA GARCÍA MONTAÑO **PhD THESIS 2007**

SUPERVISED BY JOSÉ PERAL PÉREZ

AND FRANCESC TORRADES CARNÉ

COMBINATION OF ADVANCED OXIDATION PROCESSES AND BIOLOGICAL TREATMENTS FOR COMMERCIAL REACTIVE AZO DYES REMOVAL

Memoria presentada por **Julia García Montaño** para optar al grado de Doctora en Química

Universitat Autònoma de Barcelona

Bellaterra, Junio de 2007

José Peral Pérez, Profesor Titular de Universidad del Departament de Química de la Universitat Autònoma de Barcelona,

y

Francesc Torrades Carné, Profesor Titular de Universidad del Departament d'Enginyeria Química de la ETSEIA de Terrassa, Universitat Politècnica de Catalunya,

CERTIFICAMOS:

Que la presente tesis doctoral, con título "*Combination of Advanced Oxidation Processes and Biological Treatments for Commercial Reactive Azo Dyes Removal"*, ha sido realizada bajo nuestra dirección por **Julia García Montaño** en el Departament de Química de la Universitat Autònoma de Barcelona para optar al grado de Doctora en Química.

Bellaterra, Mayo de 2007

José Peral Pérez

Francesc Torrades Carné

A todos los que quiero

Patientia et labor omnia vincit

San Agustín

Agradecimientos

Esta tesis doctoral se ha realizado gracias a la financiación de la Unión Europea (proyecto EVK1-CT-2002-00122), el Ministerio de Ciencia y Tecnología (proyecto PPQ2002-04060-C02-01), el Ministerio de Educación y Ciencia (proyecto CTQ2005-02808) y las becas de movilidad otorgadas por el Ministerio de Educación y Ciencia (*Programa de Acceso y Mejora de Grandes Instalaciones Científicas Españolas*, proyecto GIC-05-17) y la Generalitat de Catalunya (*Estades per a la recerca a fora de Catalunya*).

Quiero expresar mi gratitud al Dr. José Peral y al Dr. Francesc Torrades por los consejos y el tiempo dedicado en la dirección de esta tesis. Asimismo, agradezco el apoyo, la ayuda y la atención de todos los colegas del Grupo de Fotocatálisis y Química Verde del Departament de Química de la Universitat Autònoma de Barcelona. Particularmente al Dr. Xavier Domènech, al Dr. José Antonio Ayllón, a la Dra. María Isabel Franch y a María José Farré. Mi especial agradecimiento al Dr. José Antonio García Hortal del Departament d'Enginyeria Tèxtil i Paperera de la ETSEIA de Terrassa, Universitat Politècnica de Catalunya, y al Dr. Manuel Ignacio Maldonado y colaboradores del Grupo de Química Solar de la Plataforma Solar de Almería.

Sin olvidar a Dystar Hispania, a Ciba Specialty Chemicals y a la estación de depuración de aguas residuales de Manresa.

Finalmente, gracias a todas aquellas personas que han estado a mi lado alentándome y apoyándome durante todos estos años.

Julia.

Preface

Nowadays, the remediation of textile effluents containing persistent dyestuffs is still far away to a satisfactory solution. Consequently, the increased public concern and the tighter international regulations have challenged the environmental scientists community to explore new lines to reduce environmental problems associated with such a wastewaters.

Advanced Oxidation Processes (AOPs) are well known strong technologies for waste treatment purposes. Though, from an applied point of view, they still require further advancement and extent. A new promising application field is their integration with biological treatments, while taking advantage of the individual potentialities of each other. In this direction, the investigation developed through this doctoral dissertation deals with the coupling of an AOP –fundamentally the photo-Fenton process– and a conventional biological treatment to treat solutions polluted with commercial reactive azo dyes.

The memory, presented as a compendium of publications, is divided in the following chapters: Introduction, Goal and Scope of the Work, Materials and Methods, Results and Discussion, Concluding Remarks and Annexes.

The Introduction chapter highlights those aspects more significant for the present experimental work understanding. The main topics regarding reactive dyes and textile effluents, the conventional biological treatments, the AOPs used in this work, as well as the different likely AOPs-biological coupling strategies have been described. The chapter concludes with a brief introduction to the Life Cycle Assessment (LCA) as a tool for quantitative evaluation of the environmental repercussion of processes, such as AOP based treatments.

The Goal and Scope of the Work outlines the main scope and aims of this thesis.

The Materials and Methods chapter has been included into the memory in order to extend and detail the experimental section of publications, thus facilitating repeatability and further research in this application field.

The Results and Discussion chapter comprises the following five interrelated publications. The issue begins with an overview of the various studies –including unpublished results– emphasising major results and accomplished goals.

Decolourisation and mineralisation of homo- and hetero-bireactive dyes under Fenton and photo-Fenton conditions

Coloration Technology, 120 (2004) 188-194

Decolorization and mineralization of commercial reactive dyes under solar light assisted photo-Fenton conditions

Solar Energy, 77 (2004) 573-581

Degradation of Procion Red H-E7B reactive dye by coupling a photo-Fenton system with a sequencing batch reactor

Journal of Hazardous Materials, 134 (2006) 220-229

Combining photo-Fenton process with aerobic sequencing batch reactor for commercial hetero-bireactive dye removal

Applied Catalysis B: Environmental, 67 (2006) 86-92

Environmental assessment of different photo-Fenton approaches for commercial reactive dye removal

Journal of Hazardous Materials, 138 (2006) 218-225

Following Results and Discussion, the Concluding Remarks chapter lists the general conclusions drawn from the present work.

Finally, the Annexes encompass several unpublished results as well as some useful supporting information. The unpublished results include the below works submitted for publication. The first of them has been developed during a research stay at the Plataforma Solar de Almería (PSA, Spain).

Pilot plant scale reactive dyes degradation by solar photo-Fenton and biological processes

The testing of several biological and chemical coupled treatments for Cibacron Red FN-R azo dye removal

TABLE OF CONTENTS

Table of Contents

ABBREVIATIONS AND SYMBOLS ..... **I**

CHAPTER 1. INTRODUCTION **1**

1.1. REACTIVE DYES **3**
1.1.1. Structure of reactive dyes **4**
1.1.2. Dyeing with reactive dyes **5**
1.1.3. Environmental concern of reactive dyes **8**
1.2. TEXTILE WASTEWATERS **9**
1.2.1. Nature and environmental impact **9**
1.2.2. Textile wastewater treatments **10**
1.3. BIOLOGICAL TREATMENTS **12**
1.3.1. Fundamentals **12**
1.3.2. Aerobic treatment **14**
1.3.3. Anaerobic treatment **16**
1.3.4. Biological systems **18**
1.3.4.1. Suspended growth systems 18
1.3.4.2. Immobilised growth systems 19
1.4. ADVANCED OXIDATION PROCESSES (AOPs) **20**
1.4.1. Fenton and photo-Fenton processes **22**

1.4.1.1. Fundamental chemistry 22
1.4.1.2. Operational conditions 30
1.4.1.3. Benefits and limitations 32
1.4.1.4. Applications to wastewater treatment 33
1.4.2. Ozonation 34
1.4.2.1. Fundamental chemistry 34
1.4.2.2. Operational conditions 35
1.4.2.3. Benefits and limitations 36
1.4.2.4. Applications to wastewater treatment 37
1.5. COMBINATION OF AOPs AND BIOLOGICAL TREATMENTS 37
1.5.1. Fundamentals 37
1.5.2. Applications to wastewater treatment 40
1.6. ENVIRONMENTAL ASSESSMENT: LIFE CYCLE ASSESSMENT (LCA) 42
1.6.1. Fundamentals 42
1.6.1.1. Definition and extent 42
1.6.1.2. Methodology 44
1.6.1.3. Benefits and limitations 47
1.6.2. Applications to AOP based treatments 48
1.7. REFERENCES 50

CHAPTER 2. GOAL AND SCOPE OF THE WORK 65

CHAPTER 3. MATERIALS AND METHODS 69

3.1. PREPARATION OF SYNTHETIC DYE SOLUTIONS 71
3.2. REAGENTS 73
3.3. CHEMICAL ASSAYS 74
3.3.1. Dissolved Organic Carbon (DOC) 74
3.3.2. Chemical Oxygen Demand (COD) 74
3.3.3. Colour and aromatic content analysis by UV/Vis spectrophotometry 75
3.3.4. Hydrogen peroxide analysis by iodometric titration 76
3.3.5. Dissolved iron analysis (Fe (II) and total iron) by colorimetry 77
3.3.6. High Performance Liquid Chromatography (HPLC) 78
3.3.7. Liquid Chromatography-(Electrospray Ionisation)-Time-of-Flight Mass Spectrometry (LC-(ESI)-TOF-MS) 78
3.3.8. Ion Chromatography (IC) 79
3.3.9. Ammonium analysis by Nessler reagent 80
3.3.10. Methane analysis by Gas Chromatography (GC) 80
3.3.11. Ozone flow analysis by iodometric titration 81
3.3.12. Total and Volatile Suspended Solids (TSS, VSS) 81

3.4. BIOLOGICAL ASSAYS 82
3.4.1. Zahn-Wellens biodegradability test 82
3.4.2. Biochemical Oxygen Demand for 5 days (BOD_5) 84
3.4.3. Acute toxicity 85
3.4.4. Short-term respirometry 87
3.4.5. Anaerobic digestion assay 89
3.5. ANAEROBIC SLUDGE ADSORPTION EXPERIMENT 91
3.6. REACTORS AND EXPERIMENTAL PROCEDURES 92
3.6.1. Fenton and photo-Fenton reactors 92
3.6.1.1. Cylindrical batch reactors 92
3.6.1.2. Compound Parabolic Collector (CPC) 94
3.6.2. Ozonation set-up 97
3.6.3. Biological Reactors 98
3.6.3.1. Sequencing Batch reactor (SBR) 98
3.6.3.2. Immobilised Biomass Reactor (IBR) 100
3.7. PHOTO-FENTON IRRADIATION SOURCES 102
3.7.1. Black light 102
3.7.2. Solar radiation 103
3.8. ENVIRONMENTAL ASSESSMENT METHODOLOGY 105
3.9. REFERENCES 107

CHAPTER 4. RESULTS AND DISCUSSION 111

4.1. OVERVIEW 113
4.2. PUBLICATIONS 125
4.2.1. Decolourisation and mineralisation of homo- and hetero-bireactive dyes under Fenton and photo-Fenton conditions
Coloration Technology, 120 (2004) 188-194
4.2.2. Decolorization and mineralization of commercial reactive dyes under solar light assisted photo-Fenton conditions
Solar Energy, 77 (2004) 573-581
4.2.3. Degradation of Procion Red H-E7B reactive dye by coupling a photo-Fenton system with a sequencing batch reactor
Journal of Hazardous Materials, 134 (2006) 220-229
4.2.4. Combining photo-Fenton process with aerobic sequencing batch reactor for commercial hetero-bireactive dye removal
Applied Catalysis B: Environmental, 67 (2006) 86-92
4.2.5. Environmental assessment of different photo-Fenton approaches for commercial reactive dye removal
Journal of Hazardous Materials, 138 (2006) 218-225

CHAPTER 5. CONCLUDING REMARKS 171

ANNEXES 175

ANNEXE 1. UNPUBLISHED RESULTS 177

A.1.1. Pilot plant scale reactive dyes degradation by solar photo-Fenton and biological processes 179

Submitted for publication

A.1.2. Pathways of solar photo-Fenton degradation of Procion Red H-E7B reactive azo dye at pilot plant scale 207

A.1.3. The testing of several biological and chemical coupled treatments for Cibacron Red FN-R azo dye removal 229

Submitted for publication

ANNEXE 2. SUPPORTING INFORMATION 249

A.2.1. LC-(ESI)-TOF-MS spectra 251

A.2.2. LCA characterisation tables 261

ABBREVIATIONS AND SYMBOLS

Abbreviations and Symbols

A; Abs	Absorbance
A_o; Abs_o	Absorbance at t = 0
$Abs_{542.5}$	Absorbance at 542.5 nm wavelength
$Abs_{543.5}$	Absorbance at 543.5 nm wavelength
AEP	Aquatic Eutrophication Potential
α	Level of significance
AOB	Ammonium Oxidising Bacteria
AOP	Advanced Oxidation Process
AOX	Adsorbable Organic Halogens
AP	Acidification Potential
ARD	Abiotic Resource Depletion
BOD	Biochemical Oxygen Demand
BOD_5	Biochemical Oxygen Demand for 5 days
BOD_7	Biochemical Oxygen Demand for 7 days
C	Concentration
C_o	Concentration at t = 0
CI	Colour Index
COD	Chemical Oxygen Demand
CPC	Compound Parabolic Collector

DM	Dry Matter
DO	Dissolved Oxygen
DOC	Dissolved Organic Carbon
DOC_o	Dissolved Organic Carbon at t = 0
E	East; Energy
E^o	Standard potential
EC_{50}	Median effective concentration
FATP	Freshwater Aquatic Toxicity Potential
GC	Gas Chromatography
GWP	Global Warming Potential
$h\nu$	Photon
HPLC	High Performance Liquid Chromatography
HRT	Hydraulic Retention Time
HTP	Human Toxicity Potential
IBR	Immobilised Biomass Reactor
IC	Ion Chromatography
%INH	Percentage of inhibition
ISO	International Standards Organisation
k	Reaction rate constant
K_{eq}	Equilibrium rate constant
λ	Wavelength
λ_{max}	Maximum absorption wavelength
LCA	Life Cycle Assessment
LC-(ESI)-TOF-MS	Liquid Chromatography-(Electrospray Ionisation)-Time-of-Flight Mass Spectrometry
MAEP	Marine Aquatic Ecotoxicity Potential
MS	Mass Spectrometry
m/z	Mass to charge ratio
n	Sample size
N	North
NB	Non Biodegradable
NDIR	Non Dispersive Infrared Detector
NHE	Normal Hydrogen Electrode
NOB	Nitrite Oxidising Bacteria
OD	Oxygen Demand
OD_{st}	Oxygen Demand of the standard solution
ODP	Ozone Depletion Potential
OLR	Organic Loading Rate
PB	Partly Biodegradable

POP	Photochemical Oxidation Potential
PSA	Plataforma Solar de Almería
r_o	Maximum gradient of the degradation curve
RB	Ready Biodegradable
SBR	Sequencing Batch Reactor
SETAC	Society of Environmental Toxicology and Chemistry
SMA	Specific Methanogenic Activity
sOUR	Specific Oxygen Uptake Rate
SRT	Sludge Retention Time
t	Time
t_{30W}	Normalised illumination time
$t_{80\%}$	t_{30W} necessary to obtain around 80% mineralisation
T	Temperature
TC	Total Carbon
TEP	Terrestrial Ecotoxicity Potential
TIC	Total Inorganic Carbon
TOC	Total Organic Carbon
TOC_o	Total Organic Carbon at t = 0
TSS	Total Suspended Solids
U	Enzymatic units
UV	Ultraviolet
UV_{254}	Aromatic compounds content
UVA	Ultraviolet A
UV/Vis	Ultraviolet/Visible
V_i	Irradiated volume
V_{SBR}	SBR operational volume
V_T	Total volume
VFA	Volatile Fatty Acids
VSS	Volatile Suspended Solids
W	West
w/v	Weight to volume ratio
WWTP	Wastewater Treatment Plant

CHAPTER 1. INTRODUCTION

Chapter 1
Introduction

1.1. REACTIVE DYES

Dyes are chemical compounds characterised by absorbing in the visible region of the electromagnetic spectrum (400 to 700 nm). This is the reason why they appear to be coloured. Their application over the different affined substrates (textile materials, leather, paper, hair, etc.) is performed from a liquid in which they are completely or partially soluble [1]. They are classified based on two criteria (both used by the *Colour Index* [2], which lists all dyes and pigments commercially used for large scale coloration purposes): according to their chemical structure or according to their method of application over the substrate.

Attending to the second criteria, in the 1950s appeared the first reactive dyes [1, 3], characterised by containing one or more groups capable of forming, in general, covalent bonds between a carbon or phosphorus atom of the dye and an oxygen, nitrogen or sulphur atom of a hydroxy, an amino or a mercapto group of the substrate, respectively.

Such covalent bonds are formed with the hydroxyl groups of cellulosic fibres, with the amino, hydroxyl and mercapto groups of protein fibres and with the amino groups of polyamides. However, the reactive dye term usually refers to a dye applicable to cellulosic fibres, since reactive dyes have been essentially applied to cotton and rayon fibres, in this order.

1.1.1. Structure of reactive dyes

The structural features of a reactive dye are schematically shown in Figure 1.1 [1]. Two parts are mainly distinguishable: the chromogen and the reactive group. The first contains a chromophore group (lineal or cyclic systems with conjugated double bonds) that confers the colour to the dye, and one or more water solubilising groups, generally sulphonic groups. As chromophore, the most employed are the azo type, which suppose approximately 80% of the total (in fact, the majority of synthetic dyes currently used in the industry are azo derivatives), followed by the anthraquinonics, the phthalocyanines and those that present metal-ligand coordination bonds in their structure.

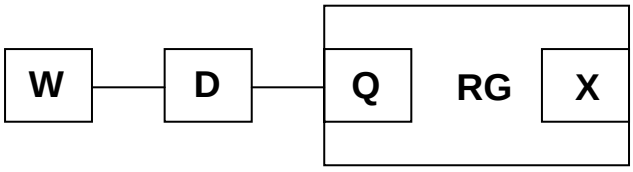

RG: electrophilic reactive group
Q: bridge link
X: nucleofugic leaving group
D: chromogen
W: water solubilising group

Figure 1.1. Structural features of a reactive dye.

The reactive group, bonded to the chromogen by a bridge link (structures generally containing the amino or imino groups), is the responsible of the interaction with the fibre [1]. This part of the molecule conditions on the chemical behaviour of the dye. The

most habitual for cellulosic fibre dyeing are the mono or dichlorotriazine and the vinylsulphone groups, though more recently reactive dyes that present fluorotriazine reactive groups in their structure have also emerged (Figure 1.2). Reactive dyes may contain only one reactive group (monoreactive dyes) or two or more of them (bi- o multi-reactive dyes). Depending on whether these reactive groups are the same or different, they can be distinguished as homo- or hetero-, respectively.

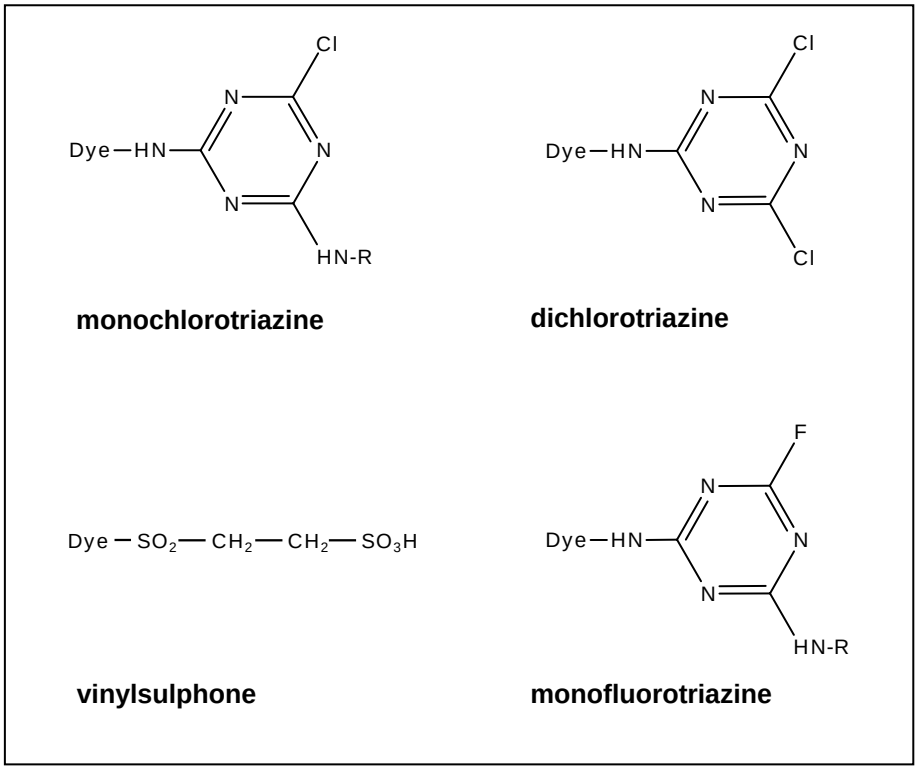

Figure 1.2. Some important reactive groups for cellulosic fibres [1, 3].

1.1.2. Dyeing with reactive dyes

The basic dyeing process of cellulosic fibres with reactive dyes takes place in three stages [3, 4]: sorption, reaction and washing of unfixed dye. This operation can be performed in batch, semicontinuous or continuous mode.

In a first step of sorption in neutral media, the dye diffuse from dyebath through the fibres, and gets fixed by way of secondary-type bonds (electrostatic forces, Van der Waals forces, hydrogen bonds and hydrophobic interactions). The addition of neutral electrolytes during this process (generally NaCl or Na_2SO_4 in a 50-80 $g \cdot l^{-1}$ dosage [5]) makes easier the sorption since they neutralise the electronegative potential of the fibre and suppresses the dye-fibre repulsion.

Once reached the sorption equilibrium, a chemical reaction (almost irreversible) initialises by adding an alkali, usually Na_2CO_3 (pH between 8 and 12 [3]). In this way, the reactive groups react with the ionised hydroxyl groups of cellulosic substrate (i.e., Cel-O^-). The temperature of dyeing ranges from ambient up to the boiling point (or even superior). Depending on the reactive group that accompanies the dye, two reaction mechanisms may be possible [4]:

- *Nucleophilic substitution mechanism*: The reactive group is constituted by a ring structure with heterocyclic nitrogens and halogens (halotriazines). The last are ousted by the cellulosate anion giving place to the covalent bond (Equation 1.1):

$$\text{Dye-X} + \text{Cel-O}^- \rightarrow \text{Dye-O-Cel} + \text{X}^- \qquad (1.1)$$

- *Nucleophilic addition mechanism*: The reactive group is formed by a double bond capable to form covalent bonds with cellulose. Frequently, this double bond is obtained from a previous elimination step under mild alkaline conditions. The vinylsulphone reactive group is an important representative of this system (Equations 1.2-1.4):

$$\text{Dye-SO}_2\text{-CH}_2\text{-CH}_2\text{-SO}_3\text{H} \xrightarrow{\text{HO}^-} \text{Dye-SO}_2\text{-CH=CH}_2 \qquad (1.2)$$

$$\text{Dye-SO}_2\text{-CH=CH}_2 + \text{Cel-O}^- \rightarrow \text{Dye-SO}_2\text{-CH}^-\text{-CH}_2\text{-O-Cel} \qquad (1.3)$$

$$\text{Dye-SO}_2\text{-CH}^-\text{-CH}_2\text{-O-Cel} \xrightarrow{\text{H}^+} \text{Dye-SO}_2\text{-CH}_2\text{-CH}_2\text{-O-Cel} \qquad (1.4)$$

Since water is also a weak nucleophilic agent, an important part of the reactive dyes undergo, in parallel, alkaline hydrolysis of the reactive group (Equations 1.5-1.7). It is a competitive reaction (around 30 times slower than the dye-fibre one) where the reactive group loses the capacity of forming the covalent bond with the fibre. Hence, for a reactive dye to be useful, the fraction of hydrolysis should be minimal. However, the degree of exhaustion (the amount of dye taken from the dyebath by the fibre) of reactive dyes is rather low (60-90%), and at the end of the dyeing process the dye is found in two forms: linked to the fibre or hydrolysed (10-40%) [5].

$$\text{Dye-X} + HO^- \rightarrow \text{Dye-OH} + X^- \quad (1.5)$$

$$\text{Dye-SO}_2\text{-CH=CH}_2 + HO^- \rightarrow \text{Dye-SO}_2\text{-CH}^-\text{-CH}_2\text{-OH} \quad (1.6)$$

$$\text{Dye-SO}_2\text{-CH}^-\text{-CH}_2\text{-OH} \xrightarrow{H^+} \text{Dye-SO}_2\text{-CH}_2\text{-CH}_2\text{-OH} \quad (1.7)$$

In a third stage, unfixed dye fraction, alkali and electrolyte are eliminated by washing, generating high coloured dye-containing effluents. Depending on the reactive dye colour intensity or the process employed, their concentration in dyebaths ranges among 10 and 10,000 $mg \cdot l^{-1}$. After the washing stage, the dye solution is diluted between 20 and 40% [6].

It is worth to mention that the incorporation of two or more reactive groups into the dye molecule (bi- o multi-reactive dyes) affords further opportunities for reaction with the fibre with a stronger dye-fibre anchorage, thus reducing the contamination of the wastewater discharged [3]. Figure 1.3 shows an example of the benefits of a hetero-bireactive dye (Cibacron FN, CIBA, Ciba Specialty Chemicals) in comparison with a monoreactive dye [7].

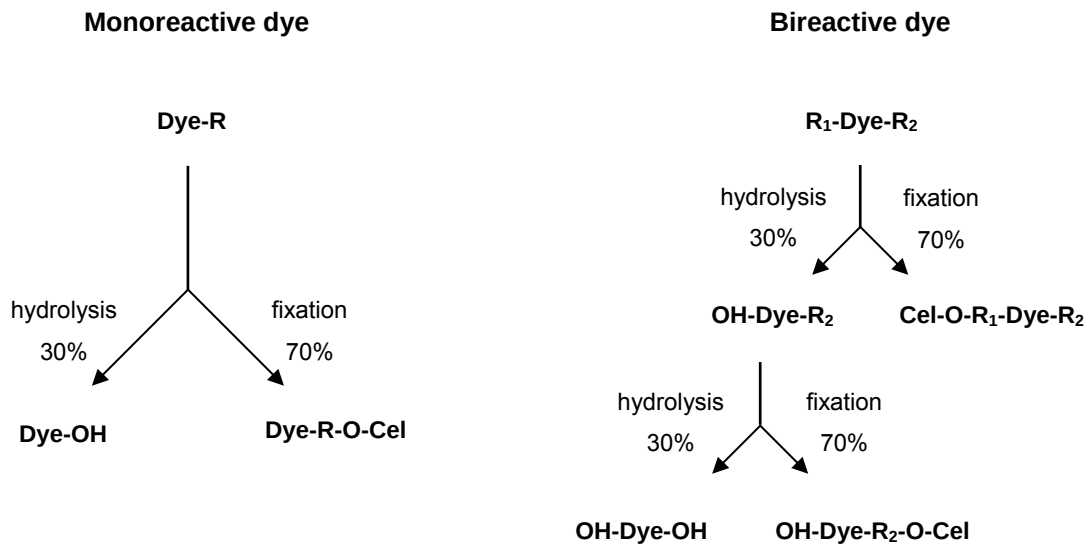

Figure 1.3. Increased fixation through bireactivity. Example of Cibacron FN (CIBA).

1.1.3. Environmental concern of reactive dyes

Reactive dyes have been identified as the most problematic compounds in textile dye effluents [8, 9]. They are characterised by their readily water solubility as well as their high stability and persistence, essentially due to their complex structure and synthetic origin. Since they are intentionally designed to resist degradation, they consequently offer a large resistance against chemical and photolytic degradation. Moreover, as many of textile dyes, reactive dyes are usually non biodegradable under typical aerobic conditions found in conventional biological treatment systems [10]. Among them, the reactive azo dyes family is of special interest. Although they are usually of non toxic nature, they may generate, under anaerobic conditions (e.g., in anaerobic sediments and in intestinal environments), breakdown products as aromatic amines considered to be potentially carcinogenic, mutagenic and toxic [11, 12].

The fact that cotton supposes one of the first textile fibre worldwide, with a yearly production that go beyond the 25 millions of tons (2005 data, see Table 1.1) [13], gives an idea of the large scale production of reactive dyes, their extensive application (nowadays, reactive dyes make 20-30% of the total dyestuff market [14]), and the

environmental pollution associated with the wastewaters generated. Besides, the large fraction of reactive dyes wasted because of their large hydrolysis degree in alkaline dyebaths further enhances the potential environmental risk of their effluents.

Table 1.1. World production of textile fibres (million tons).

	2003	2004	2005	04/05 ± %
Chemical fibres	31.8	33.8	34.1	+ 0.8
Synthetics[a]	29.5	31.3	31.5	+ 0.5
Cellulosics[b]	2.3	2.5	2.6	+ 4.9
Cotton[c]	20.7	26.3	25.1	- 4.5
Wool[c]	1.2	1.2	1.2	+ 0.4
Silk	0.1	0.1	0.1	0
Total	53.8	61.5	60.5	-1.5

[a] excl. PP fibres and tapes
[b] excl. acetate filter tow
[c] seasonal

1.2. TEXTILE WASTEWATERS

1.2.1. Nature and environmental impact

Textile mills are major consumers of water –with an average water consumption of 160 kg per kg of finished product [15]– and consequently one of the largest groups of industries causing intense water pollution. Generated wastewaters collect different effluents coming from different manufacturing unitary operations: from raw material preparation processes (i.e., desizing, scouring and bleaching), as well as from dyeing, soaping, softening, etc. These complex operations, subjected to frequent changes as a result of shifting consumers preferences, are the cause of the variable volume and the wide diversity of chemical products found in these wastewaters. Though their characteristics depend on the specific operations performed, they commonly present suspended solids, high temperature, unstable pH, high Chemical Oxygen Demand (COD), low Biochemical Oxygen Demand (BOD) and high colourisation.

As commented above, colour of textile effluents is caused by dyes employed in dyeing processes. In this sense, it is interesting to remark that about 10^6 tons and more than 10,000 different synthetic dyes and pigments are produced annually worldwide and used in dyeing and printing industries [16]. Other major pollutant types identified are biocides used in the growing or storage of the fibre (e.g., chlorinated aromatics), finishing products (e.g., synthetic resins), surfactants (e.g., alkyl phenol ethoxylates), starches, solvents, fats and greases, heavy metals (e.g., chromium), salts (e.g., carbonate, sulphate, chloride), nutrients (e.g., ammonium salts, urea, phosphate based buffers), oxidising agents (e.g., peroxide, dichromate), reducing agents (e.g., sodium sulphide), bleaching agents (e.g., hypochlorite, hydrogen peroxide) and Adsorbable Organic Halogens (AOX) formed as a result of the use of bleaching chemicals containing chloride [17].

Such wastewaters composition would cause serious impacts when encountering natural areas. High contents of organic matter originate depletion of dissolved oxygen, which has an adverse effect on the marine ecological system. Nitrogen and phosphorous nutrients content causes an increase of biomass production in aquatic environments, also leading to a depletion of dissolved oxygen (namely eutrophication). Regarding high colourisation, not only aesthetic pollution occurs (e.g., the eye can detect concentrations of 0.005 $mg \cdot l^{-1}$ of reactive dye in water [18]), but it also produces strong absorption of the sunlight responsible for the photosynthetic activity of aquatic plants, seriously threatening the whole ecosystem [19].

1.2.2. Textile wastewater treatments

In this frame, textile industry is confronted with the challenge of effective wastewater remediation. In general, the current practice in textile mills is to discharge the wastewater directly into the local environment or into the municipal sewer system. In any case, to accomplish with current local legislations (which are becoming more stringent) [20], textile mills are sometimes forced to have their own treatment plant prior discharge. The specific processes carried out at the different textile mills require a proper specific treatment, which must guarantee the wastewater decontamination. In

some cases, the combination of various basic treatments is needed to improve the overall efficiency of the wastewater treatment systems.

A varied range of methods have been developed for textile wastewater treatment at laboratory, pilot or full scale. The most widely used are coagulation-flocculation, adsorption (commonly with activated carbon), foam flotation, membrane filtration (ultrafiltration, nanofiltration or inverse osmosis), biological treatments (mainly conventional aerobic activated sludge treatments), and chemical processes (e.g., electrochemical methods or Advanced Oxidation Processes (AOPs)) [14, 21-25].

Coagulation-flocculation, adsorption, foam flotation and membrane filtration are common practices, but result in a phase transfer of pollutants, leading to another form of waste (such as spent carbon or sludge) that would require additional treatment or disposal (e.g., incineration). In view of that, destructive methods such as chemical or biological processes are desirable.

Nowadays, biological processes are the preferred choice for wastewater treatment (Section 1.3). They are relatively inexpensive, the running costs are low and the end products of complete degradation are not toxic [23]. Among them, the aerobic activated sludge processes are widely used as the main treatment for both textile and mixed textile and domestic effluents [22] (Section 1.3.4.1). However, they have proven to be markedly ineffective for handling wastewater containing synthetic textile dyes (especially for reactive and other anionic water-soluble dyes) because of their large stability. The process considerably reduces the COD, while it is almost ineffective in removing colour. Very little biodegradation of dyes occurs and adsorption onto biomass seems to be the main colour removal mechanism. Alternatively, anaerobic biodegradation may be applied for azo and other water-soluble dyes decolourisation (most types of dyes are partially degraded under anaerobic conditions, though less readily than azo dyes) [8, 9, 14, 17, 23-25]. Additionally, it offers several potential advantages such as a better removal of AOX and heavy metals [14]. Many studies have shown, however, that they generally only achieve a partial COD removal, making necessary an ensuing aerobic treatment to attain the complete degradation [10, 12, 14, 22, 23]. The effectiveness of such combined treatments have been extensively shown at laboratory and pilot scale experiments [10, 12, 22, 23], with several further applications at full scale [14, 17].

Chemical processes are destructive alternatives when biological treatments are not capable to abate both colour and COD from textile wastewater. Among them, AOPs have been proposed in the last years as powerful advanced technologies for the treatment of biorecalcitrant organic compounds [26] (Section 1.4). With their incorporation, the complete decontamination of textile wastewaters becomes feasible.

1.3. BIOLOGICAL TREATMENTS

1.3.1. Fundamentals

The first objective of biological treatment processes is to coagulate, remove the non settleable colloidal solids and to eliminate or reduce the carbonaceous organic matter present in the wastewater. Additionally, biological treatments can also be useful to reduce the inorganic concentration or to transform or remove nutrients such as nitrogen and phosphorous [27].

In synthesis, the process occurs when a group of microbial cells, by way of a series of biochemical reactions, use carbon and energy for cell growth and maintenance. Two of the most common carbon sources for the formation of microorganisms are the organic matter and inorganic carbon. Depending on whether organisms obtain the carbon from the organic or inorganic source, they are called heterotrophs (the most important group) or autotrophs, respectively. On the other hand, the energy input may be supplied by sunlight or by chemical oxidation-reduction reactions. Autotrophic organisms may take the energy from one or the other source, meanwhile heterotrophs mainly obtain the energy by way of fermentation or organic matter oxidation [27, 28].

The biological treatment can be classified into four categories: aerobic treatment or treatment in the presence of oxygen; anaerobic treatment or treatment in the absence of oxygen; anoxic treatment or treatment in the presence of nitrate or nitrite; and a combination of the aerobic and either anoxic or anaerobic processes [27]. Conventional aerobic and anaerobic processes will be more extensively developed in Sections 1.3.2 and 1.3.3, respectively. Accordingly, depending on their oxygen necessities, microorganisms can be classified as aerobic, anaerobic or facultative. The last are those

capable to adapt to either the presence or the absence of free molecular oxygen. On the other hand, biological processes can also be classified according to the microorganisms location: they can be kept suspended in the media or fixed on solid supports. The two different configurations are briefly described in Section 1.3.4.

These biotreatment units are usually composed of heterogeneous and interrelated complex biological populations. Bacteria are the main and most important microorganisms involved. Nevertheless, the metabolic activities of other minority microorganisms such as fungi, algae, protozoa and rotifers are also present, some of them with essential roles in bioremediation.

Several environmental conditions influence on the microorganisms selection, survival and growth, and consequently on the biological process operation [29]. Therefore, it is essential to effectively control some parameters such as the mixing or hydraulic regime, which determine the accessibility of the substrate to microorganisms; the oxygen availability; the nutrients availability: inorganic elements like nitrogen, phosphorous and trace elements such as sulphur, potassium, calcium and magnesium are of vital importance for cell synthesis. Additionally, organic nutrients may also be needed by some microorganisms; the pH of the medium: metabolic reactions occur fastest at optimum pH, usually defined at 6-8; the organic substrate concentration, which must be high enough to ensure biomass growth; and the temperature of the medium: the maximum growth rates generally occur between 25 and 33 ºC, although some organisms can grow above 33 ºC (this is the case, for example, of anaerobic bacteria). Depending on the temperature at which they grow best, bacteria will be grouped in three categories: cryophilic (-2-30 ºC, optimum range 12-18 ºC), mesophilic (20-45 ºC, optimum range 25-40 ºC) or thermophilic (45-75 ºC, optimum range 55-65 ºC) [27].

Every microorganism constituting the biological community has its own growth curve, which will depend on external factors like the above listed. As an example, Figure 1.4 shows the four stages of a typical growth curve of a pure bacterial culture operated in batch mode: the lag phase, the logarithmic growth phase, the stationary phase and the death phase [27, 28].

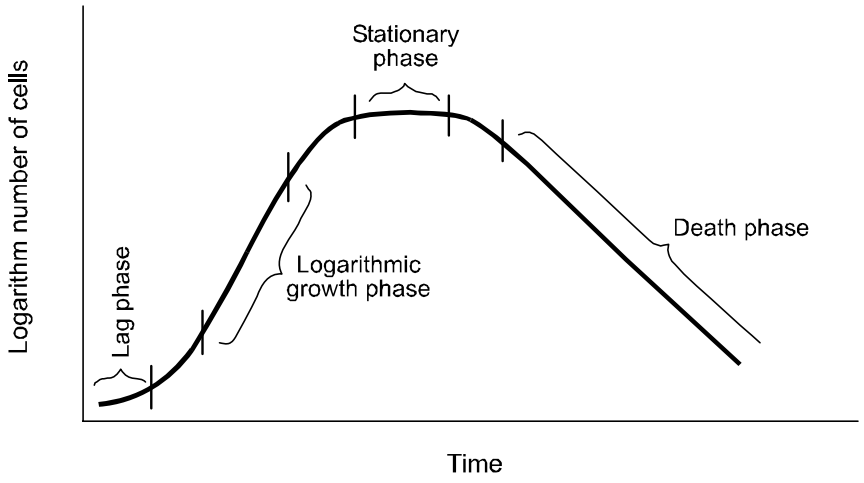

Figure 1.4. Typical bacterial growth curve [27].

Such a culture starts by inoculating a rich nutrient medium with a small number of cells. Afterwards, bacteria are acclimated to the new environmental conditions during the lag phase. This first region is characterised by little bacterial reproduction. Then, they logarithmically grow until reaching the stationary phase, where bacteria population stabilises. The stabilisation may be due to limiting substrate, limiting nutrients conditions, build up of toxic material or to equilibrium between new and old cells. Finally, during the death phase, dead cells overcome the new cells production, giving a logarithmic decrease.

1.3.2. Aerobic treatment

Aerobic treatment is usually the method of choice for biological wastewater treatment since many organic compounds are aerobically oxidisable [29]. Mainly, heterotrophic bacteria oxidise organic matter yielding carbon dioxide and water as final mineralisation products. As pointed earlier, organic matter oxidation provides the required energy (*E*) for cell synthesis. In absence of organic matter, the own cells are endogenously employed (auto-oxidation) to obtain the energy for organisms maintenance. The whole process can be described by the following simplified

biochemical reactions (Equations 1.8-1.10) [27], where CHON represents the organic matter and $C_8H_{15}O_4N$ a model cell chemical composition [30]:

Oxidation

$$CHON + O_2 \xrightarrow{\text{bacteria}} CO_2 + H_2O + NH_4^+ + \text{other final products} + E \quad (1.8)$$

Cells production

$$CHON + E \xrightarrow{\text{bacteria}} C_8H_{15}O_4N \text{ (new cells)} \quad (1.9)$$

Endogenous respiration (auto-oxidation)

$$C_8H_{15}O_4N \text{ (cells)} + 9\ O_2 \rightarrow 8\ CO_2 + NH_3 + 6\ H_2O + E \quad (1.10)$$

Though the above described endogenous respiration yields relatively simple final products (Equation 1.10), it is worth to note that some stable organic products may also be expected.

Apart from carbonaceous organic matter biodegradation, some autotrophic bacteria are capable to metabolise the inorganic compounds presents in the media. The most important inorganic compound is ammonium, which can exert a high oxygen demand by means of a two-steps biological nitrification process (Equations 1.11 and 1.12) [27]. From these reactions, autotrophic bacteria (i.e., Ammonium Oxidising Bacteria (AOB) and Nitrite Oxidising Bacteria (NOB)) gain energy, which will be used together with more NH_4^+ and inorganic carbon (CO_2, HCO_3^-) for building cell material.

$$2\ NH_4^+ + 3\ O_2 \xrightarrow{\text{AOB}} 2\ NO_2^- + 4\ H^+ + 2\ H_2O + E \quad (1.11)$$

$$2\ NO_2^- + O_2 \xrightarrow{\text{NOB}} 2\ NO_3^- + E \quad (1.12)$$

Under suitable environmental and operational conditions, nitrification process can take place jointly with the carbonaceous organic matter biodegradation. Nevertheless, the growth rates of nitrifying bacteria are slower than the heterotrophic ones, being nitrification the limiting step in the biological treatment.

The main disadvantage of the aerobic treatment is the associated sludge production. It supposes a high contribution to environmental contamination and it is an important part to be solved in aerobic treatment processes [31]. There are different technologies for exceeding sludge management. A general scheme is composed of the following steps: thickening, dewatering, stabilisation, and main treatment [32]. The sludge volume is reduced by thickening and dewatering processes. Then, it is stabilised by unit operations like lime-stabilisation, oxidation with chlorine, thermal treatment or anaerobic digestion [27]. Finally, the solid residues are usually incinerated, deposited at landfill or destined to land applications.

1.3.3. Anaerobic treatment

Anaerobic treatment mainly decomposes organic matter in absence of molecular oxygen to methane and carbon dioxide, among others (biogas). Its main and oldest application is the stabilisation of the concentrated sludge generated through aerobic wastewater treatment [27], though they can also be applied in wastewater treatment with heavy organic loads [29]. Unfortunately, anaerobic organisms are very sensitive to certain chemicals and the field of application of anaerobic treatment is not as broad as aerobic bioremediation. Nevertheless, the techniques and methods of anaerobic treatment have rapidly progressed in the last years and wastes previously thought to be not amenable to anaerobic treatment are now biotreatable [29].

The degradation proceeds as a complex chain process which requires the synergistic action of different types of facultative and anaerobic organisms [33]. It can be simplified in three separated stages: in a first stage, hydrolysing and fermenting bacteria convert complex organic compounds to Volatile Fatty Acids (VFA), alcohols, carbon dioxide, ammonium and hydrogen. The second group of hydrogen producing acetogenic bacteria converts the products of the first group into hydrogen, carbon dioxide and

acetic acid. Finally, in a third stage, methane-forming (methanogenic) bacteria convert hydrogen and carbon dioxide or acetate to methane. The biodegradation final products are responsible for the characteristic odours emitted by anaerobic treatment units.

There are also other groups of heterotrophic and autotrophic bacteria that may use the different inorganic ions present. Throughout sulphate reduction process, bacteria reduce sulphate to sulphur ion.

Due to the slow metabolism of hydrogen producing acetogenic and methane-forming bacteria, especially the responsible of propionic and acetic acids degradation, methanogenesis is the rate-limiting stage of the whole process. This fact that translates to longer degradation times than the required for the aerobic treatment units [27]. Additionally, as a difference to aerobic process, anaerobic biodegradation must be performed in a completely closed reactor with controlled thermal isolation. Anaerobic microorganisms are also more sensitive to temperature and pH than the aerobic ones. The optimum temperature ranges between 30-38 ºC and between 49-57 ºC for mesophilic and thermophilic conditions, respectively [27]. Regarding pH, it is worth to note that whether generated VFA reach a high concentration, methane-forming microorganisms may be inhibited by the own process metabolites, hampering the whole multi-stage chain [29]. Therefore, it is essential to maintain the pH over 6.2 to ensure the methanogenic organisms activity [27].

Anaerobic treatment has the advantage of a lower energy demand (expensive aeration is omitted) and a lower sludge production compared with aerobic treatment [34]. The resulting sludge is also quite well stabilised and usually suitable to be directly deposited at landfill or applied to agricultural fields. Moreover, the resulting methane is combustible and can be later exploited by conversion into thermal or mechanical energy [27].

1.3.4. Biological systems

1.3.4.1. Suspended growth systems

Suspended growth systems keep the biomass in suspension in the wastewater under treatment. The biomass grows as suspended flocs of microorganisms. Generally, some sort of mixing is employed to ensure a continuous contact with as much substrate as possible. Once the biodegradation is over, biomass flocs are removed by clarification.

This kind of systems principally consist of batch or continuous flow reactors. Aerobic activated sludge processes (Arden and Lockett, 1914 [35]), operating in continuous flow mode, are the most popular treatment for both industrial and domestic wastewaters. They consist of the introduction of the wastewater in an aerated and mixed tank containing a suspended growth culture. Once the biodegradation is carried out, biomass is settled out in a separated clarifier tank. Then, a part of this biomass is recycled back to the process and the left part periodically wasted.

On the other hand, the batch operation is the oldest and simplest type of suspended growth systems. A commonly used version is the so called Sequencing Batch Reactor (SBR), introduced by R.L. Irvine in 1971 [36], satisfactorily applied in the biodegradation of both municipal and industrial wastewaters [37]. The SBR holds the complete biological treatment in a single tank (without independent clarifier) following a timed controlled sequence composed of five stages: filling, reaction, settling, draw and idle. Wastewater enters the reactor during the filling phase. The reactions (biodegradation) initiated during filling are completed during the reaction phase by initiating the proper mixing and/or aeration strategy. This stage can take place under forced aeration allowing aerobic activity, or without forced aeration allowing anoxic and possible anaerobic reactions. Settling (separation of the biomass from treated water), draw (withdrawal of the supernatant formed during the sedimentation) and idle (time between draw and filling) complete the sequence. The exceeding sludge is wasted during the idle stage.

In comparison with conventional activated sludge processes, the SBR technology incorporates several advantages mainly because of its simplicity, flexibility of operation (even providing the capability of influencing the microbial community) as well as cost

effectiveness [37-39]. They are specially suited for wastewater treatment applications characterised by low or intermittent flow conditions [39].

1.3.4.2. Immobilised growth systems

Immobilised growth systems rely on the microorganisms attaching themselves on or within an inert solid medium that fills the reactor in the form of supports. Once finished the biodegradation, treated wastewater is drained while biomass remains fixed to the solid.

The major types of immobilised growth bioreactors consist of fixed bed, fluidised beds or rotating discs [27, 40]. In the fixed bed type reactor, the supports are located in a fixed place and do not move with the liquid. Wastewater passes through them getting in contact with adhered biomass. The supports can be large pieces like rocks, plastic sheets, redwood slats, etc. On the other hand, in the fluidised bed reactor, the supports are suspended by the upward flow of the wastewater. Small particles as sand, coal, activated carbon, ion-exchange beads and metal oxides have been used in this configuration [29]. Finally, the rotating discs configuration consists of a series of gyratory plastic discs partially submerged on the wastewater to be treated. The discs are colonised with microorganisms.

Numerous literature works have shown some advantages of immobilised over suspended biomass reactors [41]. These are the larger microbial diversity and the larger spectrum of biochemical activities; the increase of cells lifetime; the larger biomass contained per volume of bioreactor (making possible smaller reactors than suspended systems); the higher rates of degradation, with efficiencies independent of flow rates; the facility of operation (no clarification is necessary); the prevention of biomass washout; and the resistance to toxic loading (most of the biological activity takes place on the surface, which buffers most of the microorganisms from the shock of the toxic substances). Some of their disadvantages would be the mass transfer difficulty (mainly O_2) and the higher energy demand associated with aeration.

1.4. ADVANCED OXIDATION PROCESSES (AOPs)

The AOP term was firstly coined by Glaze *et al*. in 1987 [42], and include all those chemical oxidations based on the *in situ* generation of highly reactive hydroxyl radicals ($HO^{\bullet}$) as principal oxidants. Their standard potential (E^{o} = 2.80 V *versus* Normal Hydrogen Electrode (NHE)) is shown along with the ones of some common oxidants in Table 1.2 [26]. Following fluorine, hydroxyl radical is the most powerful known oxidant.

Table 1.2. Standard potential of some relevant oxidants (T = 25 ºC).

Oxidant	E^{o} V *vs* NHE
Fluorine	3.03
Hydroxyl radical	2.80
Atomic oxygen	2.42
Ozone	2.07
Hydrogen peroxide	1.78
Perhydroxyl radical	1.70
Permanganate	1.68
Chlorine dioxide	1.57
Hypochlorous acid	1.49
Chlorine	1.36

As a difference to other conventional oxidant species, the hydroxyl radical is capable to completely oxidise (i.e., mineralise) even the less reactive pollutants [43]. It reacts non selectively with organic compounds, principally by means of electrophilic addition to unsaturated bonds, addition to aromatic rings, abstraction of hydrogen, or by electron transfer (Equations 1.13-1.16) [44, 45]. Mineralisation end products generally are carbon dioxide, water and inorganic ions, without a large residues generation. The rate constants of most reactions involved are usually in the order of 10^{6}-10^{9} $l \cdot mol^{-1} \cdot s^{-1}$ [46].

$$HO^{\cdot} + RH \rightarrow R^{\cdot} + H_2O \quad (1.13)$$

$$HO^{\cdot} + \text{C=C} \rightarrow \text{HO-C-C}^{\cdot} \quad (1.14)$$

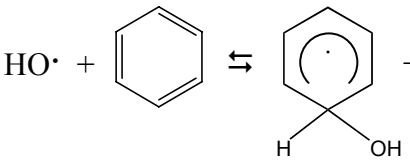

further reactions (1.15)

$$HO^{\cdot} + RH \rightarrow [RH]^{\cdot +} + HO^{-} \quad (1.16)$$

AOPs usually operate at or near to ambient temperature and pressure [42]. They can be classified according to the reaction phase (homogeneous or heterogeneous) or depending on the method used to generate the hydroxyl radical species (chemical, electrochemical, photochemical, sonochemical or radiolytic techniques). Among them, the most extensively used include: heterogeneous photocatalysis with TiO_2 (single or with H_2O_2) [47-49], treatment with ozone (often combined with H_2O_2, and/or UV) [47, 50, 51], H_2O_2/UV systems [6, 26, 51], and Fenton type reactions such as Fenton [45, 47, 52-54], photo-Fenton [45, 51, 52], or electro-Fenton processes [45, 55]. Each of them offers different ways for hydroxyl radicals production. In this sense, the versatility of AOPs becomes evident. The wide variety of techniques available, together with the little selectivity of hydroxyl radical attack, allows a better compliance with the requirements of every pollutant treatment.

The main disadvantage of AOPs is the operational cost associated with their high electrical energy input (particularly UV radiation generation) and expensive chemicals demand (H_2O_2, O_3, etc.) [56]. In fact, only wastewaters with relatively small concentrations (COD $\leq$ 5 $g \cdot l^{-1}$) can be economically treated with these technologies [43].

However, not all photochemical AOPs require irradiation of the same wavelength. Whereas direct O_3 or H_2O_2 photolysis requires photons of short wavelength (below ~ 300 nm) [57], heterogeneous photocatalysis with TiO_2 and photoassisted Fenton processes may employ photons of wavelengths up to around 400 nm [49] and 550 nm [58-60], respectively. Consequently, both AOPs could be effectively driven under solar

irradiation (wavelengths greater than 300 nm) [56, 61], reducing significantly the economic burden in a more environmentally friendly process. This fact is especially interesting for the large scale application of these processes.

Another important strategy that could lead to overcome such AOPs drawbacks is to combine AOPs with biological treatments. Under mild conditions, they can be implemented as a previous step (aimed to turn biorecalcitrant pollutants into biocompatible new compounds) or as a post-treatment (to abate the pollutants left after the biological treatment) [62]. An exhaustive analysis of this application is developed in Section 1.5.

The present work is centred in Fenton, photo-Fenton and ozonation processes, all of them operating in homogeneous reaction phase.

1.4.1. Fenton and photo-Fenton processes

1.4.1.1. Fundamental chemistry

Dark reactions

It is generally accepted the "classical" mechanism described in 1934 by Haber and Weiss [63] where, in Fenton reaction (Equation 1.17), firstly reported by H.J.H. Fenton in 1894 [64], hydroxyl radicals are generated by interaction of H_2O_2 with ferrous salts –namely the Fenton reagent–. For simplification, H_2O ligands on iron sphere coordination will be omitted from hereon.

$$Fe\,(II) + H_2O_2 \rightarrow Fe\,(III) + HO^{\bullet} + HO^{-} \qquad k = 53\text{-}76\ l{\cdot}mol^{-1}{\cdot}s^{-1} \qquad (1.17)$$

Generated Fe (III) can be reduced by reaction with exceeding H_2O_2 to form again ferrous ion and more radicals. This second process is called Fenton-like, it is slower than Fenton reaction, and allows Fe (II) regeneration in an effective cyclic mechanism

(Equations 1.18 and 1.19) [65]. Whether iron is added in small amounts, it acts as a catalyst while hydrogen peroxide is continuously consumed.

$$Fe\ (III) + H_2O_2 \rightarrow HO_2^{\cdot} + Fe\ (II) + H^+ \qquad k = 1\text{-}2\cdot10^{-2}\ l\cdot mol^{-1}\cdot s^{-1} \qquad (1.18)$$

$$Fe\ (III) + HO_2^{\cdot} \rightarrow Fe\ (II) + O_2 + H^+ \qquad k = 0.33\text{-}2.1\cdot10^{6}\ l\cdot mol^{-1}\cdot s^{-1} \qquad (1.19)$$

The rate-limiting step is the regeneration of Fe (II) (Equations 1.18 and 1.19). Ferrous ion remains at trace levels, with approximately constant Fe (III) concentration in aqueous solution.

Equations 1.20-1.22 show other important dark reactions involving ferrous ion and hydrogen peroxide (in absence of other interfering ions and organic substances). The below listed radical-radical reactions, as well as the auto-decomposition of H_2O_2 take also part of the complex process (Equations 1.23-1.26).

$$Fe\ (II) + HO_2^{\cdot} + H^+ \rightarrow Fe\ (III) + H_2O_2 \qquad k = 0.72\text{-}1.5\cdot10^{6}\ l\cdot mol^{-1}\cdot s^{-1} \qquad (1.20)$$

$$Fe\ (II) + HO^{\cdot} \rightarrow Fe\ (III) + HO^- \qquad k = 2.6\text{-}5.8\cdot10^{8}\ l\cdot mol^{-1}\cdot s^{-1} \qquad (1.21)$$

$$H_2O_2 + HO^{\cdot} \rightarrow HO_2^{\cdot} + H_2O \qquad k = 1.7\text{-}4.5\cdot10^{7}\ l\cdot mol^{-1}\cdot s^{-1} \qquad (1.22)$$

$$2\ H_2O_2 \rightarrow 2\ H_2O + O_2 \qquad (1.23)$$

$$2\ HO^{\cdot} \rightarrow H_2O_2 \qquad k = 5\text{-}8\cdot10^{9}\ l\cdot mol^{-1}\cdot s^{-1} \qquad (1.24)$$

$$2\ HO_2^{\cdot} \rightarrow H_2O_2 + O_2 \qquad k = 0.8\text{-}2.2\cdot10^{6}\ l\cdot mol^{-1}\cdot s^{-1} \qquad (1.25)$$

$$HO_2^{\cdot} + HO^{\cdot} \rightarrow H_2O + O_2 \qquad k = 1.4\cdot10^{10}\ l\cdot mol^{-1}\cdot s^{-1} \qquad (1.26)$$

The rate constants are those reported by Sychev and Isaak [66]. It is important to note that some of the reactions are believed to occur in multiple steps [45].

There are specially worth mentioning side reactions that result from Fe (III) and hydroquinone structures (typical aromatic degradation by-products generated by $HO^{\bullet}$ addition to aromatic rings (Equation 1.15)). As they build up in solution, they provide a quicker alternative for ferrous ion generation by successive one-electron transfer steps via the semiquinone radical [67, 68]. An example is shown in Equations 1.27 and 1.28:

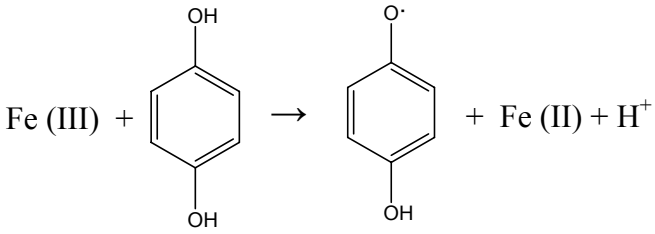

(1.27)

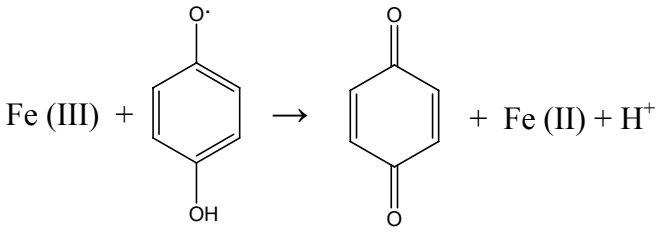

(1.28)

The resulting quinone can rapidly react with $HO_2^{\bullet}$ radical to build up the cycle (Equation 1.29) [69]:

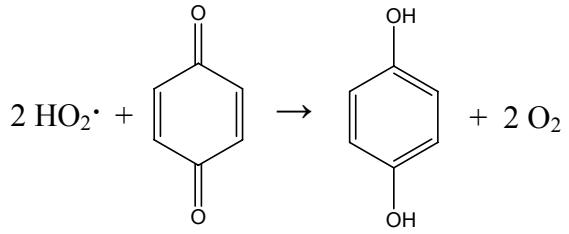

(1.29)

Finally, it should be commented that, instead of ferrous ion, the Fenton process may also be initiated by combining H_2O_2 with ferric ion (Fenton-like process). In this case, since iron catalyst cycles between II an III oxidation states, the same mechanism takes place regardless of which one is used to initiate the chain. However, Equations 1.18 and

1.19 are clearly slower than Equation 1.17, and starting with Fe (III) salt often results in a slower initial rate [45].

Photochemical reactions

The efficiency of thermal (dark) Fe (II) recycling can be enhanced by near-UV to visible light assistance [52, 57, 61, 65]. Under irradiation, ferric ion complexes can be photolysed by passing through a photoexcited transition state before charge transfer and complex dissociation (ligand-to-metal charge transfer reaction).

Especially worthy of mention is the photolysis of ferric aquo-complexes (photo-Fenton reaction, Equation 1.30), producing extra $HO^{\cdot}$ and the recovery of Fe (II) which will further react with more H_2O_2 molecules in Fenton reaction (Equation 1.17). The most important species is $[Fe\,(III)\,HO]^{2+}$ (Equation 1.31), due to a combination of its high absorption coefficient (it is known to be the most photoactive species, delivering $HO^{\cdot}$ with a quantum yield of 0.085 at 350 nm wavelength [70]) and its high concentration relative to other Fe (III) species under typical photo-Fenton pH conditions (see operational conditions in Section 1.4.1.2) [61].

$$[Fe\,(III)\,(HO)_x]^{-x+3} \xrightarrow{h\upsilon} Fe\,(II) + (x\text{-}1)\,HO^- + HO^{\cdot} \qquad (1.30)$$

$$[Fe\,(III)\,HO]^{2+} \xrightarrow{h\upsilon} Fe\,(II) + HO^{\cdot} \qquad \lambda \leq 410\ nm \qquad (1.31)$$

Photoassisted process can also drive ligand-to-metal charge transfer in the potentially photolabile complexes formed by Fe (III) and organic compounds (Equation 1.32) [60]. The ferric ion complexes formed with carboxylic acids (Equation 1.33) [59, 61] are of special importance since they frequently appear as intermediate products through Fenton type processes [45, 55]. In this case, complexes under irradiation directly produce CO_2. Additionally, they often have higher quantum yields than ferric aquo-complexes and can occur over the UV and into the visible range (up to ~ 550 nm) [59]. It is therefore typical to observe (in photoassisted processes) an increase of the

oxidation rate coinciding with carboxylic acids intermediates apparition. In this sense, it is well established that initially adding such type of organic compounds together with Fenton reagent causes the improvement of oxidation reaction yields. An example is ferrioxalate [59, 61, 71], a well known photoactive ferric polycarboxylate complex [72].

$$[Fe(III)L]^{2+} \xrightarrow{h\upsilon} Fe(II) + L^{\cdot} \qquad (L = \text{organic ligand}) \qquad (1.32)$$

$$[Fe(III)LCOO]^{2+} \xrightarrow{h\upsilon} Fe(II) + CO_2 + L^{\cdot} \qquad (1.33)$$

In photoassisted process, as in darkness, the rate-limiting step of the catalytic mechanism is the regeneration of ferrous ion.

The fate of organic free radicals

The above generated organic radicals, together with those generated in Equations 1.13-1.16, react prolonging the complex chain mechanism. Some representative reactions are shown below. Equations 1.34-1.37 would take place depending on the redox potential of the organic radical generated. The organic peroxide generated in Equation 1.37 can further react with Fe (II) similarly to Fenton reaction (Equation 1.38) [73].

$$R^{\cdot} + Fe(III) \rightarrow R^{+} + Fe(II) \qquad (1.34)$$

$$R^{\cdot} + Fe(II) \rightarrow R^{-} + Fe(III) \qquad (1.35)$$

$$R^{\cdot} + R^{\cdot} \rightarrow R\text{-}R \qquad (1.36)$$

$$R^{\cdot} + HO_2^{\cdot} \rightarrow RO_2H \qquad (1.37)$$

$$Fe(II) + RO_2H \rightarrow Fe(III) + RO^{\cdot} + HO^{-} \qquad (1.38)$$

Of special interest is the "Dorfman" mechanism (Equation 1.39) [74, 75]. The reaction between the intermediate organic radicals and O_2 forms $HO_2^{\bullet}$, which would lead to an increase in either Fe (II) (Equation 1.19) or H_2O_2 (Equation 1.20), depending on the Fe (III) to Fe (II) ratio [45]. Other reactions between intermediate organic radicals and molecular oxygen are shown in Section 1.4.1.2.

$$R^{\bullet} + O_2 \rightarrow RO_2^{\bullet} \xrightarrow{H_2O} ROH + HO_2^{\bullet} \qquad (1.39)$$

Influence of inorganic ions

Organic compounds oxidation by Fenton and photo-Fenton processes would be inhibited (in varying degrees and depending on their concentration) by inorganic species such as phosphate, sulphate, chloride and carbonate ions [75-77]. These may be initially present in wastewater or be formed as final products from original compounds undergoing degradation. Due to the high oxidation potential of $HO^{\bullet}$, this can react with such anions and be scavenged from aqueous solution leading to non reactive species. Some representative reactions are shown in Equations 1.40-1.43.

$$HO^{\bullet} + HCO_3^- \rightarrow H_2O + CO_3^{\bullet -} \qquad k = 8.5 \cdot 10^6\ l \cdot mol^{-1} \cdot s^{-1} \qquad (1.40)$$

$$HO^{\bullet} + CO_3^{2-} \rightarrow HO^- + CO_3^{\bullet -} \qquad k = 3.9 \cdot 10^8\ l \cdot mol^{-1} \cdot s^{-1} \qquad (1.41)$$

$$HO^{\bullet} + Cl^- \rightarrow [ClOH]^{\bullet -} \qquad k = 4.3 \cdot 10^9\ l \cdot mol^{-1} \cdot s^{-1} \qquad (1.42)$$

$$HO^{\bullet} + HSO_4^- \rightarrow H_2O + SO_4^{\bullet -} \qquad k = 3.5 \cdot 10^5\ l \cdot mol^{-1} \cdot s^{-1} \qquad (1.43)$$

Apart from the scavenging phenomenon, inhibition from anions may also be due to iron precipitation or to coordination to dissolved Fe (III) to form a less reactive complex. Phosphate ion, for instance, has a double detrimental effect since it both scavenges $HO^{\bullet}$ and forms insoluble complexes with Fe (III) in acidic media [45].

Additional pathways for Fe (II)/H_2O_2 reactions

Alternative pathways for Fe (II)/H_2O_2 reactions that involve other potential oxidants than free hydroxyl radicals have been reported in the literature. Thermal Fenton reaction was suggested to give a "caged" HO· loosely bound to Fe (III) that was capable of intramolecular oxidation of an organic ligand [78]. On the other hand, numerous studies have proposed the formation of aquo- or organo-complexes of a high-valent oxoiron moiety (ferryl, Fe=O, Fe (IV) or Fe (V)), responsible for the direct attack to organic matter [79-81]. In this direction, and more recently, Bossmann *et al.* [44] published evidence of an alternative oxidant in thermal and photoassissted systems (Fe (IV) oxoiron moiety, written as "Fe^{4+}_{aq}"), which may be formed by an inner-sphere two-electron transfer reaction taking place within a hydrated Fe (II) + H_2O_2 complex. Shortly later, Pignatello *et al.* [60] suggested that the irradiated process may involve the photolysis of a Fe (III) + H_2O_2 complex ([Fe (III) HOO]$^{2+}$) to form high-valent iron based oxidants. Such reactions have shown to absorb visible light photons up to 550 nm [58]. Both HO· and ferryl compounds would coexist in the Fe (II)/H_2O_2 system, and one of them would predominate depending on the operational conditions (substrate nature, Fe (II)/H_2O_2 ratio, scavengers addition, etc.) [47]. However, proposed non hydroxyl radical schemes are still rather controversial while the free HO· chain mechanism is broadly accepted for Fe (II)/H_2O_2 reactions.

Fenton reactions kinetics

The kinetics of Fenton reactions can be quite complex because of the large number of steps involved. The general rate equation for the reaction of a target organic compound may be written as follows [45]:

$$-\frac{dC_{RH}}{dt} = k_{HO\cdot}\cdot C_{HO\cdot}\cdot C_{RH} + \sum_i k_{ox_i}\cdot C_{ox_i}\cdot C_{RH} \qquad (1.44)$$

where ox_i represents additional oxidants other than HO· that may also be present, such as ferryl, C_{ox_i} is their concentration, $C_{HO\cdot}$ is the hydroxyl radical concentration and C_{RH} is the target organic compound concentration.

Since hydroxyl radical is usually regarded as the sole or most important reactive species, Equation 1.44 can be rewritten as:

$$-\frac{dC_{RH}}{dt} = k_{HO\cdot} \cdot C_{HO\cdot} \cdot C_{RH} \quad (1.45)$$

Considering that the concentration of reactive species must quickly reach a stationary state regimen during the process, and provided that $C_{HO\cdot}$ may be considered constant, the rate law may be treated as being of pseudo-first order in terms of consumption of the target organic compound:

$$-\frac{dC_{RH}}{dt} = k_{app} \cdot C_{RH} \quad (1.46)$$

Finally, by integrating, a plot of $\ln C_{RH}$ *versus* time generates a straight line whose slope corresponds to the apparent rate constant value (k_{app}) of the target organic compound degradation (Equation 1.47):

$$\ln C_{RH} = \ln C_{RH_0} - k_{app} \cdot t \quad (1.47)$$

being C_{RH_0} the initial concentration of the target organic compound.

1.4.1.2. Operational conditions

The performance of such a complex reactive system is clearly pH dependent – particularly in Fenton-like and photo-Fenton reactions– with the maximum catalytic activity at pH = 2.8 [60, 65]. For higher pH values, low activity is detected because of the decrease of free iron species due to ferric oxyhydroxides precipitation. On the other hand, the decrease of activity for pH values below the optimum is understandable taking into account (i) the inhibition of the complexation of Fe (III) with H_2O_2 in Equation 1.18 and (ii) the photoactivity of the Fe (II) species present in solution [61]. Table 1.3 gives the predominant iron species (including water ligands) at different pH ranges:

Table 1.3. Hydrated Fe (III) species in solution and the range of pH where they are predominant [61].

Fe species	pH
$[Fe\ (III)\ (H_2O)_6]^{3+}$	1-2
$[Fe\ (III)\ (HO)(H_2O)_5]^{2+}$	2-3
$[Fe\ (III)\ (HO)_2(H_2O)_4]^{+}$	3-4

As commented above, it is evident that $[Fe\,(III)\,(HO)(H_2O)_5]^{2+}$, the most photoactive species, is the dominant between pH 2 and 3. The majority of ferric ion below this pH will be $[Fe\,(III)\,(H_2O)_6]^{3+}$, with a lower irradiation absorption effectiveness [61].

Another important factor influencing the efficiency of these processes is the initial Fe (II) and H_2O_2 dosage. Although Fenton type reactions have been widely studied, there is no agreement on the ratio of H_2O_2 to Fe (II) that leads to the best mineralisation results. Different authors have reported different reactants ratios [53, 82, 83], and it seems difficult to attain a universal criterion for all type of substrates when the reaction pathways and even the oxidative species may differ in each case [44]. The optimum treatment conditions will depend on the composition and concentration of the specific water to be treated, as well as on the degree of degradation that is to be achieved. In any case, it has to be taken into account the detrimental effect of large concentrations of either H_2O_2 or Fe (II) since they can act themselves as radicals scavengers (Equations

1.21 and 1.22) [16, 65]. Undesirable competitive reactions such as Equations 1.23-1.26 could also be favoured by using inappropriate Fe (II)/H_2O_2 ratios.

As other AOPs, Fenton and photo-Fenton processes are generally carried out at room temperature. However, temperature is a key parameter that has to be taken into account. It is known that thermal Fenton process is accelerated with increasing temperature [84], although too high values (above 40 ºC) may decompose hydrogen peroxide (Equation 1.23) [85] precluding the extent of mineralisation. When photoassisted reactions are controlling the process, no beneficial effect would be observable.

Obviously, incident irradiation intensity is also another factor affecting the rate of generation of free radicals at photoassisted processes, and hence the rates of degradation of the pollutants.

Finally, it has been reported that incorporation of molecular oxygen into the complex reaction mechanism of the Fenton and photo-Fenton systems leads to greater mineralisation of target pollutants to CO_2 [45, 86]. O_2 consumption may be caused by different processes. It reacts with intermediate organic radicals to generate oxygenated intermediates (Equation 1.48) [61, 87], forming photolabile Fe (III) complexes and thus promoting overall mineralisation.

$$R^{\cdot} + O_2 \rightarrow RO_2^{\cdot} \rightarrow \text{ non radical oxygenated products} \qquad (1.48)$$

The intermediate organoperoxides formed serve to oxidise Fe (II) to Fe (III), which is photoactive (Equation 1.49).

$$RO_2^{\cdot} + \text{Fe (II)} \rightarrow RO_2^{-} + \text{Fe (III)} \qquad (1.49)$$

Finally, it generates $HO_2^{\cdot}$ by means of the before described “Dorfman” mechanism (Equation 1.39).

The direct oxidation of Fe (II) by O_2 (auto-oxidation) is too slow to be important in acidic solution [65].

1.4.1.3. Benefits and limitations

Among the different AOPs, the Fenton and, especially, the photo-Fenton processes are considered the most promising for the remediation of highly contaminated wastewaters [44].

They constitute an attractive oxidative system since do not require neither expensive reagents nor sophisticated instrumentation for pollutants destruction [43]. Iron is the fourth most abundant element on the earth, as well as non toxic and safe, whereas hydrogen peroxide, compared with other bulk oxidants, is reasonably priced, easy to handle and environmentally benign [45, 61]. At the same time, the Fenton reagent is considered a "clean" reagent [57]. Once the treatment is over, dissolved iron can be removed by precipitation just increasing the pH of the media [88]. Moreover, if the employed catalyst amount is small enough (in the order of few $mg \cdot l^{-1}$), it could remain dissolved without affecting the quality of the resulting water. Likewise, any residual hydrogen peroxide readily decomposes to O_2 and H_2O (Equation 1.23), posing no lasting environmental threat [45, 57].

Fenton type processes are capable to carry out a deep mineralisation of pollutants with, in many cases, oxidation effectiveness clearly superior than other AOPs [45, 56]. Additionally, from an economic and environmental point of view, photoassisted Fenton process may also surpass most of them. As discussed before, It makes use of photons with wavelengths from the near-UV up to visible (~ 550 nm), with the possibility of be driven under solar irradiation [56, 61]. Even so, the high operational costs derived from chemical reagents consumption are the main handicap of this technology.

Other associated drawbacks are the instability of the reagent mixture, the necessity of pH changes, the interference by some substances that complex iron ions and the possible iron oxide sludge generation and subsequent disposal [45]. In this sense, recent studies aim at the application of iron as a heterogeneous catalyst [89], providing an easy separation and the possibility of working without pH adjustments.

Finally, it should be pointed out that it is possible to take advantage of the iron precipitation capacity. Under determined experimental Fenton conditions, iron may not act just as a catalyst but also as a coagulant agent. Thereby, the pollutant removal would be due to a non oxidative process based on the $Fe(OH)_3$ co-precipitation. Some large scale plants that use a large excess of iron as well as hydrogen peroxide exploit such property [22].

1.4.1.4. Applications to wastewater treatment

The degradation of organic pollutants present in wastewater by means of Fenton, and more especially of photo-Fenton systems is a fast growing field of applied research. Illustrative bench scale studies are the treatment of pesticides [57, 58, 65], chlorinated phenolic compounds [82, 83, 90], agricultural effluents (wine-distilleries and black olive plants) [91], paper pulp bleaching effluents [92, 93] and dye-containing textile effluents [16, 19, 84, 94, 95]. Applications involving surfactants, photographic wastes and landfill leachates, have also been described [45].

At large scale, Oliveros *et al.* [96] reported the successful treatment of an industrial wastewater contaminated with xylidines (toxic intermediates of pharmaceutical and dyes and pigments industries) on a 500 l pilot plant by the photoassisted reaction. Moreover, solar pilot plants have been designed for a variety of solar driven photo-Fenton applications [77, 88, 97-100].

Fe (II)/H_2O_2 systems have also been applied at full scale, most of them on textile effluents treatments [14]. A special remark has to be made to the first commercial wastewater treatment plant applying solar driven photo-Fenton, which has been installed in Almería, Spain (Albaida Recursos Naturales y Medio Ambiente, S.A.), where wastewater coming from pesticide plastic bottles recycling is treated by solar driven photo-Fenton process [101].

Currently, an important field of investigation concerns the combination of either Fenton and/or photo-Fenton reactions (as AOPs in general) with biological treatments. Some important examples are listed in Section 1.5.2.

1.4.2. Ozonation

1.4.2.1. Fundamental chemistry

Ozone is a very powerful oxidising agent (E^o = 2.07 V *versus* NHE) (see Table 1.2), generally produced *in situ* by a high-voltage electric discharge in the presence of air or pure oxygen. It can react with organic contaminants present in wastewater by two possible mechanisms [102, 103]: the direct reaction (important at low pH), where the oxidising agent is the molecular ozone, in a slow and highly selective attack to the organic matter (especially in the case of unsaturated organic compounds); and the indirect reaction, initiated by the ozone decomposition in presence of species such as HO^-, HO_2^-, $HCOO^-$, Fe (II) or humic substances [104]. In this manner, the indirect mechanism can be significantly promoted in basic media, where hydroxide ions would initiate ozone decomposition entailing the following free radical mechanism (Equations 1.50-1.57) [50, 105-107]:

$$O_3 + HO^- \rightarrow HO_2^- + O_2 \qquad k = 70\ l{\cdot}mol^{-1}{\cdot}s^{-1} \qquad (1.50)$$

$$O_3 + HO_2^- \rightarrow HO^{\cdot} + O_2^{\cdot -} + O_2 \qquad k = 2.8{\cdot}10^6\ l{\cdot}mol^{-1}{\cdot}s^{-1} \qquad (1.51)$$

$$O_3 + O_2^{\cdot -} \rightarrow O_3^{\cdot -} + O_2 \qquad k = 1.6{\cdot}10^9\ l{\cdot}mol^{-1}{\cdot}s^{-1} \qquad (1.52)$$

$$pH \leq 8 \qquad O_3^{\cdot -} + H^+ \leftrightarrows HO_3^{\cdot} \qquad k_+ = 5{\cdot}10^{10}\ l{\cdot}mol^{-1}{\cdot}s^{-1};\ k_- = 3.3{\cdot}10^2\ s^{-1} \qquad (1.53)$$

$$HO_3^{\cdot} \rightarrow HO^{\cdot} + O_2 \qquad k = 1.4{\cdot}10^5\ s^{-1} \qquad (1.54)$$

$$pH \geq 8 \qquad O_3^{\cdot -} \leftrightarrows O^{\cdot -} + O_2 \qquad k_+ = 2.1{\cdot}10^3\ l{\cdot}mol^{-1}{\cdot}s^{-1};\ k_- = 3.3{\cdot}10^9\ s^{-1} \qquad (1.55)$$

$$O^{\cdot -} + H_2O \rightarrow HO^{\cdot} + HO^- \qquad k = 10^8\ s^{-1} \qquad (1.56)$$

$$HO^{\cdot} + O_3 \rightarrow HO_2^{\cdot} + O_2 \qquad k = 1{\cdot}10^8\text{-}2{\cdot}10^9\ l{\cdot}mol^{-1}{\cdot}s^{-1} \qquad (1.57)$$

Throughout this chain sequence, ozone gives rise to the formation of HO· radical – among others– which quickly and indiscriminately reacts with most organic compounds present in the reacting media [105]. Some of its main reaction mechanisms have been described in preceding Sections.

Both the molecular and the free radical oxidation pathways can take part in the organic compounds oxidation. One or the other mechanism would prevail depending on the composition of the specific wastewater, the ozone dosage and, mainly, the pH of the media [104]. Since the oxidative power of HO· is higher than the oxidative power of molecular ozone (see Table 1.2), it should be remarked that ozonation is a more efficient treatment when experimental conditions favour the free radical mechanism.

1.4.2.2. Operational conditions

To favour the free radical mechanism, the pH should be superior to a critical value, near neutrality [102]. However, it should be taken into account the detrimental effect of excessively high pH values because of the scavenging of HO· radicals by part of carbonate and hydrogencarbonate ions (Equations 1.40 and 1.41). In fact, the scavenging capacity of certain anions earlier described for Fenton type reactions (Section 1.4.1.1) is extended to any process involving HO·, such as ozonation.

Reaction efficiency is a function of the applied ozone dose. To attain a thorough oxidation, a high enough O_3 to contaminant molar ratio (largest than 5:1) is necessary [104].

As other AOPs, ozonation process usually operates at or near to room temperature. Though, temperature variation may cause two simultaneous opposed effects [47]: when it increases, the rate constants of the reactions consequently increase. On the contrary, the solubility of ozone drops off thus reducing the amount of ozone available for oxidation [108]. In this way, there is no clear beneficial or damaging effect associated with this variable.

Finally, it is interesting to remark that ozonation efficiency may be effectively enhanced by O_3 combination with H_2O_2 [105], UV irradiation [109] or both, and even with TiO_2 photocatalyst [110, 111] or photo-Fenton reaction [111].

1.4.2.3. Benefits and limitations

The main advantage of ozonation treatment is that, in general, it leads to a quick and efficient removal of all type of contaminants. Its strong oxidant potential is especially noticeable in those cases where other classical treatments are inefficient. Additionally, ozone is just transformed into O_2 and H_2O, and does not introduce new substances into the aqueous media.

In contrast, ozone generation requires a large amount of chemical reagent and electrical energy [56] and its lonely use would result uneconomical in industrial wastewater applications. This limitation adds to the instability of ozone in water, which needs to be continuously generated and always at site. The maximum concentrations of ozone produced in air or pure oxygen are approximately 4 and 8%, respectively [112], and depending on the water quality, the half-life of ozone is in the range of seconds to hours [50].

Another important drawback of ozonation is the low solubility of ozone in aqueous solution. As a consequence, the gas-liquid mass transfer is often the main limiting factor of the oxidation process [113]. This problem may be technically handled, for instance, by maximising the interfacial area of contact (i.e., reducing the bubble size by using small pore size ozone diffusers), by means of an increase of the contact time between the gas and the solution (large bubble columns), or by increasing the pressure [47, 114]. However, these aspects suppose additional investments to the already high capital costs related to the equipment (ozonator, abatement system for residual ozone, construction materials that can resist to its powerful oxidative capability, etc. [43]).

Both operational cost and gas-liquid mass transfer limitations should be overcome to make profitable the use of ozonation in large scale operation.

1.4.2.4. Applications to wastewater treatment

Throughout the last 20 years, the literature is full with successful applications of ozonation on a wide range of contaminant compounds in wastewater. It has been used for treatment of effluents from various industries related to pulp and paper production (bleaching and secondary effluents) [115], production and usage of pesticides [114, 116, 117], dye manufacture and textile dyeing [118, 119], wine-distillery [120] and olive mill wastewaters [121], among others. It is remarkable that, in the frame of AOP-biological treatment strategies (see Section 1.5), some of the works apply ozonation as a pre- or post-treatment of biological treatment units [120, 121]. More examples of ozonation and biological coupling systems are shown in Section 1.5.2.

Several case studies in which ozone is used in full scale units are also reported [14]. In most of them the ozonation is used to raise the final quality of the effluents (tertiary treatment).

1.5. COMBINATION OF AOPs AND BIOLOGICAL TREATMENTS

1.5.1. Fundamentals

The decontamination potential of AOPs technologies becomes evident. Nevertheless, due to the associated high investment and operational costs (electrical energy and chemicals demand), it is obvious that their application should not replace, whenever possible, the cost-effective and environmentally compatible biological treatments. However, bioremediation do not always proceeds to complete degradation. Numerous factors can affect the biodegradation process. It may depend on the environmental conditions (see Section 1.3.1) and on the nature of the chemical compounds to be degraded. Two main factors have been identified responsible for the biorecalcitrant behaviour of some organic compounds [16]: the lack of enzymes able to degrade the molecule (which will depend on the size, the nature, number and position of functional groups, etc.) and its toxic properties against the bioculture (i.e., the capability to disrupt the functions or produce the death of the microorganisms). In this sense,

organic compounds may be non biocompatible due to their toxic and/or non biodegradable character.

Biological treatment units may require, in such cases, the support of an effective complementary technique to synergistically improve the entire efficiency of the treatment. In this frame, the current research points to remediation strategies that integrate AOPs and biological treatments. As introduced in Section 1.4, AOPs can be implemented as a pre- or post-treatment of the biological process. The extent of biorecalcitrance of the different wastewaters and the organic compounds therein will decide the processes application order. Regardless, the resulting effluent should achieve the required legislation limits.

Figure 1.5 presents a possible strategic scheme to be followed in each case, derived from the general strategy proposed by Sarria *et al.* [122]. Biodegradable and non toxic wastewaters (Ready Biodegradable; RB) can be directly biotreated. Otherwise, when handling completely biorefractory wastewaters (Non Biodegradable; NB), the AOP is performed as a first step (avoiding complete mineralisation) to just enhance the biodegradability and generate a new solution capable to be subsequently treated in the biological plant. Facing the treatment of partly biocompatible wastewaters (Partly Biodegradable; PB), there are two possible alternatives: it can be firstly submitted to biological treatment (to eliminate the biodegradable fraction) and then leaded to the AOP stage to abate the remaining refractory COD; or it can be chemically treated prior the bioremediation (analogously to NB). Depending on the wastewaters characteristics, one or the other option will be preferable. Finally, it is worth to note that some specific breakdown products generated throughout the biological unit (even coming from initially biotreatable wastewaters) may accumulate in the reaction and/or inhibit the microorganisms, requiring further chemical oxidation (see Figure 1.5) [62].

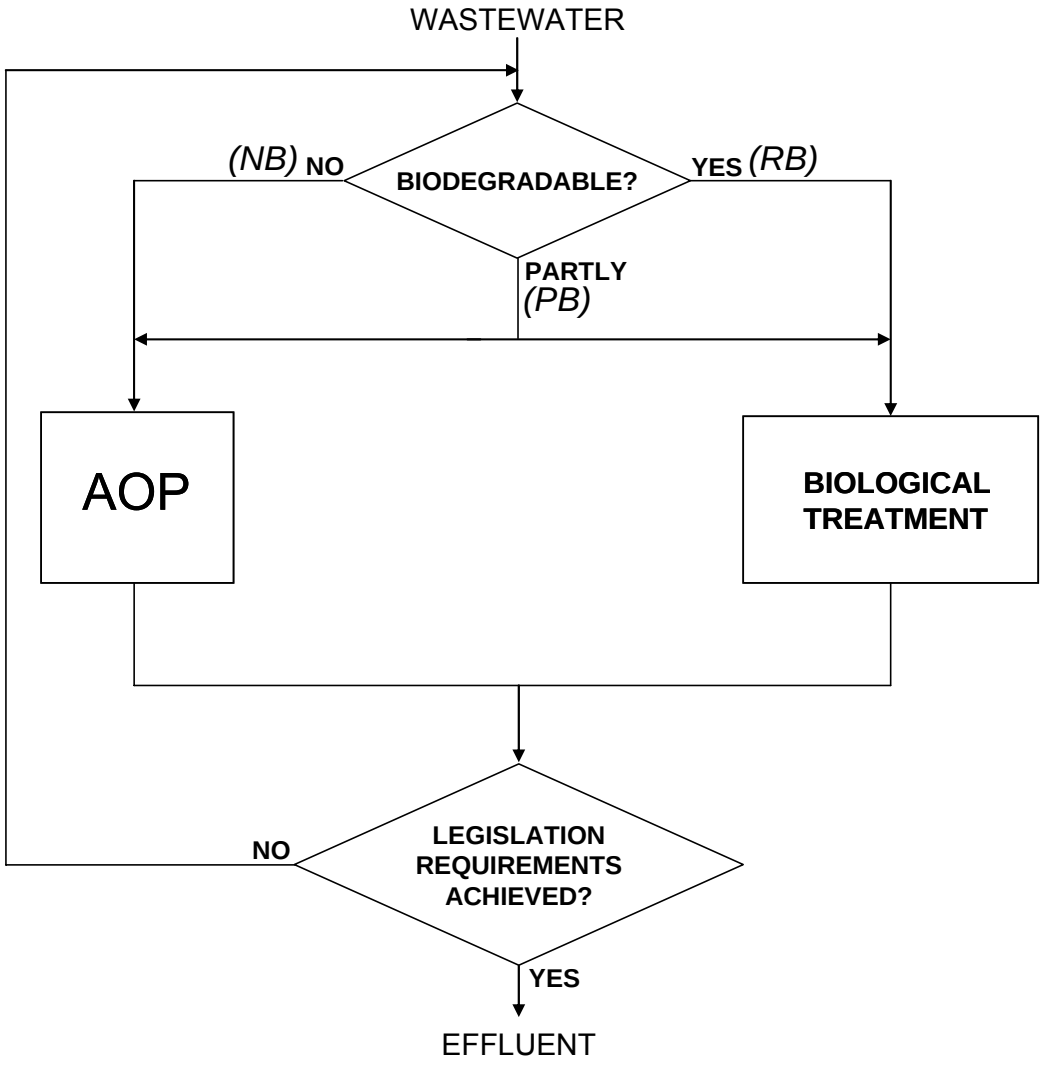

Figure 1.5. Strategy for wastewater treatment processing.

Such chemical and biological combinations intend to take advantage of the individual potentialities of each treatment, avoiding their above described drawbacks [62]. The final goal would be to minimise the AOP in front of the biological stage, while reducing at maximum its large chemicals and energy consumption. It should be commented that, to harmonise them, sample pre-treatment like pH readjustments or the removal of any bactericide residual reagent coming from the AOP should be tackled.

As deduced from Figure 1.5, a key aspect is the determination of the toxic or biodegradable nature of the original wastewater and the intermediate solutions generated. It directly influences the effectiveness of each treatment step and determines

when it would be optimal to switch processes. There is large number of tests used to provide information about biocompatibility. In this sense it is worth to note that, since many factors can influence the tests results, there is not a universal response and it is not possible to define a truly reliable method; the choice of one or the other will depend on the testing purpose [123].

Biodegradation tests are normally used to predict the biodegradation behaviour of a test material in natural or technical environments. Standardised methods such as the Zahn-Wellens assay [124] or the respirometric tests [125, 126] are commonly employed for aerobic tests. The BOD_5/COD ratio of a wastewater also constitutes a good index of screening aerobic biodegradability. It is established that contaminants with a ratio $BOD_5/COD \geq 0.4$ may be considered thoroughly biodegradable [53]. On the other hand, anaerobic biodegradability may be determined by means of methods based on the methanogenic activity measurement [127, 128], among others.

Regarding toxicity, the measurement of the inhibition activity of different microorganisms such as luminescence bacteria (e.g., the *Vibrio fischeri* [129] or the *Photobacterium phosphoreum* [130]), the crustaceans *Daphnia magna* [131], as well as the aerobic activated sludge [132] or anaerobic complex biomass [133, 134] are generally employed.

1.5.2. Applications to wastewater treatment

A wide range of studies have already stated the potential of these coupled systems to treat different model compounds and real wastewaters coming from various origins. Examples are olive mill wastewaters, paper pulp bleaching effluents, alkaline fruit cannery effluents, textile wastewaters, waters containing pesticides, wine-distillery effluents, chlorinated phenolic compounds solutions, wastewaters coming from polyester resin production, and landfill leachates, among others.

The choice of the appropriate chemical and biological unit depends on the characteristics of the wastewater and the goal of the treatment [62]. The biological process may involve isolated or mixed microorganisms cultures acting under different

oxygen environments and located on fixed solid supports or suspended in the media. Only biological processes involving mixed biomass communities are considered here. Among the proposed coupling strategies, special attention has been given to combining the AOP and aerobic biological processes, in this order. Typical sequences are composed of O_3-aerobic treatment [120, 121, 135, 136], Fenton type reactions-aerobic treatment [122, 135, 137-146] and TiO_2 photocatalysis-aerobic treatment [122, 138, 146, 147]. Also dealing with aerobic biological treatments, the inverse strategy such as the aerobic process followed by Fenton type reactions [143, 148] or ozonation [121, 149] has been reported.

On the other hand, anaerobic digestion has been followed by Fenton reagent [150], simple ozonation [150-152] or O_3 combined with H_2O_2 [151]. Other studies integrating the anaerobic biotreatment as a post-treatment of the electro-Fenton process have been already conducted [153].

Finally, more complex chemical-biological systems have also been proposed. Some examples are a treatment cycle that implies an anoxic-aerobic-O_3 sequence [154], an anaerobic-Fenton-ozonation treatment [150] or an anaerobic-aerobic-O_3-anerobic multi-stage treatment [136].

Such combined chemical-biological strategies have been mostly developed at laboratory scale, though some of them have already been scaled-up to pilot plant designs. Obviously, the last aim will be their implementation at full scale for real wastewater applications. In this sense, it is important to remark the first industrial scale application of an oxidative pre-treatment (photo-Fenton or ozone) coupled to an aerobic immobilised biomass treatment installed in Almería, Spain (DMS-Deretil) for the treatment of salted water polluted with α-methylphenylglycine [155].

1.6. ENVIRONMENTAL ASSESSMENT: LIFE CYCLE ASSESSMENT (LCA)

1.6.1. Fundamentals

1.6.1.1. Definition and extent

LCA is an environmental management tool used to assess the environmental impacts of a product[1] over the entire life cycle, "from cradle to grave". The origins of the LCA methodology can be traced to the late 1960s [156], though it is not until the 1990s when its development and standardisation takes off [157]. In 1993 the Society of Environmental Toxicology and Chemistry (SETAC) published a 'Code of Practice' [158], which presents general principles and a framework for the conduct, review, presentation and use of LCA studies. More recently, a series of international standards for LCA put together by the International Standards Organisation (ISO) have emerged. Azapagic [159] has reviewed aspects of the ISO standards, and compared them with the SETAC methodology [160]. The study shows that both methodology frameworks are similar with some differences for the interpretation phase, since ISO includes further analysis and sensibility studies.

According to ISO 14040 [161], the LCA is defined as *"A technique for assessing the environmental aspects and potential impacts associated with a product by:*

- *compiling an inventory of relevant inputs and outputs of a product system,*

- *evaluating the potential environmental impacts associated with those inputs and outputs,*

- *interpreting the results of the inventory analysis and impact assessment phases in relation to the objectives of the study".*

In synthesis, the LCA technique exhaustively examines every stage of the whole product life cycle, from the obtainment of raw materials, through its manufacture,

[1] The term product is taken in its broadest sense, including physical goods as well as services.

distribution, use (and possible reuse, recycling) and final disposal. It collects the inputs (resources) and the outputs (emissions) of each stage. These inputs and outputs are aggregated over the life cycle, and then converted into the corresponding potential impacts on the environment. The sum of such environmental impacts represents the overall environmental effect of the life cycle of the product.

The main applications of LCA are the environmental assessment of a particular product in order to detect the hot spots in their whole life cycle; the environmental comparison of different products that perform the same function; and the environmental design of new products [162]. In this way LCA can help, for instance, in marketing, strategic planning, to identify opportunities to improve the environmental aspects of a product along its life cycle, to take an industry decision, etc. [161].

The entire LCA methodology, briefly described in Section 1.6.1.2, is detailed in the following ISO standard series:

- ISO 14040 (2006). Environmental Management –Life Cycle Assessment– Principles and Framework [161].

- ISO 14044 (2006). Environmental Management –Life Cycle Assessment– Requirements and Guidelines [163].

It is worth to mention that these two standards have recently replaced –with no major changes in the context– the following ISO 14040, 14041, 14042 and 14043 series:

- ISO 14040 (1997). Environmental Management –Life Cycle Assessment– Principles and Framework [164].

- ISO 14041 (1998). Environmental Management –Life Cycle Assessment– Goal and Scope Definition and Inventory Analysis [165].

- ISO 14042 (2000). Environmental Management –Life Cycle Assessment– Life Cycle Impact Assessment [166].

- ISO 14043 (2000). Environmental Management –Life Cycle Assessment– Life Cycle Interpretation [167].

1.6.1.2. Methodology

The ISO standards establish four interrelated basic stages for LCA studies, namely goal and scope, inventory analysis, impact assessment and interpretation [161, 163] (Figure 1.6).

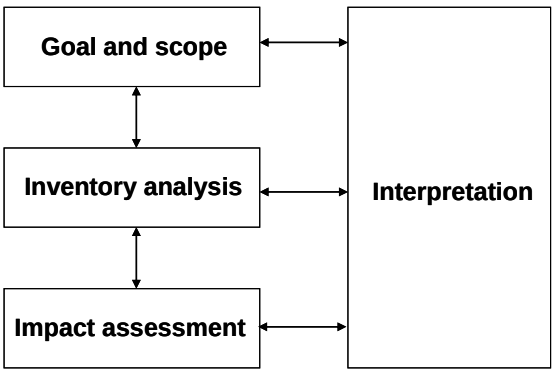

Figure 1.6. Stages in a LCA study.

Goal and scope

The goal and scope is the first stage of the LCA and probably the most important since the elements defined here determine the working plan of the entire study.

In first place, the purpose of the study is unambiguously stated and justified in relation to how the results have to be used (what will be made from obtained results and who is the study destined to). Secondly, the scope of the study must be defined. It implies, among other elements, defining the system, its boundaries (to separate all what will not be analysed), the quality of the data used (technological, temporary and geographic covering), the main hypothesis, as well as the limitations of the study. The key concern in the scope stage is the establishment of the functional unit that is the unit of product to which the environmental burdens must be referred to [168]. Its target is to provide a reference for all the inputs and outputs considered, thus allowing the assessment and comparison of their environmental impacts. It can be expressed in terms

of amount of product or be related to the amount of product needed to perform a given function.

Inventory analysis

The inventory analysis of the LCA comprises the data collection and the calculation procedures to quantify the inputs and outputs through the system boundaries. These inputs and outputs are the energy and raw materials consumed, as well as the emissions to air, water, soil, and solid waste produced. In order to make data available, several databases with standardised format are being developed in various countries.

To make the analysis easier, the system is divided in several interconnected subsystems. Usually, they are described by means of a flow diagram showing each subsystem and its interrelations (Figure 1.7). All unitary operations must comply with energy and mass conservation laws. Finally, obtained data are grouped in different categories in an inventory table.

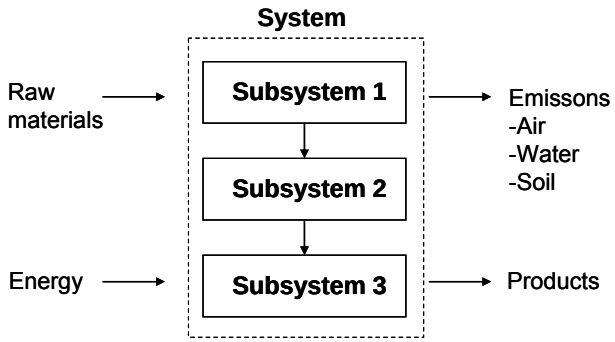

Figure 1.7. Schematic flow diagram of a system [169].

Impact assessment

The impact assessment is the phase in which the set of results –mainly the inventory table– derived from the inventory analysis is further processed in terms of potential

environmental impacts. It consists of four distinct steps: classification, characterisation, normalisation and weighting.

The first step is the classification, where the inventoried data are grouped into different impact categories according to the environmental effects they are expected to produce (potential impacts). The categories that require consideration might be internationally accepted and include representative problems such as resource depletion, human health and ecological consequences (e.g., global warming, acidification, eutrophication, photochemical oxidation, etc.).

Secondly, the characterisation step weights the different inputs and outputs contributing to the same environmental impact category. An aggregated result is obtained in a given unit of measure (characterised numeric values) generally by using equivalency factors. These equivalency factors indicate how much a substance contributes to an impact category compared with a reference substance. For instance, for global warming impact category, CO_2 and CH_4 emissions would be all weighted in kg CO_2 units (the reference substance).

Normalisation is an optional step. It is carried out in order to normalise characterisation data in relation to the actual magnitude of the impacts in some given area in a reference period.

Finally, weighting is a subjective step based on value judgements, and it is not scientific. These weighting factors may be established in a panel to directly investigate the preferences of society for reduction of environmental impacts. It must be noted that, according to ISO standards, weighting cannot be used in studies involving comparative assertions disclosed to the public.

Interpretation

Final results are analysed in the interpretation phase according to the goals and scope of the study, involving a review of all the LCA stages to check the consistency of the assumptions and the quality of the data. They are discussed in terms of the critical

sources of impacts, providing transparent conclusions and recommendations to reduce them.

1.6.1.3. Benefits and limitations

The LCA expands the debate on environmental concerns to a broad range of environmental issues by using quantitative systematic methodology.

The essential characteristic and major strength of the LCA is its holistic nature, bringing the environmental impacts into one consistent framework. All necessary inputs and outputs in many stages and operations of the life cycle are considered to be within the system boundaries. This includes not only direct inputs and outputs for production, distribution, use and final disposal, but also indirect inputs and outputs (e.g., from the initial production of the energy used) regardless of when or where they occur.

Unfortunately, according to Guinée *et al.* [162], the holistic nature of the LCA also supposes its main limitation. In fact, a cradle-to-grave analysis of a product can be only achieved at the expense of simplifying other aspects. The most important can be summarised as follows:

- LCA focuses on the environmental aspects of products, and says nothing about their economic, social and other characteristics.

- Essentially, LCA is based on linear modelling, i.e., for instance, doubling the release of a pollutant to the environment is assumed to have a double impact.

- The environmental impacts are described as "potential impacts" [161] and not as real impacts because they are not actually specified in time and space. The LCA can not address localised impacts and is typically a steady-state rather than a dynamic approach. In a context in which environmental effects depend on when, where and how they affect the environment, the LCA tool currently does not provide a satisfactory framework to predict actual effects in the environmental. Furthermore, the impacts are related to an –often– arbitrarily defined functional unit.

- LCA intends to be science based, though it involves a number of subjective technical assumptions, choices and hypothesis. To avoid arbitrariness, an important aim is to make these decisions as transparent as possible. Presented information should be clear and detailed.

- Data availability is another limitation. In spite of databases development, data are frequently obsolete, incomparable, or of questionable quality.

In this frame, it should be remarked that LCA is one among other environmental management techniques (i.e., Environmental impact assessment, Risk assessment, Cost-benefit analysis, Corporate environmental performance, Material intensity per unit service or Ecological footprint); each one characterised by its strengths and weaknesses. Obviously, no single tool can provide all information itself. Hence, for overall environmental management, a combination of complementary tools is needed for decision-making.

1.6.2. Applications to AOP based treatments

Historically, LCA has been mainly applied to a broad range of products (e.g., energy, metals and minerals, polymers, paper, textile and leather, electronic, manufacturing, agriculture, food, drinks, and also chemicals [170]). However, apart from dealing with products, the LCA also offers potential as a tool for quantitative evaluation of the environmental repercussion of processes [171].

In the context of the wastewater treatment technology, especially AOPs, the increasing awareness on environmental protection encourages the application of environmental management methods to better understand and reduce the impacts associated with a particular technique. In view of this, every wastewater treatment strategy must be developed paying special attention not only to its efficiency, but also to its potential environmental impact. In this direction, the suitability of LCA as a tool for the evaluation of chemical processes has been recently demonstrated [157, 172]. Its application requires an inventory of the energy, reagents and auxiliary materials

consumed as well as the emissions and wastes generated, providing thereby a holistic view of the environmental implications of the process.

There is extensive literature on the application of LCA to wastewater treatment systems. However, most of the studies are focused on the performance of Wastewater Treatment Plants (WWTP) dealing either with urban [31, 173, 174] or industrial wastewaters (in a lower degree) [175]. As far as the AOPs application to wastewater treatment is concerned, the number of published studies is still very scarce [176-179].

1.7. REFERENCES

[1] Zollinger H. (1991). *Color chemistry. Syntheses, properties and applications of organic dyes and pigments*. VCH, 2nd Ed., New York, USA.

[2] *Colour Index International* (2002). Society of Dyes and Colourists and American Association of Textile Chemists and Colorists, 4th Ed., www.colour-index.org.

[3] Waring D.R., Hallas G. (1994). *The chemistry and application of dyes. Topics in applied chemistry*. Plenum Press, New York, USA.

[4] Cegarra J., Puente P., Valdeperas J. (1981). *Fundamentos científicos y aplicados de la tintura de materias textiles*. Cátedra de Tintorería y Estampación de ETSIIT, Barcelona, Spain.

[5] López-Grimau V., Gutiérrez M.C. (2006). Decolourisation of simulated reactive dyebath effluents by electrochemical oxidation assisted by UV light. *Chemosphere*, 62, 106-112.

[6] Neamtu M., Siminiceanu I., Yediler A., Kettrup A. (2002). Kinetics of decolorization and mineralization of reactive azo dyes in aqueous solution by the UV/H_2O_2 oxidation. *Dyes Pigments*, 53, 93-99.

[7] *Ciba Specialty Chemicals* 124013 (1999).

[8] Carliell C.M., Barclay S.J., Naidoo N., Buckley C.A., Mulholland D.A., Senior E. (1994). Anaerobic decolourisation of reactive dyes in conventional sewage treatment processes. *Water S.A.*, 20, 341-345.

[9] Carliell C.M., Barclay S.J., Buckley C.A. (1996). Treatment of exhausted reactive dye bath effluent using anaerobic digestion: laboratory and full scale trials. *Water S.A.*, 22, 225-233.

[10] Brown D., Hamburger B. (1987). The degradation of dyestuffs –Part III– investigation of their ultimate biodegradability. *Chemosphere*, 16, 1539-1553.

[11] Pinheiro H.M., Touraud E., Thomas O. (2004). Aromatic amines from azo dye reduction: status review with emphasis on direct UV spectrophotometric detection in textile industry wastewaters. *Dyes Pigments*, 61, 121-139.

[12] Frank P. van der Zee, Villaverde S. (2005). Combined anaerobic-aerobic treatment of azo-dyes. A short review of bioreactor studies. *Water Res.*, 39, 1425-1440.

[13] *Chemical Fibers International* (2006), 2, 72.

[14] Vandevivere P.C., Bianchi R., Verstraete W. (1998). Treatment and reuse of wastewater from the textile wet-processing industry: review of emerging technologies. *J. Chem. Technol. Biot.*, 72, 289-302.

[15] EPA (1996). *Best management practices for pollution prevention in textile industry, manual*. 625R96004, Washington DC, USA.

[16] Rodrígez M., Sarria V., Esplugas S., Pulgarin C. (2002). Photo-Fenton treatment of a biorecalcitrant wastewater generated in textile activities: biodegradability of the photo-treated solution. *J. Photoch. Photobio. A*. 151, 129-135.

[17] Delée W., O'Neil C., Hawkes F.R. Pinheiro H.M. (1998). Anaerobic treatment of textile effluents: a review. *J. Chem. Technol. Biot*., 73, 323-335.

[18] O'Neill C., Hawkes F.R., Hawkes D.L., Lourenço N.D., Pinheiro H.M., Delée W. (1999). Colour in textile effluents – sources, measurement, discharge consents and simulation: a review. *J. Chem. Technol. Biot.*, 74, 1009-1018.

[19] Kuo W.G. (1992). Decolorizing dye wastewater with Fenton´s reagent. *Water Res*., 26, 881-886.

[20] *Reglamento del Dominio Público Hidráulico* (2003). Real Decreto 606/2003.

[21] Robinson T., McMullan G., Marchant R., Nigam P. (2001). Remediation of dyes in textile effluent: a critical review on current treatment technologies with a proposed alternative. *Bioresource Technol*., 77, 247-255.

[22] Mattioli D., Malpei F., Bortone G., Rozzi A. (2002). Water minimisation and reuse in textile industry. In: Lens P., Pol L.H., Wilderer P., Asano T. (Eds.). *Water recycling and resource recovery in industry: analysis, technologies and implementation*. IWA publishing, London, UK.

[23] Forgacs E., Cserháti T., Oros G. (2004). Removal of synthetic dyes from wastewaters: a review. *Environ. Int*., 30, 953-971.

[24] Pearce C.I., Lloyd J.R., Guthrie J.T. (2003). The removal of colour from textile wastewater using whole bacterial cells: a review. *Dyes Pigments*, 58, 179-196.

[25] Rai, H.S., Bhattacharyya M.S., Singh J., Bansal T.K., Vats P., Banerjee U.C. (2005). Removal of dyes from the effluent of textile and dyestuff manufacturing industry. A review of emerging techniques with reference to biological treatment. *Crit. Rev. Env. Sci. Tec*., 35, 219-238.

[26] Legrini O., Oliveros E., Braun A.M. (1993). Photochemical processes for water treatment. *Chem. Rev.*, 93, 671-698.

[27] Metcalf & Eddy (1985). *Wastewater engineering. Treatment, disposal and reuse*. Mc. Graw-Hill, Inc., 2nd Ed., New York, USA.

[28] Manahan S.E. (2005). *Environmental chemistry*. CRC Press, 8th Ed., Boca Raton, USA.

[29] Stephenson R.L., Blackburn J.B. Jr. (1998). *The industrial wastewater systems handbook*. Lewis publishers, New York, USA.

[30] Tchobanoglous G., Theisen H., Vigil S. (1993). *Integrated solid waste management: Engineering principles and management issues*. Mc. Graw-Hill, New York, USA.

[31] Hospido A., Moreira M.T., Fernández-Couto M., Feijoo G. (2004). Environmental peroformance of a municipal wastewater treatment plant. LCA case studies. *Int. J. Life Cycle Ass.*, 10, 336-345.

[32] Suh Y.J., Rousseaux P. (2002). A LCA of alternative wastewater sludge treatment scenarios. *Resour. Conserv. Recy.*, 35, 191-200.

[33] Marchaim U. (1992). *Biogas processes for sustainable development*. FAO, Agricultural services bulletin 95, Rome, Italy.

[34] O'Neill C., Hawkes F.R., Hawkes D.L., Esteves S., Willcox S.J. (2000). Anaerobic–aerobic biotreatment of simulated textile effluent containing varied ratios of starch and azo dye. *Water Res.*, 34, 2355-2361.

[35] Arden E., Lockett W.T. (1914). Experiments on the oxidation of sewage without the aid of filters. *J. Soc. Chem. Ind.*, 33, 523-539.

[36] Wilderer P.A., Irvine R.L., Goronszy M. C. (2001). *Sequencing batch reactor technology*. Scientific and technical report No 10, IWA publishing, London, UK.

[37] Mace S., Mata-Alvarez J. (2002). Review of SBR Technology for Wastewater Treatment: An Overview. *Ind. Eng. Chem. Res.*, 41, 5539-5553.

[38] Irvine R.L., Ketchum L.H. Jr. (1989). Sequencing batch reactors for biological wastewater treatment. *CRC Crit. Rev. Environ. Control.*, 18, 255-294.

[39] EPA 1999. *Wastewater technology fact sheet. Sequencing Batch Reactors*. 832-F-99-073, Washington DC, USA.

[40] Grady C.P.L., Daigger G.T., Lim H.C. (1999). *Biological wastewater treatment*. Marcel Dekker, Inc., 2nd Ed., New York, USA.

[41] Sarria V., Pulgarin C. (2007). Biological Technology Optimisation. Technical Report of the CADOX project: *A Coupled Advanced Oxidation-Biological Process for Recycling of Industrial Wastewater Containing Peristent Organic Contaminants*. Reference: CADOX-T240-EPFL-01.

[42] Glaze W.H., Kang J.W., Chaplin D.H. (1987). The Chemistry of water treatment processes involving ozone, hydrogen peroxide and ultraviolet radiation. *Ozone-Sci. Eng.*, 9, 335-352.

[43] Andreozzi R., Caprio V., Insola A., Marotta R. (1999). Advanced oxidation proceses (AOP) for water purification and recovery. *Catal. Today*, 53, 51-59.

[44] Bossmann S.H., Oliveros E., Göb S., Siegwart S., Dahlen E.P., Payawan L., Straub M., Wörner M., Braun A.M. (1998). New evidence against hydroxyl radicals as reactive intermediates in the thermal and photochemically enhanced Fenton reactions. *J. Phys. Chem. A*, 102, 5542-5550.

[45] Pignatello J., Oliveros E., MacKay A. (2006). Advanced Oxidation processes for organic contaminant destruction based on the Fenton reaction and related chemistry. *Crit. Rev. Env. Sci. Tec*., 36, 1-84.

[46] Hoigné J. (1997). Inter-calibration of OH radical sources and water quality parameters. *Water Sci. Technol*. 35, 1-8.

[47] Gogate P.R. Pandit A.B. (2004). A review of imperative technologies for wastewater treatment I: oxidation technologies at ambient conditions. *Adv. Environ. Res.*, 8, 501-551.

[48] Ioannis K., Konstantinou, Triantafyllos A. Albanis. (2004). TiO_2-assisted photocatalytic degradation of azo dyes in aqueous solution: kinetic and mechanistic investigations: A review. *Appl. Catal. B: Environ*., 49, 1-14.

[49] Herrmann J.M. (2005). Heterogeneous photocatalysis: state of the art and present applications. *Top. Catal*., 34, 49-65.

[50] Urs von Gunten (2003). Ozonation of drinking water: Part I. Oxidation kinetics and product formation. *Water Res.*, 37, 1443-1467.

[51] Gogate P.R., Pandit A.B. (2004). A review of technologies for wastewater treatment II: hybrid methods. *Adv. Environ. Res.*, 8, 553-597.

[52] Kiwi J., Pulgarin C., Peringer P. (1994). Effect on Fenton and photo-Fenton reactions on the degradation and biodegradability of 2 and 4-nitrophenols in water treatment. *Appl. Catal. B: Environ*., 3, 335-350.

[53] Chamarro E., Marco A., Esplugas S. (2001). Use of Fenton reagent to improve organic chemical biodegradability. *Water Res*., 35, 1047-1051.

[54] Neyens E., Baeyens J. (2003). A review of classic Fenton's peroxidation as an advanced oxidation technique. *J. Hazard. Mater*., 98, 33-50.

[55] Brillas E., Mur E., Sauleda R., Sànchez L., Peral J., Domènech X., Casado J. (1998). Aniline mineralization by AOP's: anodic oxidation, photocatalysis, electro-Fenton and photoelectro-Fenton processes. *Appl. Catal. B: Environ*., 16, 31-42.

[56] Bauer R., Fallman H. (1997). The photo-Fenton oxidation-a cheap and efficient wastewater treatment method. *Res. Chem. Intermediat.*, 23, 341-354.

[57] Huston P.L., Pignatello J. (1999). Degradation of selected pesticide active ingredients and commercial formulations in water by the photo-assisted Fenton reaction. *Water Res.*, 33, 1238-1246.

[58] Sun Y., Pignatello J. (1993). Photochemical reactions involved in the total mineralization of 2,4-D by $Fe^{3+}/H_2O_2/UV$. *Environ. Sci. Technol.*, 27, 304-310.

[59] Hislop K.A., Bolton J.R. (1999). The photochemical generation of hydroxyl radical in the UV-vis/ferrioxalate/H_2O_2 system. *Environ. Sci. Technol.*, 33, 3119-3126.

[60] Pignatello J., Liu D., Huston P. (1999). Evidence for an additional oxidant in the photoassisted Fenton reaction. *Environ. Sci. Technol.*, 33, 1832-1839.

[61] Safarzadeh-Amiri A., Bolton J.R., Cater S.R. (1996). The use of iron in Advanced Oxidation Processes. *J. Adv. Oxid. Technol.*, 1, 18-26.

[62] Scott J.P., Ollis D.F. (1995). Integration of chemical and biological oxidation processes for water treatment: review and recommendations. *Environ. Prog.*, 14, 88-103.

[63] Haber F., Weiss J. (1934). The catalytic decomposition of hydrogen peroxide by iron salts. *Proc. Roy. Soc. A*, 147, 332-351.

[64] Fenton H.J.H. (1894). Oxidation of tartaric acid in the presence of iron. *J. Chem. Soc.*, 65, 899-910.

[65] Pignatello J. (1992). Dark and photoassisted Fe^{3+}-catalyzed degradation of chlorophenoxy herbicides by hydrogen peroxide. *Environ. Sci. Technol.*, 26, 944-951.

[66] Sychev A.Y., Isaak V.G. (1995). Iron compounds and the mechanisms of the homogeneous catalysis of the activation of O_2 and H_2O_2 and of the oxidation of organic substrates. *Russ. Chem. Rev.*, 64, 1105-1129.

[67] Chen R., Pignatello J. (1997). Role of quinone intermediates as electron shuttles in Fenton and photoassited Fenton oxidations of aromatic compounds. *Environ. Sci. Technol.*, 31, 2399-2406.

[68] Chen R., Pignatello J. (1999). Structure-activity study of electron-shuttle catalysis by quinones in the oxidation of aromatic compounds by the Fenton reaction. *J. Adv. Oxid. Technol.*, 4, 447-453.

[69] Ma J., Song W., Chen C., Ma W., Zhao J., Tang Y. (2005). Fenton degradation of organic compounds promoted by dyes under visible irradiation. *Environ. Sci. Technol.*, 39, 5810-5815.

[70] Benkelberg H.J., Warneck P. (1995). Photodecomposition of iron (III) hydroxo- and sulfato-complexes in aqueous solution: wavelength dependence of HO and SO_4- quantum yields. *J. Phys. Chem.*, 99. 5214-5221.

[71] Safarzadeh-Amiri A., Bolton J.R., Cater S.R. (1997). Ferrioxalate-mediated solar degradation of organic contaminants in water. *Water Res.*, 31, 787-798.

[72] Hatchard C.G., Parker C.A., (1956). A sensitive chemical actinometer II. Potassium ferrioxalate as a standard chemical actinometer. *Proc. Roy. Soc. A*, 235, 518-536.

[73] Huyser E.S., Hawkins G.W. (1983). Ferrous ion catalyzed oxidations of 2-propanol with peroxyacetic acid. *J. Org. Chem.* 48, 1705-1708.

[74] Dorfman L.M., Taub I.A., Buehler R.E. (1962). Pulse radiolysis studies. I. Transient spectra and reaction-rate constants in irradiated aqueous solutions of benzene. *J. Chem. Phys.*, 36, 3051-3061.

[75] von Sonntag C., Dowideit P., Fang X., Mertens R., Pan X., Schuchmann M.N., Schuchmann H.P. (1997). The fate of hydroxyl radical in aqueous solution. *Water Sci. Technol*. 35, 9-15.

[76] De Laat J., Truong Le G., Legube B (2004). A comparative study of the effects of chloride, sulfate and nitrate ions on the rates of decomposition of H_2O_2 and organic compounds by Fe (II)/H_2O_2 and Fe (III)/H_2O_2. *Chemosphere*, 55, 715-723.

[77] Kositzi M., Antoniadis A., Poulios I., Kiridis I., Malato S. (2004). Solar photocatalytic treatment of simulated dyestuff effluents. *Sol. Energy*. 77, 591-600.

[78] Walling C., Amarnath K. (1982). Oxidation of mandelic acid by Fenton's reagent. *J. Am. Chem. Soc*., 104, 1185-1189.

[79] Rahhal S., Richter H.W. (1988). Reduction of hydrogen peroxide by the ferrous iron chelate of diethylenetriamine-N,N,N',N'',N''-pentaacetate. *J. Am. Chem. Soc*., 110, 3126-3133.

[80] Arasasinghan R.D., Cornman C.R., Balch A.L. (1989). Detection of alkylperoxo and ferryl, $(FeIV{=}O)^{2+}$, intermediates during the reaction of *tert*-butyl Hydroperoxide with iron porphyrins in toluene solution. *J. Am. Chem. Soc*., 111, 7800-7805.

[81] Rush J.D., Bielski B.H.J. (1994). Decay of ferrate (V) in neutral and acidic solutions. A premix pulse radiolysis study. *Inorg. Chem*., 33, 5499-5502.

[82] Ruppert G., Bauer R., Heisler G. (1993). The photo-Fenton reaction-an effective photochemical wastewater treatment process. *J. Photoch. Photobio. A*, 73, 75-78.

[83] Tang W.Z., Huang C.P. (1996). 2,4-Dichlorophenol oxidation kinetics by Fenton's reagent. *Environ. Technol*., 17, 1371-1378.

[84] Pérez M., Torrades F., Domènech X., Peral J. (2002). Fenton and photo-Fenton oxidation of textile effluents. *Water Res.*, 36, 2703-2710.

[85] Nesheiwat F.K., Swanson A.G. (2000). Clean contaminated sites using Fenton's reagent. *Chem. Eng. Prog*., 96, 61-66.

[86] Utset B., Garcia J., Casado J., Domènech X., Peral J. (2000). Replacement of H_2O_2 by O_2 in Fenton and photo-Fenton reactions. *Chemosphere*, 41, 1187-1192.

[87] Kunai A., Hata S., Ito S., Sasaki, K. (1986). The role of oxygen in the hydroxylation reaction of benzene with Fenton reagent. Oxygen-18 tracer sudy. *J. Am. Chem. Soc.*, 108, 6012-6016.

[88] Malato S., Blanco J., Vidal A., Alarcón D., Maldonado M.I., Cáceres J., Gernjak W. (2003). Applied studies in solar photocatalytic detoxification: an overview. *Sol. Energy*, 75, 329-336.

[89] Kiwi J., Denisov N., Gak Y., Ovanesyan N., Buffat P., Suvorova E., Gostev F., Titov A., Sarkisov O., Albers P., Nadtochenko V. (2002). Catalytic Fe^{3+} clusters and complexes in Naftion active in photo-Fenton processes. High-resolution electron microscopy and femtosecond studies. *Langmuir*, 18, 9054-9066.

[90] Pera-Titus M., García-Molina V., Baños M.A., Jiménez J. Esplugas S. (2004). Degradation of chlorophenols by means of advanced oxidation processes: a general overview. *Appl. Catal. B: Environ*., 47, 219-256.

[91] De Heredia J.B., Torregrosa J., Domínguez J.R., Peres J.A. (2001). Kinetic model for phenolic compound oxidation by Fenton's reagent. *Chemosphere*, 45, 85-90.

[92] Pérez M., Torrades F., Garcia-Hortal J.A., Domènech X., Peral J. (2002). Removal of organic contaminants in paper pulp treatment effluents by Fenton and photo-Fenton reactions. *Appl. Catal. B: Environ*., 36, 63-74.

[93] Catalkaya E.Co., Kargi F. (2007). Color, TOC and AOX removals from pulp mill effluent by advanced oxidation processes: A comparative study. *J. Hazard. Mater*., 139, 244-253.

[94] Ince N.H., Tezcanli G. (1999). Treatability of textile dye-bath effluents by advanced oxidation: Preparation for reuse. *Water Sci. Technol*., 40, 183-190.

[95] Lopez Cisneros R., Gutarra Espinoza A., Litter M.I. (2002). Photodegradation of an azo dye of the textile industry. *Chemosphere*, 48, 393-399.

[96] Oliveros E., Legrini O., Hohl M., Mueller T., Braun A.M. (1997). Large scale development of a light-enhanced Fenton reaction by optimal experimental design. *Water Sci. Technol*., 35, 223-230.

[97] Gernjak W., Krutzler T., Glaser A., Malato S., Cáceres J., Bauer R., Fernández-Alba A.R. (2002). Photo-Fenton treatment of water containing natural phenolic pollutants. *Chemosphere*, 50, 71-78.

[98] Arslan-Alaton I., Gurses F. (2004). Photo-Fenton and photo-Fenton-like oxidation of Procaine Penicillin G formulation effluent. *J. Photoch. Photobio. A*, 165, 165-175.

[99] Amat A.M., Arques A., Miranda M. A., Segui S. (2004). Photo-Fenton reaction for the abatement of commercial surfactants in a solar pilot plant. *Sol. Energy*. 77, 559-566.

[100] Maldonado M.I., Passarinho P.C., Oller I., Gernjak W., Fernández P., Blanco J., Malato S. (2007). Photocatalytic degradation of EU priority substances: A comparison between TiO_2 and Fenton plus photo-Fenton in a solar pilot plant. *J. Photoch. Photobio. A*, 185, 354-363.

[101] Blanco J., Malato S., Maldonado M.I., Vincent M., Vincent J.P., Sánchez M., Myro E. (2004). The Albaida Plant: first commercial step in solar detoxification. *Global symposium on recycling waste treatment and clean technology (REWAS'04)*, Madrid, Spain.

[102] Hoigné J., Bader H. (1976). The role of hydroxyl radical reactions in ozonation process in aqueous solutions. *Water Res.*, 10, 377-386.

[103] Hoigné J., Bader H. (1983). Rate constants of reactions of ozone with organic and inorganic compounds in water-I. Non-dissociating organic compounds. *Water Res*., 17, 173-183.

[104] Domènech X., Jardim W.F., Litter M.I. (2001). Eliminación de contaminantes por Fotocatálisis Heterogénea. In: Blesa M.A. (Ed.). *Procesos Avanzados de Oxidación para la eliminación de contaminantes*. CYTED VII-G, La Plata, Argentina.

[105] Staehelin J., Hoigné J. (1982). Decomposition of ozone in water: rate of initiation by hydroxide ions and hydrogen peroxide. *Environ. Sci. Technol*., 16, 676-681.

[106] Sehested K., Holcman J., Bjergbakke E., Hart E.J. (1984). Formation of ozone in the reaction of hydroxyl with O_3^- and the decay of ozonide ion radical at pH 10-13. *J. Phys. Chem.*, 88, 269-273.

[107] Elliot A.J., McCracken D.R., Ritchie D. (1989). Effect of temperature on atomic oxygen reactions and equilibria: a pulse radiolysis study. *Radiat. Phys. Chem*., 33, 69-74.

[108] Beltran F.J., Garcia-Araya J.F., Acedo B. (1994). Advanced oxidation of atrazine in water. Part I: ozonation. *Water Res*., 28, 2153-2164.

[109] Peyton G.R., Glace W.H. (1988). Destruction of pollutants in water with ozone in combination with ultraviolet radiation. *Environ. Sci. Technol*., 22, 761-767.

[110] Sanchez L., Peral J., Domènech X. (1998). Aniline degradation by combined photocatalysis and ozonation. *Appl. Catal B: Environ*., 19, 59-65.

[111] Piera E., Calpe J., Brillas E., Domènech X., Peral J. (2000). 2,4-Dichlorophenoxyacetic acid degradation by catalyzed ozonation: TiO_2/UVA/O_3 and Fe(II)/UVA/O_3 systems. *Appl. Catal. B: Environ.*, 27, 169-177.

[112] Nebel C. (1981). Ozone. In: Grayson M., Eckroth D. (Eds.). *Kirk-Othmer encyclopedia of chemical technology*. John Wiley and Sons, 3rd Ed., New York, USA.

[113] Roche P., Volk C., Carbonnier F., Paillard H. (1994). Water oxidation by ozone or ozone/hydrogen peroxide using the OZOTEST or PEROXOTEST methods. *Ozone-Sci. Eng.*, 16, 135-155.

[114] Chiron S., Fernandez-Alba A., Rodriguez A., García-Calvo E. (2000). Pesticide chemical oxidation: State-of-the-art. *Water Res.*, 34, 366-377.

[115] Korhonen M.S., Metsarinne S.E., Tuhkanen T.A. (2000). Removal of ethylenediaminetetraacetic acid (EDTA) from pulp mill effluents by ozonation. *Ozone-Sci. Eng.*, 22, 279-286.

[116] Adams C.D., Randtke S.J. (1992). Ozonation byproducts of atrazine in synthetic and natural waters. *Environ. Sci. Technol.*, 26, 2218-2227.

[117] Benitez F.J., Acero J.L. Real F.J., García J. (2003). Kinetics of photodegradation of pentachlorophenol. *Chemosphere*, 51, 651-662.

[118] Koyuncu I., Asfar H. (1996). Decomposition of dyes in textile wastewater with ozone. *J. Environ. Sci. Heal. A*, 31, 1035-1041.

[119] Wu J., Wang T. (2001). Ozonation of aqueous azo dye in a semi-batch reactor. *Water Res.*, 35, 1093-1099.

[120] Beltran F.J., Garcia-Araya J.F., Alvarez P.M. (1999). Wine-distillery wastewater degradation 1. Oxidative treatment using ozone and its effect on the wastewater biodegradability. 2. Improvement of aerobic biodegradation by means of an integrated (ozone)-biological treatment. *J. Agr. Food Chem.*, 47, 3911-3924.

[121] Benitez F.J., Beltran-Heredia, J., Torregrosa J., Acero J.L. (1999). Treatment of olive mill wastewaters by ozonation, aerobic digestion and the combination of both treatments. *J. Chem. Technol. Biot.*, 74, 639-646.

[122] Sarria V., Parra S., Adler N., Péringer P., Benitez N., Pulgarin C. (2002). Recent developments in the coupling of photoassisted and aerobic biological processes for the treatment of biorecalcitrant compounds. *Catal. Today*, 76, 301-315.

[123] Pagga U. (1997). Testing biodegradability with standardized methods. *Chemosphere*, 35, 2953-2972.

[124] OECD (1992). *Inherent biodegradability: modified Zahn-Wellens test*. Test 302B, Paris, France.

[125] APHA-AWWA-WEF (1992). *Standard Methods for the Examination of Water and Wastewater*. 2710 B, 18th Ed., Washington DC, USA.

[126] OECD (1992). *Manometric respirometry test.* Test 301F, Paris, France.

[127] Field J., Alvarez R.S., Lettinga G. (1988). *Ensayos anaerobios. Proc. of 4th Symposium on wastewater anaerobic treatment*, Valladolid, Spain.

[128] ISO (1999). *Water quality. Evaluation of the ultimate anaerobic biodegradability of organic compounds in digested sludge. Method by measurement of the biogas production*. ISO 11734, Geneva, Switzerland.

[129] ISO (1998). *Determination of the inhibitory effect of water samples on the light emission of Vibrio fischeri (Luminescent bacteria test)*. ISO 11348-3, Geneva, Switzerland.

[130] AFNOR (1991). *Détermination de l'inhibition de la luminescence de Photobacterium phosphoreum*. T-90-320, Paris, France.

[131] OECD (1998). *Daphnia sp., acute immobilisation test*. Test 202 part I, Paris, France.

[132] ISO (1986). *Water quality test for inhibition of O_2 consumption by activated sludge*. ISO 8192, Geneva, Switzerland.

[133] Owen W.F., Stuckey D.C., Healy J.B., Young L.Y., McCarthy P.L. (1979). Bioassay for monitoring biochemical methane potential and anaerobic toxicity. *Water Res.*, 13, 485-492.

[134] Soto M., Mendez R., Lema J.M. (1993). Methanogenic and non-methanogenic activity tests: theoretical basis and experimental set up. *Water Res.*, 27, 1361-1376.

[135] Beltrán-Heredia J., Torregrosa J., García J., Domínguez J.R., Tierno J.C. (2001). Degradation of olive mill wastewater by the combination of Fenton's reagent and ozonation processes with an aerobic biological treatment. *Water Sci. Technol.*, 44, 103-108.

[136] Libra J.A., Sosath F. (2003). Combination of biological and chemical processes for the treatment of textile wastewaters containing reactive dyes. *J. Chem. Technol. Biot.*, 78, 1149-1156.

[137] Pulgarin C., Invernizzi M., Parra S., Sarria V., Polania R., Péringer P. (1999). Strategy for the coupling of photochemical and biological flow reactors useful in mineralization of biorecalcitrant industrial pollutants. *Catal. Today*, 54, 341-352.

[138] Parra S., Sarria V., Malato S., Péringer P., Pulgarin C. (2000). Photochemical versus coupled photochemical-biological flow system for the treatment of two biorecalcitrant herbicides: metobromuron and isoproturon. *Appl. Catal. B: Environ.*, 27, 153-168.

[139] Lin S.H., Chang C.C. (2000). Treatment of landfill leachate by combined electro-Fenton oxidation and sequencing batch reactor method. *Water Res.*, 34, 4243-4249.

[140] Bertanza G., Collivignarelli C., Pedrazzani R. (2001). The role of chemical oxidation in combined chemical-physical and biological processes: experiences of industrial wastewater treatment. *Water Sci. Technol.*, 44, 109-116.

[141] Sarria V., Kenfack S., Guillod O., Pulgarín C. (2003) An innovative coupled solar-biological system at field pilot scale for the treatment of biorecalcitrant pollutants. *J. Photoch. Photobio. A*, 159, 89-99.

[142] Al Momani F., Gonzalez O., Sans C., Esplugas S. (2004). Combining photo-Fenton process with biological sequencing batch reactor for 2,4-dichlorophenol degradation. *Water Sci. Technol.*, 49, 293-298.

[143] Fongsatitkul P., Elefsiniotis P., Yamasmit A., Yamasmit N. (2004). Use of sequencing batch reactors and Fenton's reagent to treat a wastewater from a textile industry. *Biochem. Eng. J.*, 21, 213-220.

[144] Farré M.J., Domènech X., Peral J. (2006). Assessment of photo-Fenton and biological treatment coupling for Diuron and Linuron removal from water. *Water Res.*, 40, 2533-2540.

[145] Lapertot M., Ebrahimi S., Dazio, S., Rubinelli A., Pulgarin C. (2007). Photo-Fenton and biological integrated process for degradation of a mixture of pesticides. J. *Photoch. Photobio. A*, 186, 34-40.

[146] Oller I., Malato S., Sánchez-Pérez J.A., Maldonado M.I., Gassó R., Blanco J. (2007). Detoxification of wastewater containing five common pesticides by solar AOPs-Biological coupled system. *Catal. Today*, in press.

[147] Parra S., Malato S., Pulgarin C. (2002). New integrated phtocatalytic-biological flow system using supported TiO_2 and fixed bacteria for the mineralization of isoproturon. *Appl. Catal. B: Environ.*, 36, 131-144.

[148] Hong, S.W. Choi, Y.S., Kwon, G., Park K.Y. (2005). Performance evaluation of physicochemical processes for biologically pre-treated livestock wastewater. *Water Sci. Technol.*, 52, 107-115.

[149] Heinzle E., Geiger F., Fahmy M., Kut O.M. (1992). Integrated ozonation biotreatment of pulp bleaching effluents containing chlorinated phenolic compounds. *Biotechnol. Progr.*, 8, 67-77.

[150] Fang H.H.P., Lau I.W.C., Wang P. (2005). Anaerobic treatment of Hong Kong leachate followed by chemical oxidation. *Water. Sci. Technol.*, 52, 41-49.

[151] Sigge G.O., Britz T.J., Fourie P.C., Barnardt C.A., Strydom R. (2001). Use of ozone and hydrogen peroxide in the post-treatment of UASB treated alkaline fruit cannery effluent. *Water Sci. Technol.*, 44, 69-74.

[152] Beltran-Heredia J., Garcia, J. (2005). Process integration: continuous anaerobic digestion-ozonation treatment of olive mill wastewater. *Ind. Eng. Chem. Res.*, 44, 8750-8755.

[153] Khoufi S., Aloui F., Sayadi S. (2006). Treatment of olive mill wastewater by combined process electro-Fenton reaction and anaerobic digestion. *Water Res.*, 40, 2007-2016.

[154] Krull R., Hempel D.C. (2001). Treatment of dyehouse liquors in a biological sequencing batch reactor with recursive chemical oxidation. *Water Sci. Technol.*, 44, 85-92.

[155] Oller I., Gernjak W., Ramos Siles C., Muñoz J.A., Maldonado M.I., Pérez-Estrada L.A., Malato S. (2006). Industrial Scale Coupling of oxidative pre-treatment (solar photo-Fenton or ozone) and immobilised biomass activated sludge biotreatment. *4th European Meeting on Solar Chemistry and Photocatalysis: Environmental Applications (SPEA 4)*, Las Palmas de Gran Canarias, Spain.

[156] Miettinen P., Hamalainen R.P. (1997). How to benefit form decision analysis in environmental life cycle assessment (LCA). *Eur. J. Oper. Res.*, 102, 279-294.

[157] Burgess A.A., Brennan D.J. (2001). Application of life cycle assessment to chemical processes. *Chem. Eng. Sci.*, 56, 2589-2604.

[158] Consoli F., Allen D., Boustead I., de Oude N., Fava J., Franklin W., Quay B., Parrish R., Perriman R., Postlethwaite D., Seguin J., Vigon B. (1993). *Guidelines for life-cycle assessment: a code of practice*. SETAC, Brusseles, Belgium.

[159] Azapagic A. (1999). Life cycle assessment and its application to process selection, design and optimisation. *Chem. Eng. J.*, 73, 1-21.

[160] Fava J.A., Denison R., Jones B., Curran M.A. Vigon B., Selke S., Barnum J. (1991). *A technical framework for life cycle assessments*. SETAC, Brusseles, Belgium.

[161] ISO (2006). *Environmental Management –Life Cycle Assessment– Principles and Framework*. ISO 14040, Geneva, Switzerland.

[162] Guinée J.B., Gorrée M., Heijungs R., Huppes G., Kleijn R., Koning A., van Oers L., Sleeswijk A.W., Suh S., Udo de Haes H.A., Bruijn H., van Duin R., Huijbregts M.A.J. (2002). *Handbook on Life Cycle Assessment. Operational guide to the ISO Standards*. Kluwer Academic Publishers, Dordrecht, The Netherlands.

[163] ISO (2006). *Environmental Management –Life Cycle Assessment– Requirements and Guidelines*. ISO 14044, Geneva, Switzerland.

[164] ISO (1997). *Environmental management –Life Cycle Assessment– Principles and Framework*. ISO 14040, Geneva, Switzerland.

[165] ISO (1998). *Environmental Management –Life Cycle Assessment– Goal and Scope Definition and Inventory Analysis*. ISO 14041, Geneva, Switzerland.

[166] ISO (2000). *Environmental Management –Life Cycle Assessment– Life Cycle Impact Assessment*. ISO 14042, Geneva, Switzerland.

[167] ISO (2000). *Environmental Management –Life Cycle Assessment– Life Cycle Interpretation*. ISO 14043, Geneva, Switzerland.

[168] Muñoz I., Rieradevall J., Domènech X. (2005). Definición de la unidad funcional e implicaciones en el ACV. In: Clemente G., Sanjuán N., Vivancos J.L. (Eds.). *Análisis de Ciclo de Vida: aspectos metodológicos y casos prácticos*. Ed. Universidad Politécnica de Valencia, Spain.

[169] Fullana P., Puig R. (1997). *Análisis del ciclo de vida*. Ed. Rubes, Barcelona, Spain.

[170] Azapagic A. (2002). Life-cycle assessment: a tool for identification of more sustainable products and processes. In: Clark J., Macquarrie D. (Eds.). *Handbook of green chemistry and technology*. Blackwell Sience, Oxford, UK.

[171] Lee J., O'Callaghan P., Allen D. (1995). Critical review of life cycle analysis and assessment techniques & their application to commercial activities. *Res. Conserv. Recy*., 13, 37-56.

[172] Domènech X., Rieradevall J., Ayllon J.A., Peral J. (2002). How green is a chemical reaction: application of LCA to Green Chemistry. *Environ. Sci. Technol.*, 36, 5517-5520.

[173] Lundin M., Bengtsson M., Molander S. (2000). Life cycle assessment of wastewater systems: influence of system boundaries and scale on calculated environmental loads. *Environ. Sci. Technol.*, 34, 180-186.

[174] Vidal N., Poch M., Martí E., Rodríguez-Roda I. (2002). Evaluation of the environmental implications to include structural changes in a wastewater treatment plant. *J. Chem. Technol. Biot.*, 77, 1206-1211.

[175] Pillay S.D., Friedrich E., Buckley C.A. (2002). Life cycle assessment of an industrial water recycling plant. *Water Sci. Technol.*, 46, 55-62.

[176] Nijdam D., Blom J., Boere J.A. (1998). Environmental life cycle assessment (LCA) of two advanced treatment techniques. *Stud. Surf. Sci. Catal.*, 120, 763-775.

[177] Muñoz I., Rieradevall J., Torrades F., Peral J., Domènech X. (2005). Environmental assessment of different solar driven advanced oxidation processes. *Sol. Energy*, 79, 369-375.

[178] Muñoz I., Rieradevall J., Torrades F., Peral J., Domènech X. (2006). Environmental assessment of different advanced oxidation processes applied to a bleaching Kraft mill effluent. *Chemosphere*, 62, 9-16.

[179] Muñoz I., Peral J., Ayllon J.A., Malato S., Passarinho P., Domènech X. (2006). Life cycle assessment of a coupled solar photocatalytic-biological process for wastewater treatment. *Water Res.*, 40, 3533-3540.

CHAPTER 2. GOAL AND SCOPE OF THE WORK

Chapter 2

Goal and Scope of the Work

The purpose of the present work is mainly centred in the decolourisation and the mineralisation of commercial reactive azo dye solutions by combining a photo-Fenton Advanced Oxidation Process (AOP) with an aerobic biological treatment.

To better understand the complex chemical oxidative treatment, a preliminary research will be focused on the study of the most significant parameters that govern the system, i.e., initial Fenton reagent dosage, type of irradiation (darkness, artificial light and solar radiation) and temperature. With this target, Fenton and photo-Fenton processes will be applied at laboratory scale as unique treatments to carry out the complete degradation of reactive dyes. Reaction efficiencies will be evaluated in terms of decolourisation, aromatic compounds removal and mineralisation. Moreover, the acute toxicity and biodegradability evolution of dye solutions will be monitored in order to assess the viability of a sequential chemical-aerobic biological treatment.

In a second part, artificial light photo-Fenton process will be applied as a pre-treatment of a secondary aerobic biological treatment. In an exercise of optimisation, the study will aim at more efficient use of photo-Fenton conditions (i.e., minimum Fenton reagent dose and irradiation time) to generate a new solution capable to be biologically treated. Decolourisation, mineralisation, biodegradability and acute toxicity evolution will be assessed to choose the most appropriate pre-treatment conditions. The success of the chemical stage will be finally proven by feeding the generated solutions on a bench scale aerobic Sequencing Batch Reactor (SBR).

The environmental damage and/or benefit of such combined artificial light photo-Fenton-biological treatment will be evaluated and compared with single artificial light and solar driven photo-Fenton processes. The Life Cycle Assessment (LCA) tool will be applied to carry out the environmental impact evaluation. Likewise, an economic analysis of the different photo-Fenton processes will be performed and considered together with the environmental study to decide about the most suitable environmental/cost option for reactive dye removal.

The following step will be the scaling-up of laboratory experiments to pilot plant. In this way, the viability of the system will be checked in view of future real applications. Photo-Fenton oxidation will be conducted using a Compound Parabolic Collector (CPC) solar photoreactor and the biological treatment by means of an Immobilised Biomass Reactor (IBR). If applicable, the optimum conditions of the processes will be re-established. On the other hand, a mechanistic study of the degradation of a representative reactive dye by means of solar photo-Fenton process at pilot plant will be developed by means of chromatographic analyses of the different phototreated samples.

Finally, as an alternative to the chemical-aerobic biotreatment strategy, the application of an anaerobic biodegradation process as a pre-treatment of an ensuing aerobic treatment will be performed for a complete reactive dye and by-products degradation. In a second part, an AOP will follow the anaerobic process, opening the possibility of an anaerobic biological-chemical sequenced treatment for aerobically non biodegradable reactive azo dyes destruction. Ozonation and photo-Fenton AOPs will play this role.

CHAPTER 3. MATERIALS AND METHODS

Chapter 3
Materials and Methods

3.1. PREPARATION OF SYNTHETIC DYE SOLUTIONS

The reactive azo dyes used were Procion Red H-E7B (DyStar), Cibacron Red FN-R (CIBA) and a standard trichromatic system composed of Cibacron Red FN-R (CIBA), Cibacron Yellow FN-2R (CIBA), and Cibacron Navy FN-B (CIBA). The last was chosen as a model mixture of dyes that is commonly used in textile industry. All of them are commercial reactive azo dyes employed in cellulosic fibre dyeing. Their purity degree was unknown and they were used as received without further purification. Table 3.1 summarises some of their physical-chemical properties.

Procion Red H-E7B is a homo-bireactive azo dye with two monochlorotriazine reactive groups. Its chemical structure is shown in Figure 3.1. On the contrary, Cibacron Red FN-R, Cibacron Yellow FN-2R and Cibacron Navy FN-B are hetero-bireactive azo dyes of new generation whose chemical structure is not available. From such structures, only the reactive groups –the vinylsulphone and fluorotriazine groups– are known.

Table 3.1. Physical-chemical properties of studied reactive azo dyes.

Reactive dye	Colour Index	Formula	Molecular weight g·mol^{-1}	pH[a]	Solubility g·l^{-1} (30 ºC)
Procion Red H-E7B	CI Reactive Red 141	$C_{52}H_{34}O_{26}S_8Cl_2N_{14}$	1597	9.0	150[b]
Cibacron Red FN-R	CI Reactive Red 238	$C_{29}H_{15}O_{13}S_4ClFN_7Na_4$	944.2	7.0-7.5	100
Cibacron Yellow FN-2R	CI Reactive Yellow 206	-	-	7.0-7.5	100
Cibacron Navy FN-B	CI Reactive Blue 238	-	-	5.0-5.5	100

[a] 20 g·l^{-1} dye solution, except 10 g·l^{-1} Procion Red H-E7B
[b] solubility data at 20 ºC

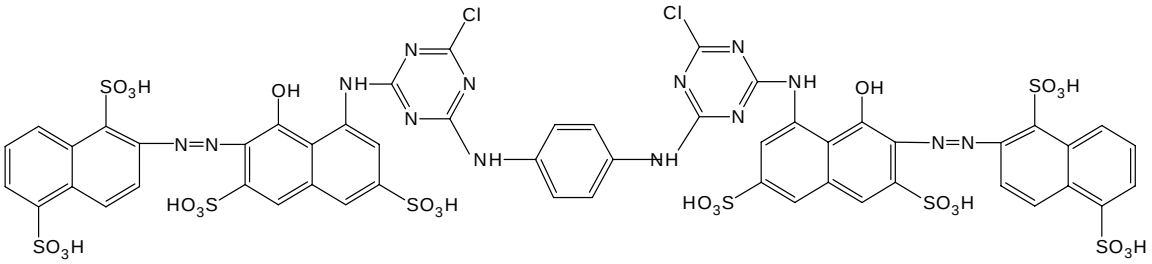

Figure 3.1. Chemical structure of Procion Red H-E7B.

Typical dye concentrations in real dyeing wastewaters were prepared to perform the experiments: solutions of 100 mg·l^{-1} of Procion Red H-E7B, 100 mg·l^{-1} of Cibacron Red FN-R, and 150.5 mg·l^{-1} of the standard trichromatic system (43.0 mg·l^{-1} of Cibacron Red FN-R, 43.0 mg·l^{-1} of Cibacron Yellow FN-2R, and 64.5 mg·l^{-1} of Cibacron Navy FN-B) were used for single Fenton and photo-Fenton processes in Sections 4.2.1 and 4.2.2 (it is worth to note that commercial dye weights included impurities, such as NaCl or Na_2SO_4). However, due to the requirements set by the detection limit of many analytical techniques, it was necessary to employ higher reactive dye concentrations when combining chemical oxidation with biological processes. Thereby, when coupling the photo-Fenton process with a subsequent aerobic biological treatment (Sections

4.2.3-4.2.5, A.1.1 and A.1.2), 250 $mg \cdot l^{-1}$ concentrations of Procion Red H-E7B and Cibacron Red FN-R were considered. For the same reason, 250, 1250 and 3135 $mg \cdot l^{-1}$ Cibacron Red FN-R concentrations were prepared for anaerobic biodegradation experiments (Section A.1.3). To simplify the matrix, only the effluent coming from dyeing process was considered. Moreover, no additives (i.e., electrolytes) were added to dye solutions.

In order to simulate real dyeing conditions, dye solutions were hydrolysed by adjusting the pH to 10.6 followed by heating to 80 ºC for 6 hours for Procion Red H-E7B, and by heating to 60 ºC for 1 hour for Cibacron Red FN-R and the standard trichromatic system (hydrolysis conditions supplied by the manufacturer). As commented in Section 1.1.2, the reactive groups of reactive dyes would have been deactivated as a result of the hydrolysis. In this way, it was expected to found a mixture of both hydrolysed and non hydrolysed forms at the end of the process.

Hydrolysed dye solutions were finally stored at 4 ºC until operation.

3.2. REAGENTS

Iron sulphate ($FeSO_4 \cdot 7H_2O$; 99.5% Merck or 98% Panreac) and hydrogen peroxide (H_2O_2; 33% w/v or 30% w/v Panreac) were used as Fenton reagent. Ozone was produced from Oxygen C-45 (99.995%, Carburos Metalicos). Reagent grade sulphuric acid and sodium hydroxide (Panreac) were used for pH adjustments. Solvents employed in chromatography were HPLC grade. All the other chemicals used throughout this study, which appear in Sections 3.3 and 3.4, were of the highest commercially available grade.

Ultra pure deionised water from a Millipore Milli-Q system (conductivity < 0.05 $\mu S \cdot cm^{-1}$, Total Organic Carbon (TOC) < 0.1 $mg \cdot l^{-1}$ C) was employed to perform all the experiments except in the case of the photo-Fenton pilot plant experiments that water was obtained from the Plataforma Solar de Almería (PSA, Spain) distillation plant (conductivity < 10 $\mu S \cdot cm^{-1}$, SO_4^{2-} = 0.5 $mg \cdot l^{-1}$, Cl^- = 0.7-0.8 $mg \cdot l^{-1}$, TOC < 0.5 $mg \cdot l^{-1}$ C).

3.3. CHEMICAL ASSAYS

3.3.1. Dissolved Organic Carbon (DOC)

The DOC is the amount of carbon in the form of CO_2 emitted when a dissolved organic substance is completely oxidised. It corresponds to the fraction of TOC that passes through a 0.45 μm pore filter [1].

Three different TOC-analyser models have been used along the present work: Shimadzu 5000, Shimadzu TOC-V_{CSH} and Shimadzu 5050A. They do not differentiate between the carbon of different compounds, but distinguish between organic and inorganic carbon. They measure the Total Carbon (TC, $mg \cdot l^{-1}$ C), the Total Inorganic Carbon (TIC, $mg \cdot l^{-1}$ C), and provide the TOC –DOC– parameter by means of TC and TIC difference.

TC measurement is based on the combustion of the aqueous sample on a platinum catalyst at 680 ºC. Thereby, all carbon is converted into CO_2 and transported by a carrier gas to a Non Dispersive Infrared Detector (NDIR). For TIC measurement, the sample is acidified with 25% (w/v) phosphoric acid. Then, carbonate and hydrogencarbonate are liberated as CO_2 and stripped from the solution by the carrier gas to the NDIR.

A linear relationship between the detector signal and the carbon concentration allows TC and TIC quantification with, respectively, potassium phthalate and sodium carbonate and hydrogencarbonate standards. Prior analysis, samples were filtered through 0.45 μm pore size (Scheleicher & Schuell, FP 30/0.45 CA-S) and quantified by duplicated.

3.3.2. Chemical Oxygen Demand (COD)

The COD is the indirect measurement of the oxygen needed for the complete oxidation of all the compounds present in solution –organic or inorganic–. It is an indirect measurement because the oxidation is carried out by a strong oxidising agent, in

this case potassium dichromate. It is usually taken as an estimation of the organic matter content in solution, in spite of the possible interference of non organic reduced species contained in the sample (Cl^-, Fe^{2+}, NO_2^-, sulphurs, etc.). For this reason, DOC is a more accurate parameter than COD for organic matter determination in water.

The analysis was assessed with Aqualytic® (0-150 and 0-1500 $mg \cdot l^{-1}$ O_2 range, Vario) or Spectroquant® (10-150 $mg \cdot l^{-1}$ O_2 range, Merck) kits by the closed reflux colorimetric method [2]. Such commercial COD kits contain suitable amounts of $K_2Cr_2O_7$, H_2SO_4, Ag_2SO_4 and $HgSO_4$ reagents. In acidic media, the sample was digested (COD reactor, HACH) with an excess of oxidant at 150 ºC for a period of 2 hours, giving place to the Cr^{3+} ion formation (visible yellow-orange to green colour change) (Equation 3.1). Ag_2SO_4 was added as catalyst for the oxidation of certain organic compounds and $HgSO_4$ to avoid any possible chloride interference by insoluble mercury chloride precipitation ($HgCl_2$).

$$Cr_2O_7^{2-} + 14\ H^+ + 6\ e^- \rightarrow 2\ Cr^{3+} + 7\ H_2O \qquad (3.1)$$

A HACH spectrophotometer detected the colour changes at 420 nm wavelength, directly providing COD data in terms of $mg \cdot l^{-1}$ O_2. Analyses were done by triplicated to check for repeatability and a potassium phthalate standard solution was analysed in parallel as a control sample.

3.3.3. Colour and aromatic content analysis by UV/Vis spectrophotometry

The UV/Vis-absorption spectra of reactive dye solutions were recorded in the 200-700 nm range by using a Shimadzu UV-1603 double beam spectrophotometer and 10 mm light path quartz cells.

Colour data were reported as the absorbance at the maximum absorption in the visible region (λ_{max} = 543.5 nm for Procion Red H-E7B, λ_{max} = 542.5 nm for Cibacron Red FN-R, and λ_{max} = 553.0-587.5 nm for the standard trichromatic system) and were taken as an estimation of reactive dyes presence in solution. On the other hand, the

absorbance at 254.0 nm wavelength (UV_{254}) was taken as the reference parameter to monitor the aromatic compounds content in solution [3].

Prior measurements, samples were filtered (0.45 μm pore size) and diluted if necessary.

3.3.4. Hydrogen peroxide analysis by iodometric titration

Hydrogen peroxide concentration was determined by the iodide titration method [4]. An excess of iodide (10 ml of 1 $mol \cdot l^{-1}$ KI) was added to 10 ml of the test sample in acidic solution (10 ml of 2 $mol \cdot l^{-1}$ H_2SO_4) with 2 ml of ammonium molibdate (50 $g \cdot l^{-1}$) as catalyst. The solution was left around 5 minutes at room temperature and protected from light in a closed bottle. Then, hydrogen peroxide reacted quantitatively with the iodide to generate the triiodide anion I_3^- ($I_2 + I^-$, dark yellow) (Equation 3.2), which was reduced again with sodium thiosulphate by titration (0.05 $mol \cdot l^{-1}$ $Na_2S_2O_3 \cdot 5H_2O$, previously standardised by potassium dichromate) (Equation 3.3). 1 $g \cdot l^{-1}$ starch was the indicator of the titration since it forms a dark blue-grey complex with the triiodide ion. At the end point, the reduction of triiodide ion turned transparent the solution.

$$H_2O_2 + 3\ I^- + 2\ H^+ \rightarrow I_3^- + 2\ H_2O \qquad (3.2)$$

$$I_3^- + 2\ S_2O_3^{2-} \rightarrow 3\ I^- + S_4O_6^{2-} \qquad (3.3)$$

According to the above reactions stoichiometry, hydrogen peroxide concentration ($C_{H_2O_2}$, $mg \cdot l^{-1}$) was calculated as shown in Equation 3.4:

$$C_{H_2O_2} = \frac{V_{S_2O_3^{2-}} \cdot C_{S_2O_3^{2-}} \cdot MW_{H_2O_2}}{2 \cdot V_{sample}} \cdot 1000 \qquad (3.4)$$

where $V_{S_2O_3^{2-}}$ is the volume of thiosulphate consumed by titration (ml), $C_{S_2O_3^{2-}}$ is the thiosulphate concentration ($mol \cdot l^{-1}$), V_{sample} is the volume of the test sample (ml) and $MW_{H_2O_2}$ is the hydrogen peroxide molecular weight. Each measurement was done by triplicated.

3.3.5. Dissolved iron analysis (Fe (II) and total iron) by colorimetry

Dissolved ferrous ion forms an orange-red chelate complex with three molecules of 1,10-phenantroline, which can be followed by colorimetry (Equation 3.5) [5]:

$$Fe^{2+} + 3\ PhH^{+} \leftrightarrows [Fe\ (Ph)_3]^{2+} + 3\ H^{+} \qquad (3.5)$$

To quantify it, 4 ml of filtered test sample (0.22 μm pore size, Millipore Millex® GN) were mixed with 1 ml of 1,10-phenantroline solution (0.1% w/v) and 1 ml of buffer solution (250 $g \cdot l^{-1}$ ammonium acetate and 700 $ml \cdot l^{-1}$ acetic acid). Such buffered conditions maintained the pH assay between 3.0 and 3.5, which ensured a rapid and quantitative development of the colour. After 1 minute, the absorbance of the solution was determined at λ = 510 nm by a Unicam-2 UV/Vis double beam Spectrometer and 10 mm light path quartz cells. To avoid possible interferences caused by the colour of the solutions, absorbance was measured against a blank solution prepared in the same way, but replacing the 1,10-phenantroline solution with deionised water.

For total dissolved iron measurement (Fe (II) and Fe (III)), a spatula tip of ascorbic acid was added to the sample. In this way, Fe (III) was reduced to its ferrous form and measured as described above.

Quantification was performed with a $FeSO_4 \cdot 7H_2O$ calibration curve, according to Lambert-Beer law (Equation 3.6):

$$Abs = \varepsilon \cdot b \cdot C \quad (3.6)$$

where Abs is the absorbance, ε is the molar extinction coefficient ($l \cdot mol^{-1} \cdot mm^{-1}$), b is the light path of the cell (mm) and C is the concentration of the compound to be measured ($mol \cdot l^{-1}$).

3.3.6. High Performance Liquid Chromatography (HPLC)

Procion Red H-E7B and Cibacron Red FN-R reactive dyes concentrations were analysed using reverse-phase liquid chromatography (flow rate 0.5 $ml \cdot min^{-1}$, injection volume 20 µl) with UV/Vis detector in a HPLC (Agilent, Series 1100) with C-18 column (Phenomenex LUNA 5 µm, 3 mm x 150 mm) at 543 nm wavelength. The column temperature was 25 °C. The mobile phases were 5 $mmol \cdot l^{-1}$ ammonium acetate (A) and methanol (B). A 15 minutes gradient elution was used from 0% to 100% B for Procion Red H-E7B and from 0% to 50% B for Cibacron Red FN-R.

Prior analysis, samples were filtered through 0.22 µm pore size and diluted 1:1 with methanol.

3.3.7. Liquid Chromatography-(Electrospray Ionisation)-Time-of-Flight Mass Spectrometry (LC-(ESI)-TOF-MS)

Procion Red H-E7B reactive dye by-products generated through photo-Fenton process were identified using LC-(ESI)-TOF-MS with positive ionisation. Separation was made using reverse-phase liquid chromatography (flow rate 0.5 $ml \cdot min^{-1}$, injection volume 20 µl) in a HPLC (Agilent, Series 1100) equipped with a 150 mm x 4.6 mm C-18 analytical column and 5 µm particle size (Zorbax Eclipse XDB-C-18). The column temperature was 25 °C. The mobile phases were 0.1% (w/v) formic acid in water (A) and acetonitrile (B). A linear gradient progressed from 5% B to 100% B in 30 minutes, and it was maintained at 100% B for 5 minutes. The HPLC system was connected to an Agilent MSD Time-of-Flight Mass Spectrometer (TOF-MS) with an Electrospray

Ionisation (ESI) interface. The accurate mass spectra were recorded from 50 to 1000 m/z (mass to charge ratio). The data recorded were processed with Applied Biosystems/MDS-SCIEX Analyst QS software (Frankfurt, Germany) with application-specific accurate mass additions provided by the Agilent MSD TOF software. The mass axis was calibrated by using the mixture provided by the manufacturer in the 50-3200 m/z range. A second orthogonal sprayer was used with a reference solution as a continuous calibration using the following reference masses: 121.0509 and 922.0098 m/z (resolution 9500 ± 500 @ 922.0098 m/z).

As a pre-treatment, 20 ml of collected samples were filtered through OASIS® HLB (hydrophilic/lipophilic balance) 6 cc (200 mg) solid-phase extraction cartridges, previously conditioned with 2 ml of methanol and 2 ml of water. Then, retained samples were washed with 4 + 4 ml of deionised water and eluted later with 2 + 2 ml of methanol. Finally, extractions were diluted 1:1 with deionised water.

3.3.8. Ion Chromatography (IC)

Ions and aliphatic carboxylic acids content in aqueous solution was determined by IC. Ammonium ion was determined with a Dionex DX-120 ion chromatograph equipped with a Dionex Ionpac CS12A 4 mm x 250 mm column. Elution was done in isocratic mode with 10 $mmol \cdot l^{-1}$ H_2SO_4 mobile phase at 1.2 $ml \cdot min^{-1}$ flow rate. On the other hand, sulphate, chloride, nitrite, nitrate and carboxylic acids concentrations (in their anionic form) were measured with a Dionex DX-600 ion chromatograph using a Dionex Ionpac AS11-HC 4 mm x 250 mm column. The elution gradient programme for anions quantification was pre-run 5 minutes with 20 $mmol \cdot l^{-1}$ NaOH, followed by an injection with 20 $mmol \cdot l^{-1}$ NaOH for 8 minutes and with 35 $mmol \cdot l^{-1}$ NaOH for 7 minutes. The flow rate was 1.5 $ml \cdot min^{-1}$. The gradient programme for carboxylate anions analysis consisted of a 10-minutes pre-run with 1 $mmol \cdot l^{-1}$ NaOH, 10 minutes with 15 $mmol \cdot l^{-1}$ NaOH, 10 minutes with 30 $mmol \cdot l^{-1}$ NaOH and 10 minutes with 60 $mmol \cdot l^{-1}$ NaOH. The flow rate was also 1.5 $ml \cdot min^{-1}$.

Samples were filtered through 0.22 μm pore size. Quantitative detection was accomplished with calibrated curves of the following standards: K_2SO_4, $NaNO_3$,

$NaNO_2$, NH_4Cl, and the corresponding sodium salt of formic, acetic, oxalic, pyruvic, and maleic carboxylic acids.

3.3.9. Ammonium analysis by Nessler reagent

Ammonium ion was also spectrophotometrically determined by Nessler colorimetric assay [6]. Nessler reagent (K_2HgI_4) was prepared from 5 g KI, 2.2 g $HgCl_2$ and 4 g NaOH in 100 ml of deionised water. To perform the analysis, 5 ml of filtered test sample (0.45 μm pore size) were mixed with 2 ml of Nessler reagent. After 10 minutes, the yellow complex formed (Equation 3.7) was measured at λ = 425 nm by a Shimadzu UV-1603 double beam spectrophotometer and 10 mm light path quartz cells.

$$NH_4^+ + 2\ [HgI_4]^{2-} + 4OH^- \rightarrow HgO{\cdot}Hg(NH_2)I + 7I^- + 3H_2O \qquad (3.7)$$

Dissolved Fe (II) may interfere in ammonium quantification. When applicable, it was removed by precipitation with sodium hydroxide prior the measurement. The calibration curves were constructed by means of standard NH_4Cl solutions, following Lambert-Beer law (Equation 3.6). Every measurement was duplicated.

3.3.10. Methane analysis by Gas Chromatography (GC)

The methane composition of biogas generated during anaerobic biodegradation assays was determined by using a HP 5890 GC equipped with a thermal conductivity detector and a Porapak Q, 3 m x 1/8" column (Supelco). The temperature of the injector was 130 ºC. A gradient of oven temperature was programmed as follows. It was initially maintained at 30 ºC for 3 minutes. Then, it was increased to 70 ºC at a 10 ºC·min^{-1} rate and finally maintained at 70 ºC for 5 minutes. The temperature of the detector was 180 ºC.

Quantification was carried out by means of a methane gas calibration curve.

3.3.11. Ozone flow analysis by iodometric titration

The quantity of ozone contained in the gas feeding the ozonation reactor was determined by iodometry [7]. The gas was bubbled during a contact time of 2 minutes through a 100 ml solution of an excess of potassium iodide (0.120 $mol \cdot l^{-1}$ KI) buffered with 0.041 $mol \cdot l^{-1}$ Na_2HPO_4 and 0.026 $mol \cdot l^{-1}$ $NaH_2PO_4 \cdot 2H_2O$. Analogously to H_2O_2 determination (Section 3.3.4), triiodide ion was formed by ozone reduction (Equation 3.8). Afterwards, the solution was acidified with 5 ml of 4.5 $mol \cdot l^{-1}$ H_2SO_4 and titrated by standardised sodium thiosulphate (0.05 $mol \cdot l^{-1}$ $Na_2S_2O_3 \cdot 5H_2O$) (see Equation 3.3). The indicator of the titration was a 1 $g \cdot l^{-1}$ starch solution.

$$O_3 + 2\ H^+ + 3\ I^- \rightarrow I_3^- + O_2 + H_2O \qquad (3.8)$$

Ozone flow (O_3, $mg \cdot min^{-1}$) was obtained stoichiometrically as shown in Equation 3.9:

$$O_3 = \frac{V_{S_2O_3^{2-}} \cdot C_{S_2O_3^{2-}} \cdot MW_{O_3}}{2 \cdot t_c} \qquad (3.9)$$

where $V_{S_2O_3^{2-}}$ is the volume of thiosulphate consumed by titration (ml), $C_{S_2O_3^{2-}}$ is the thiosulphate concentration ($mol \cdot l^{-1}$), MW_{O_3} is the ozone molecular weight and t_c is the contact time (minutes). Each measurement was done by triplicated.

3.3.12. Total and Volatile Suspended Solids (TSS, VSS)

Biomass population involved in biological processes was determined gravimetrically by means of TSS and VSS measurements [8, 9].

A well mixed sample volume was filtered through a pre-weighed glass-microfibre filter (ALBET, FV-C). Afterwards, the residue retained on the filter was dried at 103-105 ºC to a constant weight. The mass increase corresponded to the TSS, which

included all particles suspended in water that did not pass through the filter (Equation 3.10):

$$TSS = \frac{(A - B) \cdot 1000}{V_{sample}} \quad (3.10)$$

where A is the weight of the filter plus the dried residue and B is the weight of the filter, both in g units. The sample volume was in ml. TSS are given in $g \cdot l^{-1}$.

The residue from the previous test was then ignited at 550 ºC to constant weight for 15 minutes in a muffle furnace. The weight lost on combustion was the VSS (Equation 3.11), and included the non dissolved organic content of the sample:

$$VSS = \frac{(A - C) \cdot 1000}{V_{sample}} \quad (3.11)$$

where A is the weight of the filter plus the weight of residue before ignition and C is the weight of the residue plus the filter after ignition, both in g units. The sample volume was in ml. VSS are given in $g \cdot l^{-1}$.

The remained solid ash, of inorganic nature, corresponded to the Fixed Total Solids (FTS, $g \cdot l^{-1}$).

3.4. BIOLOGICAL ASSAYS

3.4.1. Zahn-Wellens biodegradability test

Indicated to determine the inherent aerobic biodegradability of organic substances in water, the Zahn-Wellens assay simulates conditions close to those of a municipal Wastewater Treatment Plant (WWTP) [10].

To perform the test, non acclimated activated sludge coming from a WWTP (Manresa, Spain) was aerated for a 24-hours period, washed repeatedly and centrifuged subsequently. Activated sludge was then suspended (TSS = 0.2-0.3 $g \cdot l^{-1}$) together with 2 l of test sample at neutral pH (the ratio between the carbon content of test sample and the dry-weight of inoculum should range from 1 to 4). Moreover, 2.5 ml of mineral medium (a concentrated solution composed of 38.5 $g \cdot l^{-1}$ NH_4Cl, 33.4 $g \cdot l^{-1}$ $NaH_2PO_4 \cdot 2H_2O$, 8.5 $g \cdot l^{-1}$ KH_2PO_4 and 21.75 $g \cdot l^{-1}$ K_2HPO_4) were also added to the media per litter of sample.

The mixture was maintained for 28 days at 22 ± 3 ºC under aeration (Dissolved Oxygen (DO) not lower than 3 $mg \cdot l^{-1}$ O_2), agitation and dark conditions. A blank assay just containing activated sludge and mineral medium, as well as a control experiment fed with a fully biodegradable standard (i.e., ethylene glycol), were run in parallel.

DOC was analysed at regular intervals and pH was readjusted between 7.0 and 8.0 if necessary. To discard loses by a possible sample adsorption onto the activated sludge, DOC was measured three hours after the beginning of the test. This one was taken as the initial value. The DOC reduction, expressed in percentage, corresponded to the % biodegradation evolution of the sample (Equation 3.12):

$$\%\ \text{Biodegradation} = \left[1 - \frac{DOC - DOC_B}{DOC_0 - DOC_{0,B}}\right] \cdot 100 \qquad (3.12)$$

where DOC is the test sample value at time of sampling, DOC_B is the blank experiment value at time of sampling, DOC_0 is the initial value of the test sample, and $DOC_{0,B}$ is the initial value of the blank.

The criteria used to consider a sample biodegradable involves the removal of 70% of the original DOC.

3.4.2. Biochemical Oxygen Demand for 5 days (BOD_5)

Indicator of the auto-purifying capacity of a wastewater, the Biochemical Oxygen Demand (BOD, $mg \cdot l^{-1}$ O_2) is a measurement of the amount of organic matter potentially biodegradable under aerobic conditions. It is one of the most widely employed parameters for the characterisation of organic pollutants in water. Concretely, the BOD_5 is based on the quantification of the oxygen consumed by a sample incubated with non acclimated aerobic microorganisms at 20 ºC for a period of 5 days. It supposes, at maximum, around 80% of the COD. Hence, to complete the biological oxidation at 20 ºC, a period of time between 21 and 28 days would be required.

The BOD_5 measurement was performed by means of a mercury-free WTW 2000 OxyTop® thermostated at 20 ± 1 ºC, which allows the BOD determination among the 0-4000 $mg \cdot l^{-1}$ O_2 range without sample dilution. The assay principle is as follows: in a closed bottle, during the oxidative degradation of organic matter, aerobic microorganisms consume dissolved oxygen gas in water. By stirring, such consumed oxygen is supplied from the bottle headspace to solution. Since the experiment is conducted at constant volume, the depletion of oxygen gas at headspace leads to a difference of pressure. Therefore, a manometer collects the data and express them directly in $mg \cdot l^{-1}$ O_2 units. To avoid interferences over the pressure lectures, carbon dioxide produced is removed with a NaOH trap (Equation 3.13).

$$2\ NaOH + CO_2 \rightarrow Na_2CO_3 + H_2O \qquad (3.13)$$

The test sample volume differs depending on the expected BOD value. Table 3.2 shows the relation between BOD and volume. In each case, the BOD lecture should be multiplied by a different factor.

As a pre-treatment, samples were adjusted to pH = 6.5-7.5 and saturated of oxygen by aeration for 2 hours. Sample containing bottles were then inoculated by adding 2 ml of the supernatant solution of a WWTP activated sludge, previously aerated for 24 hours. The required mineral medium was also supplied by adding 250 µl of buffer solution (8.5 $g \cdot l^{-1}$ $Na_2HPO_4 \cdot 2H_2O$, 2.8 $g \cdot l^{-1}$ KH_2PO_4) and 50 µl of Mg^{2+}, Ca^{2+}, Fe^{3+} and

NH_4^+ concentrated solutions (22.5 $g \cdot l^{-1}$ $MgSO_4 \cdot 7\ H_2O$; 27.5 $g \cdot l^{-1}$ $CaCl_2$; 0.25 $g \cdot l^{-1}$ $FeCl_3 \cdot 6H_2O$ and 2 $g \cdot l^{-1}$ NH_4Cl) per 100 ml of test sample [11]. Finally, any possible oxygen consumption due to nitrification was inhibited by adding 10 mg N-allylthiourea per litter of test sample.

Table 3.2. Ranges and the correlated total volume of sample.

Sample volume ml	Measuring range $mg \cdot l^{-1}$ O_2	Factor
432	0-40	1
365	0-80	2
250	0-200	5
164	0-400	10
97	0-800	20
43.5	0-2000	50
22.7	0-4000	100

The correct performance of each determination was verified with an organic standard of know BOD_5, composed of glucose and glutamic acid. Moreover, a blank experiment just containing the inoculum and mineral medium was run in parallel. The BOD_5 of the test sample was corrected by subtracting the blank lecture. To check repeatability, every assay was performed by triplicated.

3.4.3. Acute toxicity

The acute toxicity analysis determines what concentration of sample leads to the inhibition of the development or to the mortality of a group of organisms exposed to the toxicant for a short period of time, under controlled conditions [12].

At the present work, acute toxicity was assessed according to the Biotox® bacterial bioluminescence assay procedure [13], by determination of the inhibitory effect that the test sample has on the marine photobacteria *Vibrio fischeri.* It was quantified as the median effective concentration (EC_{50} parameter), which is the concentration of sample

that causes 50% decrease of light emission in relation to a 2% (w/v) sodium chloride control sample solution.

To perform every toxicity measurement, a graph is plotted by means of successive dilutions of the original test sample (containing a constant bacteria population). It displays the relationship between each concentration and their corresponding inhibition percentage after 30 minutes of exposure at 15 ºC (calculated according to Equations 3.14 and 3.15):

$$\%INH = 100 - \frac{IT_{30}}{KF \cdot IT_0} \cdot 100 \tag{3.14}$$

$$KF = \frac{IC_{30}}{IC_0} \tag{3.15}$$

where %INH is the percentage of inhibition caused by the test sample, IT_{30} is the luminescent intensity of the test sample after 30 minutes of exposure, IT_0 is the initial luminescent intensity of the test sample, KF is a correction factor, IC_{30} is the luminescent intensity of the control sample after 30 minutes of exposure and IC_0 is the initial luminescent intensity of the control sample.

The EC_{50} parameter was determined in DOC units ($mg \cdot l^{-1}$ C) by %INH = 50 interpolation, and using a standard lineal regression analysis (whether the range of pair values could not be linearised, EC_{50} could be determined using a double logarithmic system). When the DOC of the sample was lower than the EC_{50}, it was assumed to be non toxic and toxicity values were given as $EC_{50} > 100\%$.

It is remarkable that toxicity determinations may be distorted due to the partial absorption of emitted bioluminescence by coloured samples. In the present case, for every obtained intensity value, a correction factor corresponding to the intensity lost due to absorption (not to inhibition) previously calculated for every test sample concentration was applied.

As a pre-treatment, according to Biotox® test procedure, the pH of the sample (filtered through 0.45 μm membrane) was adjusted to 7.0 ± 0.2 and solid NaCl was

added to adjust salinity to 2% (w/v). Phenol and glucose solutions were used as standard toxic and non toxic samples to check the technique suitability. Every plot for EC_{50} determination was replicated twice.

3.4.4. Short-term respirometry

Short-term respirometric measurement provides information about the ready biodegradability of a sample in contact with non acclimated aerobic biomass. It is based on the measurement of the biological oxygen consumption rate –namely Oxygen Uptake Rate (OUR, $g \cdot l^{-1} \cdot min^{-1}$ O_2)– under controlled conditions [14].

The experimental set-up was composed of a closed and thermostatic liquid-static-static (LSS) respirometer (T = 25 ± 1 ºC) of 250 ml of capacity, connected to a DO-meter (Model 407510, EXTECH), an air diffuser and a mechanical stirrer (Figure 3.2). In this type of reactor, the oxygen measurement was performed in the liquid phase by keeping under static conditions both liquid and gas phases. Non acclimated activated sludge coming from a municipal WWTP (Manresa, Spain) was used as inoculum. It was aerated for a 24-hours period and subsequently diluted to 3-4 $g \cdot l^{-1}$ VSS concentration with deionised water. 10 mg N-allylthiourea per litter of sample was added for nitrification inhibition. The detailed operational strategy was as follows:

(i) A 250 ml initial solution just containing the aerobic biomass in water was aerated until a DO value around 6 $mg \cdot l^{-1}$ O_2. Afterwards, the air supply was removed and the oxygen depletion (until a final DO value not lower than 2 $mg \cdot l^{-1}$ O_2) was continuously monitored by means of the oxygen-meter. From DO evolution with time, the specific Oxygen Uptake Rate (sOUR, g $O_2 \cdot g^{-1}$ $VSS \cdot min^{-1}$) corresponding to the endogenous respiration of biomass was calculated (i.e., the oxygen consumption resulting from the respiration activity of an inoculum without any addition of a biodegradable carbon source (see Section 1.3.2)).

(ii) Biomass was settled for 1 hour. Then, 125 ml of solution were replaced by the same volume of a completely biodegradable standard solution of acetic acid, previously adjusted to neutral pH. Such standard solution was prepared to provide the same COD

than the sample to be tested. Analogously to step (i), and after the aeration of the solution, the oxygen consumption with time was monitored and finally quantified as sOUR parameter. The obtained value was corrected by subtracting the endogenous sOUR contribution. Finally, aeration and oxygen depletion processes were repeated as many times as necessary to obtain the same initial endogenous sOUR profile, providing evidence of fully acetic acid biodegradation.

(iii) The sOUR of the test sample was determined analogously to step (ii) procedure.

(iv) Biomass was fed again with a second acetic acid standard addition to check a possible respiration inhibition caused by the sample. In absence of biomass inhibition, the sOUR of both standard solutions should coincide.

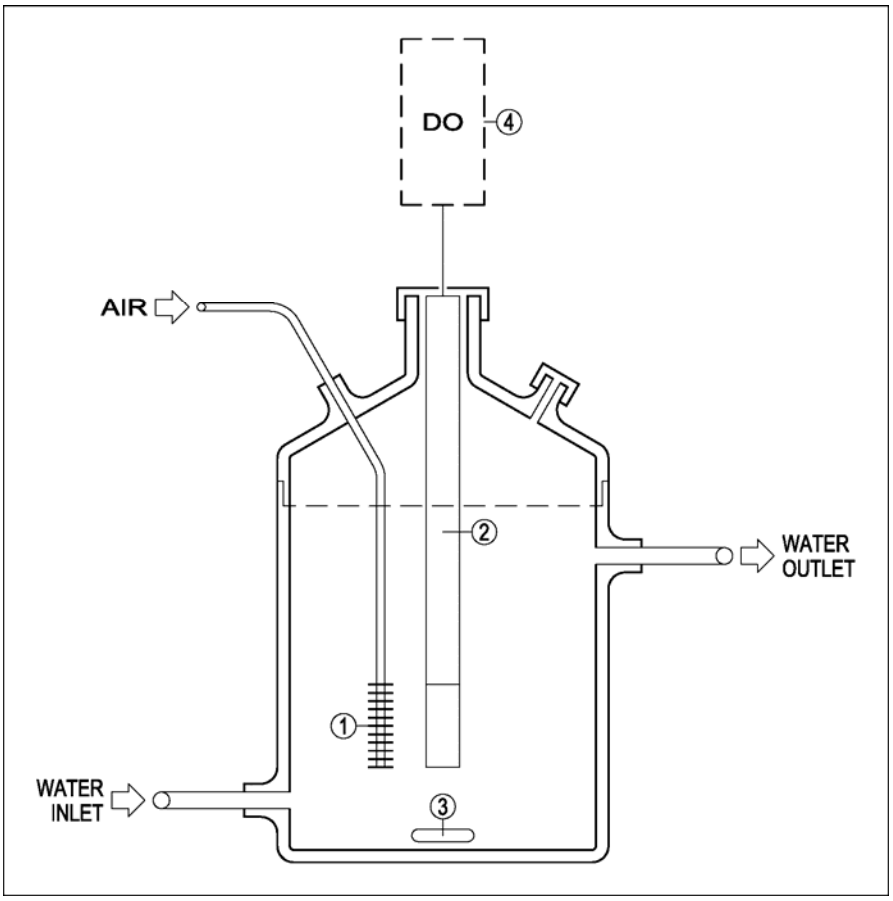

Figure 3.2. Respirometrer set-up. *1-air diffuser; 2-DO probe; 3-magnetic bar; 4- DO-meter.*

When assessing the respirometric response of aerobic biomass against a complex sample (composed of several organic compounds with different biodegradation easiness), different sOUR profiles may be observed. Therefore, to better quantify the overall behaviour of the test sample, a global parameter named accumulated Oxygen Demand (OD, g $O_2 \cdot g^{-1}$ VSS) was determined at the present work. It was calculated as the sum of the different sOUR observed multiplied by their corresponding duration times. The overall contact time with biomass was set to 30 or 120 minutes, depending on the biomass response.

Finally, the ready biodegradability of the test sample was given as the quotient between its accumulated OD and the acetic acid standard value (OD_{st}).

3.4.5. Anaerobic digestion assay

The anaerobic digestion assay provides information about the potential of a substrate to be biodegraded in a free-oxygen atmosphere. As a result of the reductive process, the complete substrate biodegradation would lead to the generation of biogas that may be followed manometrically at constant volume.

At the present work, anaerobic biodegradation was conducted in batch mode and under static conditions in closed thermostated aluminium bottles of 600 ml of capacity. The test sample volume was 500 ml and the headspace was 100 ml. The anaerobic seed sludge was a methanogenic culture obtained from a mesophilic municipal anaerobic digester (WWTP in Manresa, Spain) containing an initial TSS and VSS content of 30 and 12 $g \cdot l^{-1}$, respectively. All bottles were seeded with the same volume of original sludge to finally obtain an initial 1.5 $g \cdot l^{-1}$ VSS and 3.8 $g \cdot l^{-1}$ TSS concentration.

0.2 g of yeast extract and 2 ml of the following essential nutrients and trace elements solutions were added per litter of sample [15]: 100 $mg \cdot l^{-1}$ $Na_2S \cdot 9H_2O$ solution; a macronutrients solution composed of 170 $g \cdot l^{-1}$ NH_4Cl, 37 $g \cdot l^{-1}$ KH_2PO_4, 8 $g \cdot l^{-1}$ $CaCl_2 \cdot 2H_2O$ and 9 $g \cdot l^{-1}$ $MgSO_4 \cdot 4H_2O$; a micronutrients solution composed of 2000 $mg \cdot l^{-1}$ $FeCl_3 \cdot 4H_2O$, 2000 $mg \cdot l^{-1}$ $CoCl_2 \cdot 6H_2O$, 500 $mg \cdot l^{-1}$ $MnCl_2 \cdot 4H_2O$, 30 $mg \cdot l^{-1}$ $CuCl_2 \cdot 2H_2O$, 50 $mg \cdot l^{-1}$ $ZnCl_2$, 50 $mg \cdot l^{-1}$ H_3BO_3, 90 $mg \cdot l^{-1}$ $(NH_4)_6Mo_7O_{24} \cdot 4H_2O$, 100 $mg \cdot l^{-1}$

$Na_2SeO_3 \cdot 5H_2O$, 50 $mg \cdot l^{-1}$ $NiCl_2 \cdot 6H_2O$, 1000 $mg \cdot l^{-1}$ EDTA, 1$ml \cdot l^{-1}$ HCl 36% and 500 $mg \cdot l^{-1}$ resazurin. Additionally, 1g of $NaHCO_3$ per g of COD was added to the solution in order to maintain the pH and reduce the negative effects to methanogenesis due to the possible acidification caused by Volatile Fatty Acids (VFA) generation through the process. The pH was adjusted to 7.0 ± 0.2.

Before incubation, nitrogen gas was bubbled into the bottles to ensure anoxic conditions during biodegradation process. Temperature was maintained under mesophilic conditions at 37 ± 1 ºC. A VFA standard solution composed of acetic, propionic and butyric acids (73:21:4 weight proportion, total COD = 4500 $mg \cdot l^{-1}$ O_2 [15]), as well as a control experiment just containing anaerobic biomass, nutrients and trace elements were run in parallel. Each batch experiment was extended to 50 days.

The methanogenic activity of the anaerobic sludge was ensured by the assessment of the Specific Methanogenic Activity (SMA, $gCOD_{CH4} \cdot g^{-1}VSS \cdot day^{-1}$) of the VFA standard solution [15]. On the other hand, the parameters employed to evaluate the biodegradation of the test samples were the accumulated biogas production within the 50 days of assay (1 atm, 37 ºC), the maximum methane generation slope per unit of weight of biomass ($gCOD_{CH4} \cdot g^{-1}VSS \cdot day^{-1}$) (determined in the same way than SMA, see below), the degree of decolourisation (calculated as the absorbance at maximum wavelength in the visible region), the DOC reduction and the acute toxicity of the resultant solution (EC_{50}) after the 50 days of digestion.

Biogas production was measured at regular intervals from bottles headspace by means of a digital manometer (SMC Pressure Switch 10 bars) connected to the bottles by a valve. Biogas was sampled through an outlet located at the valve that could be opened or closed with a regulator key. The % methane composition was determined by GC (Section 3.3.10). Finally, the SMA was calculated as shown in Equation 3.16:

$$SMA = \frac{ml\,CH_4 \cdot day^{-1}}{CF \cdot VSS \cdot V_{sample}} \qquad (3.16)$$

where ml $CH_4 \cdot day^{-1}$ is the methane production rate calculated from the maximum biogas generation slope (the obtained value was corrected by subtracting the ml $CH_4 \cdot day^{-1}$ blank contribution), VSS are the initial 1.5 $g \cdot l^{-1}$ VSS concentration, sample volume are the 0.5 l of liquid volume and CF is a correction factor that allows the conversion between the methane volume and the COD. At 37 ºC and 1 atm conditions, the CF factor is 398 ml $CH_4 \cdot g^{-1}$ COD [15].

When testing the EC_{50} parameter, solutions were previously gassed with nitrogen to strip out any possible remaining H_2S gas generated through digestion. Every assay was performed at least twice.

3.5. ANAEROBIC SLUDGE ADSORPTION EXPERIMENT

Reactive dye adsorption onto anaerobic sludge experiments were conducted in 100 ml closed thermostated flasks at 37 ± 1 ºC. As in anaerobic digestion assay (Section 3.4.5), anaerobic sludge from the mesophilic municipal anaerobic digester (WWTP in Manresa, Spain) was used. Each flask contained 30 ml of reactive dye solution with 85, 250, 425, 850, 1275, 1700, 2550 and 3000 $mg \cdot l^{-1}$ concentrations, as well as anaerobic sludge at 1.5 $g \cdot l^{-1}$ VSS and 3.8 $g \cdot l^{-1}$ TSS constant values. Neither nutrients nor trace elements were added into the media. All samples were adjusted to pH = 7.0 ± 0.2. To ensure equilibrium conditions, the contact time was set at 24 hours. A control flask with anaerobic biomass suspended in deionised water was conducted in parallel. Hand shaking was occasionally conducted. Every concentration was performed by duplicated.

DOC and colour data (the maximum absorbance in the visible region at pH = 7.0) were used as dye adsorption indicators. The initial values were taken just after the preparation of the mixture and the final values 24 hours later. To perform each analysis, a well mixed volume was sampled, and the supernatant centrifuged subsequently. Both initial and final values were compared with those obtained from the control sample in order to evaluate the adsorption phenomenon.

3.6. REACTORS AND EXPERIMENTAL PROCEDURES

3.6.1. Fenton and photo-Fenton reactors

3.6.1.1. Cylindrical batch reactors

Fenton type processes performed at laboratory scale were conducted in batch mode in two different thermostatic cylindrical Pyrex cells. Initial experiments described in Sections 4.2.1 and 4.2.2 were carried out in a 130 ml cell with 28.27 cm^2 of surface. The solution volume was 100 ml. On the contrary, the rest of the bench scale experiments were conducted in a 300 ml cell with 78.54 cm^2 of surface. In this case, the solution volume was 250 ml (Sections 4.2.3 to 4.2.5) or 200 ml (Section A.1.3).

The reaction mixture inside the cells, consisting of the sample solution and the required amount of Fenton reagent, was continuously stirred with a magnetic bar. Moreover, reactors were surrounded by a water jacket that allowed the control of the reactor temperature within ± 1 ºC. A diagram of these reactors is shown in Figure 3.3.

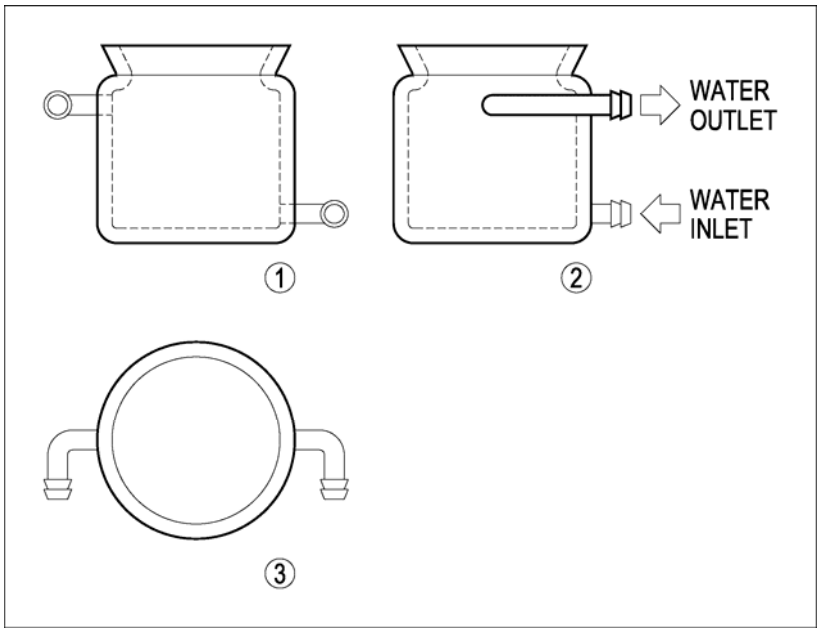

Figure 3.3. Cylindrical batch reactor. *1-front view; 2-side view; 3-upper view.*

Fenton processes were carried out in darkness. In contrast, photo-Fenton processes were performed under either artificial or solar irradiation (see irradiation sources details in Section 3.7). A 6 W Philips black light fluorescent lamp, placed over the cells, was used in artificial light photo-Fenton experiments. The distance between the lamp and the solution was 17.0 cm for the 130 ml and 7.5 cm for the 300 ml cell. The intensity of the incident light, measured by a UV light meter (Lutron UVA-365, band pass: 320-390 nm), was 0.13 and 0.60 $mW \cdot cm^{-2}$, respectively. On the other hand, solar driven photo-Fenton experiments were performed outdoors during sunny days of July at the Universitat Autònoma de Barcelona (UAB) (latitude 41º 30' N, longitude 2º 6' E). Since solar experiments were not termically controlled, temperature reached around 40 ºC at the end of the process.

To perform the experiments, the solutions were adjusted to pH = 2.8-3.0. Next, the necessary amount of iron salt was added. After its complete homogenisation, a unique pulse of the required hydrogen peroxide was added to begin the process. In artificial light photo-Fenton reaction, hydrogen peroxide addition was accomplished with the black light stabilised and experiments were carried out under continuous irradiation. Neither pH adjustments nor Fenton reagent additions were done after the beginning of the processes.

Samples were collected at regular time intervals and analysed as soon as possible. Analyses performed included DOC, COD, colour, UV_{254}, H_2O_2 concentration, NH_4^+ concentration, sOUR, BOD_5 and EC_{50}. Previous to sOUR, BOD_5 and EC_{50} biological assays, and due to the bactericide character of hydrogen peroxide, its removal from aqueous solution was necessary. Thereby, hydrogen peroxide was removed with *Catalase* enzyme (2350 U per mg: 1 U destroys 1 $\mu mol \cdot min^{-1}$ of H_2O_2 at pH = 7.0 and T = 25 ºC, Sigma) or with an excess of sodium sulphite (any remaining SO_3^{2-} was removed by bubbling O_2) [16]. On the other hand, for COD measurement, since $Cr_2O_7^{2-}$ could oxidise any reduced specie present in solution, H_2O_2 concentration (quantified by iodometric titration, Section 3.3.4) was corrected from COD values by difference [17]. However, iron interference was discarded since Fe (II) concentration was very low throughout the process. Even considering all the iron in its reduced form, the COD contribution of a 20 $mg \cdot l^{-1}$ Fe (II) initial dosage (the higher one employed) would not be higher than 3 $mg \cdot l^{-1}$ O_2.

When applying photo-Fenton process as a pre-treatment of an ensuing biological treatment, any residual hydrogen peroxide was also quenched with an excess of sodium sulphite.

3.6.1.2. Compound Parabolic Collector (CPC)

All photo-Fenton experiments carried at pilot plant scale were performed under sunlight at the PSA (latitude 37º 05' N, longitude 2º 21' W). The pilot plant (Figure 3.4) operated in batch mode and was composed by three CPCs modules in series, one tank and one recirculation pump. The collectors (1.03 m^2 each, 3.09 m^2 of total irradiated surface) faced south on a fixed platform tilted 37º (local latitude) in relation to the horizontal plane and consisted of eight parallel horizontal borosilicate glass-transparent tubes (inner diameter 29.2 mm, outer diameter 32.0 mm, length 1.37 m).

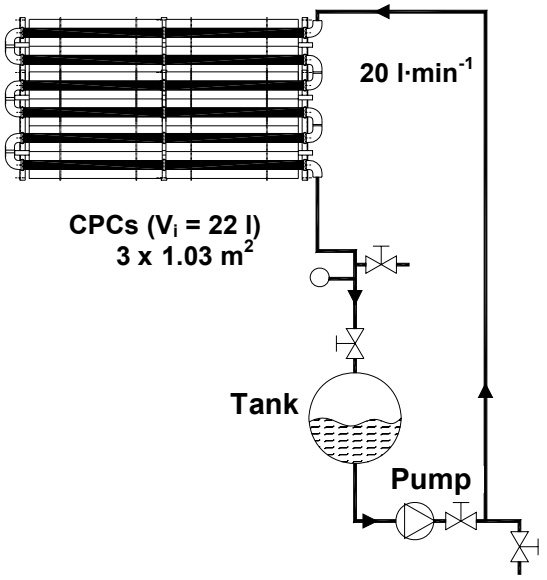

Figure 3.4. Diagram of the solar photo-Fenton pilot plant.

Under tubular conditions, water flowed steadily through the tubes at 20 $l \cdot min^{-1}$ from one CPC module to another and finally into the tank, from where the pump recirculated

it back to the CPCs. The total volume (V_T) was 35 l and it was separated in two parts: 22 l of total irradiated volume (V_i) and 13 l of dead reactor volume (tank + connecting tubes) that was not illuminated. More details about CPC photoreactor properties were described by Blanco *et al*. [18].

The reflective surface of the CPCs was formed by two connected parabolic aluminium mirrors, which redirected the radiation toward each tube attaining a low concentration factor (concentration factor = 1) (Figure 3.5). The radiation acceptance angle was 90º. In this way, all direct and diffuse incident radiation (global radiation, see Section 3.7.2) was collected. Reflected radiation was distributed around the perimeter of the tubular photoreactor, providing excellent performance in photochemical and photocatalytic applications [19].

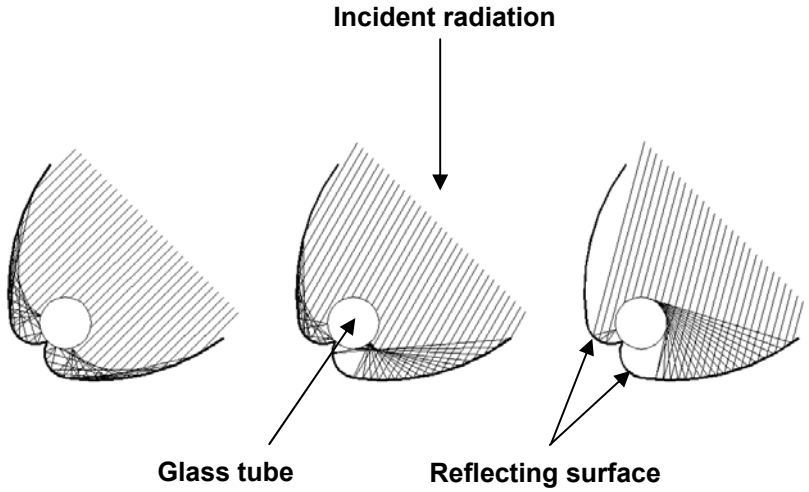

Figure 3.5. Solar ray reflection in a CPC-type solar collector.

Experiments were carried out as follows: with collectors covered, once solutions were adjusted to pH = 2.8-3.0, the necessary amount of iron salt was added to the tank. After its complete homogenisation, a unique pulse of required hydrogen peroxide was added to solution. After 5 minutes of Fenton reaction (dark process), the light protection was removed and samples were collected at regular time intervals. Neither pH

adjustments nor Fenton reagent additions were done after the beginning of the processes.

During experiments, solar ultraviolet radiation (300-400 nm) reaching the solar pilot plant was measured by a global UV radiometer (Kipp & Zonen, model CUV3), tilted 37º (the same angle as for the photoreactor), which provided data in terms of incident $W \cdot m^{-2}$.

Sample analyses included reactive dye concentration by HPLC, DOC, COD, BOD_5, H_2O_2 and iron concentrations (total and Fe (II) forms), as well as NH_4^+, NO_3^-, SO_4^{2-}, Cl^- and carboxylic acid concentrations. Analogously to the laboratory scale experiments procedure, it was necessary the removal of the remaining H_2O_2 prior the BOD_5 analysis and the H_2O_2 correction from COD measurement.

When applying photo-Fenton process as a pre-treatment of a secondary biological treatment, phototreated solutions were fed after complete H_2O_2 consumption.

The intensity of solar irradiance was never constant and could not be controlled due to multiple environmental influences (i.e., time of day or atmospheric conditions). Therefore, to better compare and evaluate the different parameters involved in different degradation processes, it was necessary to make use of a methodology that provided data in terms of incident radiation conditions throughout each experiment. In this way, using the solar ultraviolet radiation measurement at each experimental time, experiments could be compared using a corrected illumination time t_{30W} (Equation 3.17) [20]:

$$t_{30W,n} = t_{30W,n-1} + \Delta t_n \frac{UV}{30} \cdot \frac{V_i}{V_T}; \quad \Delta t_n = t_n - t_{n-1} \tag{3.17}$$

where t_n is the experimental time for each sample, UV is the average solar ultraviolet radiation measured during Δt_n and t_{30W} is the "normalised illumination time". In this case, time refers to a constant solar UV power of 30 $W \cdot m^{-2}$ (typical solar UV power on a perfect sunny day around noon) [21]. In that way, degradation could be evaluated as a function of time taking into account environmental conditions. It should be noted that

the t_{30W} normalised value only takes sense once illumination has begun (t_{30W} = 0). Consequently, negative time values were used to represent the dark Fenton process.

In those experiments, carried out in June and July months, UV intensity ranged between 14 and 37 $W \cdot m^{-2}$. Moreover, since the system was outdoors and non isolated, temperature in the reactor was in the range of 25-48 ºC.

3.6.2. Ozonation set-up

The ozonation experimental set-up consisted of a 300 ml thermostatic cylindrical Pyrex batch reactor with a working volume of 200 ml, provided with magnetic stirring and an external water jacket (Figure 3.6). By adjusting the water input through the water inlet and outlet, temperature was fixed at 23 ± 1 ºC. Ozone was obtained from an Erwin Sander 301.7 generator fed with a pure oxygen stream flowing at 1 bar. An ozone flow rate of 1.75 $g \cdot h^{-1}$ O_3 was employed to ensure saturation of the system, as determined by iodometric titration (Section 3.3.11). It was bubbled through the test sample solution by means of a metallic diffuser. Non reacted ozone was measured by means of an Erwin Sander Quantozone-1 ozone-meter, giving the measurement directly in $mg \cdot m^{-3}$, and finally destroyed with a KI trap.

Ozonation was done at different initial pH conditions: 3.0, 7.0, 10.0 and 10.5. No further pH adjustments were done after the beginning of the process. Samples were periodically taken through an outlet that could be opened or closed with a regulator key (Figure 3.6). DOC and acute toxicity (EC_{50}) data were collected. When testing the EC_{50} parameter, solutions were previously gassed with nitrogen to strip out the remaining dissolved O_3 gas.

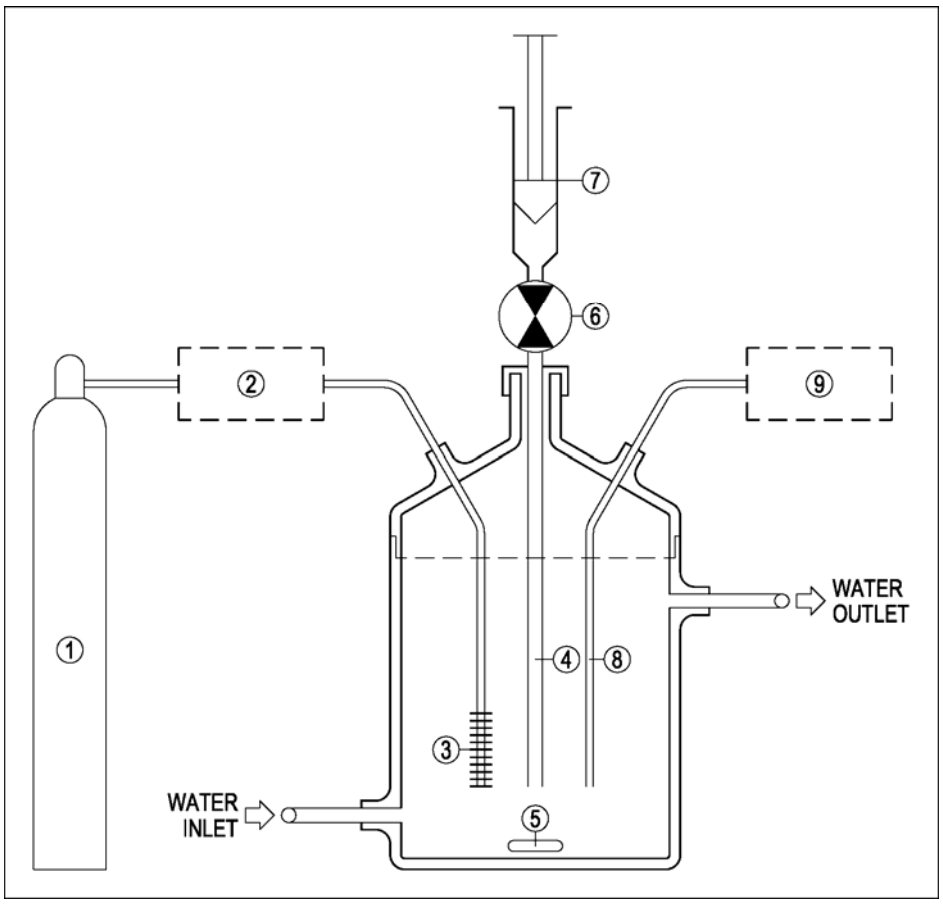

Figure 3.6. Ozonation set-up. *1-oxygen cylinder; 2-ozonator; 3-diffuser; 4-sample tube; 5-magnetic bar; 6-regulator key; 7- syringe; 8-ozone exit; 9-ozone-meter.*

3.6.3. Biological reactors

3.6.3.1. Sequencing Batch Reactor (SBR)

Aerobic biological treatment performed at laboratory scale was carried out in a SBR of 2 l –operational liquid volume (V_{SBR}) of 1.5 l–, equipped with an air diffuser and mechanical agitation. The temperature was maintained under room conditions, between 20 and 23 ºC, and DO concentration was not lower than 3 $mg \cdot l^{-1}$ O_2. Fresh biomass was used for each experiment. Suspensions of 0.6-1.0 $g \cdot l^{-1}$ VSS were prepared by diluting activated sludge collected from a municipal WWTP (Manresa, Spain).

The system operated in batch mode. Once a Hydraulic Retention Time (HRT; i.e., the average time that the effluent remains in the bioreactor, expressed in days) was fixed, according to Equation 3.18, the corresponding volume of sample was daily replaced ($V_{replaced}$, $ml \cdot day^{-1}$) by the same volume of fresh influent solution:

$$V_{replaced} = \frac{V_{SBR}}{HRT} \tag{3.18}$$

As described in Section 1.3.4.1, this process was divided under five defined stages: filling, reaction, settling, draw and idle. The whole sequence is illustrated in Figure 3.7. During the filling stage, the SBR tank was filled with the influent sample to be treated. Afterwards, aeration and agitation were switched on to begin the reaction period. Once over, both mixing and airflow were stopped to let the biomass to settle down. After 1 hour, the corresponding volume of sample (Equation 3.18) was withdrawn from the supernatant during the draw step, without disturbing the settled sludge. The SBR tank waited idle until a new fresh sample batch was added (equal to the volume decanted), and aeration-agitation was turned on again.

The whole HRT was completed when the total V_{SBR} had been replaced.

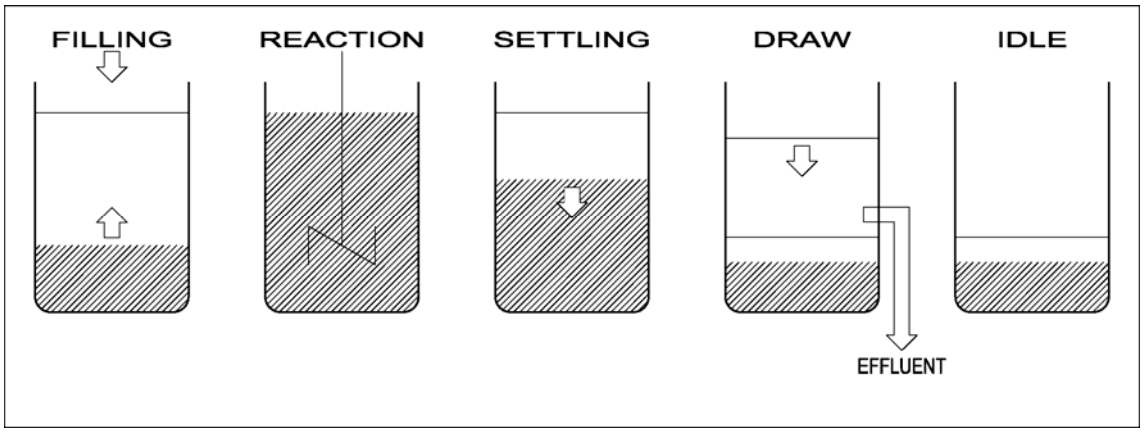

Figure 3.7. SBR operation steps.

All biodegradation experiments were carried out in two stages: preliminary run (blank run) and operation. The first one consisted of a 10-day HRT cycle where the SBR tank was fed with a fully biodegradable municipal wastewater obtained from a WWTP (Manresa, Spain). This wastewater was characterised by an average DOC of 50 $mg \cdot l^{-1}$ C and a COD of 210 $mg \cdot l^{-1}$ O_2. During this first run, aerobic biomass activity was checked, cells got adapted to experimental laboratory conditions (i.e., temperature, oxygen flow and manipulation) and the lower residual DOC that could be achieved by the SBR system (corresponding to metabolites released by biomass) was established. Once the blank run was completed, the SBR was fed with the test sample solution to begin the operation stage at the required HRT (i.e., 10, 4, 2 or 1 days). The pH of this had been previously adjusted to 6.5-7.5, and suitable amounts of the following solutions were added together to the tank: 2 ml of 101 $g \cdot l^{-1}$ $MgSO_4 \cdot H_2O$, 27.7 $g \cdot l^{-1}$ $CaCl_2$, 38.2 $g \cdot l^{1}$ NH_4Cl (at pH = 7.0) and 6 ml of 207 $g \cdot l^{-1}$ $NaH_2PO_4 \cdot H_2O$ per litter of influent sample [22]. Once over, the HRT cycle was repeated as many times as necessary to allow cells acclimation and/or to obtain repetitive results.

Influent and effluent samples DOC content, as well as the VSS were daily analysed. pH readjustment between 6.5 and 7.5 was done if necessary. A full biodegradation of the sample was assumed when attaining final DOC values close to those obtained in the previous run.

Finally, it is worth to note that, apart from the HRT, the Sludge Retention Time parameter (SRT; i.e., the average time that the sludge remains in the bioreactor) is usually controlled by sludge purging. However, due to the small scale of the SBR and the low DOC concentration used in this work, little sludge production was eliminated when withdrawing the supernatant. Consequently, sludge waste and SRT control were not found to be necessary throughout experimentation.

3.6.3.2. Immobilised Biomass Reactor (IBR)

The biological pilot plant (in the PSA) operated in batch mode and was composed by two independent modules: an IBR and a conditioner tank of 50 l (Figure 3.8). The IBR unit, which consisted of a 35 l column containing plastic fixed supports

(polypropylene, 15 mm of nominal diameter, Pall®-Ring), was seeded by aerobic activated sludge coming from a municipal WWTP (Almería, Spain). After inoculation, activated sludge was progressively fixed on polypropylene supports until TSS values in solution were near zero.

The sample volume to be treated was 45 l. It was continuously recirculated between the conditioner tank and the IBR unit at 0.5 $l \cdot min^{-1}$ ascendant flow rate. This flow rate maintained a suitable contact between the immobilised biomass and the test sample solution. A blower provided oxygen saturation conditions. Since the system was outdoors, temperature was in the range of 16-40 ºC.

The biological treatment strategy was as follows: once IBR colonisation was carried out, in order to guarantee bacteria viability and to permit a better growing and fixing on the polypropylene supports, a 45-l batch of an easily biodegradable substrate was initially added to the tank. Glucose was chosen for this role. Besides, this first batch let to establish the lower residual DOC that could be achieved by the IBR system (biomass metabolites). After its complete biodegradation, the conditioner tank was completely emptied and sequentially filled with 45-l batches of the different solutions to be treated. The pH of these had been previously neutralised to 6.5-7.5. Additionally, suitable proportions of the following solutions were supplied to the conditioner tank in order to maintain the required C:N:P (100:20:5) and C:Fe:S (100:2:2) ratios: 43.8 $g \cdot l^{-1}$ KH_2PO_4, 27.5 $g \cdot l^{-1}$ $CaCl_2$, 22.5 $g \cdot l^{-1}$ $MgSO_4.7H_2O$, 50 $g \cdot l^{-1}$ $FeSO_4.7H_2O$, 48 $g \cdot l^{-1}$ $NaHCO_3$ and 38.5 $g \cdot l^{-1}$ NH_4Cl. The KH_2PO_4, $FeSO_4.7H_2O$ and NH_4Cl volumes to be added depended on the DOC present in solution. Nevertheless, the addition of $CaCl_2$ and $MgSO_4.7H_2O$ was always fixed in 1 ml per litter of test sample and the addition of $NaHCO_3$ in 2 ml per litter of test sample.

The degree of mineralisation was followed by DOC measurement at regular time intervals (one or two times per day) until constant DOC values achievement. A Full biodegradation of the sample was assumed when attaining a final DOC close to the obtained in the previous glucose batch. Other periodical determinations carried out were the carboxylic acids concentration and NH_4^+, NO_2^- and NO_3^- ions concentration to detect parallel nitrification and denitrification processes. Moreover, TSS were determined in

order to ensure a correct sludge fixation on the plastic supports (TSS ~ 0 $g \cdot l^{-1}$). pH readjustment between 6.5 and 7.5 was done if necessary.

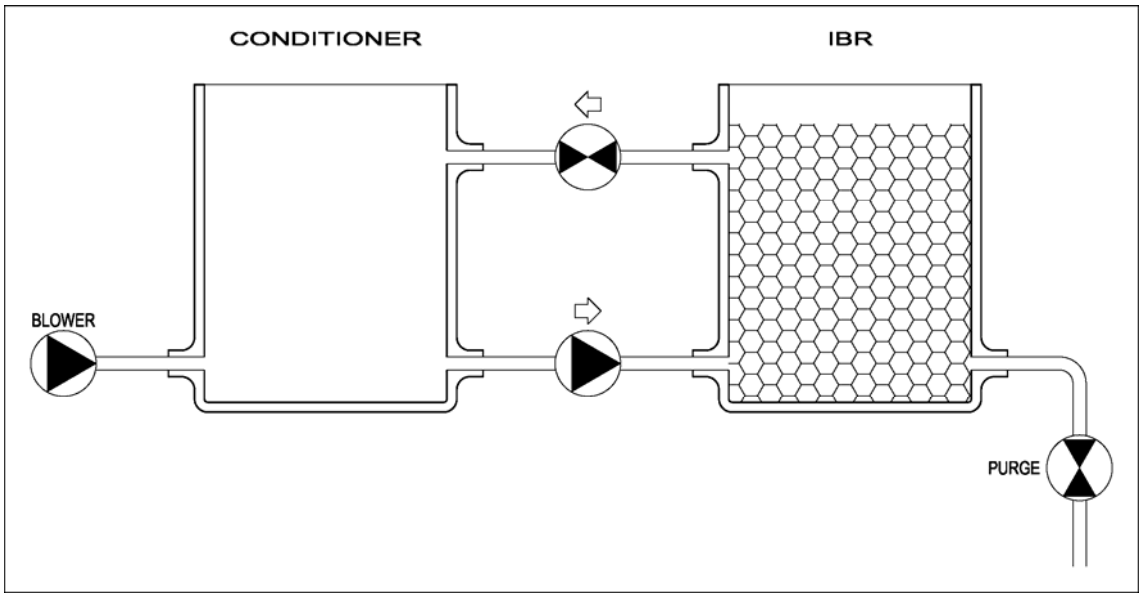

Figure 3.8. Scheme of the biological pilot plant.

3.7. PHOTO-FENTON IRRADIATION SOURCES

3.7.1. Black light

As commented above, artificial light photo-Fenton experiments performed at laboratory scale were conducted by a Philips fluorescent black light of 6 W. The emission spectrum provided by the Philips supplier is shown in Figure 3.9 (arbitrary units). As seen, irradiation is concentrated in the near-UV and visible zone of the spectrum (300-400 nm) with a maximum intensity corresponding to 348 nm wavelength.

According to the emission spectrum, this source of light is especially suited for artificial light photo-Fenton experiments since it narrowly adjusts to the absorption requirements of the process (mainly from the UV up to 410 nm wavelength). Moreover,

since it is a low power consumption lamp, it seems to be the most efficient artificial light in terms of active photons produced/energy consumed.

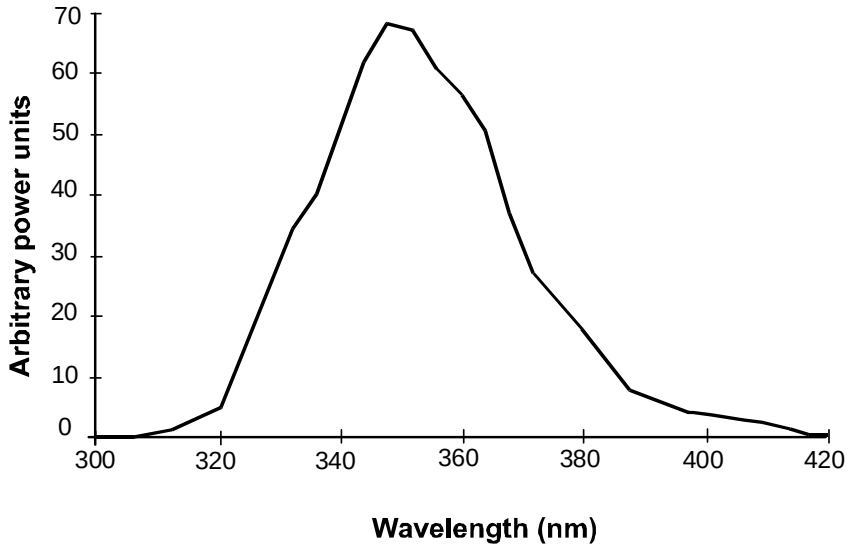

Figure 3.9. Emission spectrum of the fluorescent black light.

3.7.2. Solar radiation

A key aspect of the photo-Fenton process is the possibility of sunlight exploitation as a source of energy.

The solar radiation that reaches the earth surface, without being absorbed or scattered, is called direct radiation, meanwhile the radiation fraction that reaches de surface after being dispersed is called diffuse radiation. The sum of both is the global radiation. The proportion of each component depends on the environmental conditions. In general, the direct component of global radiation in cloudy days is at minimum and the diffuse component is at maximum, with the opposite situation in clear days.

Figure 3.10 shows the standard spectra of direct and global solar radiation at ground level on a clear day (sun-facing 37-degree tilted surface, air mass 1.5) [23, 24]. The dotted line corresponds to the extraterrestrial radiation in the same interval of wavelength.

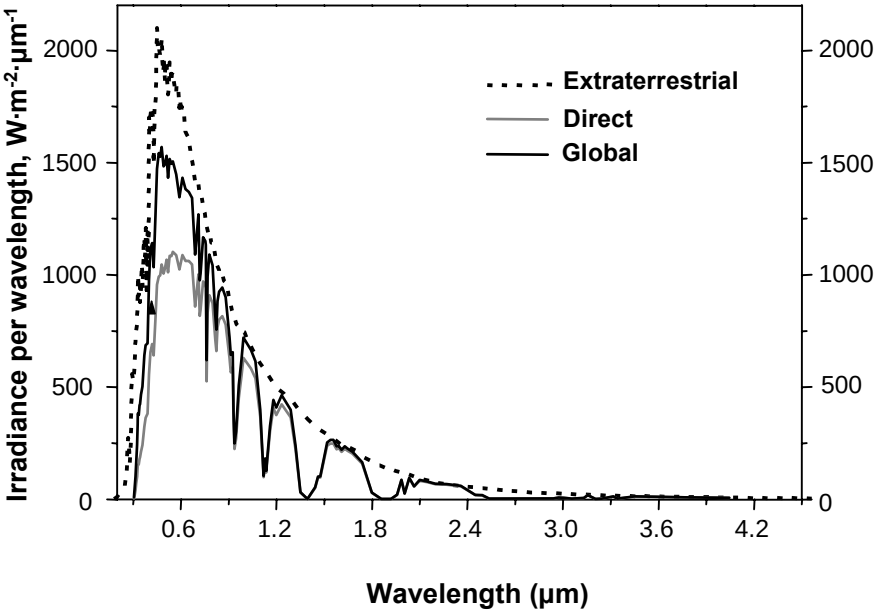

Figure 3.10. Solar radiation spectrum from 0.2 μm to 4.5 μm.

The UV radiation is a very small part of the whole solar spectrum reaching the earth surface. Measurements carried out have demonstrated that it just represents between 3.5 and 8% of the total [25], although this relation can change for a determined location between cloudy and clear days. Figure 3.11 shows the spectra of the global and direct radiation of the UV range of the above standard solar spectrum reaching the surface [26]. Between 300 and 400 nm, the direct UV radiation reaches 22 $W \cdot m^{-2}$ meanwhile the global UV radiation reaches 46 $W \cdot m^{-2}$. These two values give an idea of the cheap and abundant energy coming from the sun that is available to assist photo-Fenton reaction. Obviously, UV radiation values vary depending on location, date, time of day, season and atmospheric conditions, making necessary to know these data for every particular location in real time.

Apart from the UV radiation, and as it has been discussed in Section 1.4.1.1, photoassisted process makes also use of part of the visible solar spectrum (up to $\lambda \sim 550$ nm). Hence, it is clearly seen that solar radiation spectrum fulfil the photo-Fenton wavelength requirements.

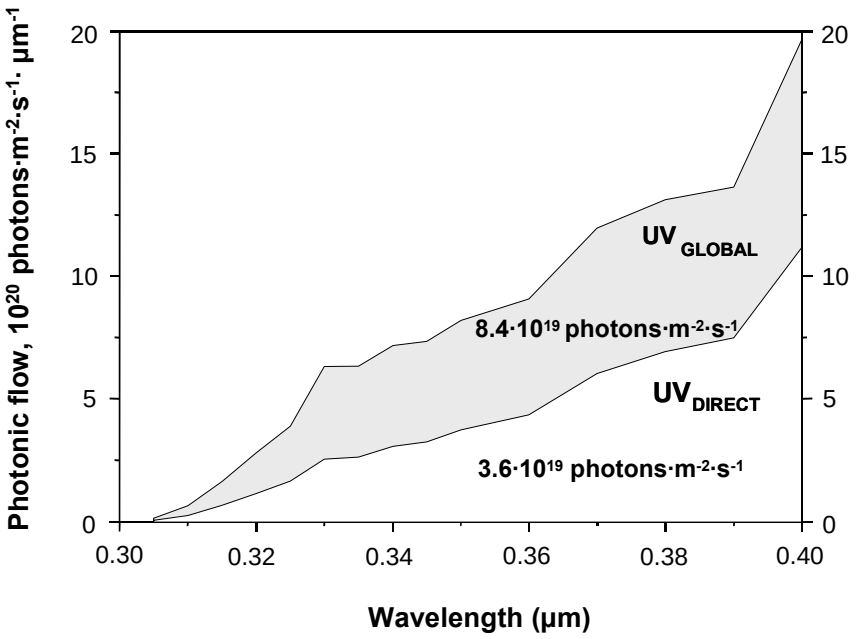

Figure 3.11. Standard UV spectrum on the earth surface.

3.8. ENVIRONMENTAL ASSESSMENT METHODOLOGY

The environmental impact of different bench scale photo-Fenton based treatments was evaluated by means of the Life Cycle Assessment (LCA) tool. As described in Section 1.6.1.2, the study was undertaken in four basic stages according to ISO 14040 standard [27]: goal and scope, inventory analysis, impact assessment, and interpretation. Among the four consecutive steps included in the impact assessment stage (i.e., classification, characterisation, normalisation and weighting), only the classification and characterisation were taken into account.

The sources and quality of data handled were taken from SigmaPro 6 software, mainly from *Ecoinvent* database version 1.1 (June 2004) [28, 29]. To carry out the environmental impact assessment, inventoried data were allocated to the following potential impact categories included in the CML 2000 method [30]:

- Abiotic Resource Depletion (ARD), which are the natural resources (including energy resources) that are regarded as non renewable in a short term.

- Global Warming Potential (GWP), which refers to the impact of human emissions on the radiative forcing of the atmosphere.

- Ozone Depletion Potential (ODP) that refers to the thinning of the stratospheric ozone layer as a result of anthropogenic emissions.

- Human Toxicity Potential (HTP) that covers the impacts on human health of toxic substances present in the environment.

- Freshwater Aquatic Toxicity Potential (FATP), which refers to the impacts of toxic substances on freshwater aquatic ecosystem.

- Marine Aquatic Ecotoxicity Potential (MAEP) that refers to the impacts of toxic substances on marine aquatic ecosystem.

- Terrestrial Ecotoxicity Potential (TEP) that refers to the impacts of toxic substances on terrestrial ecosystem.

- Photochemical Oxidation Potential (POP) that refers to the formation of photooxidants such as ozone by the action of sunlight on certain primary air pollutants.

- Acidification Potential (AP), which contains a wide variety of impacts on soil, groundwater, surface waters, biological organisms, ecosystems and materials due to acidifying pollutants like SO_2 and NO_x.

- Aquatic Eutrophication Potential (AEP) that covers all potential impacts of excessively high levels of macronutrients in the aquatic ecosystems, the most important of which are nitrogen and phosphorous.

3.9. REFERENCES

[1] APHA-AWWA-WEF (1992). *Standard Methods for the Examination of Water and Wastewater*. 5310 A, 5310 B, 18th Ed., Washington DC, USA.

[2] APHA-AWWA-WEF (1992). *Standard Methods for the Examination of Water and Wastewater*. 5220 D, 18th Ed., Washington DC, USA.

[3] Ravikumar J.X., Gurol M.D. (1994). Chemical oxidation of chlorinated organics by hydrogen peroxide in the presence of sand. *Environ. Sci. Technol*., 28, 394-400.

[4] Kormann C., Bahnemann D.W., Hoffmann M.R. (1988). Photocatalytic production of H_2O_2 and organic peroxides in aqueous suspensions of TiO_2, ZnO and desert salt. *Environ. Sci. Technol*., 22, 798-806.

[5] APHA-AWWA-WEF (1992). *Standard Methods for the Examination of Water and Wastewater*. 3500-Fe D, 18th Ed., Washington DC, USA.

[6] APHA-AWWA-WEF (1992). *Standard Methods for the Examination of Water and Wastewater*. 4500-NH_3 C, 18th Ed., Washington DC, USA.

[7] Beyer M., Walter W. (1987). *Manual de Química Orgánica*. Ed. Reverté S.A., Barcelona, Spain.

[8] APHA-AWWA-WEF (1992). *Standard Methods for the Examination of Water and Wastewater*. 2540 D, 18th Ed., Washington DC, USA.

[9] APHA-AWWA-WEF (1992). *Standard Methods for the Examination of Water and Wastewater*. 2540 E, 18th Ed., Washington DC, USA.

[10] OECD (1992). *Inherent biodegradability: modified Zahn-Wellens test.* Test 302B, Paris, France.

[11] PNE (1978). *Métodos de análisis del agua. Determinación de la demanda bioquímica de oxígeno (DBO). Método de dilución y siembra*. PNE 77-003, Madrid, Spain.

[12] Cooney J.D. (1995). Freshwater tests. In: Rand G. (Ed.). *Fundamentals in aquatic toxicology*. Taylor and Francis, 2nd Ed., Washington DC, USA.

[13] ISO (1998). *Determination of the inhibitory effect of water samples on the light emission of Vibrio fischeri (Luminescent bacteria test)*. ISO 11348-3, Geneva, Switzerland.

[14] APHA-AWWA-WEF (1992). *Standard Methods for the Examination of Water and Wastewater*. 2710 B, 18th Ed., Washington DC, USA.

[15] Field J., Alvarez R.S., Lettinga G. (1988). *Ensayos anaerobios. Proc. of 4th Symposium on wastewater anaerobic treatment*, Valladolid, Spain.

[16] Adams C.D., Scanlan P.A., Secrist N.D. (1994). Oxidation and biodegradability enhancement of 1,4-dioxane using hydrogen peroxide and ozone. *Environ. Sci. Technol*., 28, 1812-1818.

[17] Yun Whan Kang, Min-Jung Cho, Kyung-Yup Hwang (1999). Correction of hydrogen peroxide interference on standard chemical oxygen demand test. *Water Res*., 33, 1247-1251.

[18] Blanco J., Malato S., Fernández P., Vidal A., Morales A., Trincado P., Oliveira J.C., Minero C., Musci M., Casalle C., Brunote M., Tratzky S., Dischinger N., Funken K.-H., Sattler C., Vincent M., Collares-Pereira M., Mendes J.F., Rangel C.M. (2000). Compound parabolic concentrator technology development to commercial solar detoxification applications. *Sol. Energy*, 67, 317-330.

[19] Ajona J.I., Vidal A. (2000). The use of CPC collectors for detoxification of contaminated water: design, construction and preliminary results. *Sol. Energy*, 68, 109-120.

[20] Malato S., Cáceres J., Fernández-Alba A.R., Piedra L., Hernando M.D., Agüera A., Vial J. (2003). Photocatalytic treatment of diuron by solar photocatalysis: evaluation of main intermediates and toxicity. *Environ. Sci. Technol*., 37, 2516-2524.

[21] Malato S., Blanco J., Vidal A., Alarcón D., Maldonado M.I., Cáceres J., Gernjak W. (2003). Applied studies in solar photocatalytic detoxification: an overview. *Sol. Energy*, 75, 329-336.

[22] Contreras S. (2003). *Degradation and biodegradability enhancement of nitrobenzene and 2,4-dichlorophenol by means of Advanced Oxidation Processes based on ozone*. PhD thesis, Universidad de Barcelona, Spain.

[23] ASTM (1987). *Standard tables for terrestrial direct normal solar spectral irradiance for air mass 1.5*. Designation: E891-87.

[24] Hulstrom R., Bird R., Riordan C. (1985). Spectral solar irradiance data sets for selected terrestrial conditions. *Solar Cells*, 15, 365-391.

[25] Riordan C.J., Hulstrom R.L., Myers D.R. (1990). Influences of atmospheric conditions and air mass on the ratio of ultraviolet to total solar radiation. Solar Energy Research Institute (SERI)/TP-215-3895.

[26] ASTM (1987). *Standard tables for terrestrial solar spectral irradiance at air mass 1.5 for a 37º tilted surface*. Designation: E892-87.

[27] ISO (2006). *Environmental management –Life Cycle Assessment– Principles and Framework*. ISO 14040, Geneva, Switzerland.

[28] Frischknecht R., Althaus H.J., Doka G., Dones R.S., Hischier R., Jungbluth N., Nemecek T., Rebitzer G., Spielmann M. (2003). *Code of Practice*. Final report ecoinvent 2000 No 2, Swiss Centre for Life Cycle Inventories, Duebendorf, Switzerland.

[29] Frischknecht R., Althaus H.J., Doka G., Dones R.S., Heck T., Hellweg S., Hischier R., Jungbluth N., Nemecek T., Rebitzer G., Spielmann M. (2004). *Overview and Methodology*. Final report ecoivent 2000 No 1, Swiss Centre for Life Cycle Inventories, Duebendorf, Switzerland.

[30] Guinée J.B., Gorrée M., Heijungs R., Huppes G., Kleijn R., Udo de Haes H.A., Van der Voet E., Wrisberg M.N. (2002). *Life Cycle Assessment. An operational guide to ISO standards*. Centre of Environmental Science, Leiden University (CML), The Netherlands.

CHAPTER 4. RESULTS AND DISCUSSION

Chapter 4
Results and Discussion

4.1. OVERVIEW

The release of textile effluents containing reactive dyes into the environment is a dramatic source of aesthetic pollution and perturbations in aquatic life. Due to their stability and non biodegradable nature under aerobic conditions, reactive dyes are not easily amenable to conventional wastewater treatment methods. Consequently, to accomplish with current legislations, the application of specific treatment is required [1].

In this frame, Advanced Oxidation Processes (AOPs) have emerged as powerful remediation treatments to destroy refractory pollutants in water [2]. They may be applied as exclusive processes or combined with biological treatments in an attempt to reduce their large chemicals and energy consumption [3]. Among available AOPs, the Fenton and, particularly, the photo-Fenton processes are of especial interest since they achieve high reaction yields with a lower operational cost [4]. Additionally, the

photoassisted reaction presents the possibility of be driven under solar irradiation, offering further economic and environmental advantages [5].

At the present work, both Fenton and photo-Fenton processes were initially applied at bench scale to entirely decolourise and mineralise three different reactive azo dye hydrolysed solutions composed of 100 $mg \cdot l^{-1}$ of Procion Red H-E7B, 100 $mg \cdot l^{-1}$ of Cibacron Red FN-R and 150.5 $mg \cdot l^{-1}$ of a standard trichromatic system (43.0 $mg \cdot l^{-1}$ of Cibacron Red FN-R, 43.0 $mg \cdot l^{-1}$ of Cibacron Yellow FN-2R and 64.5 $mg \cdot l^{-1}$ of Cibacron Navy FN-B), respectively. The main parameters that govern the system, i.e., initial ferrous ion and hydrogen peroxide dosages, type of irradiation –artificial UVA light and solar radiation– and temperature were studied. The temperature effect is of especial interest in view of future real applications since it is unusually high in dyeing effluents considered here. Reaction efficiencies were evaluated in terms of % decolourisation, aromatic compounds removal (UV_{254} removal) and mineralisation (Dissolved Organic Carbon (DOC) removal). Finally, the possibility of an integrated photo-Fenton-aerobic biological treatment was investigated.

The following two publications, corresponding to Sections 4.2.1 and 4.2.2, encompass this first issue:

Decolourisation and mineralisation of homo- and hetero-bireactive dyes under Fenton and photo-Fenton conditions

Coloration Technology, 120 (2004) 188-194

Decolorization and mineralization of commercial reactive dyes under solar light assisted photo-Fenton conditions

Solar Energy, 77 (2004) 573-581

Both papers evidence that the studied Fenton based processes efficiently accomplished a full decolourisation and a substantial mineralisation of hydrolysed dye solutions. Regarding Fenton reagent concentrations, the best results for colour, UV_{254} and DOC removal were obtained with 10 $mg \cdot l^{-1}$ Fe (II)/100 $mg \cdot l^{-1}$ H_2O_2 for Procion Red H-E7B, 10 $mg \cdot l^{-1}$ Fe (II)/250 $mg \cdot l^{-1}$ H_2O_2 for Cibacron Red FN-R and 10 $mg \cdot l^{-1}$ Fe (II)/250 $mg \cdot l^{-1}$ H_2O_2 for the standard trichromatic system.

Under these conditions, more than 97% decolourisation was quickly attained in all solutions, both in darkness and under irradiation. However, results show that the best UV_{254} and DOC removal degree was obtained in the presence of light; dark Fenton reaction was not able to go beyond 33% DOC and 59% UV_{254} removal even at prolonged reaction times. Particularly good results were obtained when using solar light assisted photo-Fenton treatment: aromatics and DOC removal percentages were 81 and 100% for Procion Red H-E7B, 73 and 99% for Cibacron Red FN-R and 86 and 81% for the standard trichromatic system. It is remarkable that the degradation rates of solar photo-Fenton were also superior to dark and artificially irradiated processes, in this order. This higher efficiency of sunlight is attributable to the higher number of photons supplied by the sun, which also involves a visible fraction of the spectrum profitable for the photoassisted process [6, 7].

Concerning the temperature effect, values higher than room conditions manifested notable differences in colour removal, UV_{254} and mineralisation at the initial stages of dark and photoassisted processes. Thought, changes in temperature did not seem to provide any substantial advantage at long reaction times when Fe (II) concentration is low, Fenton reaction is minimal and Fenton-like or photo-Fenton reactions are controlling the process.

When assessing the possibility of an integrated photo-Fenton-aerobic biological treatment, only Procion Red H-E7B and Cibacron Red FN-R reactive dyes were considered (the standard trichromatic system was not further investigated from hereon). Their initial concentration was increased from 100 up to 250 $mg \cdot l^{-1}$ due to the requirements set by the detection limit of biological analyses. The first measure was to confirm that, as usual for textile dyes, they were not amenable to aerobic biotreatment. With this aim, Biotox® technique (acute toxicity), BOD_5/COD index (BOD_5: Biochemical Oxygen Demand for 5 days; COD: Chemical Oxygen Demand) and Zahn-Wellens biological assays were employed. As expected, both dye solutions were initially found to be non toxic, but also non biodegradable, impeding a single conventional aerobic biological treatment. Therefore, in agreement with the strategy for combined wastewater treatments proposed in Section 1.5.1, the photo-Fenton process could be performed as a pre-treatment (avoiding complete mineralisation) to just

enhance the biodegradability and generate a new solution capable to be treated in a secondary biological plant.

Initial 10 $mg \cdot l^{-1}$ Fe (II) and 125 $mg \cdot l^{-1}$ H_2O_2 Fenton reagent concentrations were arbitrarily chosen. Acute toxicity and BOD_5/COD ratio were periodically determined through photo-Fenton process in order to evaluate the biocompatibility of phototreated solutions. It should be noted that, instead of Zahn-Wellens assay, BOD_5/COD index was chosen since it provides a quicker screening of biodegradability. Obtained results were satisfactory; BOD_5/COD ratio underwent an effective increase during reaction, meanwhile non toxic oxidation products were detected. In view of this, the sequenced photo-Fenton-biological strategy was therefore possible. It is remarkable that these experiments were carried out by using the artificial irradiation source. Thus, attending to the data above reported, similar and even more favourable results were predictable when using solar radiation.

Taking such toxicity and biodegradability results as starting point, the coupling of artificial light photo-Fenton process and aerobic biological treatment for Procion Red H-E7B and Cibacron Red FN-R degradation was carried out (Sections 4.2.3 and 4.2.4, respectively). This work includes the two publications below. It is noticeable that no earlier studies regarding photo-Fenton pre-treatment of an ensuing aerobic biological process for the decontamination of real or simulated textile effluents containing reactive dyes have been found in the literature.

Degradation of Procion Red H-E7B reactive dye by coupling a photo-Fenton system with a sequencing batch reactor

Journal of Hazardous Materials, 134 (2006) 220-229

Combining photo-Fenton process with aerobic sequencing batch reactor for commercial hetero-bireactive dye removal

Applied Catalysis B: Environmental, 67 (2006) 86-92

In a first part, several experiments were carried out by modifying Fe (II)/H_2O_2 ratio and irradiation time in an attempt to establish the softest photo-Fenton conditions to make Procion Red H-E7B and Cibacron Red FN-R biocompatible. The selection of

such Fenton reagent combinations was based on the preceding optimisation reported in Section 4.2.1.

The most efficient Fenton reagent concentrations to achieve the maximum degradation levels at short irradiation times were found to be 10 $mg \cdot l^{-1}$ Fe (II)/250 $mg \cdot l^{-1}$ H_2O_2 for Procion Red H-E7B and 20 $mg \cdot l^{-1}$ Fe (II)/500 $mg \cdot l^{-1}$ H_2O_2 for Cibacron Red FN-R, with 82 and 84% mineralisation, respectively. However, since just a partial degradation was desired, such combinations were not taken into account for chemical and biological coupling applications. By stating them as the top doses limit, smaller Fe (II) and H_2O_2 amounts were considered.

The efficiency of the pre-treatment process was estimated by means of the biodegradability evolution of the phototreated solutions, determined by the BOD_5/COD ratio and respirometric measurements. The DOC evolution through the photo-Fenton process was monitored in order to determine the degree of mineralisation during the pre-treatment. Colour and acute toxicity of dyes degradation intermediates were also determined along the oxidation.

In agreement with preliminary results obtained in publications 4.2.1 and 4.2.2, all assessed solutions manifested a biodegradability increase with time, with no toxic degradation products detection. This enhancement was accompanied by the solutions decolourisation, suggesting the complete disappearance of the original dye molecules. Nevertheless, their biocompatibility degree was not always high enough and only few presumable biocompatible solutions were finally amenable to biological treatment. This process was carried out in an aerobic Sequencing Batch Reactor (SBR) working under different Hydraulic Retention Times (HRT). The DOC parameter was used as indicator of the biodegradation success.

Among the different Procion Red H-E7B tested solutions, the best results were obtained with 10 $mg \cdot l^{-1}$ Fe (II)/125 $mg \cdot l^{-1}$ H_2O_2 concentrations applied for an irradiation time of 60 minutes. On the other hand, a Fenton reagent concentration of 20 $mg \cdot l^{-1}$ Fe (II)/250 $mg \cdot l^{-1}$ H_2O_2 applied for 90 minutes made Cibacron Red FN-R solution biocompatible. Under these pre-treatment conditions, the coupled aerobic SBR system, working under steady conditions at 1 day HRT mode, successfully removed both reactive dyes metabolites from aqueous solution.

Section 4.2.5 corresponds to the publication below, which analyses the preceding combined artificial light photo-Fenton-biological oxidation system from an environmental and economic point of view. Obtained results where thereby compared with single artificial light and solar driven photo-Fenton processes, aiming to identify the most suitable approach in such a context. For this target, experimental results corresponding to Cibacron Red FN-R reactive dye degradation (Section 4.2.4) were taken as a model.

Environmental assessment of different photo-Fenton approaches for commercial reactive dye removal

Journal of Hazardous Materials, 138 (2006) 218-225

The environmental impact evaluation was carried out by means of the Life Cycle Assessment (LCA) tool. As far as LCA application to AOPs is concerned, this is the first published work dealing with an integrated AOP-biological system. The study focused on the electricity consumption, including extraction of resources, transport and energy conversion; the chemicals consumption, including extraction of resources, production of the corresponding chemicals and the different transport steps; and the air and water emissions generated through the different processes involved. The construction and the end-of-life of the systems were not taken into account. The environmental damage derived from each treatment was quantified according to the environmental categories listed in Section 3.8. LCA characterisation values (data not shown in publication 4.2.5) are given in Section A.2.2.

The economic study was performed considering the same inputs than in LCA, only taking into account the chemical and energy costs associated with operation. All other running costs and capital investments were excluded.

Obtained results were as follows. Single artificial light photo-Fenton process was found to be the wastewater treatment with a major global impact on the environment, mainly due to H_2O_2 requirements and UVA light irradiation, in this order. However, when the artificial light photo-Fenton process was applied as a pre-treatment of a biological treatment, H_2O_2 and electricity consumption were significantly reduced achieving around 45% decrease for most environmental impact categories. The heaviest

burden linked to biological treatment was attributed to exceeding sludge management, which was assumed to be composed of thickening, dewatering and stabilisation independent unit operations. Solid sludge residue was finally deposited at landfill. On the other hand, as expected, solar driven photo-Fenton process reduced the environmental impact between 10 and 50% due to the avoidance of electricity input.

When comparing both solar driven photo-Fenton and artificial light photo-Fenton-biological processes, no clear differences could be drawn for all environmental impact categories. Differentiation can be made from the economic assessment. Obviously, the artificial light photo-Fenton process was the most expensive treatment. When carrying out the treatment under solar irradiation or coupled to an ensuing biological process, the estimated relative cost decreased 13 and 44%, respectively, being the combined system the cheaper option. A reduction of H_2O_2 –the most expensive burden– and electricity consumption in favour of the biological treatment was found to be the major cause of such a decrease.

In view of this, considering both environmental and economic data to decide about the aptness of the studied wastewater treatments, the best environmental/cost option seemed to be the coupling of artificial light photo-Fenton process and biological treatment. Taking these results as a basis, it is predictable that a solar driven photo-Fenton-aerobic biological coupling system would further reduce the economic and environmental burdens. Additionally, as concluded in publications 4.2.1 and 4.2.2, solar light gives more efficient dyes degradation than artificial light, making the combined process involving sunlight very appealing from the point of view of real applications.

The following step was the scaling-up of the laboratory scale photo-Fenton-biotreatment experiments to pilot plant. In this way, the feasibility of the system was checked in view of future full scale implementations. Publications in Sections 4.2.3 and 4.2.4 were taken as starting point. Section A.1.1, corresponding to the following manuscript submitted for publication, encloses the study.

Pilot plant scale reactive dyes degradation by solar photo-Fenton and biological processes

In line with LCA and economic assessment final conclusions, the photo-Fenton process was driven under solar radiation by using a Compound Parabolic Collector (CPC) photoreactor. The biological pilot plant consisted of an Immobilised Biomass Reactor (IBR).

Firstly, photo-Fenton was applied as a stand-alone process for entire Procion Red H-E7B and Cibacron Red FN-R degradation. The 10 $mg \cdot l^{-1}$ Fe (II)/250 $mg \cdot l^{-1}$ H_2O_2 Fenton reagent dosage for Procion Red H-E7B and the 20 $mg \cdot l^{-1}$ Fe (II)/500 $mg \cdot l^{-1}$ H_2O_2 for Cibacron Red FN-R were considered. Results demonstrated the reproducibility of the laboratory system with 82% DOC removal for Procion Red H-E7B and 86% for Cibacron Red FN-R (see obtained results in publications 4.2.3 and 4.2.4). Nevertheless, in comparison with the artificial light process at laboratory, the beneficial use of sunlight with the CPC photoreactor increased the degradation rates allowing the reduction of Fe (II) concentration from 10 to 2 $mg \cdot l^{-1}$ (Procion Red H-E7B) and from 20 to 5 $mg \cdot l^{-1}$ (Cibacron Red FN-R) without efficacy loses.

Under such low Fe (II) concentrations, the biodegradability evolution of Procion Red H-E7B and Cibacron Red FN-R phototreated solutions, determined as BOD_5/COD ratio, was monitored. Analogously to the laboratory scale experiments procedure, some presumably biocompatible phototreated solutions were submitted to the IBR pilot plant. All of them were exempted of original dye and corresponded to colourless samples. Among the tested pre-treatment conditions, the best ones for a subsequent biodegradation were found to be 2 $mg \cdot l^{-1}$ Fe (II)/65 $mg \cdot l^{-1}$ H_2O_2 for Procion Red H-E7B and 5 $mg \cdot l^{-1}$ Fe (II)/225 $mg \cdot l^{-1}$ H_2O_2 for Cibacron Red FN-R, reducing the required bench scale Fenton reagent requirements (see publications 4.2.3 and 4.2.4). Both phototreated dye solutions were successfully biodegraded in 1-2 days.

The knowledge of the reaction pathways and the kinetics of formation and degradation of by-products generated along photo-Fenton is a key aspect from a practical point of view, especially in cases where it precedes a biological treatment; the success of the combined treatment depends on the nature of intermediates feeding the bioreactor. In this direction, a mechanistic study of the degradation of Procion Red H-E7B reactive dye by means of the solar photo-Fenton process at pilot plant scale complements the above work. Cibacron Red FN-R was not considered here since its molecular structure was not disclosed by the manufacturer. Again, it is noteworthy that

no studies about reactive azo dyes degradation mechanism by means of photo-Fenton process are found in the literature.

250 $mg \cdot l^{-1}$ of H_2O_2 and the lowest 2 $mg \cdot l^{-1}$ Fe (II) concentration were applied to provide appropriate degradation rates that ensure the detection of as many intermediate species as possible. The study was developed by means of different chromatographic analyses of the different phototreated samples; carboxylic acids generation, ammonium, sulphate, nitrate and chloride ions release were determined by Ion Chromatography (IC), and organic by-products identification was developed by means of Liquid Chromatography-(Electrospray Ionisation)-Time-of-Flight Mass Spectrometry (LC-(ESI)-TOF-MS) analysis. Identified intermediates and degradation pathways are detailed in Section A.1.2, entitled:

Pathways of solar photo-Fenton degradation of Procion Red H-E7B reactive azo dye at pilot plant scale

The proposed photo-Fenton degradation mechanism proceeds via a series of consecutive steps. Firstly, hydroxyl radical would preferably attack an electron-rich site, i.e., the –N=N– azo groups (the chromophore centre of dye molecules) or the carbon near the secondary amino groups. Consequently, the degradation of azo groups would give place to the quick solutions decolourisation, whereas the attack to the amino groups would lead to the rupture between benzene or naphthalene rings and the triazine moiety. Afterwards, mono- or poly-hydroxylations of benzene and naphthalene structures would be produced. A subsequent ring cleavage (loss of absorbance at 254 nm) would generate aliphatic carboxylic acids (maleic, oxalic, acetic and formic) to finally yield CO_2 and water. At the same time, triazine structures would be slowly degraded to the recalcitrant cyanuric acid, which cannot be mineralised until the end of the photo-Fenton process [8, 9]. This compound would justify the residual DOC observed at the end of the oxidation, even under the most favourable conditions (see Sections 4.2.3, 4.2.4 and A.1.1 results). It has to be noted that, in agreement with this, a remaining DOC should have also been observed at the end of reaction in publications 4.2.1 and 4.2.2. The reason of this lack of DOC is of analytical nature. Finally, heteroatoms initially present in the molecule (except those contained in the triazine ring) would be gradually released into aqueous solution as sulphate, chloride, ammonium and

nitrate anions throughout oxidation. Nitrogen constituting the azo groups could also generate N_2 gas from their direct attack by HO•.

The last issue of the present doctoral dissertation consists of the development of several biological and chemical coupled treatments as alternatives to the photo-Fenton-aerobic biological coupling strategy. This time, Cibacron Red FN-R was chosen as a representative reactive azo dye to carry out the experimentation. The following manuscript submitted for publication includes this study (Section A.1.3):

The testing of several biological and chemical coupled treatments for Cibacron Red FN-R azo dye removal

A possible sequenced anaerobic-aerobic biotreatment was initially investigated. Azo bonds may be anaerobically reduced basically leading to the corresponding aromatic amines, compounds that are recalcitrant and toxic under reducing atmosphere but theoretically susceptible to further aerobic biodegradation [10].

Three different hydrolysed Cibacron Red FN-R solutions (250, 1250 and 3135 $mg \cdot l^{-1}$) were submitted to anaerobic digestion. Biogas production, % decolourisation and DOC reduction after digestion were monitored in order to evaluate the success of the anaerobic stage. As a result, complete decolourisation occurred for all concentrations with 92-97% effectiveness. Nevertheless, no DOC removal neither biogas production was observed from dye metabolites, indicating that no methanogenesis occurred. In addition, according to Biotox® and Zahn-Wellens assays, anaerobically generated colourless solutions (presumably containing the aromatic amines derived from azo bond cleavage) were found to be more toxic than the original dye solution and aerobically non biodegradable, impeding the biological two-stage treatment to complete degradation.

Thus, in order to mineralise Cibacron FN-R metabolites, the application of an AOP as a post-treatment of the anaerobic digestion was performed. The 250 $mg \cdot l^{-1}$ Cibacron Red FN-R solution was chosen for these experiments. Besides the artificial light photo-Fenton process, ozonation was considered due to its known efficient removal of many types of contaminants. Photo-Fenton was applied under different chosen Fenton reagent

concentrations (including the 20 mg·l^{-1} Fe (II)/500 mg·l^{-1} H_2O_2), whereas ozonation was performed under different initial pH conditions. The best results were obtained by means of ozonation at pH = 10.5, achieving 83% mineralisation. In contrast, the photo-Fenton reaction was not efficient enough to completely oxidise the effluent. Just 59% of DOC removal of the anaerobically treated solution was attained under the highest tested dosage (100 mg·l^{-1} Fe (II)/2500 mg·l^{-1} H_2O_2), mostly attributable to a non oxidative process based on iron coagulation.

These results open the possibility of an anaerobic-chemical sequenced treatment for aerobically non biodegradable azo dyes removal, being of special interest for real textile wastewater applications.

References

[1] López-Grimau V., Gutiérrez M.C. (2006). Decolourisation of simulated reactive dyebath effluents by electrochemical oxidation assisted by UV light. *Chemosphere*, 62, 106-112.

[2] Andreozzi R., Caprio V., Insola A., Marotta R. (1999). Advanced oxidation proceses (AOP) for water purification and recovery. *Catal. Today*, 53, 51-59.

[3] Scott J.P., Ollis D.F. (1995). Integration of chemical and biological oxidation processes for water treatment: review and recommendations. *Environ. Prog.*, 14, 88-103.

[4] Bauer R., Fallman H. (1997). The photo-Fenton oxidation-a cheap and efficient wastewater treatment method. *Res. Chem. Intermediat.*, 23, 341-354.

[5] Safarzadeh-Amiri A., Bolton J.R., Cater S.R. (1996). The use of iron in Advanced Oxidation Processes. *J. Adv. Oxid. Technol*., 1, 18-26.

[6] Bauer R., Waldner G., Fallmann H., Hager S., Klare M., Krutzler T., Malato S., Maletzky P. (1999). The photo-Fenton reaction and the TiO_2/UV process for waste water treatment–novel developments. *Catal. Today*, 53, 131-144.

[7] Pignatello J., Liu D., Huston P. (1999). Evidence for an additional oxidant in the photoassisted Fenton reaction. *Environ. Sci. Technol*., 33, 1832-1839.

[8] Huston P.L., Pignatello J. (1999). Degradation of selected pesticide active ingredients and commercial formulations in water by the photo-assisted Fenton reaction. *Water Res.*, 33, 1238-1246.

[9] Pérez M.H., Peñuela G., Maldonado M.I., Malato O., Fernández-Ibáñez P., Oller I., Gernjak W., Malato S. (2006). Degradation of pesticides in water using solar advanced oxidation processes. *Appl. Catal. B: Environ*., 64, 272-281.

[10] Carliell C.M., Barclay S.J., Buckley C.A. (1996). Treatment of exhausted reactive dyebath effluent using anaerobic digestion: Laboratory and full-scale trials. *Water S.A.*, 22, 225-233.

4.2. PUBLICATIONS

4.2.1. Decolourisation and mineralisation of homo- and hetero-bireactive dyes under Fenton and photo-Fenton conditions.

Coloration Technology, 120 (2004) 188-194.

Torrades F., García-Montaño J., García-Hortal J.A., Núñez Ll., Domènech X., Peral J.

4.2.2. Decolorization and mineralization of commercial reactive dyes under solar light assisted photo-Fenton conditions.

Solar Energy, 77 (2004) 573-581.

Torrades F., García-Montaño J., García-Hortal J.A., Domènech X., Peral J.

4.2.3. Degradation of Procion Red H-E7B reactive dye by coupling a photo-Fenton system with a sequencing batch reactor.

Journal of Hazardous Materials, 134 (2006) 220-229.

García-Montaño J., Torrades F., García-Hortal J.A., Domènech X., Peral J.

4.2.4. Combining photo-Fenton process with aerobic sequencing batch reactor for commercial hetero-bireactive dye removal.

Applied Catalysis B: Environmental, 67 (2006) 86-92.

García-Montaño J., Torrades F., García-Hortal J.A., Domènech X., Peral J.

4.2.5. Environmental assessment of different photo-Fenton approaches for commercial reactive dye removal.

Journal of Hazardous Materials, 138 (2006) 218-225.

García-Montaño J., Ruiz N., Muñoz I., Domènech X., García-Hortal J.A., Torrades F., Peral J.

Decolorisation and mineralisation of homo- and hetero-bireactive dyes under Fenton and photo-Fenton conditions

Coloration Technology
Society of Dyers and Colourists

Francesc Torrades,[a,*] Julia García-Montaño,[b] José Antonio García-Hortal,[c] Lluís Núñez,[c] Xavier Domènech[b] and José Peral[b]

[a] *Departament d'Enginyeria Química, ETSEI de Terrassa, Universitat Politècnica de Catalunya, C/Colom 11, E-08222 Terrassa, Spain*
Email: francesc.torrades@upc.es

[b] *Departament de Química, Edifici Cn, Universitat Autònoma de Barcelona, E-08193 Bellaterra (Cerdanyola del Vallès), Spain*

[c] *Departament d'Enginyeria Tèxtil i Paperera, E.T.S.E.I. de Terrassa, Universitat Politècnica de Catalunya, C/Colom 11, E-08222 Terrassa, Spain*

Received: 10 February 2004; Accepted: 7 May 2004

The degradation of two commercial reactive dyes, CI Reactive Red 141 (homo-bireactive) and CI Reactive Red 238 (hetero-bireactive), using Fenton's reagent in the dark and under either artificial or solar irradiation, has been investigated. The main parameters that govern the complex reactive system, i.e. type of irradiation, temperature and initial concentrations of iron(II) and hydrogen peroxide, have been studied at pH 3. Temperature and the use of light have beneficial effects on the removal of colour, aromatic compounds, total organic carbon, acute toxicity, given as changes in EC_{50} values (against the marine photobacteria *Vibrio fischeri*) and changes in the biodegradability. The advanced oxidation processes used in this study have proven to be highly effective for the treatment of such types of reactive dyes and several advantages concerning the technique application arise from the study. The possibility of a combined advanced oxidation process–biological treatment is proposed.

Introduction

The textile industry produces large quantities of wastewater that is highly coloured and contains large concentrations of organic matter [1]. This type of dyehouse effluent can cause major aesthetic and environmental problems [2–4]. The major problem of colour in such effluent is produced by the residual dyes present after the dyeing process. Treatment technologies such as biological, physical and chemical processes have been used for colour removal. However, biological treatment technologies are insufficient for the decolorisation of textile wastewater [5], and the colour remains due to the non-biodegradable nature of the chromophoric groups, such as azo or nitro, bonded to the aromatic rings of the dyes. On the other hand, physical treatment technologies, such as coagulation/flocculation, activated carbon adsorption and membrane processes, can result in successful removal of colour from effluent but there is a disadvantage as these methods also lead to another form of waste (i.e. solid waste such as spent carbon or sludge).

Therefore, in the last decade, attention has focused on treatment technologies that lead to the complete destruction of the dye molecules. Among these treatments, advanced oxidation processes (AOPs) have been used for pollutant abatement due to the high oxidative power (2.8 V vs NHE) of the hydroxyl radical, the main reactive species generated by such processes. The most widely known AOPs include heterogeneous photocatalytic oxidation [6–11], treatment with ozone in basic or neutral media [often combined with hydrogen peroxide, ultraviolet (UV) light or both] [12–14], hydrogen peroxide/UV systems [2,15–18], and Fenton [4,9,19–22] and photo-Fenton reactions [9,20,23–25].

The major disadvantage of AOPs is their high electrical energy input and chemical requirements rendering them energy intensive and hence expensive treatment alternatives, thus hindering their adoption in full scale applications [26]. The production of photons with artificial light sources in particular requires an important energy input. Fortunately, the photo-Fenton reaction can be driven with low energy photons in the visible part of the spectrum. Thus, photo-Fenton processes are a potentially low cost AOP that can be run under solar irradiation [25].

In the generally accepted mechanism of reaction with Fenton's reagent, hydroxyl radicals ($^{\bullet}OH$) are produced by interaction of hydrogen peroxide with ferrous salts (Eqn 1).

$$Fe^{2+} + H_2O_2 \rightarrow Fe^{3+} + {}^{\bullet}OH + {}^{-}OH \quad k = 76.5\ l\ mol^{-1}\ s^{-1} \quad (1)$$

Iron(III) can then react with hydrogen peroxide in the so-called Fenton-like reaction (Eqns 2–4):

$$Fe^{2+} + H_2O_2 \rightleftharpoons FeOOH^{2+} + H^+ \quad K_{eq} = 3.1\times10^{-3} \quad (2)$$

$$Fe - OOH^{2+} \rightarrow HO_2^{\bullet} + Fe^{2+} \quad k = 2.7\times10^{-3}\ s^{-1} \quad (3)$$

$$Fe^{3+} + HO_2^{\bullet} \rightarrow Fe^{2+} + O_2 + H^+ \quad k < 2\times10^{3}\ l\ mol^{-1}\ s^{-1} \quad (4)$$

in order to regenerate iron(II) and, thus, supporting the Fenton process [15].

The rate of degradation of the organic pollutants by the Fenton reaction could increase if an irradiation source is present. The positive effect of irradiation on the degradation rate is due to the photoreduction of iron(III) to iron(II) ions, a step that produces new hydroxyl radicals and regenerates iron(II) ions that can further react with more hydrogen peroxide molecules. The photoreduction of iron(III) follows Eqn 5 [15]:

$$FeOH^{2+} + h\nu \rightarrow Fe^{2+} + {}^{\bullet}OH \qquad (5)$$

with $Fe(OH)^{2+}$ being the dominant iron(III) species in solution at pH 2–3. On the other hand, it has been proven that the irradiation of iron(III) and hydrogen peroxide enhances the reaction rate of oxidant production, through the involvement of high valence iron intermediates responsible for the direct attack on organic matter [27,28]. Absorption of visible light by the complex formed between iron(III) and hydrogen peroxide seems to be the cause of formation of such high valence iron-based oxidants.

As organic molecules, dyes can be the target of hydroxyl radical attack and thus, the previously described Fenton and photo-Fenton reactions can be eventually effective techniques for the removal of such contaminants from water. In this sense, the purpose of the present study is the degradation of two commercial hydrolysed reactive dyestuffs, i.e. one bis-aminochlorotriazine bifunctional (CI Reactive Red 141) and one vinylsulphone fluorotriazine heterobifunctional (CI Reactive Red 238), by using Fenton and photo-Fenton reactions. In order to achieve this, the main parameters that govern the complex reactive system, i.e. type of irradiation, temperature, initial iron(II) and hydrogen peroxide concentrations, have been studied. The analytical techniques used involved colour removal, aromatic compound removal (UV_{254}) and total organic carbon (TOC).

Moreover, an additional goal of the paper was to obtain a non-toxic and biodegradable effluent, in order to assess the possibility of a combined AOP–biological treatment. Consequently, chemical oxygen demand (COD), five day biochemical oxygen demand (BOD_5) and acute toxicity (EC_{50}) was studied.

Experimental

Reagents

Two commercially available reactive dyestuffs, CI Reactive Red 141 ($C_{52}H_{34}O_{26}S_8Cl_2N_{14}$) and CI Reactive Red 238 ($C_{29}H_{15}ClFN_7O_{13}S_4Na_4$) were supplied by Ciba.

The preparation of the dye solutions was as follows. CI Reactive Red 141 (0.1000 g) was dissolved in 1 l of distilled water to make a dye solution typical of reactive dyebath effluent (100 mg/l). The solution was adjusted to pH 10.6 using sodium hydroxide (6 mol/l), followed by heating to 80 °C in a reflux system, where it was kept for 6 h to simulate batch-dyeing conditions. The hydrolysed dye solution was then cooled to the test temperature, adjusted to pH 3 with sulphuric acid (6 mol/l) and stored at 4 °C. CI Reactive Red 238 solution (100 mg/l) was prepared in a similar manner. However, the heating was kept to 60 °C for 1 h to simulate bath-dyeing conditions.

Analytical grade hydrogen peroxide (33% w/v) and $FeSO_4 \bullet 7H_2O$ were purchased from Panreac and were used as received. For the pH adjustment solutions, concentrated reagent grade sulphuric acid and sodium hydroxide solutions, obtained from Panreac, were used. Solutions were prepared with deionised water obtained from a Millipore Milli-Q system.

Sample analysis

Chemical analysis

The absorption spectra of the dye solution were recorded by using a Shimadzu UV-1603 double beam spectrophotometer. The absorbance of the solution at the absorption maximum (λ_{max}) of the dye in the visible region (CI Reactive Red 141, λ_{max} 543.5 nm; CI Reactive Red 238, λ_{max} 542.5 nm), and the UV_{254} absorbance (aromatic content), were measured by using 10 mm light path cells.

Total organic carbon (TOC) of initial and irradiated samples was determined with a Shimadzu 5000 TOC analyser.

All COD values were determined by the close reflux colorimetric method [29] with a HACH DR-700 apparatus. The residual H_2O_2 was determined by the potassium iodide titration method [30].

Biodegradability measurements

The measurement of BOD_5 values was performed by means of a mercury-free WTW 2000 Oxytop unit thermostatted at 20 °C. Here, due to the toxic character of hydrogen peroxide, its removal with SO_3^{2-} was found to be necessary before the BOD_5 analysis, since the microorganisms used in this technique cannot endure the presence of the oxidant.

The Zahn–Wellens test was carried out under conditions close to those of a municipal wastewater treatment plant using activated sludge [31]. The activated sludge from the municipal wastewater treatment plant of Manresa (Catalonia Community, Spain) was aerated for a 24 h period and centrifuged subsequently. The centrifuged sludge was then suspended at 0.2–0.3 g/l for the Zahn–Wellens test.

Toxicity analysis

The toxicity was assessed using the Biotox technique. According to the sample preparation prior to the Biotox test, the pH of the solutions was adjusted to 7 and solid sodium chloride was added in order to adjust the salinity to 2%. Residual hydrogen peroxide was removed from the solution with *Catalase* (2350 U per mg; Sigma), according to the following specifications: 1 U destroys 1 μmol min^{-1} of hydrogen peroxide at pH 7 and temperature 25 °C. Fe ion (mainly Fe^{3+})was precipitated out prior to assay by increasing the pH.

The test is based on the determination of the acute toxicity that the sample has on the marine photobacteria *Vibrio fischeri*. The toxicity is quantified as the relative decrease of the photobacteria light emission with respect to a sample control that only contained the dilution medium, i.e. sodium chloride, 2% w/v. The analysis generates the EC_{50} parameter (the concentration of toxicant that causes a 50% decrease of the light emission), which

is determined by interpolation from a series of dilutions of the original toxicant sample that have been in contact with the photobacteria during 30 min. A graph is plotted with the *x*-axis containing TOC% (compared to the total TOC content of the initial sample) and the *y*-axis displays the light emission of the marine photobacteria that reduces to half the photobacteria light activity. EC_{50} values were expressed as a percentage of TOC of the original toxicant sample and they are inversely correlated to the toxicity (the more toxic, the lower the EC_{50} value). When the TOC of the original toxicant samples were lower than the EC_{50}, these values were given as > 100%.

Reactors and light sources

Almost all experiments were conducted in a thermostatic cylindrical Pyrex cell of 130 ml capacity. The reaction mixture inside the cell, consisting of 100 ml of dye sample (100 mg/l) and the precise amount of Fenton's reagent, was continuously stirred with a magnetic bar and the temperature fixed at the required level (25, 40 or 60 °C at ± 1 °C). In order to maintain standard conditions, the Fenton reactions were carried out in darkness [19].

When experiments with CI Reactive Red 141 were performed using solar light, the temperature rose from 33 to 42 °C at the end of the 2 h. In the case of CI Reactive Red 238, the temperature rose from 30 to 40 °C. The yearly averaged solar energy between 300–400 nm hitting the earth's surface in the south of Spain is *ca.* $3–4 \times 10^{-3}$ W cm^{-2} [32].

A 6 W Philips black-light fluorescent lamp was used in the photo-Fenton experiments with artificial light. The intensity of the incident light inside the photoreactor, measured employing a uranyl actinometer, was 1.38×10^{-9} Einstein s^{-1} for the fluorescent lamp. Based on this number, the reactor geometry and the lamp emission spectrum it was estimated that a total power of luminous energy entering the reactor was 1.3×10^{-4} W cm^{-2}.

Results and Discussion

Analysis of the hydrolysed dye samples

UV–visible spectra

The absorption spectra of the CI Reactive Red 141 solution (100 mg/l) before AOP treatment at pH 3 is characterised by two main bands, one in the visible region (λ_{max} 543.5 nm) and the other in the UV region (λ_{max} 289.0 nm) (Table 1). As indicated by Silverstein *et al.*, the visible band at 543.5 nm is due to the long conjugated π-system of aromatic rings connected by two azo groups [33]. The UV band at 289 nm is due to two adjacent rings.

In the absorption spectra of CI Reactive Red 238, there are also two main bands, one in the visible region (λ_{max} 542.5 nm) and one in the UV region (λ_{max} 286.5 nm) (Table 1).

Biodegradability measurements

Prior to treatment it was concluded, by means of a Zahn–Wellens test (data not shown), that both dyes were of non-biodegradable nature. It was also found that a BOD_5/COD ratio value of 0.10 and 0.02 was obtained for CI Reactive Red 141 and CI Reactive Red 238, respectively (Table 1).

Toxicity analysis

As the calculated EC_{50} value was greater than 100% for both dyes (> 17.68 and 29.94 ppm for CI Reactive Red 141 and CI Reactive Red 238, respectively), it can be concluded that neither dye showed any evidence of toxicity (Table 1).

Fenton and photo-Fenton reactions of the hydrolysed dyes

Reaction in the dark

In order to achieve the best degree of decolorisation and mineralisation of the dye, optimal concentrations of hydrogen peroxide and iron(II) were required. For mineralisation, a good level of hydrogen peroxide is thought to be *ca.* 1–2 times the stoichiometric requirements [23] (1 g COD = 0.03125 mol oxygen = 0.0625 mol hydrogen peroxide). The COD values for the hydrolysed dyes, before treatment, are shown in Table 1.

However, for the purposes of decolorisation, the removal of colour is associated with the break of the conjugated unsaturated bonds in molecules. Consequently, hydrogen peroxide may be used in smaller quantities than those calculated from a COD value [19], and the optimal concentration in the dye/hydrogen peroxide/iron(II) system will depend on the degree of degradation that is to be achieved. A good degree of degradation would be associated with the attainment of a decoloured, low organic loaded, biodegradable and non-toxic effluent.

For a 10 mg/l (0.18 mM) sample of iron (II), a range of concentrations of hydrogen peroxide were tested: 50, 100, 150, 250, 500 and 1000 mg/l (1.47, 2.94, 4.41, 7.35, 14.7 and 29.4 mM, respectively). For CI Reactive Red 141, the best results for colour, UV_{254} and TOC removal were obtained at a peroxide concentration of 100 mg/l (2.94 mM) (Figure 1). For CI Reactive Red 238, the best results were obtained at a peroxide concentration of 250 mg/l (7.35 mM) for colour, UV_{254} and TOC removal (Figure 2).

The treatment time had a significant effect on degradation process, as can be seen in both Figures 1 and 2. The results shown in Figure 3, show the effect of varying the treatment time at specific hydrogen peroxide concentrations with a plot of A/A_0 or TOC/TOC_0 vs time. A/A_0 is the normalised absorbance and is the quotient between the absorbance

Table 1 Environmental characterisation of the hydrolysed dye samples

Dye	Dye conc. (mg/l)	λ_{max} (nm)	TOC (mg/l)	COD (mg/l)	BOD_5	BOD_5/COD	EC_{50} (mg/l)
CI Reactive Red 141	100	543.5,289.0	17.68	50	5	0.10	> 17.68[a]
CI Reactive Red 238	100	542.5,286.5	29.24	110	2	0.02	> 29.24 [a]

a EC_{50} > 100%

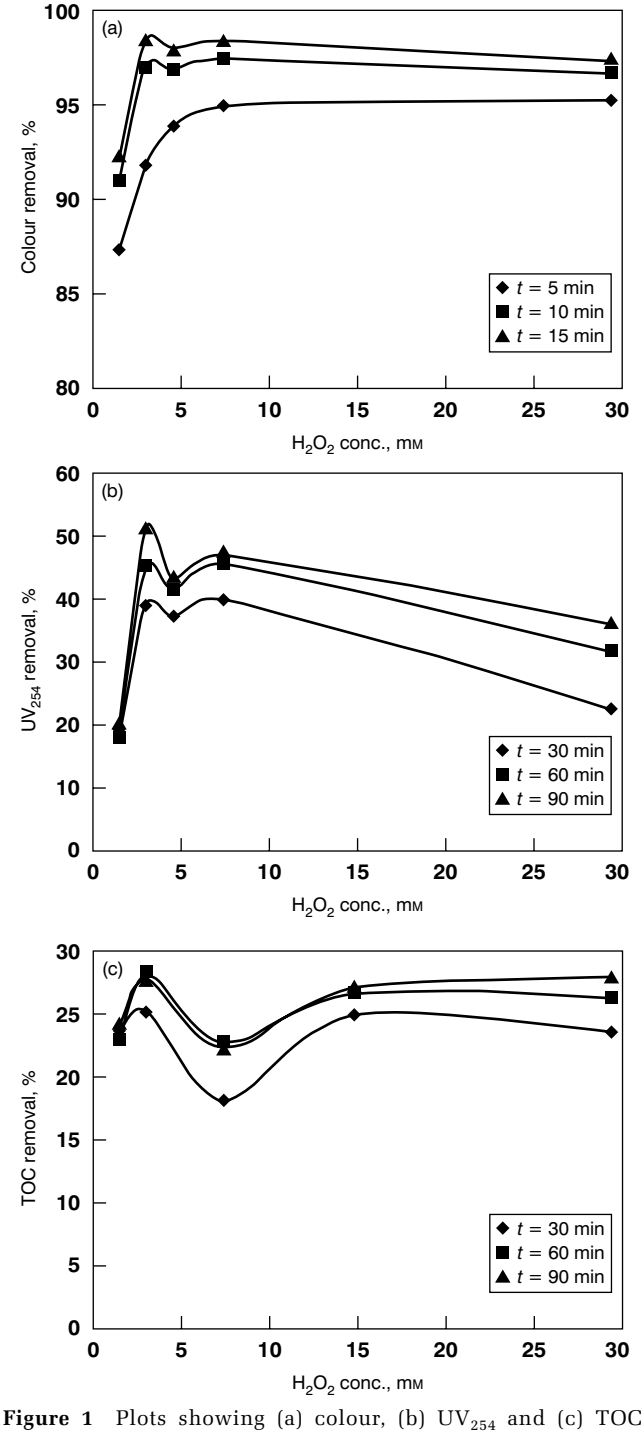

Figure 1 Plots showing (a) colour, (b) UV_{254} and (c) TOC removal for CI Reactive Red 141 for different concentrations of hydrogen peroxide; $[Fe^{2+}]_0$ = 10 mg/l (0.18 mM), pH = 3 and T = 25 °C

at time t (A) and at t = 0 (A_0). For CI Reactive Red 141, at a hydrogen peroxide concentration of 100 mg/l, more than 98% colour removal was obtained after 15 min, along with more than 50% UV_{254} and 28% TOC removal after 90 min treatment (Figure 3). The decrease of these parameters is initially fast, although it slows down for long treatment times. For CI Reactive Red 238, at a hydrogen peroxide concentration of 250 mg/l, more than 97% colour removal was obtained after 15 min treatment, along with more than 41% UV_{254} and 24% TOC removal after 90 min treatment.

For hydrogen peroxide concentrations below 100 mg/l for CI Reactive Red 141 and 250 mg/l for CI Reactive Red 238, insufficient oxidant is available to destroy the dye, as can be seen from the initial COD value. On the other hand, a further increase in oxidant concentration slows down the decolorisation and degradation processes, because hydrogen peroxide in excess acts as a hydroxyl-radical scavenger as shown by the following kinetic equation (Eqn 6) [34].

$$^{\bullet}OH + H_2O_2 \rightarrow H_2O + HO_2^{\bullet}$$
$$k = (1.2-4.5)\times 10^7 \text{ l mol}^{-1} \text{ s}^{-1} \quad (6)$$

The effect of temperature on the Fenton reaction (in the dark) was also tested. It is important to remark that in comparison to most industrial wastewater, the temperature

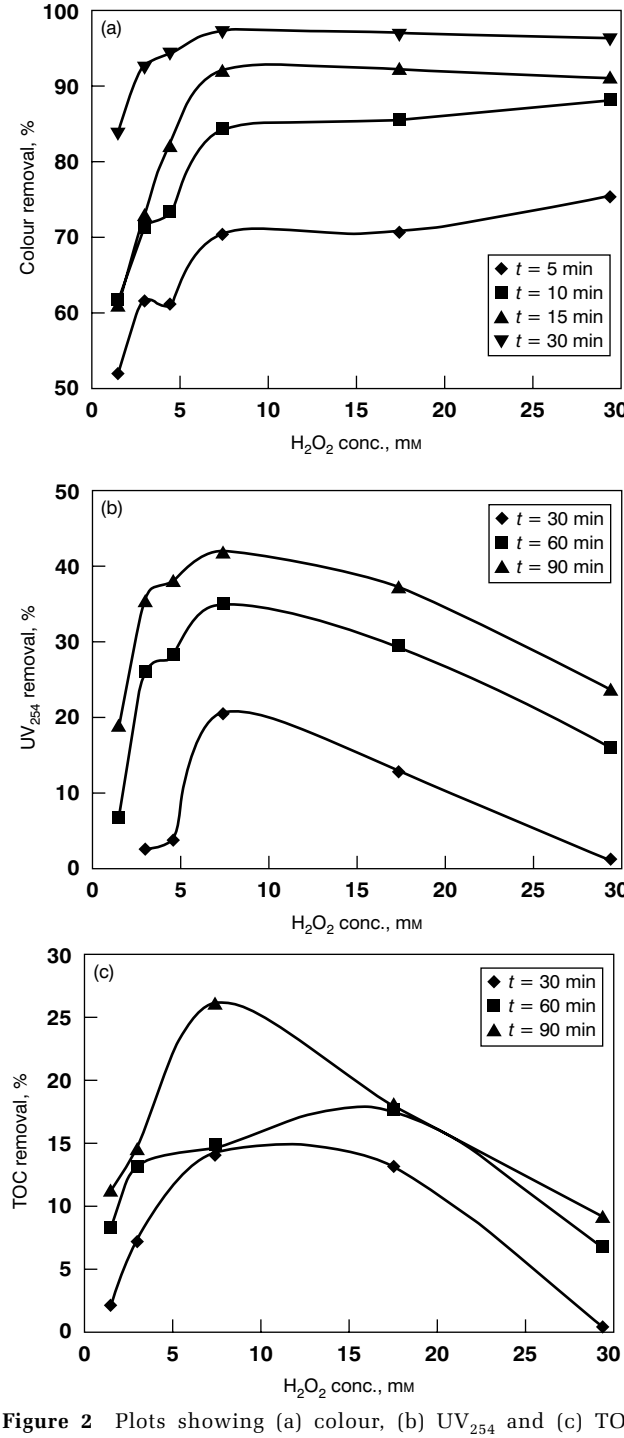

Figure 2 Plots showing (a) colour, (b) UV_{254} and (c) TOC removal for CI Reactive Red 238 for different concentrations of hydrogen peroxide; $[Fe^{2+}]_0$ = 10 mg/l (0.18 mM), pH = 3 and T = 25 °C

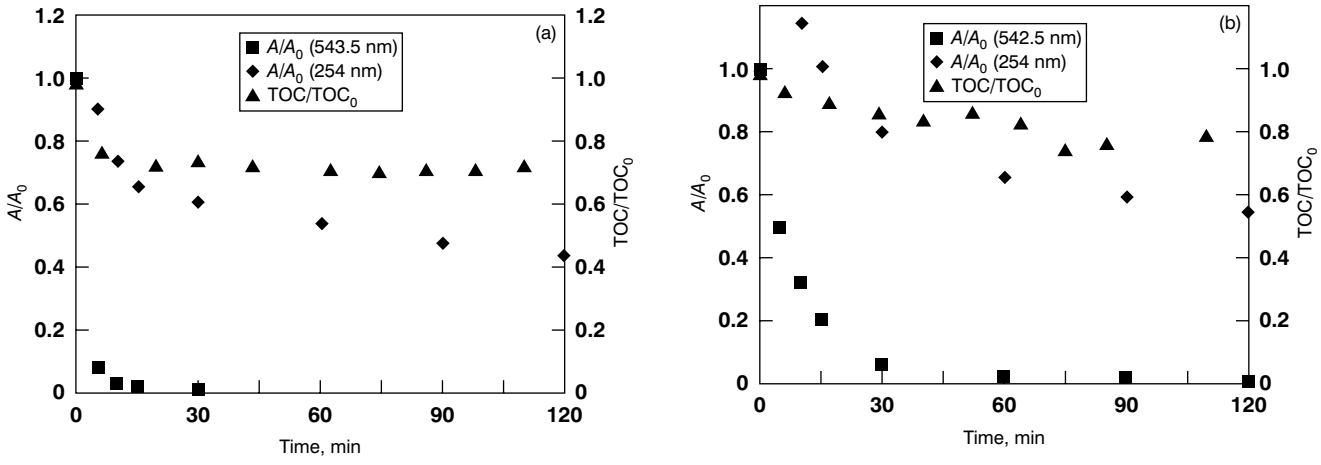

Figure 3 Colour, UV_{254} and TOC removal of (a) CI Reactive Red 141 (H_2O_2 conc., 100 mg/l) and (b) CI Reactive Red 238 (H_2O_2 conc., 250 mg/l) at various treatment times; $[Fe^{2+}]_0$ = 10 mg/l (0.18 mM), pH = 3 and T = 25 °C

of effluent from dyeing and finishing mills is unusually high. During the dyeing process, rinse water temperature higher than 40 °C is normally encountered [35]. Consequently, the effect of different temperatures (25, 40 and 60 °C) on the degree of degradation of the dye was tested. In all cases for CI Reactive Red 141 and CI Reactive Red 238, raising the temperature gave good results in relation to degradation of the dyes in terms of colour (data not shown), UV_{254} (Figure 4) and TOC (Figure 5). These results agree with the known fact that the Fenton reaction is accelerated with increasing temperatures [20,21]. It has to be said that the differences in colour removal, UV_{254} and TOC removal rate are obtained in the first 15 min of reaction. For longer reaction times, when the rate decreases changes in temperature seem to have no effect (Figures 4 and 5). This is the time region where iron(II) concentration is close to zero, the Fenton reaction is minimal, and the much slower Fenton-like reaction is controlling the process.

Reaction under irradiation

As mentioned before, when using Fenton's reagent in the presence of an irradiation source (photo-Fenton process) the rate of degradation of the organic pollutants could increase. In this sense, the effects of artificial (UVA) light and solar light on TOC and UV_{254} removal was also investigated (see Figures 4 and 5). The results show that the best UV_{254} and TOC removal rates were always obtained in the presence of light.

Although attempts to monitor colour removal were also carried out, the disappearance was too fast in presence of light. Light can play two different roles that will lead to an improvement of the reaction yields. Firstly, it drives the photo-Fenton reaction, producing extra hydroxyl radicals and the recovery of iron(II) needed in the Fenton reaction. The photo-Fenton reaction may involve direct photolysis of ferric iron (Eqn 5) or photolysis of iron(III)–peroxy complexes, or any of their potential intermediates [28].

Secondly, it can drive ligand-to-metal charge transfer in the potentially photolabile complexes formed by iron(III) and the organic compounds, a process that has been well proven for the complexes formed between iron(III) and the carboxylic acid moiety [36]. Large quantities of carboxylic acid are expected to be formed as degradation intermediates of the original organic substrate.

Additionally, solar light has the largest fraction of photons with the energy needed to drive the photoreactions involved in the present reactive system and, consequently, solar light gives the best results in UV_{254} and TOC removal (as shown in Figures 4 and 5). This opens up the possibility of extended low cost applications. For CI Reactive Red 141, a 98% TOC removal is obtained after 15 min treatment and more than 80% UV_{254} after 60 min, when using solar light as the light source. For CI Reactive Red 238 the results were more than 98% TOC removal after 45 min along with more than 70% UV_{254} after 60 min. Results of the optimised treatment systems, at a treatment time of 90 min, in terms of the parameters UV_{254} removal and TOC removal are summarised in Table 2.

It has to be pointed out that the remaining absorption at 254 nm seen in Figure 4 was due to the residual hydrogen peroxide present in the effluent and the presence of several complexes of iron that absorb photons of this wavelength. In this study, residual hydrogen peroxide concentrations (determined by the potassium iodide titration method [30]) of 5–20 mg/l were found at the end of all the experiments. Hydrogen peroxide analysis also showed a correlation between the peroxide consumption and TOC/colour/COD abatement rate. For example, in an experiment with hydrogen peroxide (125 mg/l) and CI Reactive Red 141 (250 mg/l), initial reaction rates of reagent removal were 3.4 (peroxide) and 2.7 mg/l/min (dye). In an experiment with equivalent concentrations of hydrogen peroxide and CI Reactive Red 238, initial reaction rates were 0.96 (peroxide) and 0.62 mg/l/min (dye). Clearly, a faster TOC/colour/COD removal reaction involves a faster hydrogen peroxide consumption.

The fast colour removal of the dye and the decrease of TOC and aromatic compounds is compatible with a degradation mechanism that begins with azo-bond cleavage and is followed by the hydroxylation of the aromatic ring, as indicated by several authors [37,38]. This mechanism leads to the production of sulphonated aromatic amines, carboxylic acids, quinones, carbon dioxide and other minority compounds.

The chemical observations described above are validated by the concomitant increase of biodegradability. As can be seen in Figure 6, a BOD_5/COD ratio of 0.31 and 0.21, respectively, is obtained for CI Reactive Red 141 (after

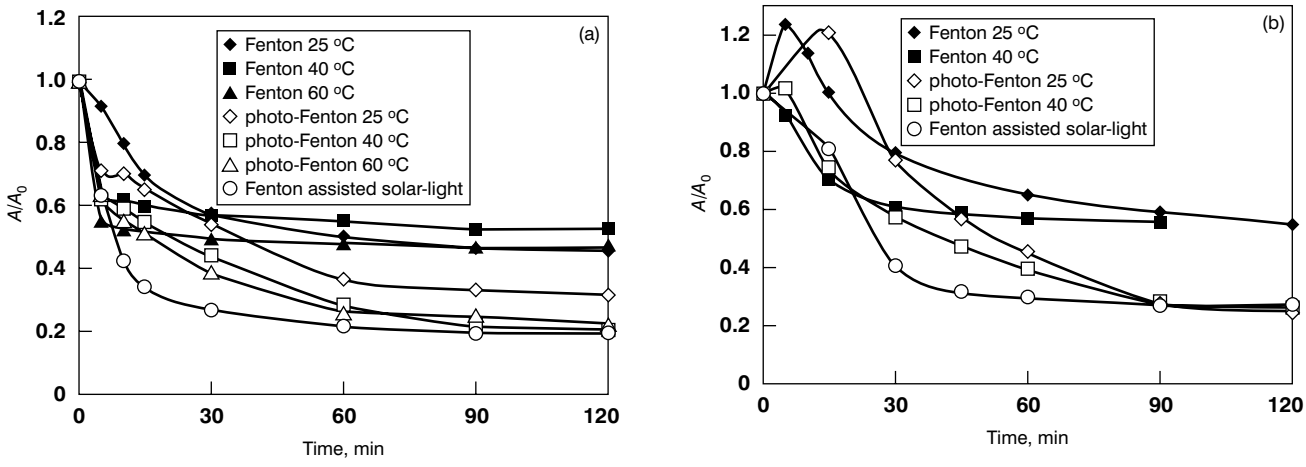

Figure 4 UV_{254} removal of (a) CI Reactive Red 141 (H_2O_2 conc., 100 mg/l) and (b) CI Reactive Red 238 (H_2O_2 conc., 250 mg/l) for different Fenton and photo-Fenton conditions; $[Fe^{2+}]_0$ = 10 mg/l (0.18 mM) and pH = 3

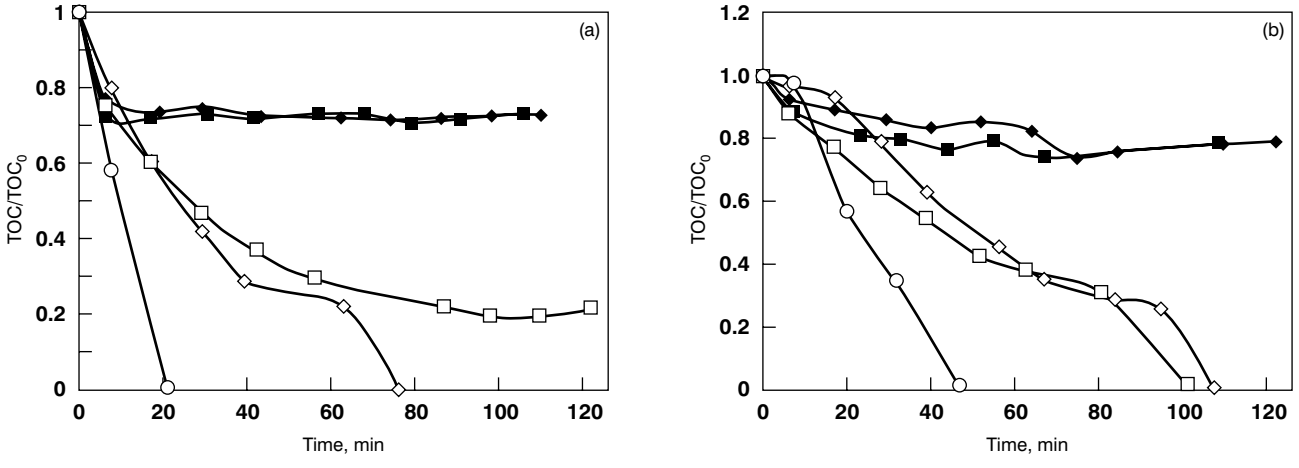

Figure 5 TOC removal of (a) CI Reactive Red 141 (H_2O_2 conc., 100 mg/l) and (b) CI Reactive Red 238 (H_2O_2 conc., 250 mg/l) for different Fenton and photo-Fenton conditions; for key see Figure 4; $[Fe^{2+}]_0$ = 10 mg/l (0.18 mM) and pH = 3

Table 2 UV_{254} and TOC removal for the hydrolysed dye samples under optimised process conditions[a]

	CI Reactive Red 141		CI Reactive Red 238	
Treatment	UV_{254} removal (%)	TOC removal (%)	UV_{254} removal (%)	TOC removal (%)
Fenton, 25 °C	51.8	28.0	41.8	24.0
Fenton, 40 °C	49.6	28.7	45.1	25.0
Photo-Fenton, 25 °C	66.9	100.0	71.7	74.0
Photo-Fenton, 40 °C	79.1	79.1	72.8	85.0
Fenton assisted solar-light	80.6	100.0[b]	73.1	98.6[c]

a Treatment time = 90 min
b Treatment time = 20 min
c Treatment time = 47 min

120 min) and CI Reactive Red 238 (after 180 min) of photo-Fenton treatment (artificial light).

It has to be pointed out that, in order to have reproducible BOD_5 results, the experiments were carried out with larger initial dye concentrations (250 mg/l) and thus, much longer reaction times are expected to achieve the same levels of degradation in the dyes. Also, as indicated in the Experimental section, due to the toxic character of hydrogen peroxide, its removal with SO_3^{2-} was found to be necessary before the BOD_5 analysis. Moreover, the COD values were corrected taking in account the residual hydrogen peroxide present.

On the other hand, the most important conclusion with respect to toxicity that can be drawn is that intermediates with higher toxicity than the initial dyes did not develop during the photo-Fenton treatment process, because the EC_{50} was greater than 100% after the various treatment times (5, 15, 60 and 120 min).

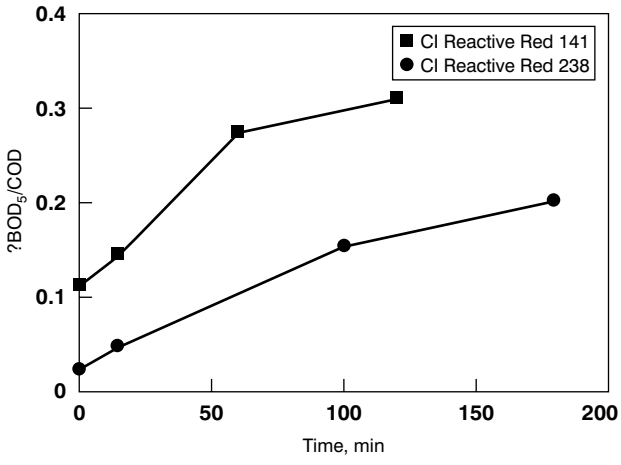

Figure 6 Variation of BOD_5/COD with treatment time for CI Reactive Red 141 (250 mg/l) and CI Reactive Red 238 (250 mg/l) (H_2O_2 conc., 125 mg/l); $[Fe^{2+}]_0$ = 10 mg/l (0.18 mM), pH = 3 and artificial light

Consequently, the positive effect of the Photo-Fenton treatment on the biodegradability of both dyes clearly indicates that coupling the photo-Fenton process with biological treatment might be a beneficial treatment approach.

Conclusions

This study has shown that, once the optimum operating conditions are established, the Fenton and photo-Fenton processes may be suitable methods for the complete decolorisation and mineralisation of effluent generated during the textile dyeing and finishing processes. In the Fenton treatment, the optimal dose of hydrogen peroxide used to degrade CI Reactive Red 141 and CI Reactive Red 238, were 100 and 250 mg/l, respectively. The introduction of artificial and solar light enhanced the Fenton process significantly. Particularly good results were obtained when using solar-light assisted Fenton treatment, opening up the possibility of low cost applications. Also, the results obtained show that the degradation of the homo-bireactive dye (CI Reactive Red 141) was easier than the hetero-bireactive dye (CI Reactive Red 238).

Moreover, the increase in the biodegradability ratio (expressed as the BOD_5/COD ratio) and the fact that no toxic oxidation products were detected during the photo-Fenton treatment have proven that chemical preoxidation allows the discharge of pretreated dyehouse effluent to sewage treatment facilities, as well as the direct disposal of the treated effluent into natural water bodies, provided that no toxic chemical contribution from other process stages of the textile manufacturing plant or dyehouse is expected.

Acknowledgements

The authors wish to thank Eduardo Puigvehí (Ciba) for the supply of dyes used in the present work, and also the Spanish government (Ministerio de Ciencia y Tecnología) for financial support (Project PPQ2002-04060-C02-01).

References

1. P Grau, *Water Sci. Technol.*, **24** (1991) 97.
2. D Georgiou, P Melidis, A Aivasidis and K Gimouhopoulos, *Dyes Pigm.*, **52** (2002) 69.
3. C O'Neill, F R Hawkes, D L Hawkes, N D Lourenço, H M Pinheiro and W Delée, *J. Chem. Technol. Biotechnol.*, **74** (1999) 1009.
4. W G Kuo, *Water Res.*, **26** (1992) 881.
5. A Uygur and E Kök, *J.S.D.C.*, **115** (1999) 350.
6. M R Hoffman, S T Martin, W Choi and D W Bahnemann, *Chem. Rev.*, **95** (1995) 69.
7. D F Ollis, in *Photochemical Conversion and Storage of Solar Energy*, Eds E Pelizzetti and M Schiavello (Dordrecht: Kluwer Academic Publishers, 1991).
8. H Lachheb, E Puzenat, A Houas, M Ksibi, E Elaloui, C Guillard and J M Herrmann, *Appl. Catal., B,* **39** (2002) 75.
9. I A Balcioglu, I Arslan and M Sacan, *Environ. Technol.*, **22** (2001) 813.
10. C M So, M Y Cheng, J C Yu and P K Wong, *Chemosphere*, **46** (6) (2002) 905.
11. C Lizama, M C Yeber, J Freer, J Baeza and H D Mansilla, *Water Sci. Technol.*, **44** (2001) 197.
12. L Sánchez, J Peral and X Domènech, *Appl. Catal., B,* **19** (1998) 59.
13. I Arslan and I A Balcioglu, *J. Chem. Technol. Biotechnol.*, **76** (2001) 53.
14. I Arslan, I A Balcioglu and D W Bahnemann, *Water Res.*, **36** (2002) 1143.
15. J Pignatello, *Environ. Sci. Technol.*, **26** (1992) 944.
16. M Neamtu, I Simiceanu, A Yediler and A Kettrup, *Dyes Pigm.*, **53** (2002) 93.
17. A M El-Dein, J A Libra and U Wiesmann, *Water Sci. Technol.*, **44** (2001) 295.
18. H-Y Shu, C-R Huang and M-C Chang, *Chemosphere*, **29** (12) (1994) 2597.
19. E G Solozhenko, N M Soboleva and V V Goncharuk, *Water Res.*, **29** (1995) 2206.
20. M Pérez, F Torrades, X Domènech and J Peral, *Water Res.*, **36** (2002) 2703.
21. M Pérez, F Torrades, J A Garcia-Hortal, X Domènech and J Peral, *Appl. Catal., B*, **36** (2001) 63.
22. E Chamarro, A Marco and S Esplugas, *Water Res.*, **35** (2001) 1047.
23. N H Ince and G Tezcanli, *Water Sci. Technol.*, **40** (1999) 183.
24. J Kiwi, C Pulgarin and P Peringer, *Appl. Catal., B,* **3** (1994) 335.
25. A Safarzadeh-Amiri, J R Bolton and S R Cater, *J. Adv. Oxid. Technol.*, **1** (1996) 18.
26. R Bauer and H Fallman, *Res. Chem. Intermed.*, **23** (1997) 341.
27. S H Bossmann, E Oliveros, S Göb, S Siegwart, E P Dahlen, L Payawan, M Straub, M Wörner and A M Braun, *J. Phys. Chem.,* **102** (1998) 5542.
28. J Pignatello, D Liu and P Huston, *Environ. Sci. Technol.*, **33** (1999) 1832.
29. *APHA-AWWA-WPCF: Standard Methods for the Examination of Water and Wastewater*, ASTM D1252-00, 17th Edn (Washington: ASTM, 1985).
30. C Kormann, D W Bahnemann and M R Hoffmann, *Environ. Sci. Technol.*, **22** (5) (1988) 798.
31. Test No. 302B, *OECD Guidelines for Testing of Chemicals*, Vol. 2 (Paris: OECS, 1996).
32. S Malato, personal communication (2003).
33. R M C Silverstein, G C Bassler and T C Morrill, *Spectrophotometric Identification of Organic Compounds* (New York: Wiley, 1991).
34. C H Walling, *Acc. Chem. Res.*, **8** (1975) 125.
35. S H Lin and C F Peng, *Water Res.*, **28** (1994) 277.
36. K A Hislop and J R Bolton, *Environ. Sci. Technol.*, **33** (18) (1999) 3119.
37. E Guivarch, S Trevin, C Lahitte and M A Oturan, *Environ. Chem. Lett.*, **1** (2003) 38.
38. J M Joseph, H Destaillats, H-M Hung and M R Hoffmann, *J. Phys. Chem. A*, **104** (2000) 301.

Available online at www.sciencedirect.com
SCIENCE DIRECT®
Solar Energy 77 (2004) 573–581
SOLAR ENERGY
www.elsevier.com/locate/solener

Decolorization and mineralization of commercial reactive dyes under solar light assisted photo-Fenton conditions

Francesc Torrades [a], Julia García-Montaño [b], José Antonio García-Hortal [c], Xavier Domènech [b], José Peral [b,*]

[a] *Departament d'Enginyeria Química, E.T.S.E.I. de Terrassa, Universitat Politècnica de Catalunya, C/Colom 11, E-08222 Terrassa, Barcelona, Spain*
[c] *Departament d'Enginyeria Tèxtil i Paperera, E.T.S.E.I. de Terrassa, Universitat Politècnica de Catalunya, C/Colom 11, E-08222 Terrassa, Barcelona, Spain*
[b] *Departament de Química, Edifici Cn, Universitat Autònoma de Barcelona, E-08193 Bellaterra, Cerdanyola del Vallès, Spain*

Received 2 December 2003; received in revised form 10 February 2004; accepted 31 March 2004
Available online 17 June 2004

Communicated by: Associate Editor Sixto Malato-Rodríguez

Abstract

The degradation of different commercial reactive dyes: a monoreactive dye (Procion Red H-E7B), an hetero-bireactive dye (Red Cibacron FN-R) and a Standard Trichromatic System, by using solar light assisted Fenton and photo-Fenton reaction is investigated. The reaction efficiencies have been compared with the ones obtained for the same system in the dark or under the assistance of an artificial light source. The use of solar light is clearly beneficial for the removal of color, aromatic compounds (UV_{254}), total organic carbon (TOC), and the increase of the BOD_5/COD ratio. The possibility of a combined advanced oxidation process (AOP)/biological treatment based on the use of sunlight is suggested.

Keywords: Reactive dyes; Decolorization; Advanced oxidation processes; Solar light; Fenton and photo-Fenton reactions

1. Introduction

Highly colored wastewaters are commonly discarded by the textile industry worldwide (Grau, 1991). The use of large amounts of dyestuffs during the dyeing stages of the textile manufacturing processes is the cause of such pollution (Georgiou et al., 2002; O'Neill et al., 1999). Apart from the aesthetic problems created when colored effluents reach the natural water currents dyes strongly absorb sunlight, thus impeding the photosynthetic activity of aquatic plants and seriously threatening the whole ecosystem (Kuo, 1992).

Most of the dyes disposed are of non-biodegradable nature and direct biological treatment of the colored effluents is not effective (Uygur and Kök, 1999). Consequently, physical or chemical treatments have to be used to completely degrade the dye, or to produce a partial degradation solution amenable to a secondary biological treatment. On the other hand, methods such as coagulation/flocculation, activated carbon adsorption and reverse osmosis can only transfer the contaminants from one phase to another leaving the problem essentially unsolved. Therefore, much attention has been paid to the development of water treatment techniques that lead to the complete destruction of the dye molecules. Due to the high oxidative power of the OH radical (2.8

* Corresponding author. Tel.: +34-93-581-2772; fax: +34-93-581-2920.
E-mail address: jose.peral@uab.es (J. Peral).

0038-092X/$ - see front matter © 2004 Elsevier Ltd. All rights reserved.
doi:10.1016/j.solener.2004.05.004

V versus NHE), several treatments based on the generation of such species, and catalogued under the designation of advanced oxidation processes (AOPs), have been used for general organic pollutant abatement. The most frequently used AOPs include: heterogeneous photocatalytic oxidation (Hoffman et al., 1995; Ollis, 1991; Pérez et al., 1997; Balcioglu et al., 2001; So et al., 2002; Lizama et al., 2001), treatment with ozone (often combined with H_2O_2, UVA or both) (Sánchez et al., 1998; Arslan and Balcioglu, 2001; Arslan et al., 2002), H_2O_2/UV systems (Georgiou et al., 2002; Neamtu et al., 2002; El-Dein et al., 2001; Shu et al., 1994), Fenton (Pignatello, 1992; Kuo, 1992; Balcioglu et al., 2001; Solozhenko et al., 1995; Pérez et al., 2002; Pérez et al., 2001; Chamarro et al., 2001) and photo-Fenton reactions (Balcioglu et al., 2001; Pérez et al., 2002; Ince and Tezcanli, 1999; Kiwi et al., 1994; Safarzadeh-Amiri et al., 1996).

Although generally effective a common drawback among AOPs is the requirement of large amounts of energy and/or chemicals to be spent (Bauer and Fallmann, 1997). Of particular importance is the fact that many of these techniques require consumption of high energy photons generated by artificial light, being the economical cost too high for practical applications. However, photo-Fenton reaction can be driven with low energy photons in the visible part of the spectrum. Thus, photo-Fenton processes are a potential low cost AOP that can be run under solar irradiation (Safarzadeh-Amiri et al., 1996).

In the generally accepted mechanism of Fenton reaction, hydroxyl radicals (OH·) are produced by interaction of H_2O_2 with ferrous salts:

$$\mathrm{Fe(II)} + \mathrm{H_2O_2} \rightarrow \mathrm{Fe(III)} + \mathrm{OH^{\cdot}} + \mathrm{OH^-} \quad (\text{rate constant}) = 76.5\ \mathrm{l\,mol^{-1}\,s^{-1}} \tag{1}$$

The rate of degradation of organic pollutants by Fenton reaction can be increased if an irradiation source is present. The positive effect of irradiation on the degradation rate is due to the photoreduction of Fe(III) to Fe(II) ions, a step that produces new OH· radicals and regenerates Fe(II) ions that can further react with more H_2O_2 molecules. The photoreduction of Fe(III) follows the equation:

$$\mathrm{FeOH^{2+}} + h\nu \rightarrow \mathrm{Fe^{2+}} + \mathrm{OH^{\cdot}} \tag{2}$$

$Fe(OH)^{2+}$ being the dominant Fe(III) species in solution at pH 2–3. On the other hand, it has been proven that the irradiation of Fe(III) + H_2O_2 mixtures, enhances the reaction rate of oxidant production, through the involvement of high valence Fe intermediates responsible for the direct attack to the organic matter (Bossmann et al., 1998; Pignatello et al., 1999). Absorption of visible light by the complex formed between Fe(III) and H_2O_2 seems to be the cause of formation of such high valence Fe-based oxidants.

As organic molecules, dyes can be the target of the OH· attack and thus, the above described Fenton and photo-Fenton reactions can be effective techniques for the removal of such contaminants from water. In this sense, the purpose of the present work is to characterize the simultaneous use of solar light and the Fenton and photo-Fenton reactions for the decolorization and mineralization of three reactive dyes: a common red dye with a monochlorotriazine reactive group (Procion red H-E7B), a last generation red dye of hetero-bireactive nature with fluorotriazine and vinylsulfone as reactive groups (Red Cibacron FN-R), and a Standard Trichromatic System. Especial emphasis has been placed in monitoring the evolution of the biodegradability of the dyes solutions during the reaction, in order to assess the possibility of a sequential AOP/biological treatment.

2. Experimental

The commercially available reactive dyestuffs, Procion Red H-E7B (CI Reactive Red 141), Cibacron Red FN-R and the components of the Standard Trichromatic System were supplied by CIBA. The preparation of dye solutions before applying Fenton and photo-Fenton processes was as follows: (a) 0.1000 g of as received Procion Red H-E7B were dissolved in 1 l of distilled water to make a dye solution typical of reactive dye-bath rinse effluents (100 $\mathrm{mg\,l^{-1}}$). The solution was adjusted to pH = 10.6 by using 6 M NaOH, followed by heating to 80 °C in a reflux system, where it was kept for 6 h to simulate bath-dyeing conditions. The hydrolyzed dye solution was then cooled to the test temperature, adjusted to pH = 3 with 6 M H_2SO_4 and stored at 4 °C. (b) The same procedure was used for the preparation of Cibacron Red FN-R solutions (100 $\mathrm{mg\,l^{-1}}$). However, to better simulate bath-dyeing conditions the heating was kept at 60 °C for 1 h. (c) 43 $\mathrm{mg\,l^{-1}}$ of Cibacron Yellow FN-2R, 43 $\mathrm{mg\,l^{-1}}$ of Cibacron Red FN-R, and 64.5 $\mathrm{mg\,l^{-1}}$ of Cibacron Navy FN-B were the concentrations of three components used in the Standard Trichromatic System (150.5 $\mathrm{mg\,l^{-1}}$ of total dye). In this case the hydrolysis was carried out at 60 °C during 1 h.

Analytical grade hydrogen peroxide 33% (m/V) and $FeSO_4 \cdot 7H_2O$ were purchased from Panreac and were used as received. Reagent grade H_2SO_4 and NaOH from Panreac were used for pH adjustments. Solutions were prepared with deionized water obtained from a Millipore Milli-Q system.

The Vis/UV-absorption spectra of the dye solutions were recorded by using a Shimadzu UV-1603 double beam spectrophotometer. The absorbance of the solutions at the absorption maximum of the dyes in the visible zone (λ_{max} = 543.5 nm for Procion red H-E7B,

$\lambda_{max} = 542.5$ nm for Cibacron FN-R, and $\lambda_{max} = 553$–587.5 for the Standard Trichromatic System), and the UV_{254} absorbance (aromatic content) were measured by using 10 mm light path cells. Total organic carbon (TOC) of initial and irradiated samples was determined with a Shimadzu 5000 TOC analyzer. All COD values were determined by the close reflux colorimetric method (APHA–AWWA–WPCF, 1985) with a HACH DR-700 apparatus. Biological oxygen demand (BOD_5) was performed by means of a Hg free WTW 2000 Oxytop unit thermostated at 20 °C. Sludge from a conventional biological wastewater treatment plant was used to prepare the high bacterial concentrations (0.2–0.3 g/l) required in the Zahn–Wellens tests (ECD, 1996).

Experiments were conducted in cylindrical Pyrex cell of 130 cm^3 capacity. The reaction mixture inside the cell, consisting of 100 ml of dye sample (100 mg/l) and the precise amount of Fenton reagent, was continuously stirred with a magnetic bar. Solar light experiments were performed during sunny days of July at Universitat Autònoma de Barcelona (45 m above sea level, 41°30′N, 2°6′E). The temperature of the reactor during those experiments rose from approximately 30 to 40 °C at the end of the 2 h. A 6 W Philips black-light fluorescent lamp was used in the artificial light photo-Fenton experiments, and the intensity of the incident light inside the photoreactor, measured employing a uranyl actinometer, was 1.38×10^{-9} Einstein s^{-1}.

3. Results

The degradation of the three dye solutions studied in this work was characterized by following two different experimental parameters: (a) absorption of the solution at 254 nm in an attempt to envisage the evolution of the aromatic moieties of the dyes; and (b) total organic carbon (TOC) in order to detect the possibility of complete organic matter removal. Also, evolution of the Vis/UV-absorption spectra with time was recorded for those experiments carried out with sunlight irradiation, being this an appropriate way of characterize the dye color evolutions during the reaction.

3.1. Procion Red

Fig. 1 shows the evolution of the absorbance at 254 nm of a 100 mg l^{-1} Procion Red solution for three different experimental situations: (a) Fenton reaction in absence of light; (b) Fenton and photo-Fenton reactions supported by irradiation with an artificial light source; and (c) Fenton and photo-Fenton reactions under solar light irradiation. The concentration of the Fenton reagent (10 mg l^{-1} Fe(II) + 100 mg l^{-1} H_2O_2) were chosen taking into account a previous and detailed study of Fenton reaction optimization during the degradation of

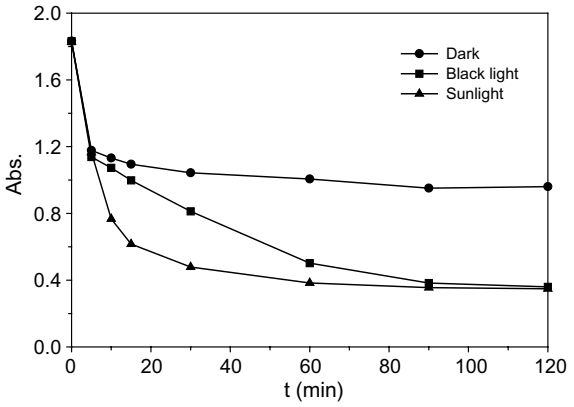

Fig. 1. Evolution of absorption at 254 nm with reaction time of Procion Red solutions (100 mg l^{-1}) for the three experimental conditions studied. $[Fe(II)]_0 = 10$ mg l^{-1}; $[H_2O_2]_0 = 100$ mg l^{-1}; pH = 3; $T = 40$ °C.

Procion Red and Cibacron dyes (Torrades et al., in press). In the three cases there is a noticeable decrease of the absorbance, specially during the first 5–10 min of the reactions. Nevertheless, there is also a clear effect attributable to the presence of light. Indeed, only minor changes of solution Vis/UV-absorption is observed after the first 10 min of Fenton reaction in the dark, and at the end of the reaction time it seems to be stabilized around 0.96 absorption units, while the use of either artificial light or sunlight produces a further absorbance decrease down to an approximated constant value of 0.35 absorption units. Although at 120 min of reaction both absorbances merge, the decrease is clearly faster when using sunlight.

Fig. 2 shows the TOC evolution during the experiments of Procion Red degradation shown in Fig. 1. A

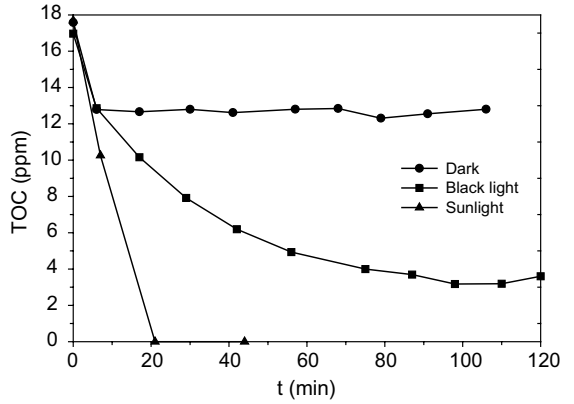

Fig. 2. TOC time course of Procion Red solutions (100 mg l^{-1}) for the three experimental conditions studied. $[Fe(II)]_0 = 10$ mg l^{-1}; $[H_2O_2]_0 = 100$ mg l^{-1}; pH = 3; $T = 40$ °C.

fast TOC decrease occurs in the first minutes of reaction, and a clear positive effect attributable to the presence of light takes place. Thus, the TOC of the solution remaining in the dark stabilizes at approximately 12.8 ± 0.5 mg l^{-1}, while artificial light stabilizes the TOC at approximately 3.6 ± 0.5 mg l^{-1}. It is noteworthy that almost complete removal of TOC is achieved in a maximum of 20 min when using sunlight, an interesting aspect if solar light is to be used in practical applications for the support of such reactive systems. It has to be pointed out that the dye molecule has a triazine moiety (see Section 1), and it is well known (Pelizzetti et al., 1992; Huston and Pignatello, 1999) that the mineralization of such structure by HO· attack is difficult and slow. Thus even in the most favourable cases a remaining TOC should have been expected in solution at the end of the reaction. The reason of the absence of TOC is of analytical nature. The initial TOC of the dye solutions were around 18 ppm, and the limit of detection of the TOC analyzer (low sensibility mode) was 1 ppm. On the other hand the dye molecule has 52 carbons (empirical formula $C_{52}H_{34}O_{26}S_8Cl_2N_{14}$), and even if all the organic carbon derived from the triazine moiety remains in solution at the end of the reaction, the corresponding TOC content would have been difficult to detect (around 1 ppm).

The evolution of the absorption spectra of Procion Red with time of reaction under solar light irradiation is shown in Fig. 3. As can be seen the large band of adsorption in the visible region, responsible of the colored character of the dye, completely disappears in less than 15 min. In fact, the visual analysis of the reaction indicated that the solution was colorless after the first 5 min of reaction. A remaining absorption in the UV region is indicative of the presence of some chemical that has a slow decay in the presence of light. The use of sunlight and Fenton reagents is, thus, an effective way of eliminating color in waters polluted with Procion Red dye.

3.2. Cibacron Red

As in the case of Procion Red the time course of absorbance at 254 nm of 100 mg l^{-1} Cibacron Red solutions were registered in the dark, under black light irradiation, and in the presence of sunlight. Fig. 4 shows the corresponding data. Again, as in the case of Procion Red, Cibacron Red absorbance in the dark during the first 20 min of reaction rapidly decreases and it remains stabilized at approximately 0.55 absorption units. The presence of light produces a further absorbance decrease, that is faster when sunlight is used as photon source. In both cases, artificial and natural light, the absorption stabilizes around 0.6 absorption units. It is also noteworthy the initial increase of absorbance observed when the reaction takes place in presence of light, specially in the case of solar light irradiation. As it will be discussed later this effect could be assigned to the absorbance of Fe(II) and H_2O_2 added in solution.

Fig. 5 shows data of TOC degradation in three experimental conditions used for Cibacron Red degradation. Again, the best scenario is attained when combining the Fenton reagents and sunlight, with almost complete TOC removal taking place in less than 50 min (see discussion above about the possible existence of non detected triazine mineralization products in solution). The assistance with black light can also lead the reactive system to a TOC level close to zero but in a much longer time (>100 min). The dark Fenton reaction alone is not

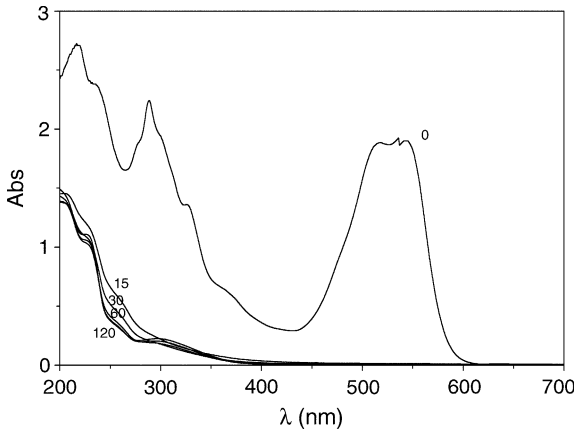

Fig. 3. Transient spectra of Procion Red solutions (100 mg l^{-1}) for the reaction carried out under solar light irradiation. The numbers indicate the reaction time (minutes) when the spectra were recorded. $[Fe(II)]_0 = 10$ mg l^{-1}; $[H_2O_2]_0 = 100$ mg l^{-1}; pH = 3; $T = 40$ °C.

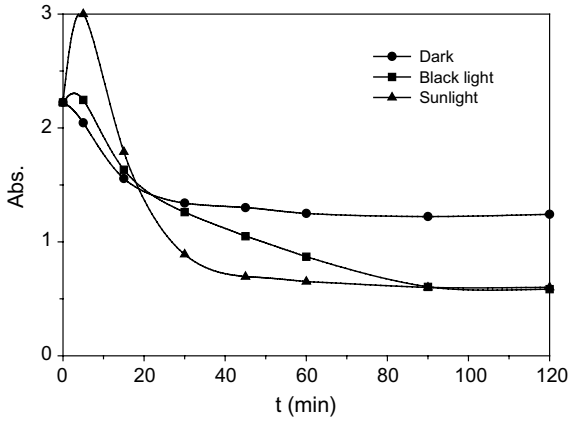

Fig. 4. Evolution of absorption at 254 nm with reaction time for Cibacron Red solutions (100 mg l^{-1}) for the three experimental conditions studied. $[Fe(II)]_0 = 10$ mg l^{-1}; $[H_2O_2]_0 = 250$ mg l^{-1}; pH = 3; $T = 40$ °C.

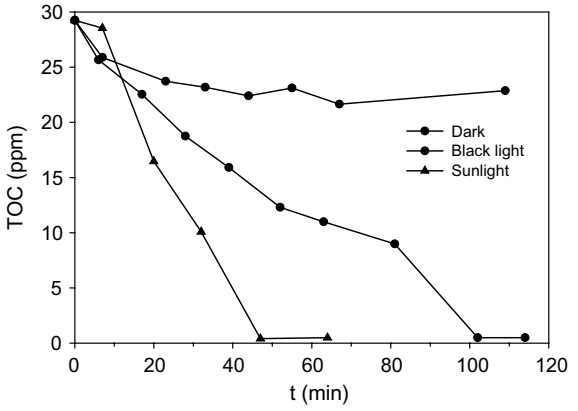

Fig. 5. TOC time course of Cibacron Red solutions (100 mg l^{-1}) for the three experimental conditions studied. $[Fe(II)]_0 = 10$ mg l^{-1}; $[H_2O_2]_0 = 250$ mg l^{-1}; pH = 3; $T = 40$ °C.

powerful in terms of TOC removal and only 25% of the solution organic content is mineralized after 110 min, when the reaction seems to have finished.

The evolution of absorption spectra of Cibacron Red with time of reaction when using solar light is shown in Fig. 6. Like in the case of Procion Red the large absorbance band in the visible region is completely removed at the end of the reaction. However, in this case the band decrease is slower, and after 15 min the dye solution still has a noticeable color. The strong absorption of the dye in the UV region also decreases and a residual absorption remains for long reaction times. The shape of the absorption bands in this region resemble the ones observed in the case of long reaction times of Procion Red degradation.

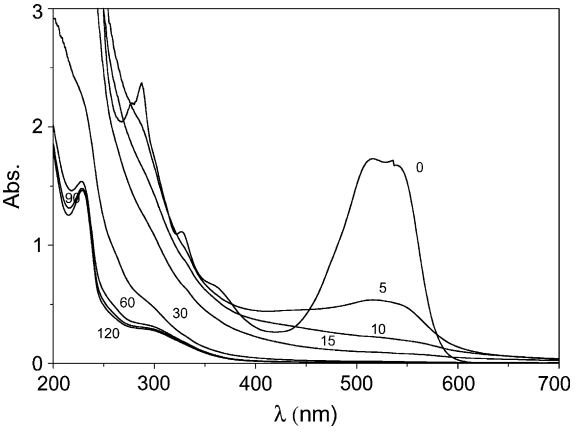

Fig. 6. Transient spectra of Cibacron Red solutions (100 mg l^{-1}) for the reaction carried out under solar light irradiation. The numbers indicate the reaction time (minutes) when the spectra were recorded. $[Fe(II)]_0 = 10$ mg l^{-1}; $[H_2O_2]_0 = 250$ mg l^{-1}; pH = 3; $T = 40$ °C.

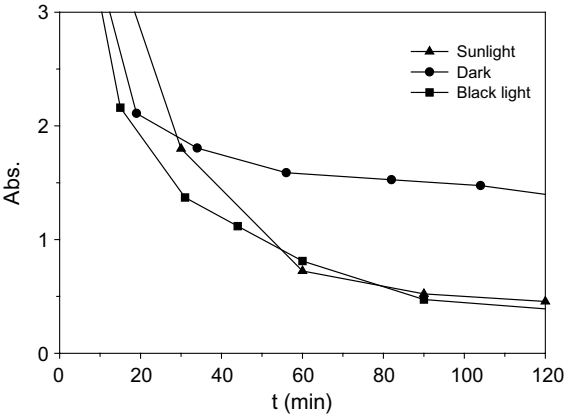

Fig. 7. Evolution of absorption at 254 nm with reaction time of the Standard Trichromatic System solutions (150 mg l^{-1}) for the three experimental conditions studied. $[Fe(II)]_0 = 10$ mg l^{-1}; $[H_2O_2]_0 = 250$ mg l^{-1}; pH = 3; $T = 40$ °C.

3.3. Standard Trichromatic System

The Standard Trichromatic System was chosen as model mixture of dyes that is widely used in the textile industry. Similar results were obtained if compared to the reactions with Procion Red and Cibacron Red solutions. The evolution of the absorbance at 254 nm with time is shown in Fig. 7. Again the simultaneous use of Fenton reagents and sunlight is an effective way of decreasing absorbance. In this case the system based on artificial light gives similar reaction rates, and very close levels of final absorbance are obtained with artificial and natural light. The dark reaction is the less efficient one, with a fast absorbance decrease in the first 20 min and a very slow decrease for longer reaction times. With this

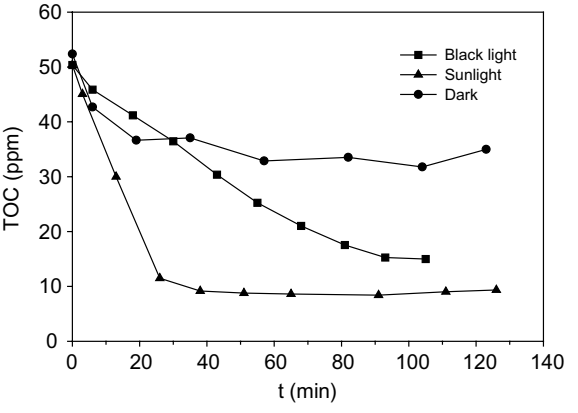

Fig. 8. TOC time course of Standard Trichromatic System solutions (150 mg l^{-1}) for the three experimental conditions studied. $[Fe(II)]_0 = 10$ mg l^{-1}; $[H_2O_2]_0 = 250$ mg l^{-1}; pH = 3; $T = 40$ °C.

dye mixture an initial absorbance increase is detected in the three experimental situations, the three of them being of similar magnitude.

The time course of TOC follows the same efficiency order: sunlight reaction > black light reaction > dark reaction (see Fig. 8). The TOC removal at the end of the dark reaction is discrete (35–40%), and it is noteworthy that, in this case, the solar light assisted reaction is not powerful enough as to completely remove TOC. A residual TOC content of approximately 9 ± 0.5 mg l^{-1} remains in solution after 120 min of reaction.

Finally, the evolution with time of the absorption spectra of the Standard Trichromatic System is shown in Fig. 9. In this case the absorption band that occupies the visible region from 400 to almost 700 nm also disappears, although taking more than 15 min for that (color disappearance). The absorption in the UV region decreases to a final shape and intensity that resembles those of Procion Red and Cibacron Red. The fact that the residual absorbance in the UV region, where both H_2O_2 and Fe aqueous species absorb, are similar for the three dye systems studied here indicates that the residual absorbance at 254 nm is caused by the presence of remaining concentrations of Fenton reagents.

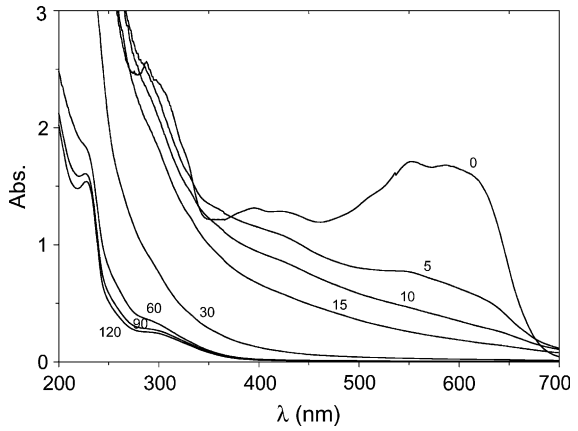

Fig. 9. Transient spectra of Standard Trichromatic System solutions (150 mg l^{-1}) for the reaction carried out under solar light irradiation. The numbers indicate the reaction time (minutes) when the spectra were recorded. $[Fe(II)]_0 = 10$ mg l^{-1}; $[H_2O_2]_0 = 250$ mg l^{-1}; pH = 3; $T = 40$ °C.

3.4. Biodegradability assays

One interesting alternative that is gaining importance among the potential techniques for non-biodegradable or toxic wastewater treatment is the combination of an AOP with a subsequent biological step. In this way the use of the AOP, the expensive part of the global procedure, is reduced to the attainment of a non-toxic and/or biodegradable solution, being the rest of the organic matter removed in the biological step. Since the dyes chosen in this study are of non-biodegradable nature (Zahn–Wellens tests were carried out to confirm this point) the above mentioned combination of treatments could be used to degrade them in aqueous solution. The key question concerning the combined use of an AOP and a biological treatment is to probe that the dye biodegradability and, particularly, the BOD_5/COD ratio increases during the AOP, approaching the value 0.4 that is considered the quantitative index for organic matter complete biodegradability (Scott and Ollis, 1995). Thus, BOD_5 and COD analysis of the treated Procion Red and Cibacron Red solutions were carried out in order to characterize the evolution of the BOD_5/COD ratio. The experiments were carried out by using the artificial light source, although attending to the data

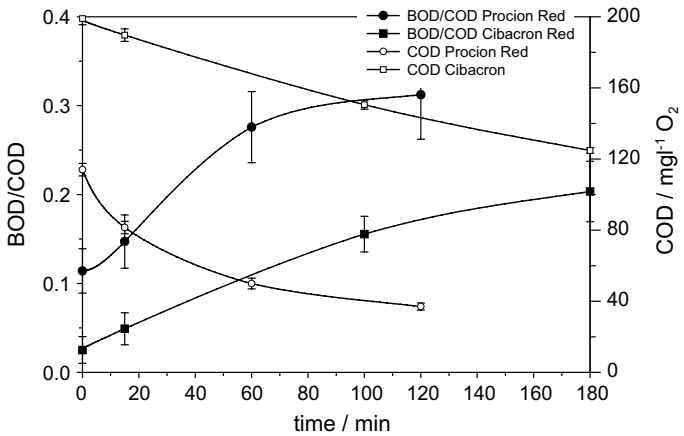

Fig. 10. Time course of the BOD_5/COD ratio and COD of 250 mg l^{-1} of Procion Red and Cibacron Red solutions under artificial light irradiation. $[Fe(II)]_0 = 10$ mg l^{-1}; $[H_2O_2]_0 = 125$ mg l^{-1}; pH = 3; $T = 25$ °C.

reported so far, similar or even more favourable situations are expected when using solar light. It is also noteworthy that, in order to have reproducible BOD_5 results the experiments were carried out with a larger initial dye concentration (250 $mg\,l^{-1}$) and thus, much longer reaction times are expected for the achievement of the same levels of TOC removal shown in Figs. 2 and 5. As can be seen in Fig. 10 the BOD_5/COD ratio increases with the reaction time, attaining values above 0.3 in the case of Procion Red and 0.2 in the case of Cibacron Red. Although these values are not above 0.4 they indicate an effective increase of biodegradability and, consequently, a possible coupling of solar assisted photo-Fenton Reaction with biological treatment.

4. Discussion

The consideration of the experimental data presented in the above section indicates a series of features expected for a Fenton based reaction. In this way, the absorbance at 254 nm of the three dye solutions always suffers a fast initial decrease, even in the dark, followed by a much slower disappearance. This can be explained with the large value of the Fenton reaction rate constant (Eq. (1), $k = 76.5\ l\,mol^{-1}\,s^{-1}$). Under the experimental conditions described here the initial 10 $mg\,l^{-1}$ of Fe(II) added to the solution would take only few seconds to completely oxidize to Fe(III) generating the corresponding stoichiometric amount of hydroxyl radicals. Is this initial amount of oxidant the one that causes the fast attack to the dye molecules causing a fast decoloration, as seen in Figs. 3, 6 and 9, along with a fast loss of the aromatic character of the dye. As indicated by several authors (Guivarch et al., 2003; Joseph et al., 2000) the attack of the hydroxyl radical to this family of dye molecules begins with the azo bond cleavage (loss of color) and it is followed by the hydroxylation of the aromatic ring (loss of absorbance at 254 nm). This mechanism leads to the production of sulfonated aromatic amines, carboxylic acids, quinones, CO_2, and other minority intermediates. On the other hand, this initial high reactivity is not enough to produce important changes of TOC since the complete mineralization of all carbons present in a dye molecule is a more complex process that needs the participation of larger amounts of oxidants and more time of reaction.

Once the initial Fe(II) has been consumed the process is controlled by the capability of the photo-Fenton reaction to regenerate it (Eq. (2)). Thus, a cycle where Fe(II) is consumed and regenerated is established, being the rate of the process controlled by the slower photo-Fenton reaction. That is the reason of the slower decrease of absorbance at 254 nm observed for the three dyes after the first minutes of reaction. In the dark reaction the photo-Fenton process takes not place, and the only way to recover Fe(II) is the so-called Fenton like reaction (Pignatello, 1992):

$$Fe^{3+} + H_2O_2 \leftrightarrow FeOOH^{2+} + H^+ \qquad K_{eq}\ \text{(equilibrium constant)} = 3.1 \times 10^{-3}\ l\,mol^{-1}\,s^{-1} \tag{3}$$

$$Fe\text{–}OOH^{2+} \rightarrow HO_2^{\cdot} + Fe^{2+} \quad k = 2.7 \times 10^{-3}\ s^{-1} \tag{4}$$

$$Fe^{3+} + HO_2^{\cdot} \rightarrow Fe^{2+} + O_2 + H^+ \qquad k < 2 \times 10^3\ l\,mol^{-1}\,s^{-1} \tag{5}$$

This is also a slow process that has only practical importance when large amounts of H_2O_2 are present in solution. This is not the present case where the concentration of H_2O_2 chosen is adjusted to the stoichiometric value needed for complete dye mineralization (e.g., COD of the Procion Red solution before reaction is approx. 50 $mg\,l^{-1}$). In consequence, the absorbance at 254 nm shows a very slow change with dark reaction time, and TOC is almost constant for long reaction times in the three dye solutions.

The presence of light is essential to maintain, through the photo-Fenton reaction, a continuous removal of the dye color and aromatic character. At this point it is important to differentiate between the results obtained with the artificial light source and the solar light. In almost all the experiments described above solar light gave more efficient degradation of the dyes than the artificial light. The wavelengths needed for the photo-Fenton reaction range from the UV up to 400 nm. The black light used was chosen because it gives a single emission band centred at 350 nm and having photons in the 300–400 nm range. It is a low power consumption lamp (6 W) that produces an output of photons that entirely matches the absorption requirements of the photo-Fenton reaction, and it seemed to be the most efficient light source in terms of active photons produced/energy consumed. As already mentioned in the experimental section the number of photons arriving to the reactor with such a lamp was 1.38×10^{-9} Einstein s^{-1}, and a simple calculation based on this number, the reactor geometry, and the lamp emission spectrum permitted to estimate a total power of luminous energy entering the reactor of $1.3 \times 10^{-4}\ W\,cm^{-2}$. This is one order of magnitude below of the yearly averaged solar energy between 300 and 400 nm arriving to the earth surface in the south of Spain (around $3\text{–}4 \times 10^{-3}\ W\,cm^{-2}$, Malato, 2003). Thus, the higher efficiency observed with the use of sunlight is basically due to the higher number of photons supplied by the sun. More powerful artificial light sources could have been tested but at the price of an increasing energy consumption. The good results obtained with sunlight along with the low economic cost and the lower environmental impact associated to the

use of this renewable energy source make the technique very appealing from the point of view of a real application.

Another aspect that has to be discussed is the remaining absorbance at 254 nm observed for the three dyes even when solar light is used. This can be explained by considering that H_2O_2 and several aqueous complexes of Fe absorb photons of this wavelength. It is obvious that the 10 mg l^{-1} of Fe(II) initially added to the solutions are still present at the end of the reactions, most probably in the form of Fe(III). On the other hand, the presence of residual amounts of H_2O_2 was proven by simple titration with standard KI solutions, basically for the correction of the COD values obtained. H_2O_2 concentrations from 5 to 20 mg l^{-1} were found at the end of all the experiments. Also, due to the toxic character of H_2O_2 its removal with SO_3^{2-} was found to be necessary before the BOD_5 analysis, since the microorganisms used in this technique cannot endure the presence of the oxidant. As pointed out in the previous section similarities exist between the residual absorption spectra observed in Figs. 3, 6 and 9, similarities that are also a probe of the similarities of the chemical species remaining in solution at the end of the three dyes degradation. Since complete TOC removal is observed in several of the experiments, these remaining species are not of organic nature, a fact that indicates that residual H_2O_2 and Fe species are the responsible for the observed absorption. Finally, another experimental observation that would be in agreement with the absorptive character of the Fenton reagents is the increase of absorbance at 254 nm that takes place at the beginning of several of the experiments (see Figs. 1, 4 and 7), when the addition of H_2O_2 and Fe(II) has just taken place, although this could also be due to organic complexes with iron, intermediates that have increased extinction coefficients, etc.

It is important to remark that, due to the unspecific character of the absorption at 254 nm as a reaction quantification parameter, care has been taken and only qualitative considerations have been made from such data.

5. Conclusions

The solar light assisted Fenton and photo-Fenton reactions have shown to efficiently decolorize and mineralize aqueous solution of three dyes commonly used in the textile dyeing and finishing industry: Procion Red, Cibacron FN-R, and a Standard Trichromatic System. The data has been compared with the degradations carried out in the dark and under an artificial light source, the use of sunlight always giving the best results. The solar photons help to accelerate the loss of the aromatic character of the dyes, as seen by following the change of absorbance at 254 nm. In parallel, there is a mineralization process, and TOC removal of Procion Red and Cibacron Red below the detection limit of the analytical technique take place in 20 and 45 min, respectively. The loss of color is also fast: Procion Red is decolorized in less than 15 min, while for the Standard Trichromatic System the process takes no more than 30 min. The ratio BOD_5/COD increases with time indicating that a partial treatment of the dye solutions increases their biodegradability and the possibility of a combined treatment based on a previous solar assisted chemical oxidation and a subsequent biological degradation. In any case, the use of the solar energy to drive this type of reactive systems in advantageous, specially if compared to the use of an artificial light source.

Acknowledgements

The authors want to thank the Spanish Government (Ministerio de Ciencia y Tecnología) for the financial support (Project PPQ2002-04060-C02-01).

References

APHA–AWWA–WPCF, 1985. Standard Methods for the Examination of Water and Wastewater. ASTM D1252-00, 17 ed. Washington, DC.

Arslan, I., Balcioglu, I.A., 2001. Advanced oxidation of raw and biotreated textile industry wastewater with O_3, H_2O_2/UV-C and their sequential application. J. Chem. Technol. Biotechnol. 76, 53–60.

Arslan, I., Balcioglu, I.A., Bahnemann, D.W., 2002. Advanced oxidation of a reactive dyebath effluent: comparison of O_3, H_2O_2/UV-C and TiO_2/UV-A processes. Water Res. 36, 1143–1154.

Balcioglu, I.A., Arslan, I., Sacan, M., 2001. Homogeneous and heterogeneous advanced oxidation of two commercial reactive dyes. Environ. Technol. 22, 813–822.

Bossmann, S.H., Oliveros, E., Göb, S., Siegwart, S., Dahlen, E.P., Payawan, L., Straub, M., Wörner, M., Braun, A.M., 1998. New evidence against hydroxyl radicals as reactive intermediates in the thermal and photochemically enhanced Fenton reactions. J. Phys. Chem. 102, 5542–5550.

Bauer, R., Fallmann, H., 1997. The photo-Fenton oxidation—a cheap and efficient wastewater treatment method. Res. Chem. Intermed. 23, 341–354.

Chamarro, E., Marco, A., Esplugas, S., 2001. Use of the Fenton reagent to improve organic chemical biodegradability. Water Res. 35, 1047–1051.

ECD Guidelines for Testing of Chemicals, 1996, vol. 2, Test 302B.

El-Dein, A.M., Libra, J.A., Wiesmann, U., 2001. Kinetics of decolorization and mineralization of the azo dye Reactive Black 5 by hydrogen peroxide and UV light. Water Sci. Technol. 44, 295–301.

Georgiou, D., Melidis, P., Aivasidis, A., Gimouhopoulos, K., 2002. Degradation of azo-reactive dyes by ultraviolet radiation in the presence of hydrogen peroxide. Dyes Pigments 52, 69–78.

Grau, P., 1991. Textile industry wastewater treatment. Water Sci. Technol. 24, 97–103.

Guivarch, E., Trevin, S., Lahitte, C., Oturan, M.A., 2003. Degradation of azodyes in water by electro-Fenton process. Environ. Chem. Lett. 1, 38–44.

Hoffman, M.R., Martin, S.T., Choi, W., Bahnemann, D.W., 1995. Environmental applications of semiconductor photocatalysis. Chem. Rev. 95, 69–96.

Huston, P.L., Pignatello, J.J., 1999. Degradation of selected pesticide active ingredients and commercial formulations in water by the photo-assisted Fenton reaction. Water Res. 33, 1238–1246.

Ince, N.H., Tezcanli, G., 1999. Treatability of textile dye-bath effluents by advanced oxidation: preparation for reuse. Water Sci. Technol. 40, 183–190.

Joseph, J.M., Destaillats, H., Hung Hui-Ming, Hoffmann, M.R., 2000. The sonochemical degradation of azobenzene and related azo dyes: rate enhancements via Fenton's reactions. J. Phys. Chem. A 104,301–307.

Kiwi, J., Pulgarin, C., Peringer, P., 1994. Effect of Fenton and photo-Fenton reactions on the degradation and biodegradability of 2 and 4-nitrophenols in water treatment. Appl. Catal. B: Environ. 3, 335–350.

Kuo, W.G., 1992. Decolorizing dye wastewater with Fenton's reagent. Water Res. 26, 881–886.

Lizama, C., Yeber, M.C., Freer, J., Baeza, J., Mansilla, H.D., 2001. Reactive dyes decolouration by TiO_2 photo-assisted catalysis. Water Sci. Technol. 44, 197–203.

Malato, S., 2003. Plataforma Solar de Almería, Personal communication.

Neamtu, M., Simiceanu, I., Yediler, A., Kettrup, A., 2002. Kinetics of decolorization and mineralization of reactive azo dyes in aqueous solution by the UV/H_2O_2 oxidation. Dyes Pigments 53, 93–99.

Ollis, D.F., 1991. Solar-assisted photocatalysis for water purification: issues, data, questions. Photochem. Convers. Storage Sol. Energy, Proc. Int. Conf., 8th.

O'Neill, C., Hawkes Freda, R., Hawkes Dennis, L., Lourenço Nidia, D., Pinheiro Helena, M., Delée, W., 1999. Colour in textile effluents—sources, measurement, discharge consents and simulation: a review. J. Chem. Technol. Biotechnol. 74, 1009–1018.

Pelizzetti, E., Carlin, V., Minero, C., Pramauro, E., Vincenti, M., 1992. Degradation pathways of atrazine under solar light and in the presence of titanium oxide colloidal particles. Sci. Total Environ. 161, 123–124.

Pérez, M., Torrades, F., Garcia-Hortal, J.A., Domènech, X., Peral, J., 1997. Removal of organic contaminants in paper pulp treatment effluents by TiO_2 photocatalyzed oxidation. J. Photochem. Photobiol. A: Chem. 109, 281–286.

Pérez, M., Torrades, F., Garcia-Hortal, J.A., Domènech, X., Peral, J., 2001. Removal of organic contaminants in paper pulp treatment effluents under Fenton and photo-Fenton conditions. Appl. Catal. B: Environ. 36, 63–74.

Pérez, M., Torrades, F., Domènech, X., Peral, J., 2002. Fenton and photo-Fenton oxidation of textile effluents. Water Res. 36, 2703–2710.

Pignatello, J., 1992. Dark and photoassisted Fe^{3+} catalyzed degradation of chlorophenoxy herbicides by hydrogen peroxide. Environ. Sci. Technol. 26, 944–951.

Pignatello, J., Liu, D., Huston, P., 1999. Evidence for an additional oxidant in the photoassisted Fenton reaction. Environ. Sci. Technol. 33, 1832–1839.

Safarzadeh-Amiri, A., Bolton, J.R., Cater, S.R., 1996. The use of iron in advanced oxidation processes. J. Adv. Oxid. Technol. 1, 18–26.

Sánchez, L., Peral, J., Domènech, X., 1998. Aniline degradation by combined photocatalysis and ozonation. Appl. Catal. B: Environ. 19, 59–65.

Scott, J.P., Ollis, D.F., 1995. Environ. Progr. 14, 88–103.

Shu, H.Y., Huang, C.R., Chang, M.C., 1994. Decolorization of mono-azo dyes in wastewater by advanced oxidation processes: a case of study of Acid Red 1 and Acid Yellow 23. Chemosphere 29, 2597–2607.

So, C.M., Cheng, M.Y., Yu, J.C., Wong, P.K., 2002. Degradation of azo dye Procion Red MX-5B by photocatalytic oxidation. Chemosphere 46, 905–912.

Solozhenko, E.G., Soboleva, N.M., Goncharuk, V.V., 1995. Decolourization of azodye solutions by Fenton's oxidation. Water Res. 29, 2206–2210.

Torrades, F., García-Montaño, J., García-Hortal, J.A., Núñez, L., Doménech, X., Peral, J., in press. Decolourization and mineralization of monoreactive and hetero-bireactive dyes under Fenton and photo-Fenton conditions. Coloration Technology, accepted for publication.

Uygur, A, Kök, E., 1999. Decolorisation treatments of azo dye waste waters including dichlorotriazinyl reactive groups by using advanced oxidation method. J. Soc. Dyers Colour 115, 350–354.

ELSEVIER

Journal of Hazardous Materials B134 (2006) 220–229

Journal of Hazardous Materials

www.elsevier.com/locate/jhazmat

Degradation of Procion Red H-E7B reactive dye by coupling a photo-Fenton system with a sequencing batch reactor

Julia García-Montaño [a], Francesc Torrades [b], José A. García-Hortal [c], Xavier Domènech [a], José Peral [a,*]

[a] *Departament de Química, Edifici Cn, Universitat Autònoma de Barcelona, E-08193 Bellaterra, Barcelona, Spain*
[b] *Departament d'Enginyeria Química, ETSEI de Terrassa (UPC), C/Colom, 11, E-08222 Terrassa, Barcelona, Spain*
[c] *Departament d'Enginyeria Tèxtil i Paperera, ETSEI de Terrassa (UPC), C/Colom, 11, E-08222 Terrassa, Barcelona, Spain*

Received 12 September 2005; received in revised form 27 October 2005; accepted 1 November 2005
Available online 15 December 2005

Abstract

A bench-scale study combining photo-Fenton reaction with an aerobic sequencing batch reactor (SBR) to degrade a commercial homo-bireactive dye (Procion Red H-E7B, 250 mg l^{-1}) was investigated. The photo-Fenton process was applied as a pre-treatment, avoiding complete mineralisation, just to obtain a bio-compatible water able to be treated by means of the SBR in a second step. In this sense, different Fenton reagent concentrations were assessed by following dye solution biodegradability enhancement (BOD_5/COD), as well as the toxicity (EC_{50}), DOC, colour ($Abs_{543.5}$) and H_2O_2 evolution with photo-Fenton irradiation time. Obtained pre-treated solutions were biologically oxidized in a SBR containing non-acclimated activated sludge. Different hydraulic retention time (HRT) in the bioreactor were tested to attain the maximum organic load removal efficiency. Best results were obtained with 60 min of 10 mg l^{-1} Fe(II) and 125 mg l^{-1} H_2O_2 photo-Fenton pre-treatment and 1 day HRT in SBR.

Keywords: Textile reactive dye; Advanced oxidation processes; Photo-Fenton reaction; Biodegradability enhancement; Sequencing batch reactor; Organic removal

1. Introduction

The textile industry daily consumes large quantities of water in dyeing and finishing processes. Generated effluents are characterized by a high content of suspended solids and heavy metals, high temperature, unstable pH, elevated chemical oxygen demand and the presence of chlorinated organic compounds, surfactants and colour [1]. The substantial amount of dyes, especially reactive dyes, used in the dyeing stage of textile manufacturing supposes an increasing environmental threat due to its refractory nature. Therefore, it is necessary to find an effective method of wastewater treatment, both in terms of limited water recourses management and the need for nature preservation.

At present, several methods have been developed to treat dye wastewater. Physicochemical treatments such as coagulation/flocculation, flotation, membrane processes or activated carbon adsorption are common practices [2–5], but they are quite inefficient and result in a phase transfer of pollutants, leaving the problem unsolved. On the other hand, single biological treatments, the most economical and environmentally friendly ones, are not a suitable alternative when working with toxic and/or non biodegradable wastewaters [6]. In fact, most of disposed dyes are of non-biodegradable nature and standard biological treatment of their coloured effluents is not effective [7].

Therefore, destructive treatment methods for the remediation of recalcitrant or hazardous pollutants are currently under investigation. In this direction, *Advanced Oxidation Processes* (AOPs), based on the generation of highly reactive hydroxyl radicals ($HO^{\bullet}$, $E = 2.8$ V versus NHE) as primary oxidant, appear as the emerging alternatives for the organic pollutants abatement [8]. Among them, the *Fenton* and *photo-Fenton* type reactions are very promising since they achieve high reaction yields with a low treatment cost [9]. Fenton and photo-Fenton methods have been successfully applied to treat reactive dyes [10,11] as well as textile effluents [12,13].

In the accepted mechanism of *Fenton* reaction [14], hydroxyl radicals ($HO^{\bullet}$) are generated by interaction of H_2O_2 with ferrous

* Corresponding author. Tel.: +34 93 581 2772; fax: +34 93 581 2920.
E-mail address: jose.peral@uab.es (J. Peral).

0304-3894/$ – see front matter © 2005 Elsevier B.V. All rights reserved.
doi:10.1016/j.jhazmat.2005.11.013

salts [reaction (1)]:

$$\mathrm{Fe(II)} + \mathrm{H_2O_2} \rightarrow \mathrm{Fe(III)} + \mathrm{HO^\bullet} + \mathrm{HO^-}$$
$$k = 76.51\,\mathrm{mol^{-1}\,s^{-1}} \quad (1)$$

Then, Fe(III) can be reduced by reaction with exceeding H_2O_2 to form again ferrous ion and more radicals. This second process is called *Fenton-like*, is slower than Fenton reaction and allows Fe(II) regeneration giving place to a catalytic mechanism [reactions (2)–(4)]:

$$\mathrm{Fe(III)} + \mathrm{H_2O_2} \leftrightarrows \mathrm{FeOOH^{2+}} + \mathrm{H^+} \quad K_{eq} = 3.1 \times 10^{-3} \quad (2)$$

$$\mathrm{FeOOH^{2+}} \rightarrow \mathrm{HO^\bullet}_2 + \mathrm{Fe(II)} \quad k = 2.7 \times 10^{-3}\,\mathrm{s^{-1}} \quad (3)$$

$$\mathrm{Fe(III)} + \mathrm{HO^\bullet}_2 \rightarrow \mathrm{Fe(II)} + \mathrm{O_2} + \mathrm{H^+}$$
$$k < 2 \times 10^3\,\mathrm{l\,mol^{-1}\,s^{-1}} \quad (4)$$

Degradation of the organic pollutants in the *Fenton* reaction can increase in presence of an irradiation source (*photo-Fenton* reaction). In this case, the regeneration of Fe(II), with production of new $HO^\bullet$ radicals, follows a photoreduction process [reactions (5) and (6)]:

$$\mathrm{Fe(III)} + \mathrm{H_2O} \rightarrow \mathrm{FeOH^{2+}} + \mathrm{H^+} \quad (5)$$

$$\mathrm{FeOH^{2+}} \xrightarrow{h\upsilon} \mathrm{Fe(II)} + \mathrm{HO^\bullet} \quad \lambda = 410\,\mathrm{nm} \quad (6)$$

Since the reaction requires radiations up to 410 nm [15], photo-Fenton reaction offers the possibility to be driven under solar irradiation, becoming a cost-effective process [16,17]. Nevertheless, Fenton and photo-Fenton methods have some drawbacks: necessity of pH changes, sludge generation and, mainly, high operational costs due to the chemical reagents consumption. In this sense, chemical oxidation alone can often be prohibitive for wastewater treatment.

Recently, several studies have proposed the combination of single AOP and biological treatments to avoid the drawbacks of each other [18–22]. With this aim, the AOP is performed as a first step to just enhance the biodegradability and generate a new effluent able to be treated in a biological plant, while reducing operational costs.

The biological treatment is carried out in a sequencing batch reactor (SBR). There are large facilities incorporating the SBR design, mainly because of its simplicity, flexibility of operation, as well as cost effectiveness [23,24]. In this sense, SBR is considered an attractive alternative to conventional biological wastewater treatment systems, but with a unique tank for reaction and sedimentation stages. Therefore, in a controlled time sequence, usually SBR-type bioreactors operate under five defined phases: filling, aeration-reaction, activated sludge settling, draw and idle. With respect to applications, SBRs have been successfully employed in the biodegradation of both municipal and industrial wastewaters [25], as well as for the degradation of textile wastewaters in combined systems [18].

Accordingly, it is clear from the above discussion that SBR is an appropriate alternative in the combined AOP-biological treatment of the wastewaters studied here. In the present work, a representative reactive dyestuff employed in cellulosic fibre dyeing (Procion Red H-E7B) is taken as a model compound. The paper aims at more efficient use of chemical oxidants to carry out the photo-Fenton pre-treatment. In this sense, an important indicator of the pre-treatment effectiveness will be the increase of the biodegradability under minimum Fenton reagent doses. Subsequently, different photo-treated dye solutions will be fed to the SBR to evaluate the best photo-Fenton conditions. Moreover, the hydraulic retention time needed to obtain maximum organic load removal in the bioreactor is studied.

2. Experimental

2.1. Synthetic dye solution

A commercial homo-bireactive azodye, Procion Red H-E7B (C.I. Reactive Red 141, empirical formula $C_{52}H_{34}O_{26}S_8Cl_2N_{14}$), composed of two monochlorotriazine reactive groups, was supplied by DyStar and used as received without any purification. The chemical structure of the dye is shown in Fig. 1. The initial concentration of Procion Red H-E7B for all the experiments was 250 mg l^{-1}, a value that is among typical dye concentrations in real textile wastewaters [26]. In order to simulate batch-dyeing conditions, the dye was hydrolysed, by adjusting the pH of synthetic solutions to 10.6, followed by heating to 80 °C for 6 h. Finally, the hydrolysed dye solutions were stored at 4 °C after pH adjustment between 2.8 and 3.0, being ready for AOP operation.

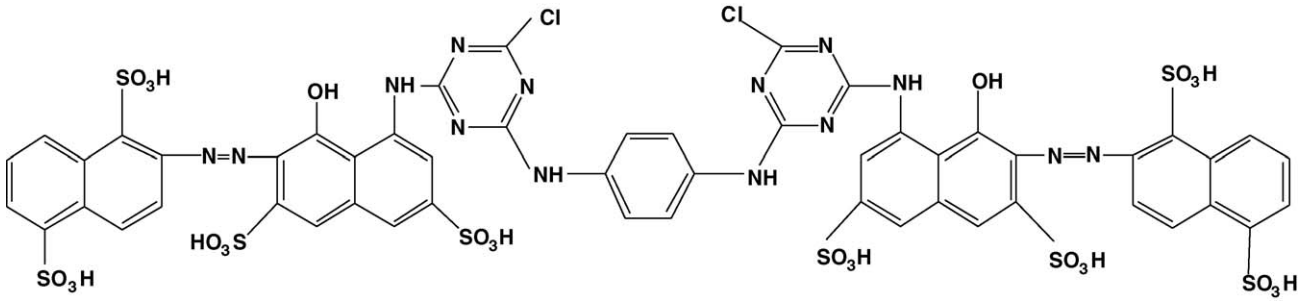

Fig. 1. Chemical structure of Procion Red H-E7B.

2.2. Photo-Fenton oxidation reagent

The hydroxyl radical, $HO^{\bullet}$, was generated in situ by the addition of the following reagents in aqueous media: hydrogen peroxide, H_2O_2, Panreac, 33% (w/v) and ferrous sulphate, $FeSO_4{\cdot}7H_2O$, Merck, 99.5%.

2.3. Photo-chemical reactor

Photo-Fenton oxidation was carried out using a cylindrical Pyrex thermostatic cell of 300 ml of capacity ($T = 23 \pm 1\,^{\circ}C$), equipped with a magnetic stirrer to provide good mixing with the defined Fenton reagent inside the reactor. The dye solution volume was 250 ml. A 6 W Philips black light fluorescent lamp, which basically emits at 350 nm, was used as artificial light source. The intensity of the incident light, measured employing an uranyl actinometer, was 1.38×10^{-9} Einstein s^{-1}.

2.4. SBR biomass

The bioreactor was seeded with activated sludge coming from the recirculation stage of a municipal Wastewater Treatment Plant, WWTP, in Manresa (Catalonia, Spain). The biomass population of the collected activated sludge, usually expressed as volatile suspended solids (VSS, $g\,l^{-1}$) [27], fluctuated within the range 2.85–4.94 $g\,l^{-1}$. Then, to perform every experiment with approximately the same initial cells concentration, the SBR was seeded by diluting the original activated sludge to a VSS value of 1 $g\,l^{-1}$.

2.5. SBR set-up and operation conditions

The biological treatment system was composed of a 2 l aerobic bench-scale sequencing batch reactor, equipped with an air diffuser and agitation. The operating liquid volume was 1.5 l. Temperature was maintained under room conditions, between 21 and 23 °C, while keeping the concentration of dissolved oxygen (DO, $mg\,l^{-1}$ O_2) not lower than 3 $mg\,l^{-1}$ O_2. Fresh biomass was used for the performance of each run.

The SBR operation strategy was as follows: once the hydraulic retention time was fixed, the bioreactor was fed with the required sample volume during the filling stage. At the end of the aeration-reaction period, the agitation and the airflow were switched off to allow to settle the activated sludge for 1 h. Afterwards, the corresponding volume of treated solution was decanted from the supernatant during the draw step, according to the defined HRT. Finally, the reactor was fed with the same volume of fresh solution and the aeration-agitation turned on again. This process was repeated cycle by cycle as many times as necessary to allow cells acclimation and/or to obtain repetitive results.

Daily analyses carried out were VSS, DO, dissolved organic carbon (DOC, $mg\,l^{-1}$ C) (influent and effluent samples content) and pH adjustment between 6.5 and 7.5 if necessary. Suitable proportions of essential biological nutrients ($MgSO_4$, $CaCl_2$, NH_4Cl and NaH_2PO_4 buffer at pH 7) were also added to the solution [28].

2.6. Chemical assays

The UV/vis-absorption spectra were recorded by using a Shimatzu UV-1603 double beam spectrophotometer in the 200–700 nm range. The maximum absorption in the visible region ($\lambda_{max} = 543.5$ nm) was taken as an estimation of the dye presence in solution. DOC was determined with a Shimadzu TOC-V_{CSH} analyser with a solution of potassium phthalate as standard of calibration. Chemical oxygen demand (COD, $mg\,l^{-1}$ O_2) was assessed by the closed reflux colorimetric method with a HACH DR/2000 spectrophotometer [28]. H_2O_2 consumption was tested by the potassium iodide titration method [29]. Accordingly, correction was made in the COD measurement for residual H_2O_2 [30]. Determination of total suspended solids (TSS, $g\,l^{-1}$) and volatile suspended solids (VSS, $g\,l^{-1}$) was carried out gravimetrically following Standard Methods recommendations [28].

2.7. Biological assays

Residual hydrogen peroxide was removed from the solution with *Catalase* (2350 U mg^{-1}; Sigma), according to the following specifications: 1 U destroys 1 μmol min^{-1} of hydrogen peroxide at pH 7 and temperature 25 °C. Fe ion (mainly Fe(III)) was precipitated before the assays by increasing the pH. The toxicity was assessed using the Biotox® technique. According to the sample preparation procedure prior to the Biotox® test, the pH of the solutions was adjusted to 7 and solid sodium chloride was added in order to adjust salinity to 2%.

The test is based on the determination of the acute toxicity that the sample has on the marine photobacteria *Vibrio fischeri*. The toxicity is quantified as the relative decrease of the photobacteria light emission with respect to a sample control that only contains the dilution medium, i.e. sodium chloride, 2% (w/v). The analysis generates the EC_{50} parameter (the concentration of toxicant that causes a 50% decrease of light emission), which is determined by interpolation from a series of dilutions of the original toxicant sample that have been in contact with the photobacteria during 30 min. A graph is plotted with the *x*-axis containing % DOC (compared to the total DOC content of the initial sample) and the *y*-axis displays the inhibition percent. EC_{50} values were expressed as percentage of DOC of the original sample. When the DOC of the original samples were lower than the EC_{50}, these values were given as >100%. Phenol and glucose solutions were used as standard toxic and non toxic samples to check the technique suitability.

The measurement of biochemical oxygen demand for 5 days (BOD_5, $mg\,l^{-1}$ O_2) was performed by means of a mercury-free WTW 2000 Oxytop thermostated at 20 °C. When BOD_5 determination took place during the photo-treatment stage, due to the toxic character of hydrogen peroxide, its removal with the precise amount of SO_3^{2-} [31] was found to be necessary.

The Zahn–Wellens test was carried out under conditions close to those of a conventional municipal wastewater treatment plant. Activated sludge coming from the Manresa WWTP was used to prepare the 0.2 $g\,l^{-1}$ of TSS required in the test specifications [32].

The experimental set-up to perform the short-term respirometry test was composed of a closed and thermostatic 250 ml respirometer ($T = 25 \pm 1\,^{\circ}C$), connected to a dissolved oxygen-meter (Model 407510, EXTECH), an air diffuser and a mechanical stirrer. Results were determined as specific oxygen uptake rate (OUR, $g\,O_2\,g^{-1}$ VSS min^{-1}) of the sample, while biodegradability was estimated by comparing the oxygen demand (OD, $g\,O_2\,g^{-1}$ VSS) within the first 2 h of reaction with the oxygen demand of an acetic acid solution (OD_{st}, $g\,O_2\,g^{-1}$ VSS), a completely biodegradable standard with the same COD than the sample.

3. Results and discussion

3.1. Untreated wastewater characteristics

The parameters employed to characterize the wastewater were the DOC, colour ($Abs_{543.5}$), acute toxicity (EC_{50}) and BOD_5/COD index and OD/OD_{st} as biodegradability indicators. Their values in the original dye solution are shown in Table 1. The absorption spectrum of the dye has a large band centred at 543.5 nm, responsible of the red colour of the solution.

As seen in Table 1, it is noticeable the low biodegradability of the synthetic textile wastewater, expressed as a BOD_5 to COD ratio. This relation shows that only a 10% of the chemically oxidable fraction is able to be biologically oxidised as well. Apart from the BOD_5 to COD estimation, the Zahn–Wellens test was carried out to investigate the potential of a biological treatment as a single process to remove the reactive dye. As it has been mentioned before, the experiment takes place under conditions close to those of a conventional WWTP, using non-acclimated activated sludge as inoculum. Two concentrations of dye (125 and 250 $mg\,l^{-1}$) were tested in order to discover if any toxicity effect was present. Obtained results clearly reveal that the biodegradability associated to both concentrations of Procion Red H-E7B is almost negligible (Fig. 2). The activated sludge has not removed any DOC within the 28 days of contact, with no sign of adaptation. This behaviour contrasts with the experiment performed with ethylene glycol, a completely biodegradable standard, which achieved an 85% of biodegradation under the same conditions in just 4 days. Once the 28 days period was completed, ethylene glycol was added to the dye solutions to discard a possible inhibition caused by the sample (data not shown). Again, the standard was consumed in few days, demonstrating that the biomass was still active or not inhibited.

Table 1
Chemical characterisation of 250 $mg\,l^{-1}$ hydrolysed Procion Red H-E7B in the synthetic textile effluent

DOC ($mg\,l^{-1}$ C)	44.96 ± 1.55[a]
EC_{50} ($mg\,l^{-1}$ C)	>44.96[b]
BOD_5 ($mg\,l^{-1}$ O_2)	12 ± 2[a]
COD ($mg\,l^{-1}$ O_2)	115 ± 2[a]
BOD_5/COD	0.10 ± 0.02[a]
OD/OD_{st}	0.04

[a] $n = 3$, $\alpha = 0.05$.
[b] $EC_{50} > 100\%$.

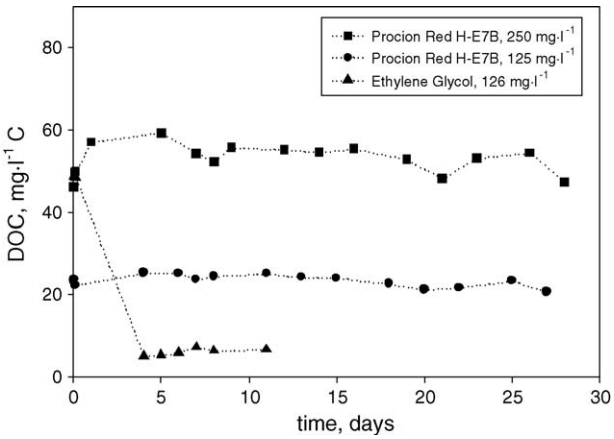

Fig. 2. Zahn–Wellens assay. DOC evolution of hydrolysed Procion Red H-E7B solutions (250 and 125 $mg\,l^{-1}$) and the biodegradable standard ethylene glycol (126 $mg\,l^{-1}$).

As a complementary assay, respirometric measurements where made to provide more information about biomass activity during the reactive dye biodegradation. In agreement with BOD_5/COD and Zahn–Wellens biodegradability tests, short-term respirometry test declares the non biodegradability of untreated wastewater (Table 1, OD/OD_{st} index).

Finally, results from the acute toxicity assessment of the dyestuff by means of Biotox® assay show that EC_{50} was greater than 100% or >44.96 $mg\,l^{-1}$ C (Table 1). This means that the concentration present in solution did not cause the 50% inhibition of the bacteria. It should be noted that toxicity assays could be distorted due to disturbances in luminescence measurements caused by intensive coloured dye solutions. In this case, it was necessary to take into account the lost of light due to absorption just applying a correction factor previously determined for every sample dilution.

Based on the above results, we conclude that Procion Red H-E7B is a non toxic but non biodegradable reactive dye. No aerobic biological treatment would be effective enough to remove the pollutant. Therefore, it could be a suitable compound to carry out the photo-Fenton reaction and biological treatment coupling strategy.

3.2. Photo-Fenton reaction as a pre-treatment process and biodegradability enhancement

The photo-Fenton process was applied in order to improve the dye solution biodegradability, avoiding complete mineralisation, as a previous step of an ensuing biological treatment. In this sense, preliminary experiments were firstly carried out to find suitable ferrous salt and hydrogen peroxide doses needed to biocompatibilize the synthetic wastewater with a second SBR stage.

An extended study about optimisation of Procion Red H-E7B reactive dye oxidation with photo-Fenton reaction has been previously reported elsewhere by our group [33]. Based on those findings, few Fenton reagents doses were tested in the present work (a serial of three experiments): 5 $mg\,l^{-1}$ Fe(II) and 125 $mg\,l^{-1}$ H_2O_2, 10 $mg\,l^{-1}$ Fe(II) and 125 $mg\,l^{-1}$ H_2O_2, 10 $mg\,l^{-1}$ Fe(II) and 250 $mg\,l^{-1}$ H_2O_2. Fig. 3 shows

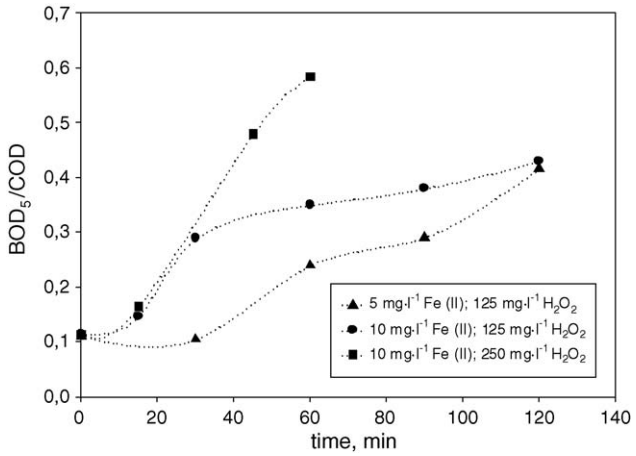

Fig. 3. Evolution of BOD_5/COD ratio vs. irradiation time at different Fenton reagent doses for hydrolysed Procion Red H-E7B, 250 mg l^{-1}, pH 3 and $T = 23\,^{\circ}C$.

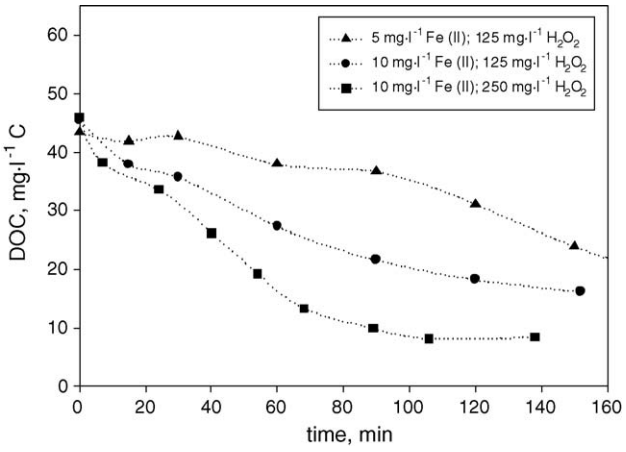

Fig. 5. Evolution of DOC vs. irradiation time at different Fenton reagent doses for hydrolysed Procion Red H-E7B, 250 mg l^{-1}, pH 3 and $T = 23\,^{\circ}C$.

the biodegradability evolution of every assessed condition, expressed as BOD_5 to COD index. Contaminants with a ratio of $BOD_5/COD \geq 0.4$ are generally accepted as biodegradable, while those with ratios situated among 0.2 and 0.3 units result partially biodegradable. Apart from biodegradability enhancement, residual H_2O_2 is also a key parameter to decide the suitable irradiation time when photo-Fenton reaction is employed as a previous step, before the biological treatment. It should be minimum and, due to its associated bactericide potential, eliminated prior feeding the bioreactor [34]. Fig. 4 shows its evolution. Finally, the concentration of DOC was also monitored during the course of photo-Fenton oxidation, and is represented in Fig. 5.

As the reaction proceeded, for every tested condition, solutions suffered a biodegradability increase achieving BOD_5 to COD ratios around 0.4. However, necessary irradiation time differ for each initial pair of Fenton reagent concentrations. The highest one, 10 mg l^{-1} Fe(II) and 250 mg l^{-1} H_2O_2, was able to reach the 0.58 units within 60 min of reaction. Nevertheless, it could be notice that an unnecessary mineralisation had taken place with this too high H_2O_2 dose (65% DOC removal, Fig. 5). On the other hand, the experiments with the lower concentration

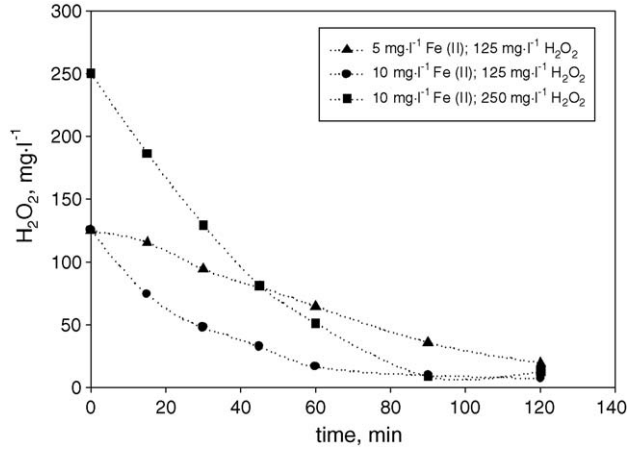

Fig. 4. Evolution of H_2O_2 vs. irradiation time at different Fenton reagent doses for hydrolysed Procion Red H-E7B, 250 mg l^{-1}, pH 3 and $T = 23\,^{\circ}C$.

(125 mg l^{-1}) required longer irradiation times as a compensation but, in both cases, high enough BOD_5/COD values were obtained along with lower mineralisation and, in the case of 10 mg l^{-1} of iron(II), with smaller remaining hydrogen peroxide levels (Figs. 4 and 5). According to the above argument, we conclude that 10 mg l^{-1} Fe(II) and 250 mg l^{-1} H_2O_2 would be the optimum concentration to complete mineralise the studied dye, but not for a partial degradation desired when using photo-Fenton as a pre-treatment. In fact, theoretical stoichiometric hydrogen peroxide required to complete oxidize the dye is 245 mg l^{-1} (1 g COD = 0.0312 mol oxygen = 0.0625 mol hydrogen peroxide). Consequently, this concentration is too high to be considered for AOP and biological coupling applications. In contrast, smaller Fenton reagent doses (5 mg l^{-1} Fe(II), 125 mg l^{-1} H_2O_2 and 10 mg l^{-1} Fe(II), 125 mg l^{-1} H_2O_2) seem to be appropriate to just enhance biodegradability to high enough levels. On the other hand, longer irradiation times will not be a drawback since the final goal of photo-Fenton reaction application is the use of solar light. Sunlight can give better results when compared with the performance of some artificial sources and, as discussed in the Section 1, with the possibility of low cost applications. In fact, the beneficial use of solar light has been already proved by our group for the removal of colour, aromatic compounds (Abs_{254}) and dissolved organic carbon of different commercial reactive dyes, such as Procion Red H-E7B [35].

Furthermore, when treating textile dyestuffs with biological processes, it has been reported that a narrow relationship exists between colour and non biodegradability [36]. In fact, single conventional biological treatment plants are not suitable methods for decolourising textile wastewaters. Based on this affirmation, it seemed possible to obtain bio-treatable solutions once the colour had disappeared. If we compare the BOD_5 to COD index evolution (Fig. 3) with absorbance data (Fig. 6), it is noticeable that biodegradability improves as solution colour disappears. Finally, it should be pointed out that this biodegradability enhancement was also exhibited in short-term respirometry measurements. For instance, consumed oxygen within the first 2 h of respirometry increased for all pre-treated solutions

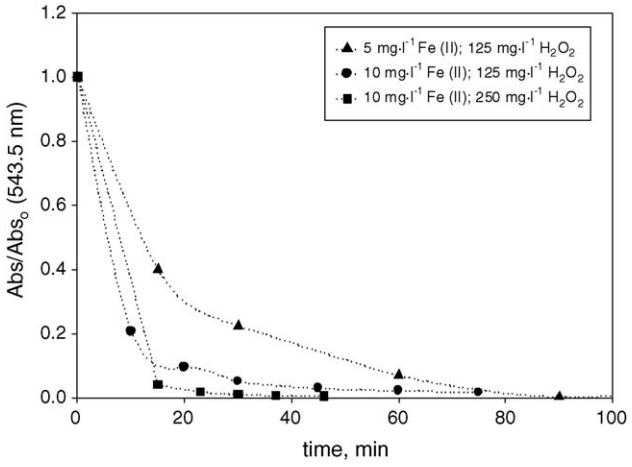

Fig. 6. Evolution of colour vs. irradiation time at different Fenton reagent doses for hydrolysed Procion Red H-E7B, 250 mg l^{-1}, pH 3 and $T = 23\,^{\circ}C$.

tested, even taking into account that COD decreases during the pre-treatment.

It may be possible that, while initial reactive dye was degraded, some other compounds with more inhibitor effect than the parent compound were formed. In this sense, apart from biodegradability measurements, acute toxicity after 30, 60 and 120 min of irradiation with the 5 mg l^{-1} Fe(II), 125 mg l^{-1} H_2O_2 and 10 mg l^{-1} Fe(II), 125 mg l^{-1} H_2O_2 photo-Fenton conditions was assessed. As happened with the untreated solution (Table 1), EC_{50} values were larger than the DOC content at every measurement time ($EC_{50} > 100\%$). There was no evidence of toxic by-products development during the photo-Fenton process. Therefore, the coupling of photo-Fenton with a biological treatment was presumably not conditioned by the possible toxic nature of reactive dye intermediates generated in the first step.

3.3. Aerobic SBR

Since the irradiated solution was in the acid pH range (2.8–3.0), it was neutralised with sodium hydroxide prior feeding into the SBR. Moreover, any residual hydrogen peroxide was quenched with an excess of sodium sulphite to avoid further reactions and to prevent its bactericide effect inside the bioreactor [31]. The remaining sulphite was removed by bubbling O_2. Taking into account such precautions, photo-treated Procion Red H-E7B samples could be introduced into the biological system.

3.3.1. Preliminary run

In order to guarantee the cells viability and to estimate the lower residual DOC that could be achieved within the SBR system, this was initially fed with a completely biodegradable wastewater and a 10 day HRT cycle was carried out. This blank run was performed before every cycle of SBR experiments with municipal wastewater coming from the WWTP, a water characterised by an average DOC of 50 mg l^{-1} C and COD of 210 mg l^{-1} O_2.

During this preliminary run, almost complete DOC removal was observed in every experiment, with a constant residual value of 11.87 ± 1.54 mg l^{-1} C corresponding to the metabolites released by the biomass. In addition, along this period, cells were adapted to the experimental laboratory conditions such as temperature, oxygen flow and manipulation, and the VSS content stabilised along every preliminary run around 0.85 g l^{-1}.

3.3.2. Effect of different photo-Fenton pre-treatments and HRT

After the preliminary run, a set of four different hydraulic retention times (10, 4, 2 and 1 days) were tested. The duration of the HRT may determine the grade of organic load removal achieved, expressed as DOC in this study. For the same experimental conditions, at least three cycles were carried out in order to obtain reproducible results. The HRT = 10 days experiment was run only twice because the residual DOC stabilized within 2 cycles.

The pretended goal was, after determining BOD_5/COD ratios of the pre-treated samples and choosing different HRT, to attain maximum DOC removal with residual DOC values close to those obtained in each previous blank run (biomass metabolites). A summary of the characteristics of the influent sample and the performance of the SBR is presented in Tables 2 and 3. Initially, an irradiation time of 60 min for a 10 mg l^{-1} Fe(II), 125 mg l^{-1} H_2O_2 photo-Fenton process was chosen to generate the feed of the bioreactor. The resulting solution was slightly yellow, without trace of red colour and with a 0.35 ± 0.05 BOD_5/COD ratio (Table 2). The mineralisation during the pre-treatment was 39%, with a small remaining H_2O_2 of 16.5 mg l^{-1}. The DOC content of the SBR influent was 26.90 ± 0.55 mg l^{-1} C.

Table 2
Summary of experimental results for the 10 mg l^{-1} Fe(II), 125 mg l^{-1} H_2O_2 conditions in photo-Fenton process and SBR coupling system

Pre-treatment (min)	Initial DOC[a] (mg l^{-1} C)	BOD_5/COD[b]	EC_{50} (mg l^{-1} C)	HRT, days	Cycles	OLR (mg l^{-1} day^{-1} C)	Residual DOC[a] (mg l^{-1} C)	SBR % DOC removal
60	25.60 ± 0.47	0.35 ± 0.05	>25.60[c]	10	2	2.560	12.82 ± 0.63	49.1
60	28.39 ± 0.01	0.35 ± 0.05	>28.39[c]	2	5	14.20	14.51 ± 0.36	48.9
60	27.79 ± 0.81	0.35 ± 0.05	>27.79[c]	1	15	27.79	13.23 ± 0.36	52.4
30	38.65 ± 0.33	0.29 ± 0.02	>38.65[c]	2	3	19.32	25.71 ± 1.37	33.4
30	37.58 ± 0.47	0.29 ± 0.02	>37.57[c]	4	3	9.395	23.99 ± 0.75	36.2

[a] Replicate data have been determined with a minimum of 5 values and $\alpha = 0.05$.
[b] $n = 3$, $\alpha = 0.05$.
[c] $EC_{50} > 100\%$.

Table 3
Summary of experimental results for the 5 mg l^{-1} Fe(II), 125 mg l^{-1} H_2O_2 conditions in photo-Fenton process and SBR coupling system

Pre-treatment (min)	Initial DOC[a] (mg l^{-1} C)	BOD_5/COD[b]	EC_{50} (mg l^{-1} C)	HRT (days)	Cycles	OLR (mg l^{-1} day^{-1} C)	Residual DOC[a] (mg l^{-1} C)	SBR % DOC removal
60	38.17 ± 1.01	0.25 ± 0.03	>38.17[c]	2	8	19.08	24.81 ± 0.86	35.0
60	38.12 ± 0.84	0.25 ± 0.03	>38.12[c]	4	3	9.53	24.13 ± 0.56	37.2

[a] Replicate data have been determined with a minimum of 5 values and $\alpha = 0.05$.
[b] $n = 3$, $\alpha = 0.05$.
[c] $EC_{50} > 100\%$.

At the beginning, an HRT = 10 days was fixed to insure a reaction period long enough to determine the maximum biodegradation percentage. As a result, a 49.1% DOC removal was obtained along the whole biological run, with no need of acclimation period (percent of reduction calculated from influent DOC). The attained residual DOC, 12.82 ± 0.63 mg l^{-1} C, coincided with the remaining content previously determined in the blank run. It should to be remarked that this residual DOC value settles the lowest threshold of DOC removal. However, obtained results showed that it may be possible to reduce the HRT without renouncing to attain maximum biodegradation. A low and stable residual DOC is reached after 2 days in the first SBR cycle. Cycle time duration corresponding to 2 and 1 day were consequently tested. From Table 2 it is noticeable that when HRT decreases, it increases the steady-state organic loading rate (OLR, mg l^{-1} day^{-1} C). Moreover, it should be pointed out that, for the three studied experiments, initial VSS level decreased until a stabilized value, just when % DOC removal became stable (see Fig. 7).

As predicted, organic load removals for HTR = 2 and 1 day show similar efficiencies than for HRT = 10 days, but making necessary an acclimation period of 2 and 4 days, respectively. Nevertheless, since minimum SBR cycle time duration is to be accomplish, 1 day cycle was chosen as the suitable HRT for a 60 min, 10 mg l^{-1} Fe(II), 125 mg l^{-1} H_2O_2 photo-Fenton pre-treatment. Afterwards, SBR process was continued for 15 cycles to check that SBR worked under steady conditions (Fig. 7). On average, residual DOC was 13.23 ± 0.36 mg l^{-1} C after the fourth cycle, with no more than 4.74% fluctuation in DOC values, while VSS remained stable around 0.41 g l^{-1}. The DOC removal rate was 14.85 mg l^{-1} day^{-1} C. In those steady-state conditions, daily BOD_5 to VSS ratio was 0.04 mg O_2 mg^{-1} VSS. Finally, once the 15 days of operation were over, a blank run (by adding biodegradable municipal wastewater as influent to the adapted biomass) was performed to ensure that the remaining biomass was able to reduce DOC to a residual value around 12 mg l^{-1} C.

The next step of the study was to try to reduce the pre-treatment irradiation time of photo-Fenton process, by maintaining the same Fenton reagent dose, in order to evaluate the pre-treatment duration effect. In this sense, it should be pointed out that pre-treatment times beyond 60 min were not considered since this was enough to obtain an effluent that can be completely degraded in the biological reactor. With this aim, some new SBR runs were performed with a pre-treatment irradiation time of 30 min (Table 2). This time reduction involves an increase in organic carbon load to an average concentration of 37.91 ± 0.42 mg l^{-1} C, a remaining H_2O_2 of 47.6 mg l^{-1} and a 0.29 ± 0.02 BOD_5/COD ratio (Table 2). As a difference with the 60 min one, this influent was characterised by a visible slight brown colour. A 2 day HRT was fixed as starting point. As it can be seen in the table, an increase of the remaining DOC takes place when comparing with the 60 min experiment under the same conditions. The obtained residual DOC was 25.71 ± 1.37 mg l^{-1} C, far away from the 14.51 mg l^{-1} C value. In any case, good performance of the SBR was observed since operating parameters were properly maintained throughout each run. The VSS

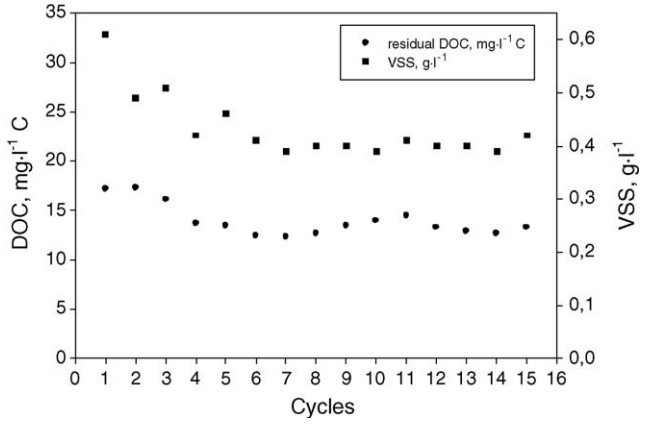

Fig. 7. VSS evolution and final DOC concentration for the 60 min, 10 mg l^{-1} Fe(II) 125 mg l^{-1} H_2O_2 photo-Fenton pre-treatment and 1 day HRT SBR cycle.

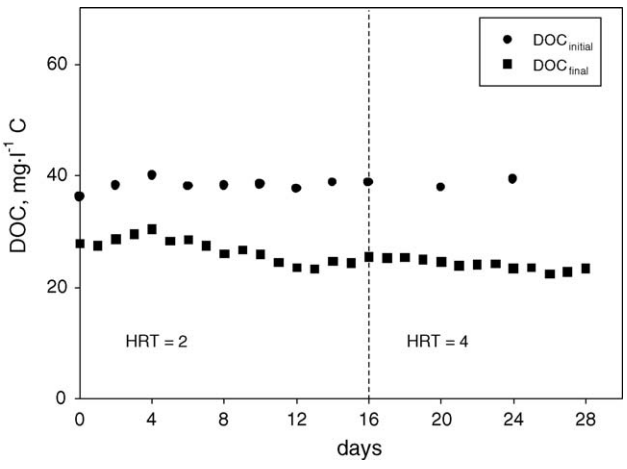

Fig. 8. Initial and final DOC for the 60 min, 5 mg l^{-1} Fe(II), 125 mg l^{-1} H_2O_2 photo-Fenton conditions and SBR coupling system. HRT = 2 and 4 days.

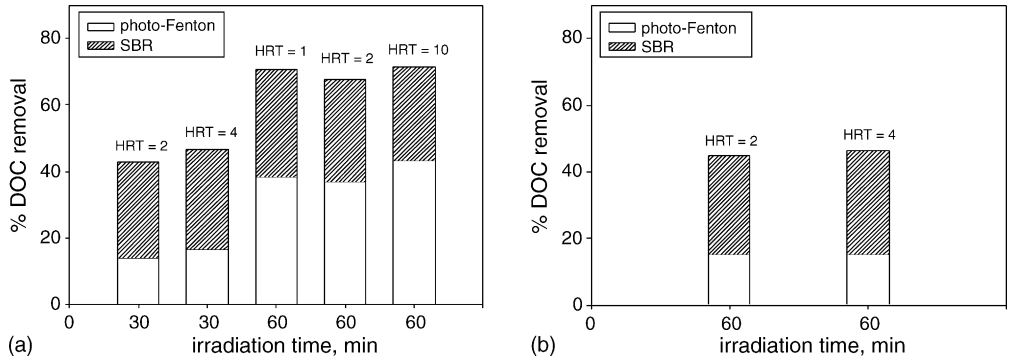

Fig. 9. % DOC removal in photo-Fenton pre-treatment and SBR coupling system as a function of pre-treatment irradiation time and HRT: (a) 10 mg l^{-1} Fe(II), 125 mg l^{-1} H_2O_2; (b) 5 mg l^{-1} Fe(II), 125 mg l^{-1} H_2O_2.

arrived to a steady-state while final DOC fluctuated slightly from cycle to cycle. In an attempt to ascertain if there was any chance to improve the situation, an increase of the bioreactor cycle time from 2 to 4 days was probed. However, in spite of extending the reaction period, the bioreactor response showed a similar behaviour. Moreover, data reveal that a 1 day HRT in the SBR would give the same remaining DOC. Therefore, biodegradability of 30 min pre-treated reactive dye was not high enough, while hydraulic retention time did not seem to influence the removal percentage values. In conclusion, sample irradiation for 60 min under 10 mg l^{-1} Fe(II), 125 mg l^{-1} H_2O_2 photo-Fenton pre-treatment conditions proves to be necessary to generate an effluent able to be completely biodegraded in the SBR.

Finally, a pair of SBR runs coupled to the 5 mg l^{-1} Fe(II), 125 mg l^{-1} H_2O_2 photo-Fenton process were assessed (Table 3). To establish time-comparable conditions to the ones presented above, the irradiation pre-treatment time chosen was 60 min. At that point, Procion Red H-E7B intermediates were characterized by a 0.25 ± 0.03 BOD_5/COD index, slight brown colour, 64.6 mg l^{-1} of non-reacted H_2O_2 and a substrate concentration of 38.15 ± 0.64 mg l^{-1} C. As previously stated, HRT of tested bio-treatment cycles were, initially, 2 days and extended later to 4 days to discard any HRT limitation in the DOC percent reduction (Fig. 8). Table 3 clearly reveals that, although DOC removal of both tested runs was not high, it was neither affected by the HRT. In fact, Fig. 8 exhibits that, as happened with the 30 min, 10 mg l^{-1} Fe(II) and 125 mg l^{-1} H_2O_2 pre-treatment, 24 h SBR cycle would be time enough to reach the same final DOC content. Residual values for 2 and 4 days runs were 24.81 ± 0.86 and 24.13 ± 0.56 mg l^{-1} C, respectively.

With regard to VSS evolution, it should be pointed out that the bioreactor did not manage to work under stable operation until the fourth cycle of the 2 days HRT experiment. During the first cycles bacteria experimented a slight adaptation until stable VSS and reproducible final DOC values were achieved. Due to this behaviour, and proceeding in a different way with respect to the other SBR experiments, biomass was reused from one run to the other to avoid such acclimation period.

It is noteworthy that this set of experiments showed a similar biodegradation percent than the 30 min of irradiation, 10 mg l^{-1} Fe(II), 125 mg l^{-1} H_2O_2 photo-Fenton pre-treatment. Although with Fe(II) concentration of 5 mg l^{-1}, the ratio BOD_5/COD is not close to 0.4, it seems reasonable that longer irradiation times (more than the 1 h tested) would eventually produce a biodegradable solution, an interesting possibility taking into account the potential use of sunlight in the photo-Fenton reaction.

In summary, studied AOP and SBR coupling show higher degradation efficiencies when working under the 10 mg l^{-1} Fe(II), 125 mg l^{-1} H_2O_2 photo-Fenton pre-treatment conditions. This DOC removal efficiency was affected by the irradiation time, being significantly higher in the case of 60 min. Fig. 9 compares the DOC removal of all the studied runs, taking into account the percentage of mineralisation reached by the coupling of both stages. Under most favourable conditions a 71% removal with respect to the initial DOC in coloured dye solution was obtained. This percentage dropped around 45% in the other combined treatments. Finally, it is remarkable that the residual DOC values oscillated around 12 mg l^{-1} C, setting a lower threshold for DOC removal.

With regard to the hydraulic retention time effect, no remarkable differences in DOC removal were found between different assessed cycle times. For instance, the 60 min of 10 mg l^{-1} Fe(II), 125 mg l^{-1} H_2O_2 photo-Fenton pre-treatment, the most effective one, allowed to reduce HRT from 10 to 1 day without lost of biodegradability (Fig. 9). This fact let us to conclude that SBR efficiency is not time dependent over 1 day HRT. Nevertheless, the SBR behaviour when reducing the hydraulic retention time below 24 h has not been studied, being not possible to discard an HRT effect below this cycle time duration.

4. Conclusions

Results have demonstrated that photo-Fenton reaction can be successfully used as a pre-treatment process to biocompatibilize Procion Red H-E7B reactive dye solutions. With partial oxidation run under mild conditions, dye solution became decolourised and more biodegradable, as well as non toxic. Photo-treated solutions were subsequently biodegraded in an aerobic sequencing batch reactor working under different hydraulic retention times.

Best pre-treatment results were obtained with 60 min of photo-Fenton irradiation time and 10 mg l^{-1} Fe(II), 125 mg l^{-1} H_2O_2 of initial reagents concentrations. At these conditions, BOD_5/COD index went from 0.10 up to 0.35 units just with

39% mineralisation and 16.5 mg l^{-1} of residual H_2O_2. On the other hand, data comparison for every tested HRT in SBR shows that the biological process efficiency appeared to be independent of the changes carried out in the cycle time duration. Therefore, 1 day (the minimum one tested) was chosen as the suitable HRT for SBR operation. Low residual DOC values obtained were close to those previously obtained in a blank run, assuming complete biodegradability. In addition, a good performance of the bioreactor was observed since operating parameters (VSS and residual DOC content) were properly maintained within each experiment.

On the other hand, when trying to reduce the 10 mg l^{-1} Fe(II) and 125 mg l^{-1} H_2O_2 photo-Fenton process duration from 60 to 30 min, it was not possible to attain enough biodegradation percentage levels, showing that photo-treated water was not biodegradable enough to feed the SBR. The same behaviour was observed in the 60 min, 5 mg l^{-1} Fe(II) and 125 mg l^{-1} experiment. In any case, results exhibit that DOC removal was not conditioned by the studied HRT.

In summary, the use of photo-Fenton type reactions as a pre-treatment allows the SBR system to remove Procion Red H-E7B reactive dye from aqueous solution, fact which improves the low success of aerobic biological removal of dye colour. Moreover, it should be pointed out that, taking the studied artificial light photo-Fenton process as starting point, more favourable results are expected when using solar light, both in terms of photo-Fenton pre-treatment effectiveness as well as energy consumption.

Acknowledgements

The authors wish to thank to CICYT (project PPQ2002-04060-C02-01) and European Commission (CADOX project, EVK1-CT-2002-00122) for financial support.

References

[1] N.H. Inze, M.I. Stefan, J.R. Bolton, UV/H_2O_2 degradation and toxicity reduction of textile azo dyes: Remazol Black-B, a case study, J. Adv. Oxid. Technol. 2 (3) (1997) 442–448.
[2] B.T. Tan, T.T. Teng, A.K. Omar, Removal of dyes and industrial dye wastes by magnesium chloride, Water Res. 34 (2000) 3153–3160.
[3] S.H. Lin, C.C. Lo, Treatment of textile wastewater by Foam flotation, Environ. Technol. 17 (8) (1996) 841–849.
[4] L. Tan, R.G. Sudan, Removing colour from a groundwater source, J. Am. Water Works Assoc. 84 (1992) 79–87.
[5] S.H. Lin, Adsorption of disperse dye by powdered activated carbon, J. Chem. Technol. Biotechnol. 57 (1993) 387–391.
[6] A. Uygur, E. Kök, Decolorisation treatments of azo dye waste waters including dichlorotriazinyl reactive groups by using advanced oxidation method, JSDC 115 (11) (1999) 350–354.
[7] D. Brown, B. Hamburger, The degradation of dyestuffs. Part III. Investigation of their ultimate biodegradability, Chemosphere 16 (1987) 1539–1553.
[8] R. Andreozzi, V. Caprio, A. Insola, R. Marotta, Advanced oxidation processes (AOP) for water purification and recovery, Catal. Today 53 (1999) 51–59.
[9] R. Bauer, H. Fallman, The photo-Fenton oxidation—a cheap and efficient wastewater treatment method, Res. Chem. Intermed. 23 (1997) 341–354.
[10] M. Neamtu, A. Yediler, I. Siminiceanu, A. Kettrup, Oxidation of commercial reactive azo dye aqueous solutions by the photo-Fenton and Fenton-like processes, J. Photochem. Photobiol. A: Chem. 161 (2003) 87–93.
[11] K. Swaminathan, S. Sandhya, A. Carmalin Sophia, K. Pachhade, Y.V. Subrahmanyam, Decolorization and degradation of H-acid and other dyes using ferrous-hydrogen peroxide system, Chemosphere 50 (2003) 619–625.
[12] M. Pérez, F. Torrades, X. Domènech, J. Peral, Fenton and photo-Fenton oxidation of textile effluents, Water Res. 36 (2002) 2703–2710.
[13] M. Rodrígez, V. Sarria, S. Esplugas, C. Pulgarin, Photo-Fenton treatment of a biorecalcitrant wastewater generated in textile activities: biodegradability of the photo-treated solution, J. Photochem. Photobiol. A: Chem. 151 (2002) 129–135.
[14] F. Haber, J. Weiss, The catalytic decomposition of hydrogen peroxide by iron salts, Proc. R. Soc. Series A 147 (1934) 332–351.
[15] P.L. Huston, J. Pignatello, Degradation of selected pesticide active ingredients and commercial formulations in water by the photo-assisted Fenton reaction, Water Res. 33 (1999) 1238–1246.
[16] M. Pérez, F. Torrades, X. Domènech, J. Peral, Removal of organic compounds in paper pulp treatment effluents under Fenton and photo-Fenton conditions, Appl. Catal. B: Environ. 36 (2002) 63–74.
[17] A. Safarzadeh-Amiri, J.R. Bolton, S.R. Cater, The use of iron in advanced oxidation processes, J. Adv. Oxid. Technol. 1 (1996) 18–26.
[18] P. Fongsatitkul, P. Elefsiniotis, A. Yamasmit, N. Yamasmit, Use of sequencing batch reactors and Fenton's reagent to treat a wastewater from a textile industry, Biochem. Eng. J. 21 (2004) 213–220.
[19] S. Parra, V. Sarria, S. Malato, P. Péringer, C. Pulgarin, Photochemical versus coupled photochemical–biological flow system for the treatment of two biorecalcitrant herbicides: metobromuron and isoproturon, Appl. Catal. B: Environ. 27 (2000) 153–168.
[20] C. Pulgarin, M. Invernizzi, S. Parra, V. Sarria, R. Polania, P. Péringer, Strategy for the coupling of photochemical and biological flow reactors useful in mineralization of biorecalcitrant industrial pollutants, Catal. Today 54 (1999) 341–352.
[21] V. Sarria, S. Parra, N. Adler, P. Péringer, N. Benitez, C. Pulgarin, Recent developments in the coupling of photoassisted and aerobic biological processes for the treatment of biorecalcitrant compounds, Catal. Today 76 (2002) 301–315.
[22] F. Al Momani, O. Gonzalez, C. Sans, S. Esplugas, Combining photo-Fenton process with biological sequencing batch reactor for 2,4-dichlorophenol degradation, Water Sci. Technol. 49 (4) (2004) 293–298.
[23] R.L. Irvine, L.H. Ketchum Jr., Sequencing batch reactors for biological wastewater treatment, CRC Crit. Rev. Environ. Control. 18 (1989) 255–294.
[24] P.A. Wilderer, R.L. Irvine, M.C. Gorzonsky (Eds.), Sequencing Batch Reactor Technology, International Water Association, London, 1999.
[25] S. Mace, J. Mata-Alvarez, Review of SBR technology for wastewater treatment: an overview, Ind. Eng. Chem. Res. 41 (2002) 5539–5553.
[26] M. Neamtu, I. Siminiceanu, A. Yediler, A. Kettrup, Kinetics of decolorization and mineralization of reactive azo dyes in aqueous solution by the UV/H_2O_2 oxidation, Dyes Pigments 53 (2002) 93–99.
[27] W.W. Eckenfelder, J.L. Musterman, Activated Sludge Treatment of Industrial Wastewater, Technomic Publishing Co., Lancaster, Pennsylvania, USA, 1995.
[28] APHA-AWWA-WPCF, Standard Methods for the Examination of Water and Wastewater, ASTM D1252-00, 17th ed, Washington, DC, 1989.
[29] C. Kormann, D.W. Bahnemann, M.R. Hoffmann, Photocatalytic production of H_2O_2 and organic peroxides in aqueous suspensions of TiO_2, ZnO and desert salt, Environ. Sci. Technol. 22 (5) (1988) 798–806.
[30] Y.W. Kang, M.-J. Cho, K.-Y. Hwang, Correction of hydrogen peroxide interference on standard chemical oxygen demand test, Water Res. 33 (5) (1999) 1247–1251.
[31] C.D. Adams, P.A. Scanlan, N.D. Secrist, Oxidation and biodegradability enhancement of 1,4-dioxane using hydrogen peroxide and ozone, Environ. Sci. Technol. 28 (1994) 1812–1818.
[32] ECD Guidelines for Testing of Chemicals, vol. 2, Test 302B, 1996.

[33] F. Torrades, J. García-Montaño, J.A. García-Hortal, Ll. Núñez, X. Domènech, J. Peral, Decolorisation and mineralisation of homo- and hetero-bireactive dyes under Fenton and photo-Fenton conditions, Color. Technol. 120 (2004) 188–194.
[34] J.P. Scott, D.F. Ollis, Integration of chemical and biological oxidation processes for water treatment: review and recommendations, Environ. Progress. 14 (1995) 88–103.
[35] F. Torrades, J. García-Montaño, J.A. García-Hortal, X. Domènech, J. Peral, Decolorization and mineralization of commercial reactive dyes under solar light assissted photo-Fenton conditions, Sol. Energy 77 (2004) 573–581.
[36] H. Chun, W. Yizhong, Decolorization and biodegradability of photocatalytic treated azo dyes and wool textile wastewater, Chemosphere 39 (12) (1999) 2107–2115.

Available online at www.sciencedirect.com
ScienceDirect
Applied Catalysis B: Environmental 67 (2006) 86–92
APPLIED CATALYSIS B: ENVIRONMENTAL
www.elsevier.com/locate/apcatb

Combining photo-Fenton process with aerobic sequencing batch reactor for commercial hetero-bireactive dye removal

Julia García-Montaño [a], Francesc Torrades [b], José A. García-Hortal [c], Xavier Domènech [a], José Peral [a,*]

[a] Departament de Química, Edifici Cn, Universitat Autònoma de Barcelona, E-08193 Bellaterra, Barcelona, Spain
[b] Departament d'Enginyeria Química, ETSEI de Terrassa (UPC), C/Colom 11, E-08222 Terrassa, Barcelona, Spain
[c] Departament d'Enginyeria Tèxtil i Paperera, ETSEI de Terrassa (UPC), C/Colom 11, E-08222 Terrassa, Barcelona, Spain

Received 30 January 2006; received in revised form 7 April 2006; accepted 16 April 2006
Available online 24 May 2006

Abstract

A synthetic textile effluent containing an hetero-bireactive dye (Cibacron Red FN-R, 250 mg l^{-1}) was treated by coupling photo-Fenton process with an aerobic sequencing batch reactor (SBR). The study is focused on the selection of suitable mild photo-Fenton conditions (Fe(II)/H_2O_2 reagents and irradiation time) that performs as a pre-treatment of a secondary biological treatment. Decolourisation ($Abs_{542.5}$), biodegradability enhancement (determined by BOD_5/COD index and respirometric methods) and dye degradation intermediates toxicity (Biotox® technique) were the parameters employed to verify the chemical stage effectiveness. From different assessed photo-Fenton conditions, a Fenton reagent concentration of 20 mg l^{-1} Fe(II) and 250 mg l^{-1} H_2O_2, applied for an irradiation time of 90 min, was found to be an effective process to bio-compatibilize the studied wastewater. The SBR, working under steady conditions in a 24-h-cycle mode, made available an 80% DOC removal in the combined oxidation system.

Keywords: Reactive azodye; Photo-Fenton's oxidation; Biodegradability enhancement; Aerobic sequencing batch reactor; Coupled oxidation system

1. Introduction

Wastewater produced in the natural fibre dyeing plant is characterised, in general, by its high colouration. The high consumption of reactive dyes, mainly in the cotton industry, originates environmental and aesthetic problems due to their low fixing degree to the fibre. Therefore, an important percentage of the dye (10–40%) remains unfixed in its hydrolysed form in the washing liquors [1]. Like many textile dyestuffs, reactive dyes are not removed under the aerobic conditions of standard biological treatment [2]. Additionally, under anaerobic conditions, they are readily reduced to potentially hazardous aromatics [3]. Consequently, to accomplish with current regulations, the application of specific treatments is required.

Advanced oxidation processes (AOPs) are powerful remediation technologies, which generate highly reactive hydroxyl radicals ($HO^{\bullet}$, $E = 2.8$ V versus NHE), able to mineralise almost all toxic and non-biologically degradable compounds [4]. These destructive treatments suppose an alternative to conventional physical and chemical treatment techniques, effective for colour removal but consisting only in a phase transfer of pollutants that requires additional treatment or disposal [5–8].

Fenton and photo-Fenton reactions are AOPs where oxidant species are generated from hydrogen peroxide and Fe(II)/Fe(III) as a catalytic couple. In Fenton reaction [9], ferrous salts react with hydrogen peroxide to generate the hydroxyl radicals as follows (reaction (1)):

$$\mathrm{Fe(II)} + \mathrm{H_2O_2} \rightarrow \mathrm{Fe(III)} + \mathrm{HO^{\bullet}} + \mathrm{HO^-} \quad k = 76.51\,\mathrm{mol^{-1}\,s^{-1}} \tag{1}$$

The rate of contaminants degradation can be considerably increased via photochemical reaction in the photo-Fenton process [10]. The effect of UV is the direct $HO^{\bullet}$ formation and regeneration of Fe(II) from the photolysis of the $FeOH^{2+}$ complex in solution (reaction (2)). The reduction of Fe(III)

* Corresponding author. Tel.: +34 93 581 2772; fax: +34 93 581 2920.
E-mail address: jose.peral@uab.es (J. Peral).

0926-3373/$ – see front matter © 2006 Elsevier B.V. All rights reserved.
doi:10.1016/j.apcatb.2006.04.007

back to Fe(II) is needed for the catalytic progress of the Fenton reaction:

$$FeOH^{2+} \xrightarrow{h\nu} Fe(II) + HO^{\bullet} \quad \lambda \leq 410\,nm \qquad (2)$$

Although Fenton and photo-Fenton type reactions offer successful pollutant removal with relatively low operational costs [11] and with the possibility of efficient sun radiation exploitation [12], expenses associated to reagents and energy consumption are their main disadvantage (shared by all AOPs). In order to overcome the economical drawback, and considering that biological treatment is the most desirable wastewater treatment in terms of environmental impact, a two-stage chemical/biological process is being currently proposed by many researchers when working with toxic and/or non-biodegradable waters [13–16]. Complete mineralisation would be avoided in the chemical process, being the goal the generation of a new biocompatible effluent.

Therefore, the photo-Fenton reaction was employed in the current work as a pre-treatment for further aerobic treatment of a representative reactive dye: hydrolysed Cibacron Red FN-R hetero-bireactive azodye. Few different Fe(II)/H_2O_2 doses were tested. The biodegradability evolution of the dye solution with time, estimated by means of BOD_5/COD index and respirometric tests, was assessed in order to judge the efficiency and the most appropriate conditions of the chemical stage. The mineralisation degree and the dye intermediates toxicity (EC_{50} parameter) were also evaluated. Photo-treated solutions were subsequently submitted to an aerobic sequencing batch reactor (SBR), an efficient alternative to conventional biological systems for a wide variety of model pollutants and real wastewaters biodegradation [17–19]. The effectiveness of the coupling process in dyestuff degradation was investigated.

2. Experimental

2.1. Hydrolysed dye solutions

A commercial hetero-bireactive azodye, Cibacron Red FN-R (CI Reactive Red 238, empirical formula $C_{29}H_{15}ClFN_7O_{13}S_4Na_4$, 944.2 g mol^{-1}) was supplied by CIBA and used as received without further purification. The chemical structure was confidential and not available. The initial Cibacron Red FN-R concentration for all the experiments was 250 mg l^{-1}. In order to simulate batch-dyeing conditions, the dye was hydrolysed by adjusting the pH of synthetic solutions to 10.6, followed by heating to 60 °C for 1 h. Finally, pH of the hydrolysed dye solutions was adjusted between 2.8 and 3.0 (the optimum pH for photo-Fenton process) and stored at 4 °C until AOP operation.

2.2. Chemicals

All chemicals used throughout this study were of the highest commercially available grade. Analytical grade hydrogen peroxide (33% (w/v), Panreac) and $FeSO_4{\cdot}7H_2O$ (99.5%, Merck) were used as received to generate hydroxyl radical ($HO^{\bullet}$) in aqueous solution. For the pH adjustment, concentrated reagent grade sulphuric acid and sodium hydroxide solutions (Panreac) were used. All solutions were prepared with deionised water obtained from a Millipore Milli-Q system.

2.3. SBR inoculum

The aerobic SBR was seeded with activated sludge coming from a municipal wastewater treatment plant (WWTP) in Manresa (Catalonia, Spain). Biomass concentration in biological suspensions was determined as volatile suspended solids (VSS, g l^{-1}) [20]. For all performed experiments, the bioreactor was seeded with approximately the same initial cell population by diluting the original activated sludge to a VSS value of 0.6 g l^{-1}.

2.4. Photo-chemical reactor

Photo-Fenton oxidation was conducted in a thermostated ($T = 23 \pm 1$ °C) well-stirred cylindrical Pyrex cell of 300 ml of capacity. The dye solution volume was 250 ml. A 6 W Philips black light fluorescent lamp, which basically emits at 350 nm, was used as artificial light source. The intensity of the incident light, measured employing an uranyl actinometer, was 1.38×10^{-9} einstein s^{-1}.

2.5. Aerobic SBR experimental conditions

The biological treatment system was composed of a 2 l aerobic bench-scale sequencing batch reactor, equipped with an air diffuser and agitation. The operating liquid volume was 1.5 l. The fill-and-draw SBR procedure is described elsewhere [16]. Temperature remained stable and close to room conditions, between 21 and 23 °C. The concentration of dissolved oxygen (DO, mg l^{-1} O_2) was kept above 3 mg l^{-1} O_2. Daily analyses of VSS, DO and dissolved organic carbon (DOC, mg l^{-1} C) (influent and effluent samples content) were carried out, and pH adjustment between 6.5 and 7.5 was done if necessary. Suitable proportions of nutrients ($MgSO_4$, $CaCl_2$, NH_4Cl and NaH_2PO_4 buffer at pH 7) were also added to the solution [20].

2.6. Chemical assays

UV/vis-absorption spectra were recorded by using a Shimatzu UV-1603 double beam spectrophotometer in the 200–700 nm range. All colour data are reported as absorbance at the maximum absorption in the visible region (λ_{max} = 542.5 nm). DOC was determined with a Shimadzu TOC-V_{CSH} analyser. Chemical oxygen demand (COD, mg l^{-1} O_2) was assessed by the closed reflux colorimetric method with a HACH DR/2000 spectrophotometer [20]. H_2O_2 consumption was tested by the potassium iodide titration method [21]. Accordingly, correction was made in the COD measurement for residual H_2O_2 [22]. Determination of total suspended solids (TSS, g l^{-1}) and volatile suspended solids

(VSS, g l^{-1}) was carried out gravimetrically following Standard Methods procedure [20].

2.7. Biological assays

Acute toxicity was assessed using the Biotox® bacterial bioluminiscence assay, by determination of the inhibitory effect that the sample has on the marine photobacteria *Vibrio fischeri*. To perform the measurement, residual hydrogen peroxide was removed from the media with Catalase (2350 U mg^{-1}, Sigma) according to the following specifications: 1 U destroys 1 μmol min^{-1} of hydrogen peroxide at pH 7 and temperature 25 °C. The toxicity effect was quantified as the EC_{50} parameter (the concentration of toxicant that causes a 50% decrease of light emission after 30 min of exposure at 15 °C), expressed as percentage of DOC of the original sample. Phenol and glucose solutions were used as standard toxic and non-toxic samples to check the technique suitability. Colour correction was applied in coloured solutions toxicity determinations.

The measurement of biochemical oxygen demand for 5 days (BOD_5, mg l^{-1} O_2) was performed by means of a mercury-free WTW 2000 Oxytop thermostated at 20 °C. When BOD_5 determination took place during the photo-treatment stage, due to the harmful character of hydrogen peroxide, its removal with an excess of SO_3^{2-} [23] was found to be necessary. Any remaining sulphite was removed by bubbling O_2.

The Zahn–Wellens test was carried out under conditions close to those of a conventional municipal wastewater treatment plant. Non-acclimated activated sludge coming from the Manresa WWTP was used to prepare the 0.3 g l^{-1} of TSS required in the test specifications [24].

The experimental set up used to perform the short-term respirometry test was composed of a closed and thermostatic 250 ml respirometer ($T = 25 \pm 1$ °C), connected to a dissolved oxygen-meter (Model 407510, EXTECH), an air diffuser and a mechanical stirrer. Suspensions of 3–4 g l^{-1} VSS were used as inoculum. Results were determined as specific oxygen uptake rate (sOUR, g O_2 g^{-1} VSS min^{-1}) of the sample, while ready biodegradability was estimated as the quotient between the accumulated oxygen demand within the first 30 min of contact with biomass (OD, g O_2 g^{-1} VSS, calculated by multiplying the sOUR by the considered time) and the oxygen demand of an acetic acid solution (OD_{st}, g O_2 g^{-1} VSS), a completely biodegradable standard with the same COD than the sample. *N*-Allylthiourea was added for nitrification inhibition.

3. Results and discussion

3.1. Hydrolysed dye solution characterisation

Results of the characterization of the 250 mg l^{-1} hydrolysed Cibacron Red FN-R solution are shown in Table 1. Cibacron Red FN-R is a non-toxic reactive azodye since there was no bacterial inhibition response at the studied DOC sample concentration: EC_{50} parameter >100% (>79.46 mg l^{-1} C). On the other hand, the dye is of non-biodegradable nature. Both BOD_5/COD and OD/OD_{st} index manifest its nearly null biodegradability, with 0.02 and 0.04 values, respectively (Table 1). Moreover, as a complementary long-term biodegradability study, two concentrations (125 and 250 mg l^{-1} Cibacron Red FN-R) were assessed with the Zahn–Wellens test to investigate the potential of a single aerobic biological treatment to remove the reactive dye (data not shown). Obtained results exhibited that bacteria were not able to remove any DOC within the 28 days of contact, with no sign of adaptation capacity.

Table 1
Chemical characterisation of 250 mg l^{-1} hydrolysed Cibacron Red FN-R in the synthetic textile effluent

DOC (mg l^{-1} C)	79.46 ± 1.34[a]
EC_{50} (mg l^{-1} C)	>79.46[b]
BOD_5 (mg l^{-1} O_2)	5 ± 5[a]
COD (mg l^{-1} O_2)	199 ± 10[a]
BOD_5/COD	0.02 ± 0.02[a]
OD/OD_{st}	0.04

[a] $n = 3$; $\alpha = 0.05$.
[b] $EC_{50} > 100\%$.

The data of all the biological experiments evidence that no traditional activated sludge system would be effective enough to remove Cibacron Red FN-R from aqueous solution. Subsequently, photo-Fenton reaction coupled to a biological process appears to be a suitable strategy for successful dyestuff treatment.

3.2. Photo-Fenton pre-treatment: biocompatibility assessment

Several experiments were carried out by modifying the Fe(II)/H_2O_2 ratio in an attempt to establish suitable conditions to bio-compatibilize Cibacron Red FN-R reactive dye solutions. The efficiency of the pre-treatment process was estimated by means of the biodegradability evolution of the photo-treated synthetic wastewater, estimated by BOD_5/COD and OD/OD_{st} biodegradability indicators. The DOC evolution through the photo-Fenton process was also monitored in order to determine the degree of mineralisation during the pre-treatment. Finally, colour ($Abs_{542.5}$), acute toxicity (EC_{50}), as well as hydrogen peroxide concentration were determined along the oxidation.

From preliminary experiments, 20 mg l^{-1} Fe(II) and 500 mg l^{-1} H_2O_2 was found to be the most efficient Fenton reagent combination to degrade the hetero-bireactive dye under study, achieving the maximum decolourisation and mineralisation levels at short irradiation time (Fig. 1). However, since just a partial degradation was desired when using photo-Fenton as a pre-treatment, such combination was not considered for chemical and biological coupling applications. By considering it as the top dose limit, the following Fe(II) and H_2O_2 concentrations were tested to establish minimum suitable biological pre-treatment conditions: 10 mg l^{-1} Fe(II) combined with 125, 250 and 500 mg l^{-1} H_2O_2, and 20 mg l^{-1} Fe(II) combined with 250 mg l^{-1} H_2O_2. BOD_5/COD and DOC progression with time are shown in Figs. 2 and 3, respectively.

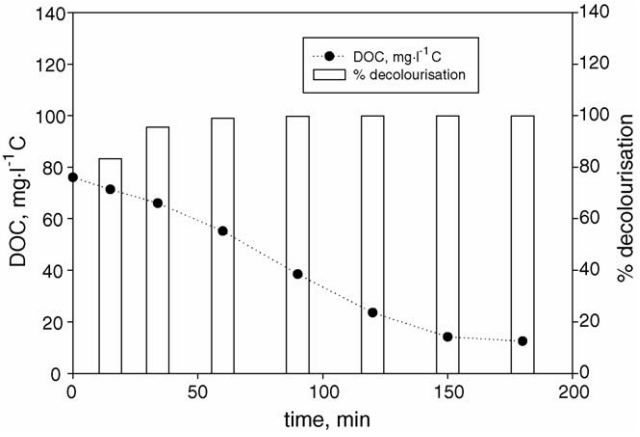

Fig. 1. Decolourisation and mineralisation of 250 mg l^{-1} hydrolysed Cibacron Red FN-R under 20 mg l^{-1} Fe(II), 500 mg l^{-1} H_2O_2 photo-Fenton conditions (pH 3 and $T = 23$ °C).

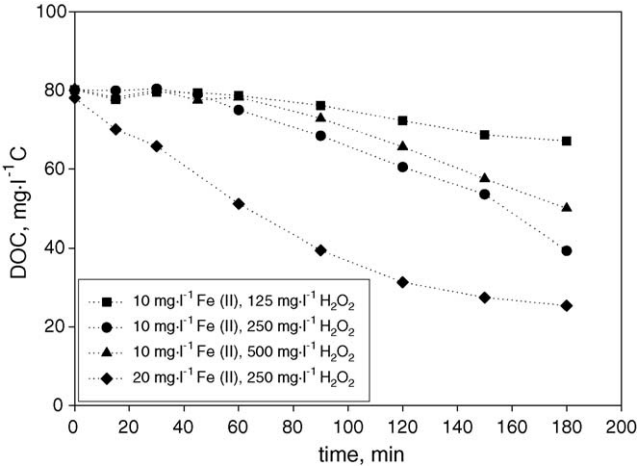

Fig. 3. DOC evolution vs. irradiation time at different Fenton reagent doses for hydrolysed Cibacron Red FN-R, 250 mg l^{-1} (pH 3 and $T = 23$ °C).

It can be observed that all photo-Fenton Fe(II)/H_2O_2 doses involve an increase of biodegradability during the course of the oxidation. Nevertheless, only wastewaters with a BOD_5/COD ratio $\geq$0.3–0.4 are generally accepted as biodegradable. Based on such requirement, the 10 mg l^{-1} Fe(II)/125 mg l^{-1} H_2O_2 process was discarded as a pre-treatment since it was not able to achieve biocompatible BOD_5/COD ratios. On the other hand, as it can be seen from Figs. 2 and 3, the 10 mg l^{-1} Fe(II)/500 mg l^{-1} H_2O_2 Fenton dose gives worst biodegradability and mineralisation degrees than the 10 mg l^{-1} Fe(II)/250 mg l^{-1} H_2O_2 one. A large hydrogen peroxide excess with respect to the Fe(II) catalyst probably promoted both the auto-decomposition of H_2O_2 and the competitive scavenging of $HO^\bullet$ by H_2O_2, according to reactions (3) and (4) [25]. In this sense, the 10 mg l^{-1} Fe(II)/500 mg l^{-1} H_2O_2 combination was not taken into account for the coupling system.

$$2H_2O_2 \rightarrow 2H_2O + O_2 \quad (3)$$

$$H_2O_2 + HO^\bullet \rightarrow HO_2^\bullet + H_2O \quad (4)$$

Therefore, the 10 mg l^{-1} Fe(II)/250 mg l^{-1} H_2O_2 and 20 mg l^{-1} Fe(II)/250 mg l^{-1} H_2O_2 experiments, with suitable BOD_5/COD and mineralisation levels, were chosen to generate the fed of the bioreactor. The following irradiation times that render biocompatible intermediate solutions were tested: 150 min for the lower and 60 and 90 min for the higher Fenton dose. BOD_5/COD index, %DOC removal as well as remaining H_2O_2 values at chosen photo-Fenton conditions are compared in Table 2. All obtained solutions correspond to colourless samples. As an example, Fig. 4 compares the untreated dyestuff spectrum with the corresponding after the 90 min, 20 mg l^{-1} Fe(II) and 250 mg l^{-1} H_2O_2 photo-Fenton process. The other two oxidising conditions generate similar absorbance profiles, with the absence of the large visible band characteristic of azodyes. On the other hand, the UV band remaining below 350 nm would correspond to colourless organic by-products. This phenomenon indicates that the parent compound Cibacron Red FN-R reactive dye had been completely removed during the chemical stage, before feeding

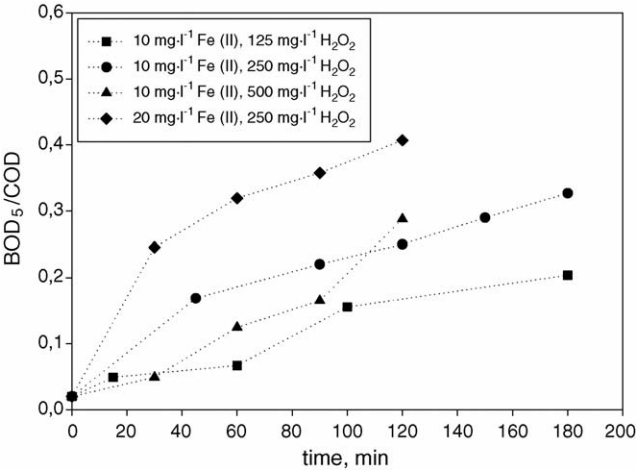

Fig. 2. BOD_5/COD evolution vs. irradiation time at different Fenton reagent doses for hydrolysed Cibacron Red FN-R, 250 mg l^{-1} (pH 3 and $T = 23$ °C).

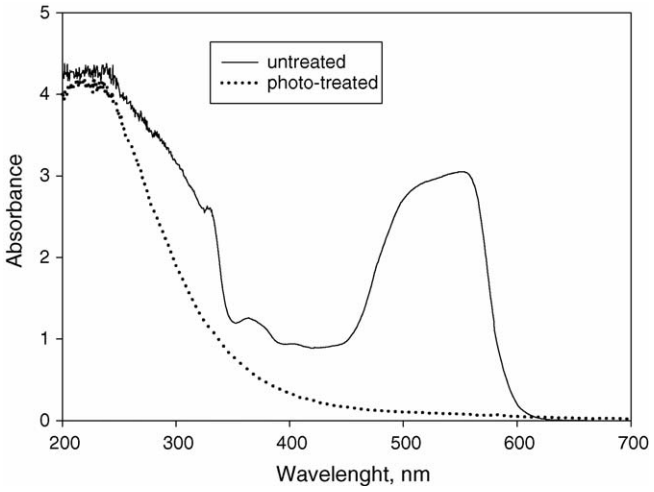

Fig. 4. Absorption spectrum of untreated and photo-treated 250 mg l^{-1} hydrolysed Cibacron Red FN-R, photo-Fenton conditions: 20 mg l^{-1} Fe(II), 250 mg l^{-1} H_2O_2, irradiation time = 90 min (pH 3 and $T = 23$ °C).

Table 2
BOD_5/COD, OD/OD_{st} index, H_2O_2 concentration and %DOC removal at different chosen Fenton reagent doses and irradiation times

Fenton reagent (mg l^{-1})	Irradiation time (min)	Residual H_2O_2 (mg l^{-1})	%DOC removal	BOD_5/COD[a]	OD/OD_{st}
10 Fe(II), 250 H_2O_2	150	98.6	32.6	0.29 ± 0.02	0.21
20 Fe(II), 250 H_2O_2	60	76.5	35.6	0.32 ± 0.03	0.34
20 Fe(II), 250 H_2O_2	90	21.2	49.6	0.36 ± 0.05	0.52

[a] $n = 3$; $\alpha = 0.05$.

into the bioreactor. In this sense, it should be pointed out that the observed decolourisation and the biodegradability enhancement may involve the same chemical steps, in agreement with the bio-refractory nature associated to coloured samples.

The biodegradability enhancement was also exhibited in short-term respirometry assays. Respirometric measurements where made to provide more information about the ready biomass activity in front of the generated intermediates. For all pre-treated solutions tested, the OD/OD_{st} index experimented a significant increase within the first 30 min of contact with biomass (with respect to the initial 0.04 value), with a data trend in agreement with that corresponding to the BOD_5/COD index (Table 2). These results evidence that more readily biodegradable intermediates were generated after the parent compound chemical oxidation. After the photo-treated sample consumption, the same biomass was fed again with acetic acid to discard a possible inhibition of respiration caused by the sample. Results were compared with data obtained from a first acetic acid measurement performed before the photo-treated dye addition. As the oxygen demand and the sOUR of the standard were properly reproduced, it can be assumed that no toxic compounds were formed during the photo-Fenton process. Fig. 5 shows an example of respirometry corresponding to the accumulated oxygen demand evolution with time of 90 min, 20 mg l^{-1} Fe(II) and 250 mg l^{-1} H_2O_2 photo-Fenton pre-treatment with respect to the demand of an acetic acid solution with the same COD than the sample (measured before and after biomass contact with the treated dye addition). From the figure,

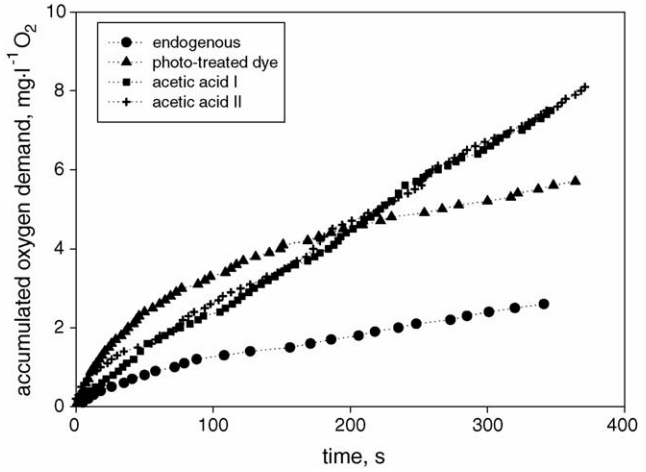

Fig. 5. Comparison of accumulated oxygen demand evolution of the photo-treated dyestuff after 90 min, 20 mg l^{-1} Fe(II), 250 mg l^{-1} H_2O_2 photo-Fenton process and the biodegradable acetic acid standard (first and second addition) (VSS = 3.92 g l^{-1}, pH 7 and $T = 25$ °C).

it can be clearly seen that microorganisms showed a fast O_2 uptake when feeding with photo-treated dye (even larger than the uptake of the acetic acid solutions), achieving the endogenous oxygen uptake rate once finished the ready biodegradation.

Finally, the acute toxicity of the chosen bioreactor influent was also determined with Biotox® bioluminiscence assay. As happened with the untreated solution (Table 1), the EC_{50} parameter was larger than the DOC content for all tested times ($EC_{50} > 100\%$), indicating that the discoloured effluent was non-toxic and would not inhibit the bacterial activity of the further biological treatment. These results corroborate respirometric tests conclusions.

3.3. Aerobic sequencing batch reactor

All experiments in SBR were carried out in two stages: start-up and operation. During the start-up period (one 10-day hydraulic retention time (HRT) cycle) the influent was a completely biodegradable municipal wastewater obtained from the WWTP, with no photo-treated dye added. The purpose of this preliminary step (so-called blank run) was to ensure the biomass viability and to establish, as a reference, the lower residual DOC that could be achieved by the SBR system. The steady DOC obtained, attributed to the metabolites released by the biomass, remained stable at 10.09 ± 0.39 mg l^{-1} C and settles the lowest boundary of DOC removal.

The operation period was performed once the blank cycle was completed. Different biodegradation runs were assessed by feeding the bioreactor with the presumably biocompatible selected photo-treated solutions. The pH of these had been previously readjusted from 2.8 to 3.0, to neutral, and they were treated with the required amount of SO_3^{2-} to remove the hydrogen peroxide remaining from photo-Fenton reaction.

The experimental results for each coupled chemical and SBR process are summarised in Table 3. Initially, an HRT of 2 days was defined. The cycle was repeated as many times as necessary to allow cells acclimation and/or to obtain repetitive results. Data from Table 3 clearly exhibits a DOC removal improvement in SBR when increasing the Fenton catalyst from 10 to 20 mg l^{-1} Fe(II). DOC removal for 150 min, 10 mg l^{-1} Fe(II)/250 mg l^{-1} H_2O_2 pre-treatment was 46.6%, with a residual value of 28.62 ± 1.02 mg l^{-1} C, far away from the 10.09 ± 0.39 mg l^{-1} C established as the limit in the blank run. On the other hand, when working under the 20 mg l^{-1} Fe(II)/250 mg l^{-1} H_2O_2 oxidising conditions, the percentage of mineralisation in SBR achieved 58.1% and 59.7% after 60 and 90 min of irradiation, respectively. Therefore, the level of

Table 3
Summary of experimental results for different assessed photo-Fenton conditions and SBR processes

Photo-Fenton		SBR					
$Fe(II)/H_2O_2$ (mg l^{-1})	Irradiation time (min)	Influent DOC[a] (mg l^{-1} C)	Influent BOD_5/COD[b]	HRT (days)	Cycles	Residual DOC[a] (mg l^{-1} C)	%DOC removal
10/250	150	53.57 ± 1.36	0.29 ± 0.02	2	10	28.62 ± 1.02	46.6
20/250	60	51.17 ± 0.82	0.32 ± 0.03	2	7	21.43 ± 0.49	58.1
	90	38.15 ± 1.49	0.36 ± 0.05	2	8	15.38 ± 0.79	59.7
		41.92 ± 0.81		1	15	16.62 ± 0.62	60.4

[a] Replicate data have been determined with a minimum of eight values and $\alpha = 0.05$.
[b] $n = 3$; $\alpha = 0.05$.

biodegradation increased more than 10 units when doubling the ferrous salt dose. Although data practically show identical percentage of DOC removal in the bioreactor for both experiments, an irradiation period of 90 min seems to be necessary to precede the biological stage since the DOC concentration of the final effluent (15.38 ± 0.79 mg l^{-1} C) was lower than the attained when 60 min pre-treatment had just taken place (21.43 ± 0.49 mg l^{-1} C). The residual DOC content was just around 5 mg l^{-1} C above the previously defined in the blank run. Thus, it could be assumed that the applied treatment has successfully removed the reactive dye from aqueous solution. A longer chemical pre-treatment was not considered since it would suppose to overcome the 50% mineralisation during photo-Fenton process, while the final aim of the present work was to minimise the chemical step in front of the biological one.

In an attempt to improve the percentage of DOC mineralisation in the bioreactor, the same set of experiments was developed by extending the hydraulic retention time to 4 days. Results revealed that the DOC elimination was not limited by the cycle time duration, since the %DOC removal was exactly the same (data not shown) than the obtained in the short cycle. Consequently, it can be concluded that overall SBR efficiency depends on the nature of the intermediates associated to each pre-treatment.

The dissimilarities between different assessed photo-Fenton and SBR coupled runs are better reflected in Fig. 6. This compares the DOC removal taking into account the percentage of mineralisation reached by both oxidation stages. The hydraulic retention time in the bioreactor was 2 days. It is noticeable that 90 min, 20 mg l^{-1} Fe(II) and 250 mg l^{-1} H_2O_2 were the most favourable pre-treatment conditions for the combined strategy proposed, with an 80% global DOC removal achieved. As discussed before, it should be remarked that the degree of organic matter removal was limited by the remaining DOC in the effluent corresponding to the biomass metabolites. On the other hand, it can be stated that 150 min, 10 mg l^{-1} Fe(II)/250 mg l^{-1} H_2O_2 and 60 min, 20 mg l^{-1} Fe(II)/250 mg l^{-1} H_2O_2 photo-Fenton conditions were not able to generate enough biocompatible dye by-products, giving place to 64% and 73% DOC removal efficiencies, respectively.

Once established the best photo-Fenton pre-treatment conditions, since maximum SBR removal rate is to be accomplish, the next step of the study was to reduce the hydraulic retention time in the bioreactor. In this direction, a new SBR run was performed in a 24-h-cycle mode after 90 min, 20 mg l^{-1} Fe(II) and 250 mg l^{-1} H_2O_2 photo-Fenton reaction (Table 3). In addition, the biological process was continued for 15 cycles to check that SBR was working under steady conditions. Results were as follows. With respect to the %DOC removal and final DOC concentration, once achieved the steady state, SBR behaved in the same way than with 2 and 4 days operation times, with 60.4% elimination and 16.62 ± 0.62 mg l^{-1} C residual DOC value. The steady state organic inlet rate was 41.92 mg l^{-1} day^{-1} C; the DOC removal rate was 25.37 mg l^{-1} day^{-1} C, and the volatile suspended solids stabilised at 0.56 ± 0.03 g l^{-1} after the third cycle. Fig. 7 shows the input, output and removed DOC within the 15 cycles. Such stable operational parameters evidence the good performance of the sequencing batch reactor.

Photo-Fenton pre-treatment allows traditional activated sludge to remove Cibacron Red FN-R reactive dye, originally bio-recalcitrant under aerobic media. On the other hand, as it has been discussed in Section 1, reactive dyes are potentially reduced under anaerobic conditions. In this direction, preliminary anaerobic degradation tests of Cibacron Red FN-R solutions have been conducted in an attempt to determine its biodegradability degree in absence of oxygen (data not

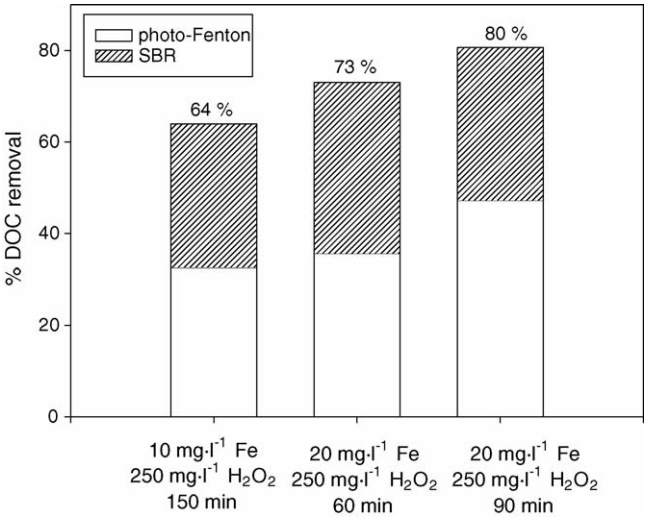

Fig. 6. %DOC removal in photo-Fenton pre-treatment and SBR coupling system as a function of photo-Fenton conditions (HRT in SBR = 2 days).

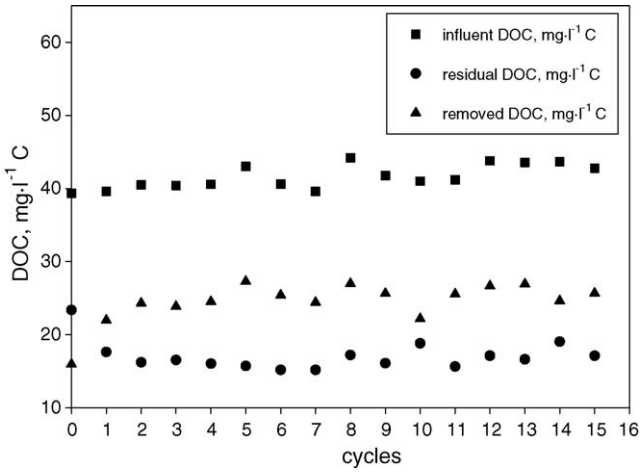

Fig. 7. Influent, removed and residual DOC for the 90 min, 20 mg l^{-1} Fe(II), 250 mg l^{-1} H_2O_2 photo-Fenton pre-treatment and 24-h SBR cycle (stabilised VSS = 0.56 ± 0.03 g l^{-1}).

shown). Complete decolourisation occurred but with no mineralisation, since no DOC removal neither biogas production was observed. In addition, generated colourless solutions were toxic and aerobically not biodegradable.

In this frame, further experiments will be performed applying the photo-Fenton reaction as a post-treatment of Cibacron Red FN-R anaerobic degradation.

4. Conclusions

Photo-Fenton process is an effective pre-treatment for the degradation of Cibacron Red FN-R hetero-bireactive dye in an aerobic sequencing batch reactor. With an efficient use of chemical oxidants, dye was degraded into non-toxic and biodegradable colourless species, able to be treated in the biological plant.

Biodegradation efficiency due to different chemical oxidation degree was determined. Best pre-treatment conditions correspond to a Fenton reagent concentration of 20 mg l^{-1} Fe(II)/250 mg l^{-1} H_2O_2 and an irradiation time of 90 min. BOD_5/COD and OD/OD_{st} biodegradability indicators went up from 0.02 and 0.04 to 0.36 and 0.52 values, respectively, while complete decolourisation and 49.6% mineralisation were obtained. Other assessed Fe(II)/H_2O_2 combinations and photo-Fenton irradiation times were not able to bio-compatibilize the synthetic effluent.

Hydraulic retention times of 4, 2 and 1 days were assessed in the bioreactor, giving the same biodegradation yields. To achieve maximum daily DOC removal, 1-day cycle time duration was established as the minimum SBR mode operation.

A stable 80% DOC removal was achieved for the combined system, with a residual DOC content of 16.62 ± 0.62, near to the 10.09 ± 0.39 mg l^{-1} C limit marked by the presence of biomass metabolites. Moreover, a stabilised biomass population (VSS = 0.56 ± 0.03 g l^{-1}) and a DOC removal rate of 25.37 mg l^{-1} day^{-1} C manifested that SBR was working under steady conditions.

Acknowledgements

This work was supported by CICYT (project PPQ2002-04060-C02-01) and European Commission (CADOX project, EVK1-CT-2002-00122).

References

[1] V. López-Grimau, M.C. Gutiérrez, Chemosphere 62 (1) (2006) 106–112.
[2] D. Brown, B. Hamburger, Chemosphere 16 (1987) 1539–1553.
[3] C. O'Neill, F.R. Hawkes, S.R.R. Esteves, D.L. Hawkes, S.J. Wilcox, J. Chem. Technol. Biotechnol. 74 (1999) 993–999.
[4] R. Andreozzi, V. Caprio, A. Insola, R. Marotta, Catal. Today 53 (1999) 51–59.
[5] B.T. Tan, T.T. Teng, A.K. Omar, Water Res. 34 (2000) 3153–3160.
[6] S.H. Lin, C.C. Lo, Environ. Technol. 17 (8) (1996) 841–849.
[7] L. Tan, R.G. Sudan, J. Am. Water Works Assoc. 84 (1992) 79–87.
[8] S.H. Lin, J. Chem. Technol. Biotechnol. 57 (1993) 387–391.
[9] F. Haber, J. Weiss, Proc. R. Soc. Series A 147 (1934) 332–351.
[10] J. Pignatello, Environ. Sci. Technol. 26 (1992) 944–951.
[11] R. Bauer, H. Fallman, Res. Chem. Intermed. 23 (1997) 341–354.
[12] A. Safarzadeh-Amiri, J.R. Bolton, S.R. Cater, J. Adv. Oxid. Technol. 1 (1996) 18–26.
[13] J.P. Scott, D.F. Ollis, Environ. Prog. 14 (1995) 88–103.
[14] S. Parra, S. Malato, C. Pulgarín, Appl. Catal. B: Environ. 36 (2002) 131–144.
[15] J. Beltrán-Heredia, J. Torregrosa, J. García, J.R. Domínguez, J.C. Tierno, Water Sci. Technol. 44 (5) (2001) 103–108.
[16] J. García-Montaño, F. Torrades, J.A. García-Hortal, X. Domènech, J. Peral, J. Hazard. Mater. 134 (2006) 220–229.
[17] S.S. Mangat, P. Elefsiniotis, Water Res. 33 (3) (1999) 861–867.
[18] M.C. Tomei, M.C. Annesini, S. Bussoletti, Water Res. 38 (2004) 375–384.
[19] S. Mace, J. Mata-Alvarez, Ind. Eng. Chem. Res. 41 (2002) 5539–5553.
[20] APHA–AWWA–WPCF, Standard Methods for the Examination of Water and Wastewater, ASTM D1252-00, 17th ed., APHA–AWWA–WPCF, Washington, DC, 1989.
[21] C. Kormann, D.W. Bahnemann, M.R. Hoffmann, Environ. Sci. Technol. 22 (5) (1988) 798–806.
[22] Y.W. Kang, M.-J. Cho, K.-Y. Hwang, Water Res. 33 (5) (1999) 1247–1251.
[23] C.D. Adams, P.A. Scanlan, N.D. Secrist, Environ. Sci. Technol. 28 (1994) 1812–1818.
[24] OECD Guidelines for Testing of Chemicals, Test 302B, vol. 2, 1996.
[25] M. Rodrígez, V. Sarria, S. Esplugas, C. Pulgarin, J. Photochem. Photobiol. A: Chem. 151 (2002) 129–135.

ELSEVIER

Journal of Hazardous Materials A138 (2006) 218–225

Journal of Hazardous Materials

www.elsevier.com/locate/jhazmat

Environmental assessment of different photo-Fenton approaches for commercial reactive dye removal

Julia García-Montaño [a], Nilbia Ruiz [a], Iván Muñoz [a], Xavier Domènech [a], José A. García-Hortal [b], Francesc Torrades [c], José Peral [a,*]

[a] *Departament de Química, Edifici Cn, Universitat Autònoma de Barcelona, E-08193 Bellaterra, Barcelona, Spain*
[b] *Departament d'Enginyeria Tèxtil i Paperera, ETSEIA de Terrassa (UPC), C/Colom 11, E-08222 Terrassa, Barcelona, Spain*
[c] *Departament d'Enginyeria Química, ETSEIA de Terrassa (UPC), C/Colom 11, E-08222 Terrassa, Barcelona, Spain*

Received 20 April 2006; received in revised form 18 May 2006; accepted 19 May 2006
Available online 26 May 2006

Abstract

An environmental study using life cycle assessment (LCA) has been applied to three bench-scale wastewater treatments for Cibacron Red FN-R hetero-bireactive dye removal: artificial light photo-Fenton process, solar driven photo-Fenton process and artificial light photo-Fenton process coupled to a biological treatment. The study is focused on electricity and chemicals consumption, transports and atmosphere and water emissions generated by the different processes involved. Results show that the artificial light photo-Fenton process is the worst treatment in terms of environmental impact. On the other hand, both solar driven and coupled to biological photo-Fenton processes reduce significantly the environmental damage, although none can be identified as the best in all impact categories. The major environmental impact is attributed to the H_2O_2 consumption and to the electrical energy consumption to run the UVA lamp. An economic analysis of the different photo-Fenton processes has also been performed and the results are discussed together with those obtained from the environmental assessment.

Keywords: Textile reactive dye; Photo-Fenton's oxidation; Sunlight; Biological treatment; Life cycle assessment; Economic study

1. Introduction

Reactive dyes have been identified as the most environmental problematic compounds in textile dye effluents [1]. Therefore, in the last decade, attention has been focused on the development of new treatment technologies that leads to complete destruction of the dye molecules. Among these treatments, advanced oxidation processes (AOPs) are a powerful alternative to conventional treatment methods for wastewater decontamination [2]. These treatments are based on the in situ generation of highly reactive hydroxyl radicals as a primary oxidant species ($HO^{\bullet}$). These radicals are high oxidant species ($E = 2.8$ V versus NHE) that are able to mineralise almost all recalcitrant organic compounds under mild experimental conditions. Among the considered AOPs, the Fenton and photo-Fenton type reactions are very promising since they achieve high reaction yields with a low treatment cost [3]. In Fenton reaction, hydroxyl radicals are generated by interaction of H_2O_2 with ferrous salt in aqueous media. The rate of contaminant degradation is considerably increased via photochemical reaction in the photo-Fenton process. Moreover, since the reaction requires radiations up to 410 nm [4], photo-Fenton reaction offers the possibility of sunlight exploitation.

On the other hand, AOPs are currently being object of the development for new application areas. When working with toxic or non-biodegradable wastewaters, AOPs are employed as a pre-treatment of standard biological treatments. Complete mineralisation is avoided in the chemical process, being the goal the generation of a new biocompatible effluent [5,6]. In any case, every strategy must be developed paying special attention to its potential environmental impact. In this way, environmental factors must be taken into account for the most suitable water treatment technique selection.

In this paper, a representative commercial hetero-bireactive dye, 250 mg/l Cibacron Red FN-R, is taken as a model compound for the environmental impact assessment of different lab-scale wastewater treatments. The photo-Fenton reaction, under

* Corresponding author. Tel.: +34 93 581 2772; fax: +34 93 581 2920.
E-mail address: jose.peral@uab.es (J. Peral).

0304-3894/$ – see front matter © 2006 Elsevier B.V. All rights reserved.
doi:10.1016/j.jhazmat.2006.05.061

both artificial and solar irradiation, is applied as a single process to degrade the pollutant. In another scenario, just partially photo-treated dye solution was subsequently submitted to an aerobic sequencing batch reactor (SBR), that is an efficient alternative to conventional biological systems for a wide variety of model pollutants and real wastewaters biodegradation [7].

The life cycle assessment (LCA) tool, according to ISO 14.040 Standard [8], is applied to carry out the environmental impact evaluation. Four distinguishable phases constitute the LCA sequence: (1) goal and scope, in which the purpose, scope, main hypothesis and data quality are defined, (2) inventory analysis, in which data are collected in order to quantify the inputs and outputs of the system, (3) impact assessment, where potential environmental impacts are identified and characterised, and (4) interpretation, in which the results of the inventory analysis and impact assessment are discussed in the light of the goals set in the beginning of the study, identifying the areas for environmental improvement of the system under study.

Finally, an economic study based on adding the costs of all chemicals and energy consumption through the life cycle of the different treatments has also been considered and discussed together with the environmental assessment.

2. Materials and methods

2.1. Synthetic dye solution

A commercial hetero-bireactive azodye, Cibacron Red FN-R (C.I. Reactive Red 238, $C_{29}H_{15}ClFN_7O_{13}S_4Na_4$) was supplied by CIBA and used as received without further purification. The initial Cibacron Red FN-R concentration for all the experiments was 250 mg/l. In order to simulate batch-dyeing conditions, the dye was hydrolysed by adjusting the pH of synthetic solutions to 10.6, followed by heating to 60 °C for 1 h. Finally, pH of the hydrolysed dye solutions was adjusted between 2.8 and 3.0 for AOP operation. The dissolved organic carbon (DOC) of the synthetic effluent was 79.46 ± 1.34 mg/l C and the BOD_5/COD index was 0.02 ± 0.02 ($n = 3$, $\alpha = 0.05$).

2.1.1. Photo-Fenton oxidation

Photo-Fenton oxidation was conducted in a thermostated ($T = 23 \pm 1$ °C) well-stirred cylindrical Pyrex cell of 300 ml of capacity (78.54 cm^2 surface). The dye solution volume was 250 ml. Analytical grade hydrogen peroxide (33% w/v, Panreac) and $FeSO_4 \cdot 7H_2O$ (99.5%, Merck) were used as received to generate hydroxyl radical ($HO^\bullet$) in aqueous solution. A 6 W Philips black light fluorescent lamp, situated over the reactor, was used for artificial light photo-Fenton experiments. The intensity of the incident UVA light, measured employing a luminometer, was 0.6 mw/cm^2. Solar light experiments were performed during sunny days of July at Universitat Autònoma de Barcelona (45 m a.s.l., 41°30′N, 2°6′E).

2.2. Biological treatment

The biological treatment system was composed of a 2 l aerobic bench-scale sequencing batch reactor (SBR), equipped with an air diffuser and agitation. The activated sludge, coming from a municipal wastewater treatment plant (WWTP) in Manresa (Catalonia, Spain), was initially around 0.6 g/l of volatile suspended solids (VSS) concentration. The operating liquid volume was 1.2 l and the hydraulic retention time was 24 h. Temperature remained stable and close to room conditions, between 21 and 23 °C. The concentration of dissolved oxygen (DO) was kept above 3 mg/l O_2. Daily analyses of VSS, DO and DOC were carried out, and pH adjustment between 6.5 and 7.5 was done if necessary. Suitable proportions of nutrients ($MgSO_4$, $CaCl_2$, NH_4Cl and NaH_2PO_4 buffer at pH 7) were also added to the solution [9].

2.3. Analysis

DOC was determined with a Shimadzu TOC-V_{CSH} analyser. Chemical oxygen demand (COD, mg/l O_2) was assessed by the closed reflux colorimetric method with a HACH DR/2000 spectrophotometer [9]. H_2O_2 consumption was tested by the potassium iodide titration method [10]. Accordingly, correction was made in the COD measurement for residual H_2O_2 [11]. Determination of total suspended solids (TSS, g/l) and VSS was carried out gravimetrically [9]. The measurement of biochemical oxygen demand for 5 days (BOD_5, mg/l O_2) was performed by means of a mercury-free WTW 2000 Oxytop thermostated at 20 °C. Ammonium ion concentration was determined by *Nessler* colorimetric assay [9].

2.4. Life cycle assessment methodology

The environmental impact assessment is focused on the following small-scale wastewater treatments: artificial light photo-Fenton process (scenario 1), solar driven photo-Fenton process (scenario 2) and artificial light photo-Fenton process coupled to a biological treatment (scenario 3). The DOC parameter has been used as indicator of pollutant removal.

A preliminary optimisation study to degrade Cibacron Red FN-R reactive dye was carried out by testing the following Fenton reagent dose: 10 mg/l Fe (II) combined with 125, 250 and 500 mg/l of H_2O_2, and 20 mg/l Fe (II) combined with 250 and 500 mg/l H_2O_2 concentrations [12]. The best experimental conditions that give rise to a more efficient dye degradation were 20 mg/l Fe (II) and 500 mg/l H_2O_2, which lead to a maximum mineralisation level (around 80–90% of the initial DOC) after relatively short irradiation times (Fig. 1). These conditions were used for single photo-Fenton processes (scenarios 1 and 2). On the other hand, when the photo-Fenton oxidation was just applied as a pre-treatment (scenario 3), the H_2O_2 dose was reduced in order to soften the chemical consumption. In this way, 20 mg/l Fe (II) and 250 mg/l H_2O_2 were enough to bio-compatibilize the effluent. After an irradiation time of 90 min, with just 49.6% mineralisation and 21 mg/l remaining H_2O_2, BOD_5/COD ratio went from 0.02 ± 0.02 up to 0.36 ± 0.05 ($n = 3$, $\alpha = 0.05$) (Fig. 2), close to 0.4, which is the characteristic value for completely biodegradable wastewaters [13]. Afterwards, the aerobic SBR treatment was performed until achieving 80% global

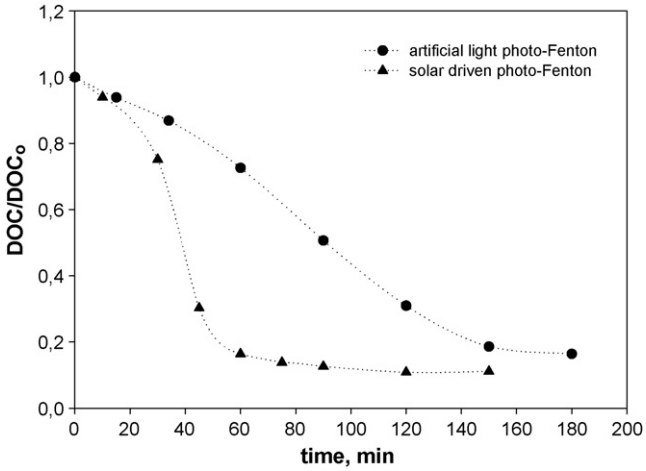

Fig. 1. DOC/DOC$_o$ evolution vs. time for 250 mg/l Cibacron Red FN-R degradation with artificial and solar light photo-Fenton reaction: 20 mg/l Fe (II), 500 mg/l H_2O_2, pH 3 and T = 23 °C.

DOC removal (accumulated in the chemical plus biological stages).

The functional unit (the unit of service to which the environmental burdens must be referred) has been defined as "the removal of 80% DOC from 1.2 l of 250 mg/l Cibacron Red FN-R synthetic effluent". To achieve this % DOC elimination, single artificial light and solar driven photo-Fenton processes required 150 and 50 min of treatment periods, respectively (Fig. 1). Residual hydrogen peroxide concentrations of 19 mg/l were found at the end of both experiments.

The flow diagrams and boundaries considered to perform the LCA are shown in Figs. 3 and 4. The inputs and outputs included are: (i) the electricity consumption by the different processes involved, including extraction of resources, transport and energy conversion, (ii) the chemicals consumption, including extraction of resources, production of the corresponding chemicals and the different transport steps, and (iii) the air and water emissions generated through the considered scenarios. The construction and the end-of-life of each system have not been considered.

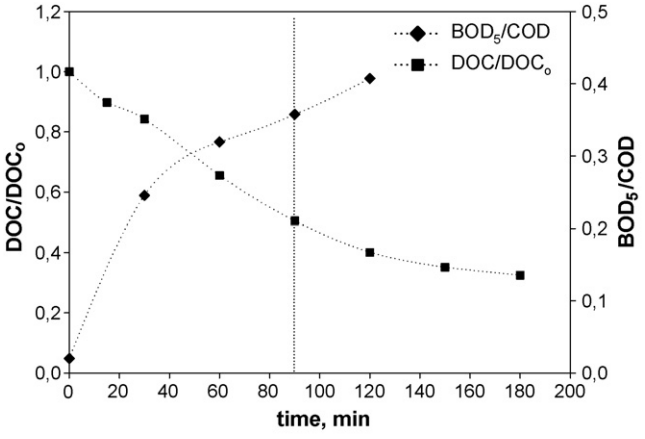

Fig. 2. DOC/DOC$_o$ and BOD$_5$/COD evolution vs. time for 250 mg/l Cibacron Red FN-R degradation with artificial light photo-Fenton reaction: 20 mg/l Fe(II), 250 mg/l H_2O_2, pH 3 and T = 23 °C.

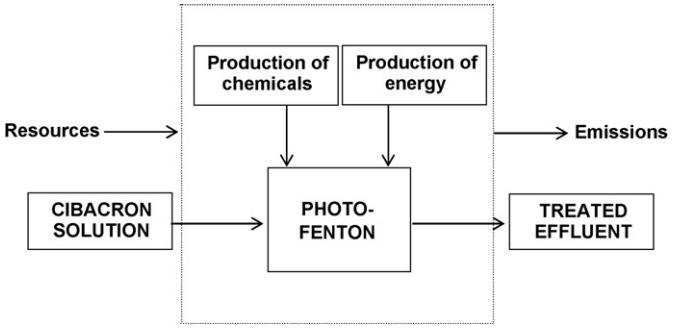

Fig. 3. Simplified flow diagram and system boundaries for scenarios 1 and 2.

The main environmental burdens associated to the defined systems and referred to the functional unit have been inventoried. The sources and quality of the data handled in this assessment, mostly obtained from Ecoinvent database version 1.1 [14,15], are detailed in Table 1.The main hypothesis assumed in the inventory phase of the LCA are the following: as a general consideration, those inputs, outputs or processes common to all the evaluated scenarios have been excluded, i.e., auxiliary reagents consumption for pH adjustments or residual iron sludge recovery for disposal.

2.4.1. Photo-Fenton process

(1) The energy used to run the black light has been assumed to be electricity delivered from the European grid. In order to consider operational conditions similar to those employed in a full-scale photochemical reactor, 100% efficiency has been considered. This implies to assume that all the UV-photons emitted by the lamp reach the solution. In the laboratory set-up, this efficiency has been calculated to be only around 0.8% (0.6 mW/cm^2 UVA light measured by the luminometer multiplied by the 78.54 cm^2 photo-reactor surface).
(2) H_2O_2 and $FeSO_4$ are assumed to be produced in Spain and delivered from the supplier to the site by 16 t-trucks over a 50 km distance.
(3) It is assumed that residual H_2O_2 is totally decomposed after each photo-Fenton process.
(4) CO_2 emissions have been estimated from DOC mineralised by chemical oxidation.
(5) Residual DOC, COD and ammonium ion content have been considered for final effluent impact assessment.

Table 1
Summary of data used in the inventory phase of the LCA

Dataset
Electricity, low voltage, production UCTE, at grid/UCTE S [28]
Hydrogen peroxide, 50% in H_2O, at plant/RER S [29]
Iron sulphate, at plant/RER S [28]
Quicklime, milled, packed, at plant/CH S [30]
Acrylonitrile, at plant/RER S [31]
Heat diesel B250 [25]
Transport, lorry 16 t/CH S [32]

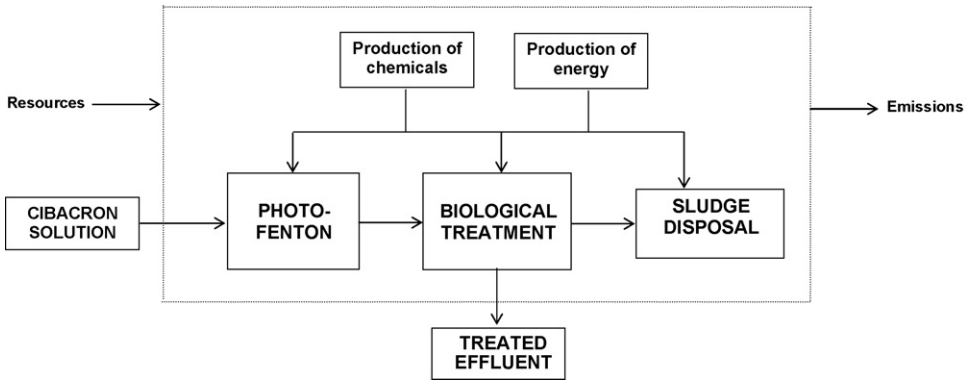

Fig. 4. Simplified flow diagram and system boundaries for scenario 3.

2.4.2. Biological treatment

(1) It is considered that the bench-scale sequencing batch reactor behaved as a real conventional biological treatment process. A municipal WWTP with a 0.76 VSS/TSS ratio is chosen as a model for the estimation, assuming an excess sludge production of 0.55 mg VSS per mg COD consumed [16].
(2) External electricity consumption for mechanical aeration equipment has been considered. In this way, the figure 1.5 kg O_2/kWh [17] has been taken into account. The consumed oxygen, required for nitrification and organic matter oxidation processes, has been determined from removed COD in the bioreactor (34 mg per functional unit) minus the COD fraction assimilated by biomass for cells grown, quantified as 1.42 mg COD per mg VSS of sludge production [16].
(3) The CO_2 emissions have been determined from oxygen requirements, considering that O_2 is mainly employed to oxidise organic substrate.
(4) It is considered a subsequent sludge treatment system composed of several independent unit processes [18]: thickening, dewatering and stabilisation processes. By means of this treatment, a dewatered sludge with 31% final dry matter content (DM) is obtained. About 50 kWh of electricity and 4 kg of polymers are considered to be consumed at the thickening and 40 kWh and 5 kg of polymer at dewatering per ton of DM of sludge. On the other hand, 200 kg lime per ton of DM of sludge is needed for stabilisation while 5 kWh of electricity is consumed for pumping and mixing it [18].
(5) It is assumed that solid residues from exceeding sludge management are finally deposited at landfill. The main environmental emissions from landfill (leachate and landfill gas) are calculated according to the ORWARE (Organic Waste Research) theoretical model [19,20]. By means of this model, the air/water/land distribution of different elements present at landfill is obtained, considering a period of 100 years for biochemical stabilisation after anaerobic sludge digestion. An input to the model is the sludge composition: $C_8H_{15}O_4N$ (typical municipal WWTP sludge, [21]), which is anaerobically degraded according to reaction (1) [21].

$$C_8H_{15}O_4N + 3H_2O \rightarrow 4.5CH_4 + 3.5CO_2 + NH_3 \quad (1)$$

The model considers that leachate generated at landfill is treated biologically and that recovered biogas (99% both CO_2 and CH_4, [22]) is totally burned in a torch. It is assumed a 50% of capture efficiency for biogas [23] and 90% for leachate [24]. Fugitive biogas and leachate reach atmosphere and aquatic media, respectively. Considered removal yields for captured leachate in subsequent biological treatment are 90% for both COD and BOD_7 [22] and 80% for $N–NH_4^+$ [23]. Atmosphere emissions and the management of sludge generated at leachate treatment have been excluded from the inventory.

With respect to the energy requirements, 1.8 l diesel consumption per ton of fresh sludge is considered for machinery operation at landfill [22]. The energy consumption (electricity) for leachate treatment has been quantified as a function of the BOD_7 and NH_4^+ eliminated, following the ORWARE methodology. The electricity consumption for biogas pumping is considered to be 0.013 kWh/m^3. It has been determined indirectly from BUWAL 250 database [25], which gives 1.35 kWh/t of residue that produces 200 m^3 of biogas (from which 53% of biogas is captured). Inventory data for inorganic compounds and energy requirements at landfill resulting from calculations are shown in Table 2.
(6) All reagents used have been supposed to be produced in Spain and delivered by 16 t-trucks. The assumed distance for lime and polymer employed in biological sludge disposal processes was 50 km. The average distance for the sludge transport between the municipal WWTP and the landfill site has also been considered to be 50 km.
(7) Residual DOC, COD, ammonium and nitrate ions content in the treated effluent have been considered for final effluent impact assessment. Nitrate concentration has been estimated considering that all disappeared NH_4^+ (5.4 mg per functional unit, minus the N fraction assimilated by biomass for cells grown quantified according to a $C_8H_{15}O_4N$ VSS sludge composition) was completely oxidised to NO_3^- through aerobic biodegradation.

In Table 3 data concerning energy, chemicals consumption, and generated emissions per functional unit for every considered scenario are summarized.

Table 2
Inventory for WWTP sludge (31% DM) deposited at landfill per functional unit

Inputs	
Transport	
Truck 16 t (t km)	4.97×10^{-6}
Energy	
Diesel (l)	1.72×10^{-7}
Electricity (kWh)	4.35×10^{-9}
Outputs[a]	
Atmosphere emissions	
CH_4 (mg)	2.27
CO_2 (mg)	25.4
NH_3 (mg)	0.01
NO_x (mg)	0.09
Water emissions	
COD (mg)	0.05
NH_4^+ (mg)	0.45
NO_3^- (mg)	1.90

[a] Outputs related chemicals and energy consumed are not included here, but in corresponding life cycle inventory dataset.

The impact assessment for each wastewater treatment was carried out considering the following potential environmental impacts categories included in the CML 2000 method [26]: abiotic resource depletion (ARD), global warming potential (GWP), ozone depletion potential (ODP), human toxicity potential (HTP), freshwater aquatic toxicity potential (FATP), marine aquatic ecotoxicity potential (MAEP), terrestrial ecotoxicity potential (TEP), photochemical oxidation potential (POP), acidification potential (AP) and aquatic eutrophication potential (AEP).

Table 3
Energy usage, chemicals consumption and generated emissions per functional unit for considered scenarios (excluding landfill inventory)

	Scenario 1	Scenario 2	Scenario 3
Inputs			
Grid electricity (kWh)	6.28×10^{-4}		3.84×10^{-4}
H_2O_2 50% (mg)	1200	1200	600
Truck 16 t (t km)	5.94×10^{-5}	5.94×10^{-5}	2.97×10^{-5}
$FeSO_4$ (g)	0.065	0.065	0.065
Truck 16 t (t km)	3.25×10^{-6}	3.25×10^{-6}	3.25×10^{-6}
CaO (mg)			4.92
Truck 16 t (t km)			2.46×10^{-7}
Acrylonitrile (mg)			0.22
Truck 16 t (t km)			1.11×10^{-8}
Outputs[a]			
Atmosphere emissions			
CO_2 (mg)	287.5	280.9	170.5
Water emissions			
COD (mg)	46	42	36
DOC (mg)	16.93	18.74	19.94
NH_4^+ (mg)	7.16	4.79	1.76
NO_3^- (mg)			12.50

[a] Outputs related chemicals and energy consumed are not included here, but in corresponding life cycle inventory dataset.

2.5. Economic study

An economic study has been performed for the three reactive dye treatments on the basis of the previously defined functional unit. The same boundaries than in the LCA are considered, taking into account chemical and energy costs employed during operation phases. All other running costs and capital investments are excluded.

3. Results and discussion

Table 4 shows the characterised values obtained for the different environmental impacts and the considered scenarios. Relative scores are represented graphically in Fig. 5, in which the highest environmental impact is set to 100% for each category. In view of this, scenario 1 is the wastewater treatment with a major global impact on the environment, with highest scores for every considered impact indicator (Table 4). However, when the photo-Fenton process is applied as a pre-treatment of a secondary biological treatment (scenario 3), impacts decrease considerably achieving around 45% reduction for most categories (Fig. 5). Fig. 6 exhibits, for single (a) and combined (b) artificial light photo-Fenton processes, the relative contributions to the impact categories of the different stages of the life cycle: H_2O_2 and iron sulphate production and consumption, associated transports, biological treatment and sludge management (without WWTP emissions), grid electricity production and use, and finally emissions from chemical and biological oxidation steps. In both cases, the major impact contribution is attributed to H_2O_2 consumption, followed by the electricity requirements of the UVA lamp. It is worth to note that, for both scenarios, air and water emissions have an important effect on AEP due to NH_4^+ and NO_3^- ions content; also it is significant the contribution to GWP due to the CO_2 emitted during chemical and biological stages. Finally, the reagents transport effect and iron salt consumption are not considered important since together represent less than 5% in all categories. From manifested similarities of both scenarios contributions profiles, it could be stated that the

Table 4
Characterisation of the different environmental impacts for considered scenarios

Category	Unit	Scenario 1	Scenario2	Scenario 3
ARD	kg Sb	8.1×10^{-6}	5.6×10^{-6}	4.4×10^{-6}
GWP	kg CO_2	1.3×10^{-3}	9.7×10^{-4}	8.2×10^{-4}
ODP	kg CFC 11	7.9×10^{-11}	6.5×10^{-11}	4.2×10^{-11}
HTP	kg 1,4-D[a]	2.4×10^{-3}	2.2×10^{-3}	1.2×10^{-3}
FATP	kg 1,4-D[a]	1.7×10^{-4}	1.5×10^{-4}	8.8×10^{-5}
MAEP	kg 1,4-D[a]	4.9×10^{-1}	2.6×10^{-1}	2.7×10^{-1}
TEP	kg 1,4-D[a]	1.1×10^{-5}	4.7×10^{-6}	6.3×10^{-6}
POP	kg C_2H_4	1.8×10^{-7}	1.0×10^{-7}	1.2×10^{-7}
AP	kg SO_2	4.3×10^{-6}	2.4×10^{-6}	2.5×10^{-6}
AEP	kg PO_4^{3-}	3.7×10^{-6}	2.8×10^{-6}	2.8×10^{-6}

ARD, abiotic resource depletion; GWP, global warming potential; ODP, ozone depletion potential; HTP, human toxicity potential; FATP, freshwater aquatic toxicity potential; MAEP, marine aquatic ecotoxicity potential; TEP, terrestrial ecotoxicity potential; POP, photochemical oxidation potential; AP, acidification potential; AEP, aquatic eutrophication potential.

[a] 1,4-Dichlorobenzene.

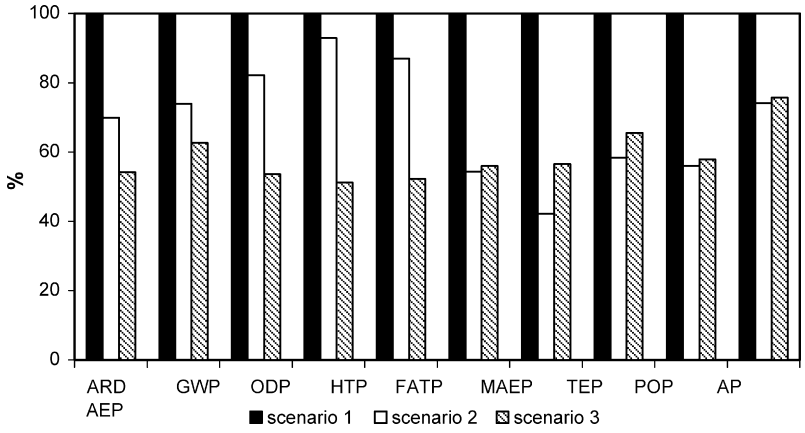

Fig. 5. Characterisation values of the different environmental impacts for considered scenarios.

chemical stage in the combined treatment supposes the main impact, since the biological treatment and subsequent processes only slightly contribute (12–17%) to the GWP, POP and AEP categories. Therefore, it becomes evident that the lower H_2O_2 concentration and the shorter irradiation time employed in the artificial light photo-Fenton pre-treatment are the main factors responsible of the impact scores reduction presented in Table 4 for scenario 3.

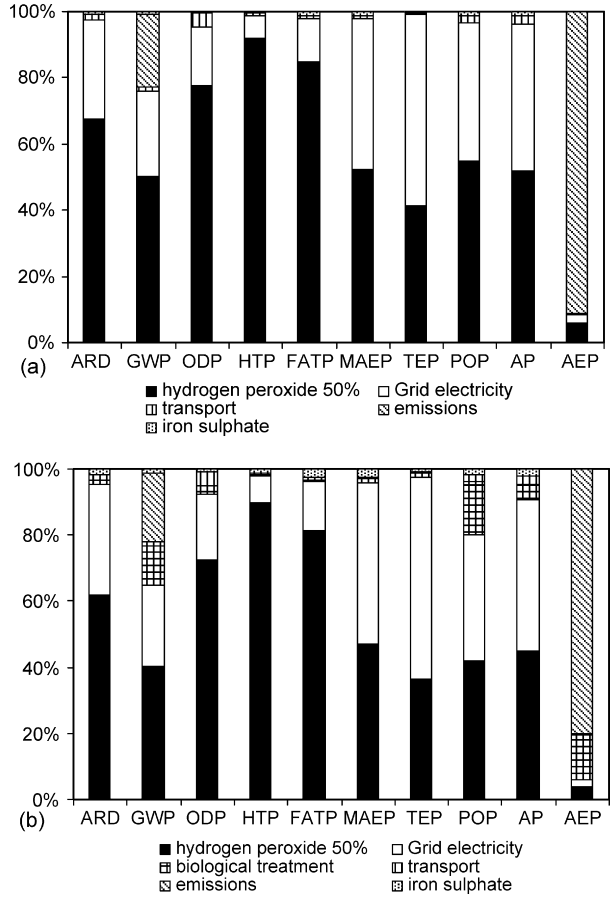

Fig. 6. Relative contributions to the respective impact categories of the different stages of the life cycle for scenarios 1 (a) and 3 (b).

The characterised values for the different environmental impact categories are also reduced when no artificial UVA light is employed (scenario 2) (Table 4). Since there is no use of electricity from the grid, environmental impacts are directly associated with the production of hydrogen peroxide, whose contribution supposes more than 93% for most categories (data not shown). It should be noted that, apart from the impact reduction attainment, solar light gives more efficient dye degradation than artificial light (Fig. 1). This higher efficiency observed with the use of sunlight is basically due to the higher number of photons between 300 and 400 nm arriving to the earth surface in Spain [27] (estimated around 3–4 mW/cm^2).

When comparing scenario 2 with the artificial light photo-Fenton process coupled to the biological treatment (scenario 3), it is difficult to distinguish which treatment would be more environmentally friendly since data notably vary depending on the category considered (Fig. 5). Solar driven photo-Fenton process offers better results than the coupled system for MAEP, TEP, POP, AP and AEP. This behaviour can be attributed to the major electricity contribution to these impact categories (Fig. 6). However, since electricity does not suppose a large burden for the rest of indicators (as H_2O_2 does), solar driven photo-Fenton impacts are not further reduced and the coupled system becomes more environmentally benign. In any case, obtained results allow concluding that both, scenarios 2 and 3, are more environmentally friendly alternatives than artificial light photo-Fenton process.

The considered wastewater treatments have also been assessed from an economic point of view. Employed unitary prices and cost per functional unit of the different inputs are shown in Tables 5 and 6, respectively. Fig. 7 displays the overall costs as a percentage of the most expensive treatment. From Table 6 and Fig. 7, it can be stated that the artificial light photo-Fenton process is the most expensive treatment. When carrying out the treatment under solar irradiation or coupled to an ensuing biological process, the estimated relative cost decreased in a 13 and 44%, respectively, being the combined system the cheaper option. A reduction of H_2O_2 dosage and electricity consumption for UVA irradiation (which contribute in an 81% and 14% cost for scenario 1, respectively) in favour of the biological treatment are the major cause since biological and sludge management

Table 5
Unitary costs considered for economic study

Product	Price (€)	Source
Electricity (kWh)	0.07	[33]
H_2O_2 50% (kg)	0.22	Hera-Segasa S.L. Barcelona, Spain
$FeSO_4$ (kg)	0.25	Albaida Recursos Naturales y Medio Ambiente S.L. Almería, Spain
Landfill (kg)	0.07	[34]
CaO (kg)	0.09	DSM-Deretil, Almería, Spain
Polymer (kg)	2.69	DSM-Deretil, Almería, Spain; Hera-Segasa S.L. Barcelona, Spain

Table 6
Economic cost per functional unit of the different inputs for considered scenarios

	Cost (€)		
	Scenario 1	Scenario 2	Scenario 3
Electricity	4.4×10^{-5}		2.7×10^{-5}
H_2O_2 50%	2.6×10^{-4}	2.6×10^{-4}	1.3×10^{-4}
$FeSO_4$	1.6×10^{-5}	1.6×10^{-5}	1.6×10^{-5}
Landfill			6.8×10^{-6}
CaO			4.4×10^{-7}
Polymer			5.9×10^{-7}
Total	3.2×10^{-4}	2.8×10^{-4}	1.8×10^{-4}

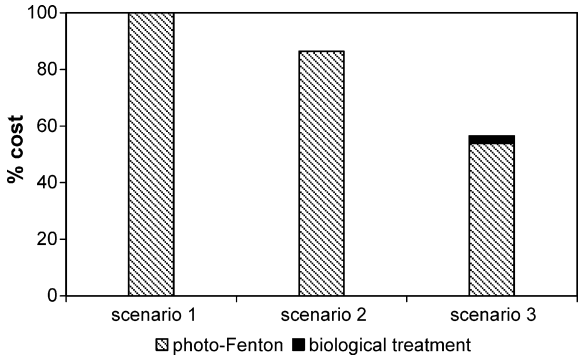

Fig. 7. Relative economic cost per functional unit for considered scenarios.

processes just suppose a 4.5% of the global combined treatment cost (Fig. 7).

In view of this, considering both environmental and economic data to decide about the suitability of the studied wastewater treatments, the best environmental/cost option seems to be the coupling of artificial light photo-Fenton process and biological treatment (scenario 3). On the other hand, artificial light photo-Fenton treatment appears as the worst option in both assessments mainly due to the high hydrogen peroxide and energy demand, in this order.

4. Conclusions

A LCA study has been performed to determine the environmental suitability of three small-scale wastewater treatments for Cibacron FN-R reactive dye removal: artificial light photo-Fenton process, solar driven photo-Fenton process and artificial light photo-Fenton process coupled to a biological treatment.

The artificial light photo-Fenton process is the most environmentally harmful treatment, mainly due to H_2O_2 consumption which presents the higher environmental impact and scores for almost all the categories considered. The electricity requirements for UVA light irradiation appear in a second place. Finally, as in the other considered scenarios, air and water emissions generated during dye oxidation have an important effect on AEP and GWP indicators while iron salt consumption and chemicals transport to the treatment plant barely contribute in a representative way.

When artificial light photo-Fenton reaction is applied as a biological pre-treatment, H_2O_2 dose and electricity consumption are significantly reduced giving place to around 45% diminution for most environmental impact categories. However, both continue to be the highest burdens of the combined process. In contrast, the biological stage becomes environmentally advantageous since it just contributes with small quantities (among 12–17%) in GWP, POP and AEP indicators. When comparing it with the solar driven photo-Fenton process, no clear preferences can be drawn from all impacts categories. Although using solar energy as a source of photons avoids electricity consumption, it just gives better environmental benefits than the combined system in five categories from the 10 evaluated since it maintains a large H_2O_2 consumption. On the other hand, from the economic point of view, the coupled process appears to be better achieving a 44% cost diminution with respect to the most expensive one, in front of the 13% reduction attained with the solar assisted process.

As a final remark, and taking these results as starting point, it is predictable that a solar driven photo-Fenton process coupled to a biological treatment would be the best economic and environmental option to remove Cibacron FN-R hetero-bireactive dye from textile effluent.

Acknowledgement

The authors wish to thank to MEC (project CTQ 2005-02808) for financial support.

References

[1] C.M. Carliell, S.J. Barclay, C.A. Buckley, Treatment of exhausted reactive dye bath effluent using anaerobic digestion: laboratory and full scale trials, Water S.A. 22 (1996) 225–233.
[2] R. Andreozzi, V. Caprio, A. Insola, R. Marotta, Advanced oxidation processes (AOP) for water purification and recovery, Catal. Today 53 (1999) 51–59.
[3] R. Bauer, H. Fallman, The photo-Fenton oxidation–a cheap and efficient wastewater treatment method, Res. Chem. Intermediat. 23 (1997) 341–354.
[4] P.L. Huston, J. Pignatello, Degradation of selected pesticide active ingredients and commercial formulations in water by the photo-assisted Fenton reaction, Water Res. 33 (1999) 1238–1246.
[5] J. García-Montaño, F. Torrades, J.A. García-Hortal, X. Domènech, J. Peral, Degradation of Procion Red H-E7B reactive dye by coupling a photo-Fenton system with a sequencing batch reactor, J. Hazard. Mater, in press.
[6] V. Sarria, S. Parra, N. Adler, P. Péringer, N. Benitez, C. Pulgarin, Recent developments in the coupling of photoassisted and aerobic biological processes for the treatment of biorecalcitrant compounds, Catal. Today 76 (2002) 301–315.

[7] S. Mace, J. Mata-Alvarez, Review of SBR technology for wastewater treatment: an overview, Ind. Eng. Chem. Res. 41 (2002) 5539–5553.
[8] ISO 14040, Environmental management – Life Cycle Assessment – Principles and Framework, Switzerland, 1997.
[9] APHA-AWWA-WPCF, Standard Methods for the Examination of Water and Wastewater, ASTM D1252-00, 17th ed., APHA-AWWA-WPCF, Washington, DC, 1989.
[10] C. Kormann, D.W. Bahnemann, M.R. Hoffmann, Photocatalytic production of H_2O_2 and organic peroxides in aqueous suspensions of TiO_2, ZnO and desert salt, Environ. Sci. Technol. 22 (5) (1988) 798–806.
[11] Y.W. Kang, M.-J. Cho, K.-Y. Hwang, Correction of hydrogen peroxide interference on standard chemical oxygen demand test, Water Res. 33 (5) (1999) 1247–1251.
[12] J. García-Montaño, F. Torrades, J.A. García-Hortal, X. Domènech, J. Peral, Combining photo-Fenton process with aerobic sequencing batch reactor for commercial hetero-bireactive dye removal, Appl. Catal. B-Environ, in press.
[13] E. Chamarro, A. Marco, S. Esplugas, Use of Fenton reagent to improve organic chemical biodegradability, Water Res. 35 (2001) 1047–1051.
[14] R. Frischknecht, H.J. Althaus, G. Doka, R.S. Dones, R. Hischier, N. Jungbluth, T. Nemecek, G. Rebitzer, M. Spielmann, Code of Practice, Final report ecoinvent 2000 No. 2, Swiss Centre for Life Cycle Inventories, Duebendorf, Switzerland, 2003.
[15] R. Frischknecht, H.J. Althaus, G. Doka, R. Dones, T. Heck, S. Hellweg, R. Hischier, N. Jungbluth, T. Nemecek, G. Rebitzer, M. Spielmann, Overview and Methodology, Final Report Ecoivent 2000 No. 1, Swiss Centre for Life Cycle Inventories, Duebendorf, Switzerland, 2004.
[16] C. Jiménez-González, R.M. Overcash, A. Curzons, Waste treatment modules—a partial life cycle inventory, J. Chem. Technol. Biot. 70 (2001) 707–716.
[17] Metcalf & Eddy, Wastewater engineering: treatment, disposal and reuse, McGraw-Hill, Singapore, 1991.
[18] Y. Suh, P. Rousseaux, A LCA of alternative wastewater sludge treatment scenarios, Resour. Conserv. Recy. 35 (3) (2002) 191–200.
[19] K. Mingarini, Systems Analysis of Organic waste with Emphasis on Modelling of the Incineration and the Landfilling Process, Licentiate Thesis, Department of Environmental Technology and Work Science, KTH, Stockholm, 1996.
[20] M. Dalemo, The ORWARE simulation model. Anaerobic Digestion and Sewage plant Sub-models, Licentiate Thesis, AFR-Report 152, Swedish Institute of Agricultural Engineering, Swedish University of Agricultural Sciences (SLU), Swedish Environmental Protection Agency, Uppsala, 1997.
[21] G. Tchobanoglous, H. Theisen, S. Vigil, Integrated Solid Waste Management: Engineering Principles and Management Issues, McGraw-Hill, Singapore, 1993.
[22] X. Domènech, J. Rieradevall, P. Fullana, Application of life cycle assessment to landfilling, Int. J. Life Cycle Assessment 2 (3) (1997) 141–144.
[23] P. Nielsen, M. Hauschild, Product specific emissions from municipal solid waste landfills. Part I: landfill model, Int. J. Life Cycle Assessment 3 (3) (1998) 158–168.
[24] J. Bez, G. Goldhan, M. Heyde, Waste treatment in product specific life cycle inventories. An approach of material-related modelling. Part II: sanitary Landfill, Int. J. Life Cycle Assessment 3 (2) (1998) 100–105.
[25] K. Habersatter, Ökoinventare für Verpackungen, Bundesamt Für Umwelt, Wald, Und Landschaft (BUWAL), Schriftenreihe Umwelt 250, Bern, 1996.
[26] J.B. Guinée, M. Gorree, R. Heijungs, G. Huppes, R. Kleijn, H.A. Udo de Haes, E. Van der Voet, M.N. Wrisberg, Life Cycle Assessment. An Operational Guide to ISO Standards, vols. 1–3, Centre of Environmental Science, Leiden University (CML), The Netherlands, 2002.
[27] S. Malato, Plataforma Solar de Almería, Personal communication, 2003.
[28] R. Dones, C. Bauer, B. Burger, M. Faist, R. Frischknecht, T. Heck. N. Jungbluth, A. Röder, Sachbilanzen von Energiesystemen: Grundlagen für den ökologischen Vergleich von Energiesystemen und den Einbezug von Energiesystemen in Ökobilanzen für die Schweiz, Final report ecoinvent 2000 No 6, Swiss Centre for Lyfe Cycle Invenrories, Paul Scherrer Institut Villigen, Switzerland, 2003.
[29] H.J. Althaus, M. Chudacoff, R. Hischier, N. Jungbluth, A. Primas, M. Osses, Life Cycle Inventories of Chemicals, Final Report Ecoinvent 2000 No. 8, Swiss Centre for Life Cycle Inventories, Duebendorf, Switzerland, 2003.
[30] D. Kellenberger, H.J. Althaus, N. Jungbluth, T. Künniger, Life Cycle Inventories of Building Products, Final Report Ecoinvent 2000 No. 7, Swiss Centre for Life Cycle Inventories, Duebendorf, Switzerland, 2003.
[31] R. Hischier, Life Cycle Inventories of Packaging and Graphical Paper, Final Report Ecoinvent 2000 No. 11, Dübendorf, Swiss Centre for Life Cycle Inventories, Switzerland, 2004.
[32] M. Spielmann, T. Kägi, O. Tietje, Life Cycle Inventories of Transport Services, Final Report Ecoinvent 2000 No. 14, Swiss Centre for Life Cycle Inventories, Duebendorf, Switzerland, 2003.
[33] J. Roca, Engineering and management of renewable energies, Master's degree (Sessions 41, 42), Institut Català de Tecnologia, 2001.
[34] W. Jenseit, H. Stahl, V. Wollny, R. Wittlinger, Recovery Options for Plastic Parts from End-of-Life Vehicles: an Eco-Efficiency Assessment, prepared by Öko-Institut e.V. for APME, Darmstadt, Deutschland, 2003.

CHAPTER 5. CONCLUDING REMARKS

Chapter 5

Concluding Remarks

The main conclusions drawn from the various studies of the present thesis can be summarised as follows:

1. Fenton and photo-Fenton Advanced Oxidation Processes (AOPs) accomplish, under optimum reagents concentrations, a full decolourisation and a substantial mineralisation of the studied reactive azo dye solutions.

2. The degradation efficiency of both artificial and solar driven photo-Fenton processes is superior to the dark process due to the positive effect of the irradiation source. Particularly good results are obtained when using solar radiation.

3. Temperatures above than room temperature notably accelerate the initial stages of Fenton and photo-Fenton processes though do not provide any considerable advantage at long reaction times.

4. Photo-Fenton process can be effectively used as a pre-treatment of an aerobic biological treatment. With a partial oxidation run under proper mild conditions, dye solutions become decolourised, biodegradable as well as non toxic.

5. The combined photo-Fenton-aerobic biological treatment completely decolourises and mineralises the studied reactive dyes solutions.

6. The artificial light photo-Fenton-aerobic biological process is a better economic and environmental option than single artificial light or solar driven photo-Fenton processes. The major economic/environmental burden is mainly attributed to hydrogen peroxide requirements, followed by the electrical energy consumption to run the UVA lamp.

7. The solar driven photo-Fenton-aerobic biological system would be the best option in terms of photo-Fenton pre-treatment effectiveness, environmental impact and operational cost.

8. Focusing on future full scale implementations, either single photo-Fenton or photo-Fenton-aerobic biotreatment may be successfully scaled-up from laboratory to pilot plant.

9. The photo-Fenton degradation sequence appears to begin with the hydroxyl radical attack to azo groups, giving place to the solutions decolourisation. The following aromatics degradation generates either short chain carboxylic acids – finally yielding CO_2 and water– or the recalcitrant triazine moiety. An important part of the heteroatoms initially present in the molecule gradually appear as innocuous final products of inorganic nature.

10. The sequenced anaerobic-aerobic biological treatment is not a plausible technology for the complete decolourisation and mineralisation of the reactive dye under study. Conversely, AOPs can be efficiently performed as a post-treatment of an anaerobic biological treatment, supposing an attractive alternative to the chemical-aerobic biotreatment strategy.

ANNEXES

Annexe 1

Unpublished Results

A.1.1. Pilot plant scale reactive dyes degradation by solar photo-Fenton and biological processes

Julia García-Montaño[a,*], Leonidas Pérez-Estrada[b], Isabel Oller[b], Manuel I. Maldonado[b], Francesc Torrades[c], José Peral[a]

[a]*Departament de Química, Edifici Cn, Universitat Autònoma de Barcelona, 08193 Bellaterra (Barcelona), Spain*

[b]*Plataforma Solar de Almería-CIEMAT. Carretera Senés km4, 04200 Tabernas (Almería), Spain*

[c]*Departament d'Enginyeria Química. ETSEIA de Terrassa (UPC), C/Colom, 11, 08222 Terrassa (Barcelona), Spain*

Submitted for publication

*Corresponding author

J. García-Montaño: julia@qf.uab.es

Abstract

Solar photo-Fenton reaction as a stand-alone process and as a pre-treatment of an aerobic biological treatment for Procion Red H-E7B and Cibacron Red FN-R reactive dyes degradation has been carried out at pilot plant scale. Photo-Fenton oxidation was conducted using a Compound Parabolic Collector (CPC) solar photoreactor and the biological treatment by means of an Immobilised Biomass Reactor (IBR). Artificial light photo-Fenton experiments carried out at laboratory scale have been taken as starting point. When applying photo-Fenton reaction as a single process, 10 $mg \cdot l^{-1}$ Fe (II) and 250 $mg \cdot l^{-1}$ H_2O_2 for 250 $mg \cdot l^{-1}$ Procion Red H-E7B treatment and 20 $mg \cdot l^{-1}$ Fe (II) and 500 $mg \cdot l^{-1}$ H_2O_2 for 250 $mg \cdot l^{-1}$ Cibacron Red FN-R treatment closely reproduced prior laboratory mineralisation results, with 82 and 86% Dissolved Organic Carbon (DOC) removal, respectively. Nevertheless, the use of sunlight with the CPC photoreactor increased the degradation rates allowing the reduction of Fe (II) concentration from 10 to 2 $mg \cdot l^{-1}$ (Procion Red H-E7B) and from 20 to 5 $mg \cdot l^{-1}$ (Cibacron Red FN-R) without efficacy loses. Carboxylic acids, SO_4^{2-}, NH_4^+ and NO_3^- generation were monitored along dyes solution mineralisation. Finally, in the combined photo-Fenton-biological system, reagents doses of 5 $mg \cdot l^{-1}$ Fe (II) and 225 $mg \cdot l^{-1}$ H_2O_2 for Cibacron Red FN-R and 2 $mg \cdot l^{-1}$ Fe (II) and 65 $mg \cdot l^{-1}$ H_2O_2 for Procion Red H-E7B were enough to generate biodegradable solutions to feed the IBR, even improving bench scale results.

Keywords: Immobilised Biomass Reactor; Photo-Fenton; Pilot plant; Reactive dyes; Sunlight

1. Introduction

Textile industry consumes large volumes of water in dyeing and finishing operations. In textile dyebaths, the degree of fixation of dyes is never complete resulting in dye-containing effluents [1]. The release of such coloured wastewaters to the environment is a dramatic source of aesthetic pollution, eutrophication and perturbations in aquatic life. Due to their chemical stability, most manufactured dyes are not amenable to common chemical or biological treatments. The increased public concern and the stringent international environmental standards (ISO 14001, November 2004) have prompted the need to develop novel treatment methods for converting organic contaminants, such as dyestuffs, to harmless final products.

Advanced Oxidation Processes (AOPs) are powerful technologies for the remediation of wastewaters containing recalcitrant organic pollutants [2]. Although AOPs include different reacting systems, their mechanisms are basically characterised by the *in situ* generation of highly reactive and non selective hydroxyl radicals ($HO^{\bullet}$, E^{o} = 2.8 V *versus* NHE), able to oxidise and mineralise almost all organic compounds to CO_2, H_2O and inorganic ions. Among available AOPs, the Fenton and photo-Fenton processes are of special interest because they offer high reaction yields with a low treatment cost [3]. In dark Fenton reaction (Equation 1, H_2O ligands on iron sphere coordination are omitted in the successive), hydroxyl radicals are generated by interaction of H_2O_2 with ferrous salts. Generated Fe (III) can be reduced by reaction with exceeding H_2O_2 to form again ferrous ion in a catalytic mechanism (Equations 2 and 3) [4].

$$Fe\,(II) + H_2O_2 \rightarrow Fe\,(III) + HO^{\bullet} + HO^{-} \quad (1)$$

$$Fe\,(III) + H_2O_2 \rightarrow HO_2^{\bullet} + Fe\,(II) + H^{+} \quad (2)$$

$$Fe\,(III) + HO_2^{\bullet} \rightarrow Fe\,(II) + O_2 + H^{+} \quad (3)$$

Radiation can play different roles that lead to an improvement of the reaction yields. It drives photo-Fenton reaction by means of ferric aquo-complexes photolysis, producing extra HO· and the recovery of Fe (II) needed in Fenton reaction (Equation 4, being $[Fe\,(III)\,HO]^{2+}$ the dominant ferric species in solution at pH = 2-3) [5]. The irradiated process may also involve photolysis of a Fe (III)-H_2O_2 complex to form high-valent iron intermediates, which can directly oxidize organic matter [6]. Moreover, it can drive ligand-to-metal charge transfer in the potentially photolabile complexes formed by Fe (III) and organic compounds (Equation 5), a process that has been well proven for the complexes formed between Fe (III) and the carboxylic acid moiety [7]. In photo-Fenton system, as in the dark process, iron acts as a catalyst and the rate-limiting step is the regeneration of ferrous ion.

$$[Fe\,(III)\,HO]^{2+} \xrightarrow{h\upsilon} Fe\,(II) + HO\cdot \qquad (4)$$

$$[Fe\,(III)\,L]^{2+} \xrightarrow{h\upsilon} Fe\,(II) + L\cdot \qquad (L = \text{organic ligand}) \qquad (5)$$

Since photoassisted processes may require radiations from UV up to visible (~ 550 nm) [7, 8], they present the possibility of be driven under solar irradiation offering additional economic and environmental advantages. Another important improvement for the reduction of economic and environmental impacts is the performance of the AOP as a pre-treatment of a conventional biological treatment, a suitable approach for the removal of non biodegradable compounds in water. Lower amounts of chemicals and energy are supplied to achieve an intermediate solution fully biodegradable [9-11].

The bench scale artificial light assisted photo-Fenton process alone and as a pre-treatment of an aerobic biological process for the degradation of two textile reactive dyes (Procion Red H-E7B, a homo-bireactive dye with two monochlorotriazine groups, and Cibacron Red FN-R, a hetero-bireactive dye with vinylsulphone and fluorotriazine reactive groups) has been previously reported by our group [10, 12, 13]. Taking into consideration such experiments, the scaling-up from laboratory to pilot plant is performed in this work. Photo-Fenton experiments are conducted at the Plataforma Solar de Almería (PSA, Spain) in a Compound Parabolic Collector (CPC) photoreactor

under solar irradiation. Initially, single photo-Fenton process with different Fe (II) concentrations is applied in order to mineralise reactive dye solutions. Dissolved Organic Carbon (DOC), H_2O_2 and Fe evolution, original dye disappearance, carboxylic acids generation and inorganic ions release are studied as a function of irradiation time. Additionally, biodegradability enhancement as a function of H_2O_2 consumed is screened to assess the possibility of a combined chemical-aerobic biological process. In a second part, solar photo-Fenton precedes an aerobic biological treatment which is carried out in an Immobilised Biomass Reactor (IBR). The minimum H_2O_2 dosages needed to generate completely biodegradable phototreated solutions are quantified. Finally, the viability of the photo-Fenton process (single or coupled to biotreatment) to treat the above reactive dyes when extending laboratory experiments to a pilot plant is discussed.

2. Experimental

2.1. Synthetic dye solutions

Commercial Procion Red H-E7B (CI Reactive Red 141, $C_{52}H_{34}O_{26}S_8Cl_2N_{14}$, DyStar) and Cibacron Red FN-R (CI Reactive Red 238, $C_{29}H_{19}O_{13}S_4ClFN_7$, CIBA) reactive dyes were used as received to prepare synthetic dye solutions. Their purity degree was unknown. The molecular formula of Procion Red H-E7B is shown in Figure 1. Cibacron Red FN-R chemical structure was not disclosed by the supplier. Initial concentrations of commercial dyes were 250 $mg \cdot l^{-1}$. In order to convert them into the form normally found in industrial effluents, solutions were hydrolysed by adjusting the pH to 10.6 followed by heating to 80 ºC for 6 hours and 60 ºC for 1 hour for Procion Red H-E7B and Cibacron Red FN-R, respectively. Their initial features were as follows: DOC: 39 ± 1 and 69 ± 2 $mg \cdot l^{-1}$ C ($n = 3$, $\alpha = 0.05$); Chemical Oxygen Demand (COD): 108 and 200 $mg \cdot l^{-1}$ O_2; BOD_5/COD ratio: 0.10 and 0.02.

2.2. Chemicals

All chemicals used throughout this study were of the highest commercially available grade. Iron sulphate ($FeSO_4 \cdot 7H_2O$, Panreac) and hydrogen peroxide (H_2O_2 30% w/v, Panreac) were used as received. Sulphuric acid and sodium hydroxide solutions were used for pH adjustments. Water in the pilot plant was obtained from the PSA distillation plant (conductivity < 10 $\mu S \cdot cm^{-1}$, SO_4^{2-} = 0.5 $mg \cdot l^{-1}$, Cl^- = 0.7-0.8 $mg \cdot l^{-1}$, Total Organic Carbon (TOC) < 0.5 $mg \cdot l^{-1}$ C). Ultra pure deionised water from a Milli-Q (Millipore Co) system was employed to prepare all the reagent solutions.

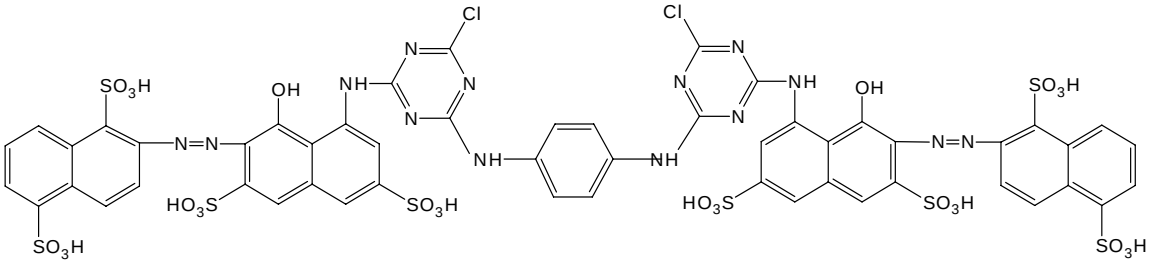

Figure 1. Chemical structure of Procion Red H-E7B.

2.3. Sample analysis

DOC was determined with a TOC Shimadzu 5050A analyser provided with an ASI-5000A Shimadzu Auto-sampler. COD was assessed by the closed reflux colorimetric method [14] with a Spectroquant® kit (10-150 $mg \cdot l^{-1}$ O_2 range, Merck). The measurement of Biochemical Oxygen Demand for 5 days (BOD_5) was performed by means of a mercury-free WTW 2000 Oxytop thermostated at 20 ºC. Reactive dyes were analysed using reverse-phase liquid chromatography (flow rate 0.5 $ml \cdot min^{-1}$) with UV/Vis detector in a HPLC (Agilent, Series 1100) with C-18 column (Phenomenex LUNA 5 µm, 3 mm x 150 mm) at 543 nm wavelength. The mobile phases were 5 $mmol \cdot l^{-1}$ ammonium acetate (A) and methanol (B). A 15 minutes gradient elution was used from 0% to 100% B for Procion Red H-E7B and from 0% to 50% B for Cibacron Red FN-R. Ammonium was determined with a Dionex DX-120 ion chromatograph

equipped with a Dionex Ionpac CS12A 4 x 250 mm column. Isocratic elution was done with 10 mmol·l^{-1} H_2SO_4 at 1.2 ml·min^{-1} flow rate. Anion and carboxylic acids concentrations (in their anionic form) were measured with a Dionex DX-600 ion chromatograph using a Dionex Ionpac AS11-HC 4 x 250 mm column. The elution gradient programme for anions was pre-run 5 minutes with 20 mmol·l^{-1} NaOH, followed by an injection with 20 mmol·l^{-1} NaOH for 8 minutes and with 35 mmol·l^{-1} NaOH for 7 minutes. The flow rate was 1.5 ml·min^{-1}. The gradient programme for carboxylate anions analysis consisted of a 10-minutes pre-run with 1 mmol·l^{-1} NaOH, 10 minutes with 15 mmol·l^{-1} NaOH, 10 minutes with 30 mmol·l^{-1} NaOH, and 10 minutes with 60 mmol·l^{-1} NaOH. The flow rate was also 1.5 ml·min^{-1}. Iron determination was done by colorimetry (Unicam-2, UV/Vis Spectrometer CV2) with 1,10-phenantroline [14]. H_2O_2 consumption was quantified by the potassium iodide titration method [15]. Determination of Total Suspended Solids (TSS) was carried out gravimetrically, following Standard Methods [14].

2.4. Photo-Fenton experimental set-up

All photo-Fenton experiments were carried out under sunlight in a pilot plant at the PSA (latitude 37º 05' N, longitude 2º 21' W). The pilot plant (Figure 2) operated in batch mode and was composed by three CPCs (concentration factor = 1), one tank and one recirculation pump.

The collectors (1.03 m^2 each) faced south on a fixed platform tilted 37º (local latitude), and consisted of eight parallel horizontal borosilicate glass-transparent tubes. Two parabolic aluminium mirrors redirected the radiation toward each tube. Water flowed directly at 20 l·min^{-1} from one CPC module to another and finally into the tank, from where the pump recirculated it back to the CPCs. The total volume (V_T) was 35 l and was separated in two parts: 22 l of total irradiated volume (V_i) and 13 l of dead reactor volume (tank + connecting tubes) that was not illuminated. More details about CPC reactor are described elsewhere [16].

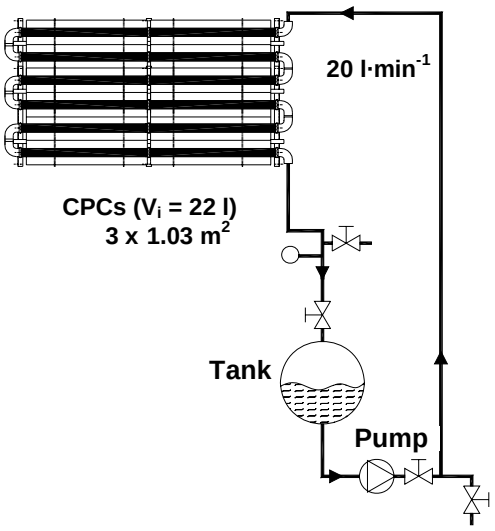

Figure 2. Scheme of the solar photo-Fenton pilot plant.

Experiments were performed as follows: with collectors covered, after pH adjustment around 2.8-3.0, the necessary amount of iron salt and hydrogen peroxide was added to the tank. After 5 minutes of homogenisation (dark Fenton reaction), the cover was removed and samples were collected at regular time intervals. Solar ultraviolet radiation (300-400 nm) was measured by a global UV radiometer (Kipp & Zonen, model CUV 3), tilted 37º as CPCs, which provided data in terms of incident $W \cdot m^{-2}$. This gives an idea of the energy reaching any surface in the same position with regard to the sun. In that way, incident radiation could be evaluated as a function of time taking into account cloudiness and other environmental conditions. Thus, experiments could be compared using a corrected illumination time t_{30W} (Equation 6) [17],

$$t_{30W,n} = t_{30W,n-1} + \Delta t_n \frac{UV}{30} \cdot \frac{V_i}{V_T}; \quad \Delta t_n = t_n - t_{n-1} \tag{6}$$

were t_n is the experimental time for each sample, UV is the average solar ultraviolet radiation measured during Δt_n, and t_{30W} is the "normalised illumination time". In this case, time refers to a constant solar UV power of 30 $W \cdot m^{-2}$ (typical solar UV power on a perfect sunny day around noon). During the present work experimentation, UV

intensity ranged between 14 and 37 $W \cdot m^{-2}$. Since the system was outdoors, temperature in the reactor was in the range of 25-48 ºC.

2.5. IBR set-up and operation conditions

The biological pilot plant operated in batch mode and was composed by two independent modules, an IBR and a conditioner tank (50 l). The IBR unit, which consisted of a 35 l column containing plastic supports (polypropylene, 15 mm of nominal diameter, Pall®-Ring), was colonised by activated sludge from a municipal wastewater treatment plant (Almería, Spain). The operational liquid volume was 45 l. Recirculation was maintained between the conditioner tank and the IBR at 0.5 $l \cdot min^{-1}$ flow rate. The system was not thermally controlled and temperature was in the range of 16-40 ºC. A blower provided oxygen saturation conditions.

The biological treatment strategy was as follows: once IBR inoculation was carried out, in order to guarantee bacteria viability and to permit better growing and fixing on the supports, a 45-l batch of glucose (an easily biodegradable substrate) was added to the tank. After complete biodegradation, the tank was completely emptied and sequentially filled with 45-l batches of different phototreated solutions coming from the photo-Fenton stage. H_2O_2 had been completely consumed before the addition of solutions (proven by iodometric titration) and the pH of these had been previously readjusted from 2.8-3.0 to neutral. The mineralisation of the pre-treated effluent was followed by DOC measurement at regular time intervals (one or two times per day). Other periodical determinations carried out were the evolution of carboxylic acids initially present, NH_4^+, NO_2^- and NO_3^- ions in order to detect parallel nitrification and denitrification reactions, and TSS to ensure a correct sludge fixation on polypropylene supports (TSS in solution near zero). pH readjustment between 6.5 and 7.5 was done if necessary. Suitable proportions of mineral medium were also supplied to solution in order to maintain the required C:N:P (100:20:5) and C:Fe:S (100:2:2) ratios.

3. Results and discussion

3.1. Preliminary bench scale degradation of reactive dyes

The application of photo-Fenton reaction as a single process and as a pre-treatment of an aerobic biological treatment for Procion Red H-E7B and Cibacron Red FN-R degradation was previously developed at laboratory scale [10, 12, 13]. Photo-Fenton oxidation was conducted at 23 ºC with a 6 W black light (6 $W \cdot m^{-2}$ UVA intensity, measured by a luminometer) situated over a 250 ml photoreactor. Biodegradation was carried out under room conditions in a 1.5 l Sequencing Batch Reactor (SBR). The best results obtained for a 250 $mg \cdot l^{-1}$ initial reactive dye dosage were as follows: when applying photo-Fenton as a stand-alone process, 10 $mg \cdot l^{-1}$ Fe (II), 250 $mg \cdot l^{-1}$ H_2O_2 for Procion Red H-E7B, and 20 $mg \cdot l^{-1}$ Fe (II), 500 $mg \cdot l^{-1}$ H_2O_2 for Cibacron Red FN-R were found to be the most efficient Fenton reagent combinations to achieve the maximum degradation levels at short irradiation times: 82 and 84% DOC removal after 100 and 150 minutes of black light irradiation, respectively. These optimal H_2O_2 experimental values closely match the stoichiometrically required to completely oxidize the dyes (1 g COD = 0.0312 mol O_2 = 0.0625 mol H_2O_2). On the other hand, in the combined chemical-biological oxidation system, 10 $mg \cdot l^{-1}$ Fe (II), 125 $mg \cdot l^{-1}$ H_2O_2 photo-Fenton conditions for 60 minutes (39% mineralisation) and 20 $mg \cdot l^{-1}$ Fe (II), 250 $mg \cdot l^{-1}$ H_2O_2 for 90 minutes (50% mineralisation) were necessary to make the homo- and hetero-bireactive dyes biocompatible, respectively. Under these pre-treatment conditions, the coupled SBR system fully removed both reactive dyes metabolites from aqueous solution

3.2. Photo-Fenton degradation at pilot plant scale

In order to scale-up bench scale experiments, the same photo-Fenton conditions (10 $mg \cdot l^{-1}$ Fe (II), 250 $mg \cdot l^{-1}$ H_2O_2 and 20 $mg \cdot l^{-1}$ Fe (II), 500 $mg \cdot l^{-1}$ H_2O_2) were initially applied for Procion Red H-E7B and Cibacron Red FN-R degradation at pilot plant. DOC and H_2O_2 evolution as t_{30W} function is shown in Figures 3 and 4. As observed when working at laboratory scale, a fast mineralisation took place until the achievement

of a constant residual DOC of recalcitrant nature. The % DOC removal was 82% for Procion Red H-E7B (residual DOC ~ 7 $mg \cdot l^{-1}$ C) and 86% for Cibacron Red FN-R (residual DOC ~ 9 $mg \cdot l^{-1}$ C), providing evidence of the reproducibility of the laboratory system. However, it is noteworthy that the solar photo-Fenton process at the pilot plant needs shorter times for dye degradation than the artificial light process at laboratory. Maximum mineralisation levels for homo- and hetero-bireactive dyes were attained at t_{30W} = 13 and 22 minutes, respectively.

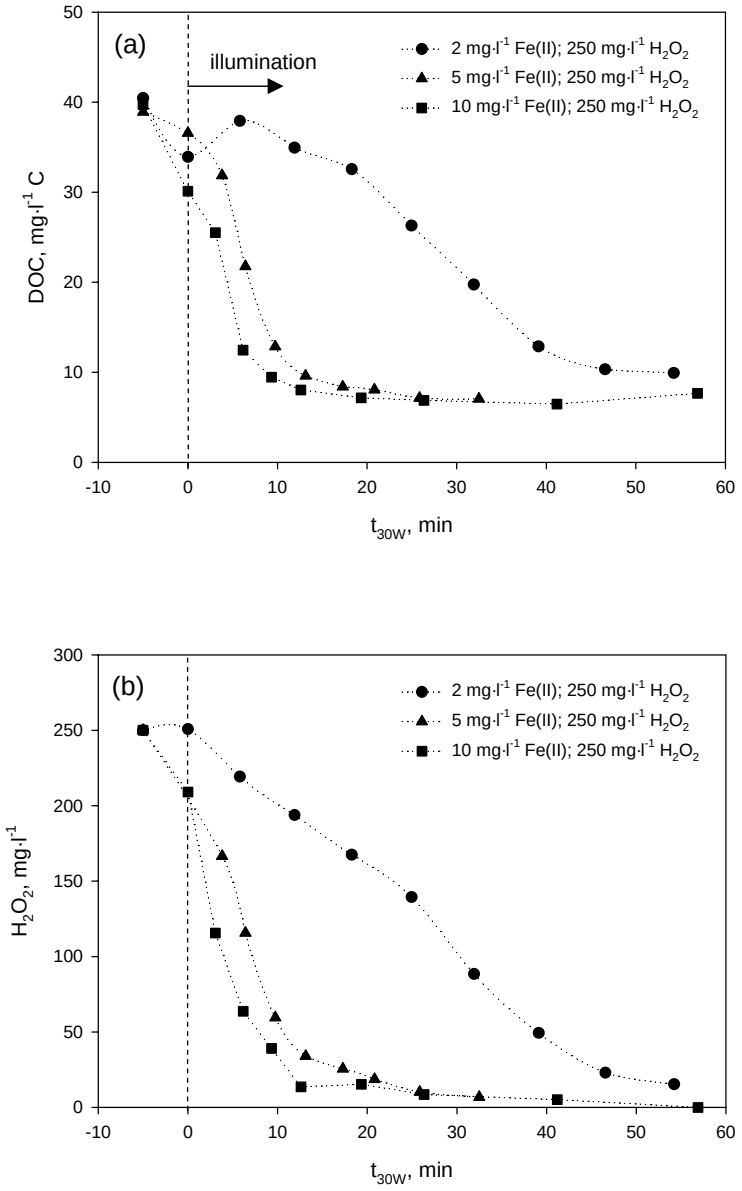

Figure 3. DOC (a) and H_2O_2 (b) evolution *versus* t_{30W} at different initial Fe (II) concentrations for 250 $mg \cdot l^{-1}$ hydrolysed Procion Red H-E7B degradation; H_2O_2 = 250 $mg \cdot l^{-1}$, pH = 2.8.

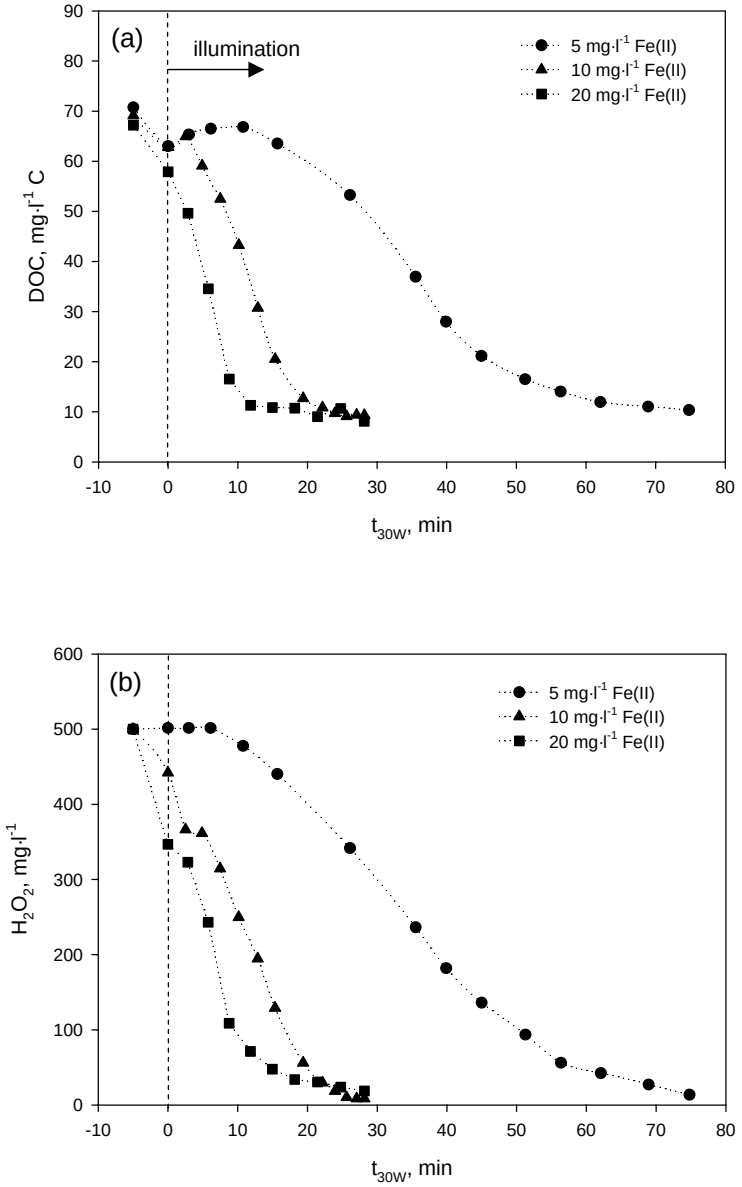

Figure 4. DOC (a) and H_2O_2 (b) evolution *versus* t_{30W} at different initial Fe (II) concentrations for 250 mg·l^{-1} hydrolysed Cibacron Red FN-R degradation; H_2O_2 = 500 mg·l^{-1}, pH = 2.8.

3.2.1. Effect of Fe (II) dose

With the base of the photo-Fenton conditions applied at the laboratory, initial Fe (II) concentration effect was evaluated while maintaining H_2O_2 concentration. The intention was to determine the lowest amount of iron necessary to effectively carry out the photo-Fenton process in the solar photoreactor. Therefore, 2 and 5 mg·l^{-1} catalyst concentrations were evaluated and compared with 10 mg·l^{-1} Fe (II) for Procion Red H-

E7B (Figure 3), and 5 and 10 $mg \cdot l^{-1}$ to 20 $mg \cdot l^{-1}$ Fe (II) for Cibacron Red FN-R (Figure 4). DOC and H_2O_2 parameters were monitored *versus* t_{30W}. Overall reaction rate constants could not be calculated since the mineralisation rate did not follow simple kinetic models. This complex behaviour is due to the fact that DOC is the sum of different product concentrations along several simultaneous reactions. Therefore, the t_{30W} necessary to obtain around 80% mineralisation (defined as $t_{80\%}$) and the maximum gradient of the degradation curve (formally the slope of the tangent at the inflexion point, r_0) were chosen to compare the experiments (Table 1). As it can be observed, the higher initial iron concentrations caused the faster mineralisation, although all tested Fe (II) dosages leaded to the same final degradation level.

Table 1. Comparison of $t_{80\%}$ and r_0 parameters related to reactive dye degradation for different Fe (II) concentrations. 250 $mg \cdot l^{-1}$ hydrolysed Procion Red H-E7B, 250 $mg \cdot l^{-1}$ H_2O_2; 250 $mg \cdot l^{-1}$ hydrolysed Cibacron Red FN-R, 500 $mg \cdot l^{-1}$ H_2O_2; pH = 2.8.

Fe (II)	**2 $mg \cdot l^{-1}$**		**5 $mg \cdot l^{-1}$**		**10 $mg \cdot l^{-1}$**		**20 $mg \cdot l^{-1}$**	
	$t_{80\%}$ min	**r_0 $mg \cdot l^{-1} \cdot min^{-1}$ C**	**$t_{80\%}$ min**	**r_0 $mg \cdot l^{-1} \cdot min^{-1}$ C**	**$t_{80\%}$ min**	**r_0 $mg \cdot l^{-1} \cdot min^{-1}$ C**	**$t_{80\%}$ min**	**r_0 $mg \cdot l^{-1} \cdot min^{-1}$ C**
Procion Red H-E7B	55	0.49	21	3.88	13	4.20	-	-
Cibacron Red FN-R	-	-	56	0.68	19	2.51	11	5.15

Besides, the H_2O_2 concentration presented the same decreasing profile than DOC (Figures 3 and 4), revealing that both parameters dropped off together and maintained the same correlation regardless of initial Fe (II) concentration. Hence, it can be concluded that 2 $mg \cdot l^{-1}$ and 5 $mg \cdot l^{-1}$ were large enough catalyst doses to degrade, without losing photo-Fenton efficacy, Procion Red H-E7B and Cibacron Red FN-R, respectively. These results are interesting since a low iron concentration would avoid the separation step –based on $Fe(OH)_3$ precipitation– at the end of the oxidation process. Finally, the catalyst evolution (in its total and ferrous form) in relation to t_{30W} is represented in Figure 5. The fast decrease of Fe (II) concentration in relation to the total

iron evidences that, as it has been commented on the introduction section, the rate-limiting step of the catalytic process is the regeneration of ferrous ion from its oxidised form.

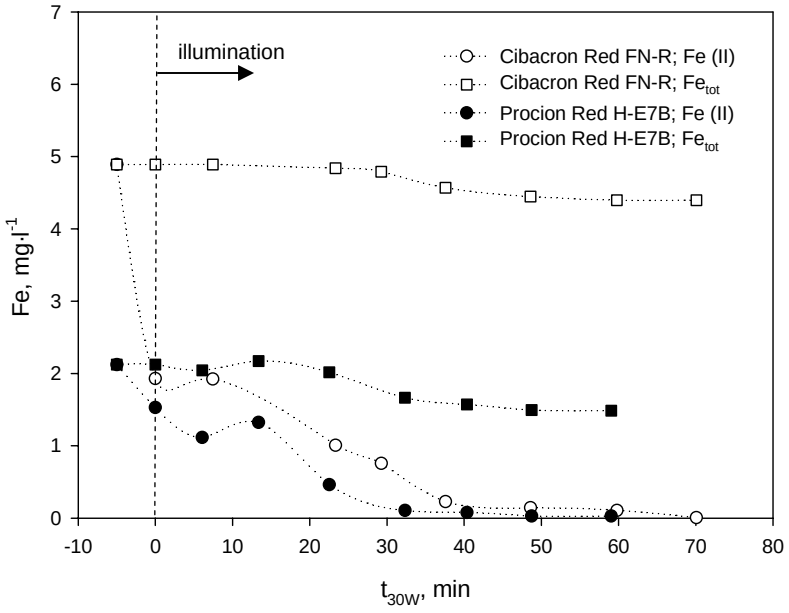

Figure 5. Fe (II) and total iron evolution *versus* t_{30W}. 250 mg·l^{-1} hydrolysed Procion Red H-E7B, 2 mg·l^{-1} Fe (II), 250 mg·l^{-1} H_2O_2; 250 mg·l^{-1} hydrolysed Cibacron Red FN-R, 5 mg·l^{-1} Fe (II), 500 mg·l^{-1} H_2O_2; pH = 2.8.

The original dye degradation was monitored by HPLC and UV/Vis detector. Procion Red H-E7B dye completely disappeared before illumination (t_{30W} = 0 minutes) for all Fe (II) concentrations tested, while just the 5 mg·l^{-1} Fe (II) one allowed to detect Cibacron Red FN-R further than dark Fenton process. The fast dye depletion was accompanied by the solutions decolourisation. Concentration decrease in relation to t_{30W} when applying the lowest Fe (II) concentrations is shown in Figure 6. When comparing reactive dye degradation with mineralisation (Figures 3(a) and 4(a)), it is noticeable that complete dye disappearance takes place before mineralisation begin (no kinetic analysis was possible due to the fast parent compound degradation). This behaviour appears to suggest a sequenced oxidation mechanism in which HO· (of electrophilic nature) preferably attacks the chromophore centre of the dye molecule (an electron-rich site) [18], giving place to the solution bleaching. Afterwards, mono- or poly-hydroxylations

of the aromatic rings would be produced [19, 20]. Heteroatoms initially present in the molecule would be released as anions at their highest oxidation degree. Finally, a subsequent ring cleavage would generate aliphatic carboxylic acids to finally produce CO_2 and water [21, 22].

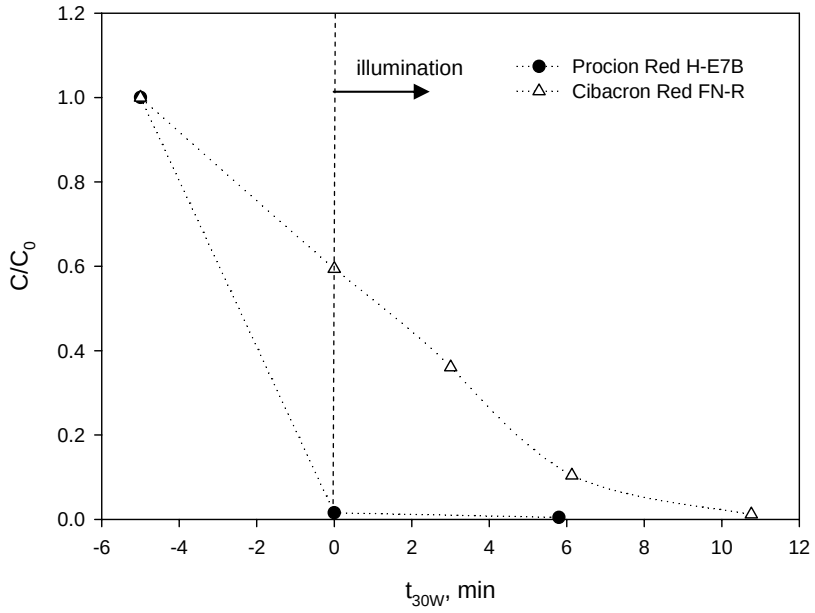

Figure 6. Relative concentration evolution *versus* t_{30W}. 250 mg·l^{-1} hydrolysed Procion Red H-E7B, 2 mg·l^{-1} Fe (II), 250 mg·l^{-1} H_2O_2; 250 mg·l^{-1} hydrolysed Cibacron Red FN-R, 5 mg·l^{-1} Fe (II), 500 mg·l^{-1} H_2O_2; pH = 2.8.

3.2.2. Carboxylic acids and inorganic compounds generation

2 mg·l^{-1} Fe (II) and 250 mg·l^{-1} H_2O_2 for Procion Red H-E7B, and 5 mg·l^{-1} Fe (II) and 500 mg·l^{-1} H_2O_2 for Cibacron Red FN-R photo-Fenton conditions were applied in order to determine carboxylic acid intermediates and inorganic compounds. These low Fe (II) concentrations were employed to provide appropriate degradation rates (not too high) that ensure the detection of as many intermediate species as possible. As a result, formic (C_1), acetic (C_2), oxalic (C_2) and maleic (C_4) acids appeared at measurable concentrations during both dyes photooxidation. Pyruvic acid (C_3) was also detected during Cibacron Red FN-R phototreatment (Figure 7).

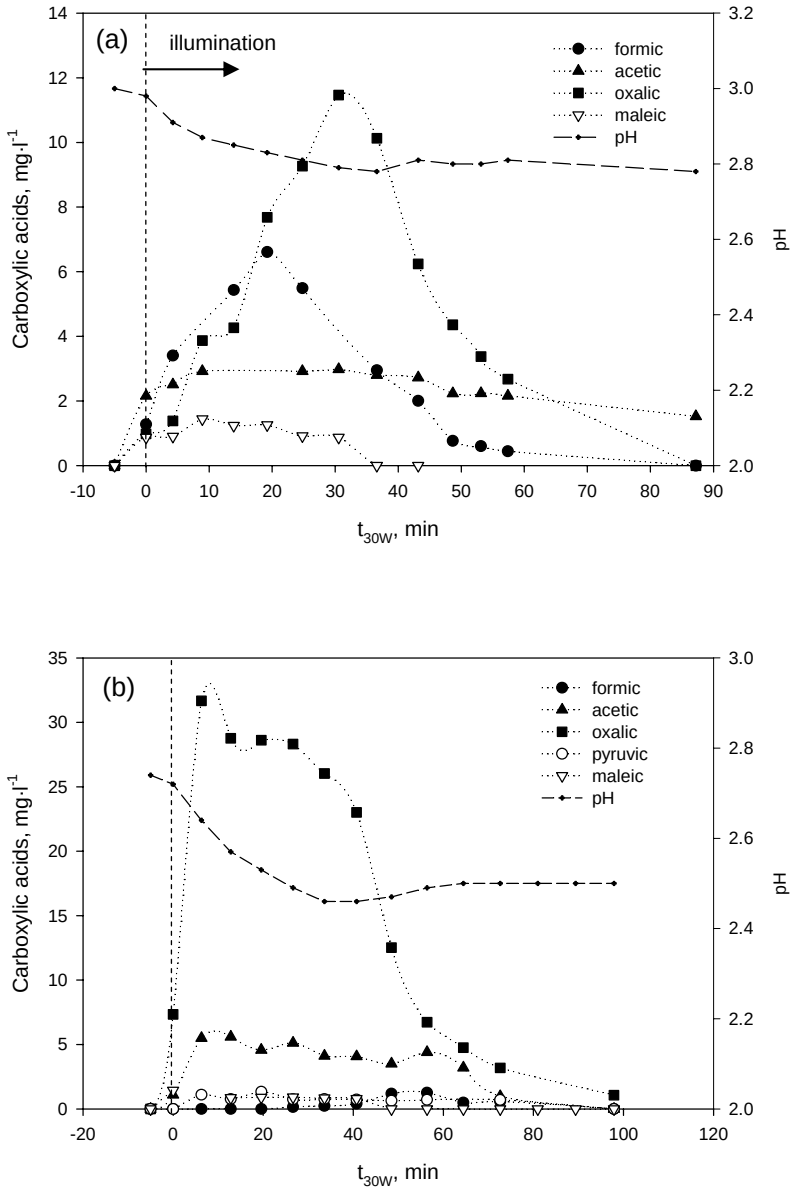

Figure 7. Carboxylic acids concentration *versus* t_{30W}. (a) 250 mg·l^{-1} hydrolysed Procion Red H-E7B, 2 mg·l^{-1} Fe (II), 250 mg·l^{-1} H_2O_2 (b) 250 mg·l^{-1} hydrolysed Cibacron Red FN-R, 5 mg·l^{-1} Fe (II), 500 mg·l^{-1} H_2O_2.

A significant pH diminution was also observed coinciding with such acids generation. Although they were present in solution from the early stages of the photo-Fenton process, their global concentration reached a maximum around t_{30W} = 30 minutes for Procion Red H-E7B and between t_{30W} = 13 and 40 minutes for Cibacron Red FN-R, indicating that they were produced via progressive oxidation of higher molecular weight species. It should be pointed out that, at maximum concentration, the detected

carboxylic acids stood for 24% of the total DOC present in solution. Afterwards, their concentration decreased in agreement with the DOC removal until achieve low values or completely disappear (pH stabilisation). 1.1 $mg \cdot l^{-1}$ of oxalic acid and 1.5 $mg \cdot l^{-1}$ of acetic acid were found for Cibacron Red FN-R and Procion Red H-E7B, respectively, being the 3 and 9% of the remaining recalcitrant DOC observed at the end of each photo-Fenton process (Figures 3(a) and 4(a)).

As referred to in the introduction, another important mechanism for the conversion of Fe (III) to Fe (II) is the photoexcitation of the complexes formed between Fe (III) and organic matter, especially carboxylic acids (Equation 7). These photochemical reactions, often with larger quantum yields than the excitation of Fe (III) aquo-complexes [7], would lead to a faster mineralisation than the direct oxidation by $HO^{\cdot}$. In agreement with this, it is noticeable that the apparition of the carboxylic acid intermediates, which becomes significant at t_{30W} = 15-20 minutes of irradiation time (Figure 7), results in an increased DOC destruction rate (Figures 3(a) and 4(a)).

$$[Fe(III)LCOO]^{2+} \xrightarrow{h\upsilon} Fe(II) + CO_2 + L^{\cdot} \quad (7)$$

Besides DOC elimination, dyes mineralisation implies the appearance of inorganic ions. According to the oxidation reactions proposed (Equations 8 and 9), SO_4^{2-} and NO_3^- anions were expected to appear in the media. In order to establish the mass balance of the different elements, and taking into account that the purity of the commercial dyes was unknown, all the initial DOC content of the samples was attributed to dye molecules. The difference between the sample weight and the DOC was attributed to inorganic impurities (such as NaCl or Na_2SO_4).

Procion Red H-E7B

$$C_{52}H_{34}O_{26}S_8Cl_2N_{14} + 76.5\,O_2 \rightarrow 52\,CO_2 + 14\,NO_3^- + 8\,SO_4^{2-} + 2\,Cl^- + 32\,H^+ + H_2O \quad (8)$$

Cibacron Red FN-R

$$C_{29}H_{19}O_{13}S_4ClFN_7 + 41.5\,O_2 \rightarrow 29\,CO_2 + 7\,NO_3^- + 4\,SO_4^{2-} + Cl^- + F^- + 17H^+ + H_2O \quad (9)$$

The kinetics of appearance of the inorganic anion SO_4^{2-} are presented in Figure 8(a). Sulphate was gradually released into the solution, in parallel to DOC removal, up to a recovery of 92% for Procion Red H-E7B and 95% for Cibacron Red FN-R. During the mineralisation process, the $-SO_3H$ group (see Procion Red H-E7B structure, Figure 1) may be directly substituted by $HO^{\cdot}$ resulting in the release of SO_4^{2-} [23]. The vinylsulphone reactive group of Cibacron Red FN-R (chemical structure not disclosed) would also lead to the sulphate anion formation.

Small nitrate and ammonium concentrations were detected in solution. It is well known that ammonium oxidation by $HO^{\cdot}$ is not a favourable process in acid media, taking place slowly [24]. Figure 8(b) shows the total nitrogen concentration corresponding to both NH_4^+ and NO_3^- ions generated through dye mineralisation. As can be seen, the complete balance of N was not obtained, attaining just 1.1 $mg \cdot l^{-1}$ N for Procion Red H-E7B (9% recovery) and 4.2 $mg \cdot l^{-1}$ N for Cibacron Red FN-R (22% recovery). This incomplete nitrogen mass balance has already been observed in photocatalytic processes by other authors [22, 25, 26]. Such results seem to be indicative of the presence of other N-containing products different than the expected. For instance, taking into account the existence of triazine rings in the initial structure of the studied dyes, which cannot be mineralised until the end by photo-Fenton process [25], it is predictable the presence of triazine derivates in the solution (i.e., ammeline (5N), ammelide (4N) and cyanuric acid (3N)). Only the two N linked to the triazine ring would be mineralised (the other three N atoms would remain in the triazine ring). The presence of these species could also justify the residual DOC observed at the end of the photo-Fenton process (Figures 3(a) and 4(a)). For example, in the case of Procion Red H-E7B, the two triazine rings would constitute around 65% of the total final DOC. Other studies have reported that nitrogen atoms constituting the azo group would lead to N_2 gas generation as a result of the $HO^{\cdot}$ attack [20, 21]. More work on degradation product analysis and identification is needed to reveal the complex fate of nitrogen.

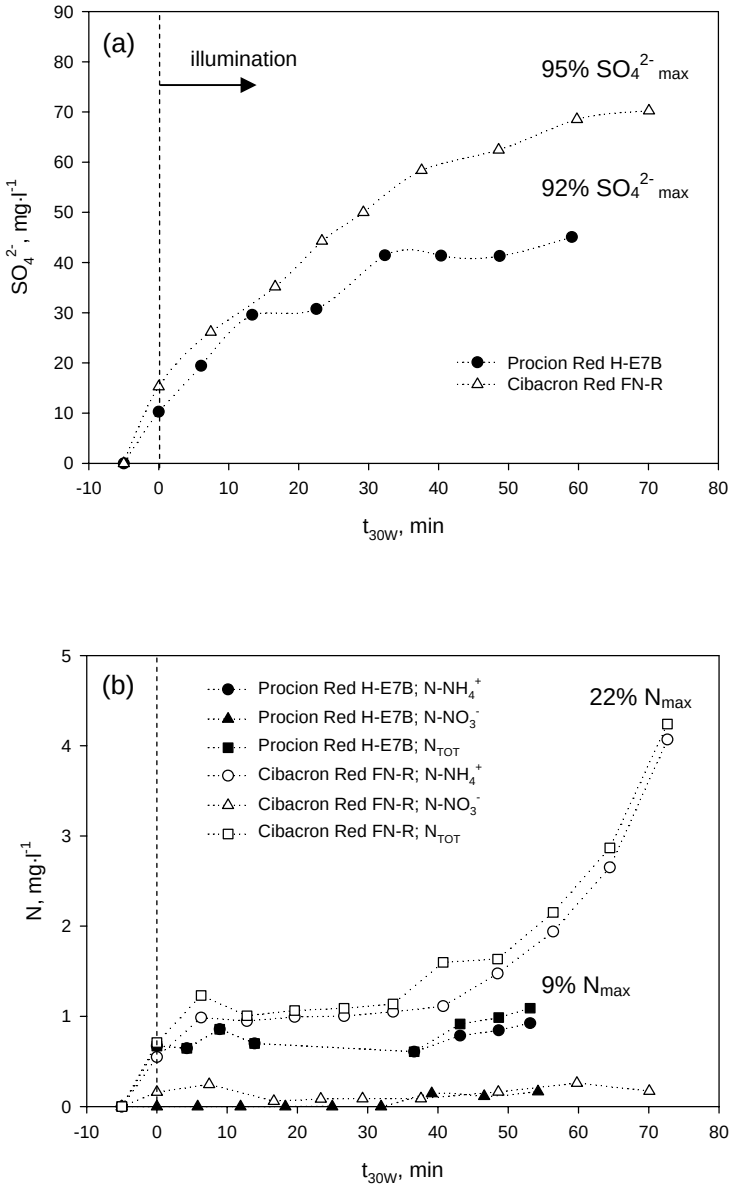

Figure 8. Sulphate ion (a) and inorganic nitrogen (b) release *versus* t_{30W}. 250 mg·l^{-1} hydrolysed Procion Red H-E7B, 2 mg·l^{-1} Fe (II), 250 mg·l^{-1} H_2O_2; 250 mg·l^{-1} hydrolysed Cibacron Red FN-R, 5 mg·l^{-1} Fe (II), 500 mg·l^{-1} H_2O_2; pH = 2.8.

3.2.3. Biodegradability enhancement

The biodegradability evolution of Procion Red H-E7B and Cibacron Red FN-R phototreated solutions, expressed as BOD_5/COD ratio, was determined in order to evaluate photo-Fenton suitability as a previous step of an aerobic biological treatment. 2 mg·l^{-1} Fe (II) for the homo- and 5 mg·l^{-1} Fe (II) for the hetero-bireactive dye were

employed to carry out the oxidation. As pointed out above, the lowest iron concentration was used to avoid the need for Fe separation at the end of the chemical oxidation, before the biological process. Hydrogen peroxide was gradually added to determine the minimum concentration able to generate a biocompatible effluent. Each new H_2O_2 pulse was added after complete H_2O_2 consumption. BOD_5/COD ratio *versus* H_2O_2 added is represented in Figure 9. It is seen that solutions become amenable to biodegradation while increasing the H_2O_2 consumption, easily attaining the BOD_5/COD = 0.4 value characteristic of thoroughly biodegradable wastewaters [27].

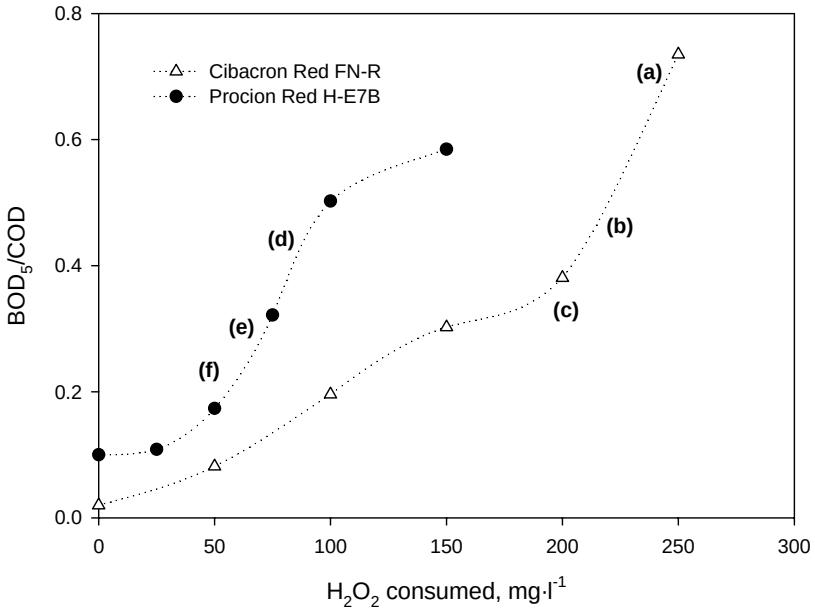

Figure 9. BOD_5/COD evolution *versus* H_2O_2 consumption for 250 mg·l^{-1} hydrolysed Procion Red H-E7B (2 mg·l^{-1} Fe (II)) and 250 mg·l^{-1} hydrolysed Cibacron Red FN-R (5 mg·l^{-1} Fe (II)); pH = 2.8.

3.3. Immobilised Biomass Reactor

Cibacron Red FN-R and Procion Red H-E7B phototreated solutions were submitted to the IBR pilot plant. As it has been described in the experimental section, a first batch of glucose (DOC around 80 mg·l^{-1} C) was added to the conditioner tank to ensure the biomass viability. This also let to establish the lower residual DOC that could be achieved by the IBR system (~ 20 mg·l^{-1} C, biomass metabolites). Afterwards, the

phototreated samples were added following a pre-designed sequence. For Cibacron Red FN-R solutions (5 $mg \cdot l^{-1}$ Fe (II)): (a) 250 $mg \cdot l^{-1}$ H_2O_2 (DOC = 24 $mg \cdot l^{-1}$ C); (b) 225 $mg \cdot l^{-1}$ H_2O_2 (DOC = 34 $mg \cdot l^{-1}$ C); (c) 200 $mg \cdot l^{-1}$ H_2O_2 (DOC = 42 $mg \cdot l^{-1}$ C). For Procion Red H-E7B solutions (2 $mg \cdot l^{-1}$ Fe (II)): (d) 80 $mg \cdot l^{-1}$ H_2O_2 (DOC = 29 $mg \cdot l^{-1}$ C); (e) 65 $mg \cdot l^{-1}$ H_2O_2 (DOC = 33 $mg \cdot l^{-1}$ C); (f) 50 $mg \cdot l^{-1}$ H_2O_2 (DOC = 39 $mg \cdot l^{-1}$ C). The strategy was to start the treatment with the more biodegradable samples (larger H_2O_2 concentration used) changing later to the ones with a lower BOD_5/COD ratio, trying to find out the minimum H_2O_2 dose to successfully perform the chemical-biological treatment with a minimum mineralisation degree in the chemical stage. Proceeding in this way, bacteria would be able to get used to the phototreated wastewater. Full biodegradation was assumed when attaining residual DOC values close to those obtained in the previous glucose batch (~20 $mg \cdot l^{-1}$ C).

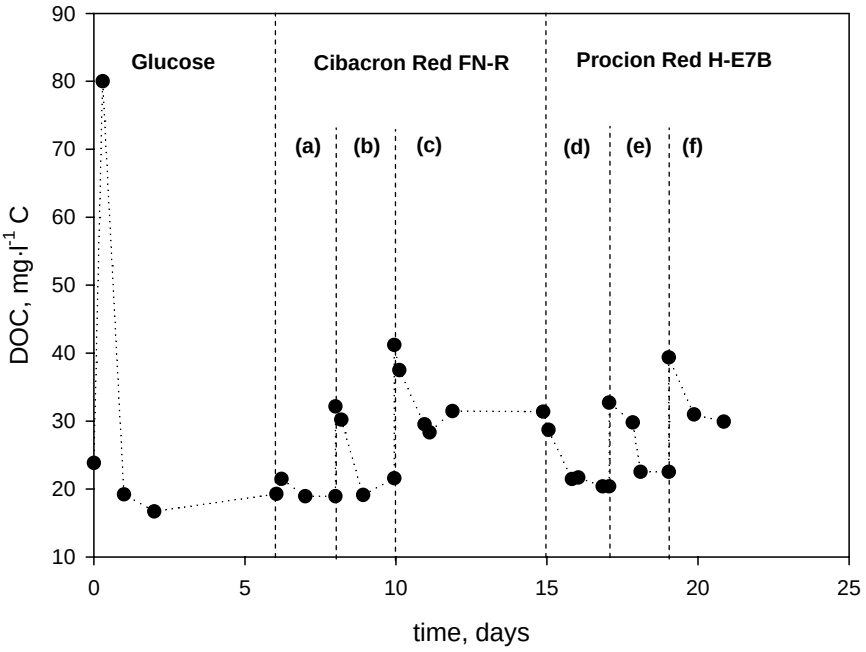

Figure 10. IBR operation after photo-Fenton pre-treatment: 250 $mg \cdot l^{-1}$ hydrolysed Cibacron Red FN-R, 5 $mg \cdot l^{-1}$ Fe (II), (a) 250 $mg \cdot l^{-1}$ H_2O_2 (b) 225 $mg \cdot l^{-1}$ H_2O_2 (c) 200 $mg \cdot l^{-1}$ H_2O_2; 250 $mg \cdot l^{-1}$ hydrolysed Procion Red H-E7B, 2 $mg \cdot l^{-1}$ Fe (II), (d) 80 $mg \cdot l^{-1}$ H_2O_2 (e) 65 $mg \cdot l^{-1}$ H_2O_2 (f) 50 $mg \cdot l^{-1}$ H_2O_2.

From Figure 10, it is clear that Cibacron Red FN-R solution was completely biodegraded in 1-2 days when adding 250 (a) and 225 $mg \cdot l^{-1}$ H_2O_2 (b) in the photo-

Fenton stage. However, the IBR was not able to degrade the hetero-bireactive dye by-products generated when using only 200 $mg \cdot l^{-1}$ H_2O_2 (c). The same behaviour was observed for Procion Red H-E7B. The effluents resulting from 80 (d) and 65 $mg \cdot l^{-1}$ H_2O_2 (e) treatments were fully biodegraded while the 50 $mg \cdot l^{-1}$ H_2O_2 one (f) was not enough biocompatible to feed the biological pilot plant. HPLC analysis revealed that original dyes were not present in solution after the considered phototreatments. This fact attributes the non biodegradability of (c) and (f) solutions to the presence of dyestuff by-products of biorecalcitrant nature. Finally, it is remarkable that the obtained biocompatible effluents ((a), (b), (d) and (e)) presented the maximum aliphatic carboxylic acids concentration (of biodegradable nature). The differences between the assessed photo-Fenton conditions are reflected in Figure 11. This compares the percentage of mineralisation reached by each stage of the coupling. The residual DOC values oscillated around 20 $mg \cdot l^{-1}$ C, settling a lower threshold for DOC removal.

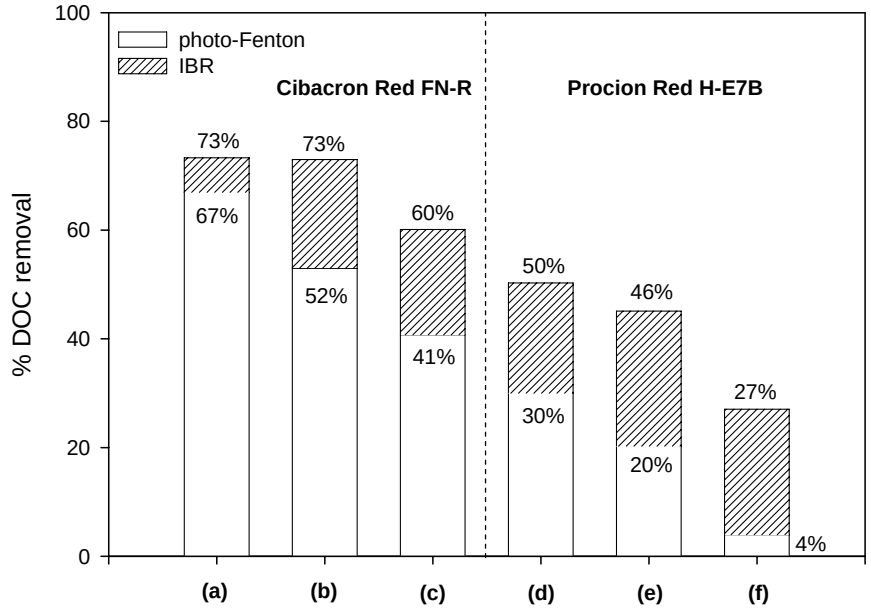

Figure 11. % DOC removal in photo-Fenton pre-treatment and IBR coupling system as a function of photo-Fenton conditions: 50 $mg \cdot l^{-1}$ hydrolysed Cibacron Red FN-R, 5 $mg \cdot l^{-1}$ Fe (II), (a) 250 $mg \cdot l^{-1}$ H_2O_2 (b) 225 $mg \cdot l^{-1}$ H_2O_2 (c) 200 $mg \cdot l^{-1}$ H_2O_2; 250 $mg \cdot l^{-1}$ hydrolysed Procion Red H-E7B, 2 $mg \cdot l^{-1}$ Fe (II), (d) 80 $mg \cdot l^{-1}$ H_2O_2 (e) 65 $mg \cdot l^{-1}$ H_2O_2 (f) 50 $mg \cdot l^{-1}$ H_2O_2.

Nitrification and denitrification reactions were followed by NH_4^+, NO_2^- and NO_3^- ion concentration measurements. A complete nitrification was achieved at the end of each batch biodegradation, indicating that the IBR system was working properly. Moreover, aliphatic carboxylic acids initially present in the pre-treated effluent were completely removed from the solutions.

Concluding, as happens when working under laboratory conditions, the photo-Fenton reaction can be successfully used as a pre-treatment to biocompatibilise the studied reactive dye solutions. Among the tested pre-treatment conditions, the best ones for a subsequent biodegradation at pilot plant are 5 $mg \cdot l^{-1}$ Fe (II), 225 $mg \cdot l^{-1}$ H_2O_2 for Cibacron Red FN-R and 2 $mg \cdot l^{-1}$ Fe (II), 65 $mg \cdot l^{-1}$ H_2O_2 for Procion Red H-E7B. BOD_5/COD values around 0.4 were achieved (Figure 9), with 52 and 20% mineralisation levels, respectively.

3.4. Main differences between laboratory and pilot plant

There are some fundamental differences between the photo-Fenton experiments carried out in the laboratory and in the pilot plant. First of all, the source of irradiation and the temperature were significantly different. A 6 W black light was used in the laboratory (6 $W \cdot m^{-2}$ UVA), while the pilot plant reactor was irradiated by the complete sunlight spectrum. Taking the 30 $W \cdot m^{-2}$ value as an estimation of the 300-400 nm energy arriving to the earth surface around noon, the luminous energy entering the photoreactor from the artificial black light was 5 times below. Additionally, it should be noted that the PSA radiometer measured only the 300-400 nm bandwidth of the solar spectrum, while photo-Fenton reaction also makes use of part of the visible spectrum [8]. This fact favours the pilot plant results and complicates the comparison with laboratory experiments. The high levels of temperature reached during solar photo-Fenton experimentation (from 25 up to 48 ºC) also increased dyes removal rates due to the beneficial effect of temperature on Fenton reaction [28].

The photoreactor configuration also differed from one system to another, leading to different efficiencies with regard to radiation. At laboratory, with the artificial light over the batch reactor, all dye volume was under irradiation, but the depth and the aromatic

content of solutions caused a strong absorption and impeded the radiation penetration towards the bottom of the system. On the contrary, CPC tubes geometry allowed all the illuminated volume to receive the radiation (they illuminate the complete perimeter of the tubular receiver, rather than just the front of it), increasing the optical and quantum efficiency of photo-Fenton process [16].

As observed before, the mineralisation degree was narrowly reproduced when scaling-up from laboratory to pilot plant the 10 $mg \cdot l^{-1}$ Fe (II), 250 $mg \cdot l^{-1}$ H_2O_2 photo-Fenton conditions for Procion Red H-E7B and the 20 $mg \cdot l^{-1}$ Fe (II), 500 $mg \cdot l^{-1}$ H_2O_2 for Cibacron Red FN-R. The reduction of irradiation times (from 100 and 150 minutes of black light irradiation to t_{30W} = 13 and 22 minutes, respectively) was a direct consequence of the above explained factors. This fast reaction rate allowed the photo-Fenton pilot system to reduce the catalyst concentration from 10 to 2 $mg \cdot l^{-1}$ for Procion Red H-E7B and from 20 to 5 $mg \cdot l^{-1}$ for Cibacron Red FN-R without loosing mineralisation efficacy (see Figures 3 and 4).

In the combined chemical-biological treatment, similar photo-Fenton pre-treatment conditions than laboratory were necessary to completely biocompatibilise Cibacron Red FN-R solution at pilot plant. The best dosages obtained were 250 $mg \cdot l^{-1}$ H_2O_2 at laboratory and 225 $mg \cdot l^{-1}$ H_2O_2 at pilot plant, leading to 50 and 52% partial mineralisation, respectively. However, for Procion Red H-E7B dye degradation, photo-Fenton oxidation at pilot plant improved laboratory results reducing the H_2O_2 requirements from 125 to 65 $mg \cdot l^{-1}$ and the mineralisation degree from 39 to 20%.

4. Conclusions

The pilot plant performance of solar photo-Fenton process for Procion Red H-E7B and Cibacron Red FN-R reactive dyes mineralisation closely reproduced previous laboratory artificial light results. 82 and 86% mineralisation was accomplished by adding 10 $mg \cdot l^{-1}$ Fe (II) and 250 $mg \cdot l^{-1}$ H_2O_2 to 250 $mg \cdot l^{-1}$ Procion Red H-E7B solutions and 20 $mg \cdot l^{-1}$ Fe (II) and 500 $mg \cdot l^{-1}$ H_2O_2 to 250 $mg \cdot l^{-1}$ Cibacron Red FN-R solutions, respectively.

The irradiation time was reduced in relation to the artificial light process from 100 and 150 minutes (black light irradiation) to 13 and 22 minutes (normalised t_{30W} values),

basically due to the higher amount of UV photons supplied by the sun, the involvement of the visible fraction of sunlight spectrum, and the solar photoreactor configuration, which collects and redirects to the solution all the radiation reaching the aperture area of the CPCs. The fast reaction rates allowed the pilot system to reduce the iron concentration from 10 to 2 $mg \cdot l^{-1}$ for Procion Red H-E7B and from 20 to 5 $mg \cdot l^{-1}$ for Cibacron Red FN-R without loosing photo-Fenton efficacy.

Formic, acetic, oxalic and maleic acids appeared during both dyes photooxidation. Pyruvic acid intermediate was also detected for Cibacron Red FN-R dye. Sulphur was stoichiometrically released into the solution as sulphate ion, with 92-95% recovery. The nitrogen mass balance was not completed as only 9-22% of total N was detected as inorganic nitrogen (NH_4^+ and NO_3^-) at the end of the treatment. These results are indicative of the generation of other N-containing products, such as N_2 gas and the recalcitrant triazine ring.

Finally, solar photo-Fenton process at pilot plant can be successfully used as a biological pre-treatment. With just 5 $mg \cdot l^{-1}$ Fe (II) and 225 $mg \cdot l^{-1}$ H_2O_2 (Cibacron Red FN-R) and 2 $mg \cdot l^{-1}$ Fe (II) and 65 $mg \cdot l^{-1}$ H_2O_2 (Procion Red H-E7B) reagent doses, dye solutions became enough biocompatible to be fully biodegraded in the IBR pilot plant. In comparison with bench scale experiments, the performance of the combined chemical-biological treatment appears to be superior.

Acknowledgements

The authors wish to thank to the Ministerio de Educación y Ciencia (project CTQ 2005-02808) for financial support and the "Programa de Acceso y Mejora de Grandes Instalaciones Científicas Españolas" (project GIC-05-17).

References

[1] C. O'Neill, F.R. Hawkes, D.L. Hawkes, N.D. Lourenço, H.M. Pinheiro, W. Delée, J. Chem. Technol. Biotechnol. 74 (11) (1999) 1009-1018.

[2] R. Andreozzi, V. Caprio, A. Insola, R. Marotta, Catal. Today 53 (1999) 5-59.

[3] R. Bauer, H. Fallman, Res. Chem. Intermed. 23 (1997) 34-354.

[4] J. Pignatello, Environ. Sci. Technol. 26 (1992) 944-951.

[5] A. Safarzadeh-Amiri, J.R. Bolton, S.R. Cater, J. Adv. Oxid. Technol. 1 (1996) 18-26.

[6] J. Pignatello, D. Liu, P. Huston, Environ. Sci. Technol. 33 (1999) 1832-1839.

[7] K.A. Hislop, J.R. Bolton, Environ. Sci. Technol. 33 (1999) 3119-3126.

[8] R. Bauer, G. Waldner, H. Fallmann, S. Hager, M. Klare, T. Krutzler, S. Malato, P. Maletzky, Catal. Today. 53 (1999) 131-144.

[9] M.J. Farré, X. Domènech, J. Peral, Water Res. 40 (2006) 2533-2540.

[10] J. García-Montaño, F. Torrades, J.A. García-Hortal, X. Domènech, J. Peral, Appl. Catal. B: Environ. 67 (2006) 86-92.

[11] V. Sarria, S. Kenfack, O. Guillod, C. Pulgarín, J. Photochem. Photobio. A 159 (2003) 89-99.

[12] J. García-Montaño, F. Torrades, J.A. García-Hortal, X. Domènech, J. Peral, J. Hazard. Mater. 134 (2006) 220-229.

[13] F. Torrades, J. García-Montaño, J.A. García-Hortal, Ll. Núñez, X. Domènech, J. Peral, Color. Technol. 120 (2004) 188-194.

[14] APHA-AWWA-WEF, Standard Methods for the Examination of Water and Wastewater, 18th Ed., Washington, DC, 1992.

[15] C. Kormann, D.W. Bahnemann, M.R. Hoffmann, Environ. Sci. Technol. 22 (5) (1988) 798-806.

[16] J. Blanco, S. Malato, P. Fernández, A. Vidal, A. Morales, P. Trincado, J.C. Oliveira, C. Minero, M. Musci, C. Casalle, M. Brunote, S. Tratzky, N. Dischinger, K.-H. Funken, C. Sattler, M. Vincent, M. Collares-Pereira, J.F. Mendes, C.M. Rangel, Sol. Energy. 67 (2000) 317-330.

[17] S. Malato, J. Cáceres, A.R. Fernández-Alba, L. Piedra, M.D. Hernando, A. Agüera, J. Vial, Environ. Sci. Technol. 37 (2003) 2516-2524.

[18] C. Galindo, P. Jacques, A. Kalt, J. Photoch. Photobio. A. 130 (2000) 35-47.

[19] E. Guivarch, S. Trevin, C. Lahitte, M.A. Oturan, Environ. Chem. Lett. 1 (2003) 38-44.

[20] C. Hu, Yu J.C., Z. Hao, P.K. Wong, Appl. Catal. B: Environ. 42 (2003) 47-55.

[21] M. Karkmaz, E. Puzenat, C. Guillard, J.M. Herrmann, Appl. Catal. B: Environ. 51 (2004) 183-194.

[22] M. Stylidi, D.I. Kondarides, X.E. Verykios, Appl. Catal. B: Environ. 40 (2003) 271-286.

[23] H. Lachheb, E. Puzenat, A. Houas, M. Ksibi, E. Elaloui, C. Guillard, J.M. Herrmann, Appl. Catal. B: Environ. 39 (2002) 75-90.

[24] A. Bravo, J. García, X. Domènech, J. Peral, J. Chem. Res. S (1993) 376-377.

[25] M.H. Pérez, G. Peñuela, M.I. Maldonado, O. Malato, P. Fernández-Ibáñez, I. Oller, W. Gernjak, S. Malato, Appl. Catal. B: Environ. 64 (2006) 272-281.

[26] M. Lapertot, C. Pulgarín, P. Fernández-Ibáñez, M.I. Maldonado, L. Pérez-Estrada, I. Oller, W. Gernjak, S. Malato, Water Res. 40 (2006) 1086-1094.

[27] E. Chamarro, A. Marco, S. Esplugas, Water Res. 35 (2001) 1047-1051.

[28] M. Pérez, F. Torrades, X. Domènech, J. Peral, Water Res. 36 (2002) 2703-2710.

A.1.2. Pathways of solar photo-Fenton degradation of Procion Red H-E7B reactive azo dye at pilot plant scale

Generated intermediates and reaction pathways of Procion Red H-E7B reactive azo dye degradation by means of photo-Fenton Advanced Oxidation Process (AOP) have been investigated. The study complements the work previously reported in Section A.1.1, entitled: **Pilot plant scale reactive dyes degradation by solar photo-Fenton and biological processes**.

Analogously, photo-Fenton experiments were carried out under sunlight at pilot plant scale in a 35 l Compound Parabolic Collector (CPC) (set-up and experimental conditions detailed in Section 3.6.1.2) at the Plataforma Solar de Almería (PSA, Spain). Solar irradiation began after 5 minutes of dark Fenton reaction. Ultraviolet radiation (300-400 nm) reaching the solar pilot plant was measured by a global UV radiometer (Kipp & Zonen, model CUV3). Experiments were thereby evaluated by using the normalised illumination time t_{30W}, which takes into account cloudiness and other environmental conditions (t_{30W} calculation method in Section 3.6.1.2). Throughout them, UV intensity ranged between 19 and 37 $W \cdot m^{-2}$. Since the system was outdoors and non isolated, temperature in the reactor rose from 26 to 44 ºC.

Applied photo-Fenton conditions were 2 $mg \cdot l^{-1}$ of Fe (II) and 250 $mg \cdot l^{-1}$ of H_2O_2. These provided appropriate degradation rates that ensure the detection of as many breakdown products as possible. In order to convert Procion Red H-E7B reactive dye into the form normally found in industrial textile effluents, 250 $mg \cdot l^{-1}$ solutions (Dissolved Organic Carbon (DOC) = 40 ± 1 $mg \cdot l^{-1}$ C; n = 3, $\alpha = 0.05$) were hydrolysed by adjusting the pH to 10.6 followed by heating to 80 ºC for 6 hours.

DOC was determined with a TOC Shimadzu 5050A analyser (Section 3.3.1). Chloride ion was determined by Ion Chromatography (IC) (Section 3.3.8). The original dye degradation was monitored by High Performance Liquid Chromatography (HPLC) and UV/Vis detector (Section 3.3.6). Organic by-products identification was developed by means of Liquid Chromatography-(Electrospray Ionisation)-Time-of-Flight Mass Spectrometry (LC-(ESI)-TOF-MS) analysis of the different phototreated samples (experimental conditions and samples pre-treatment in Section 3.3.7). Among other

chromatographic techniques, Liquid Chromatography-Mass Spectrometry (LC-MS) has become the preferred analytical instrument for analysing relatively polar and non volatile organic molecules without derivation. Furthermore, Time-of-Flight analysis Mass Spectrometry (TOF-MS) with Electrospray Ionisation (ESI) has gained popularity due to its sensibility, theoretically unlimited mass range, high mass resolution and capability for highly accurate mass determination [1].

Finally, in order to elucidate such a complex degradation mechanism, previously reported data (Section A.1.1) regarding carboxylic acids, SO_4^{2-}, NH_4^+ and NO_3^- generation through photodegradation have also been considered and discussed together with LC-(ESI)-TOF-MS results.

A.1.2.1. Degradation products of Procion Red H-E7B

The mineralisation profile of Procion Red H-E7B dye (Figure A.1.1) photodegradation is shown in Figure A.1.2. Its complete oxidation stoichiometry would be as follows (Equation A.1.1):

$$C_{52}H_{34}O_{26}S_8Cl_2N_{14} + 76.5\ O_2 \rightarrow 52\ CO_2 + 14\ NO_3^- + 8\ SO_4^{2-} + 2\ Cl^- + 32\ H^+ + H_2O \quad (A.1.1)$$

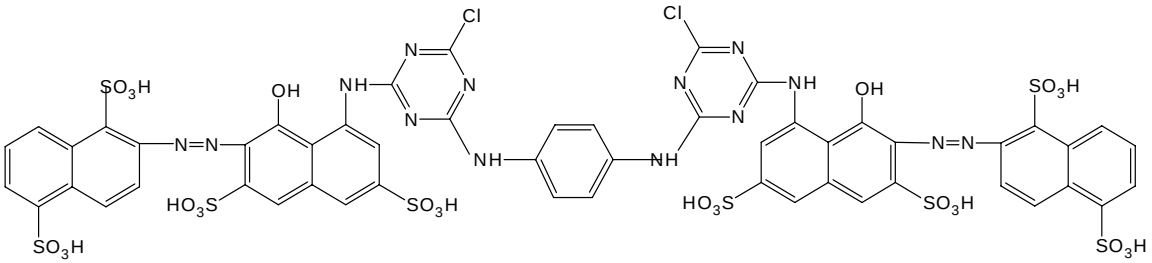

Figure A.1.1. Chemical structure of Procion Red H-E7B.

After t_{30W} ~ 15 minutes of irradiation, it is noticeable a fast mineralisation until the achievement of a constant residual DOC of recalcitrant nature. These results imply that some kind of organic compounds were still present even with prolonged photodegradation.

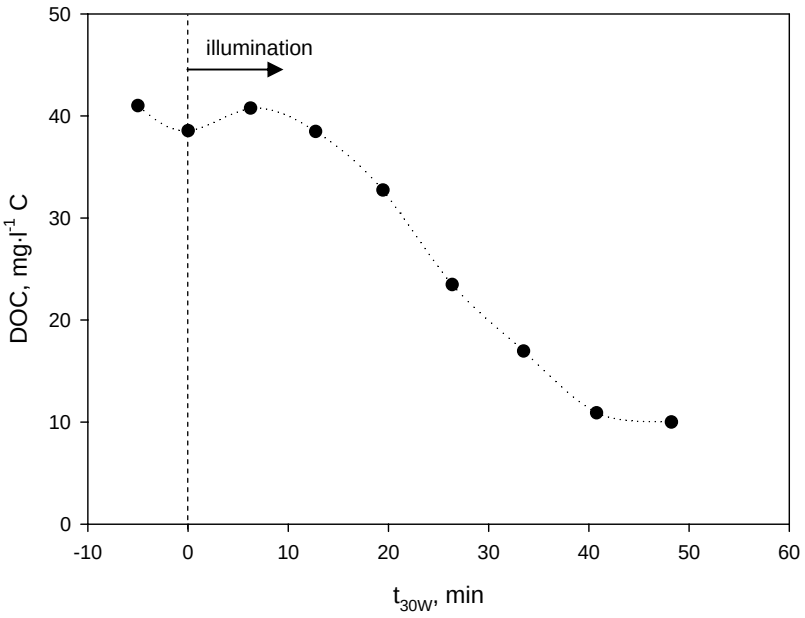

Figure A.1.2. DOC evolution *versus* t_{30W} for 250 mg·l^{-1} hydrolysed Procion Red H-E7B; photo-Fenton conditions: 2 mg·l^{-1} Fe (II), 250 mg·l^{-1} H_2O_2, pH = 2.8.

On the other hand, analogously to Procion Red H-E7B degradation observed in Section A.1.1 (Figure 6), all treated samples were exempted of original dye since it quickly disappeared before illumination (t_{30W} = 0 minutes) (data not shown). This fast parent compound disappearance was accompanied by the solution bleaching. By comparing both DOC and dye concentration data, it is worth to note that complete dye and colour depletion took place before the beginning of mineralisation (disappearance of DOC).

Degradation samples corresponding to t_{30W} = 0, 6, 13 and 19 minutes were chosen to investigate generated Procion Red H-E7B by-products. As commented above, they were analysed by means of LC-(ESI)-TOF-MS technique. Oxidation led to the formation of a high number of degradation products. Among them, a total of 18 different aromatic

compounds were identified. As an example, Figure A.1.3 shows the LC-(ESI)-TOF-MS full-scan chromatogram of the main identified compounds after t_{30W} = 6 minutes of solar photo-Fenton treatment. The tentative molecular structures of all of them are drawn in Figure A.1.4.

Identification was based on accurate mass measurements that enabled empirical formulas to be calculated with an elemental composition calculator tool, generating a list of best-match hits. The proposal of the best chemical structure was based on prior knowledge of the molecule pattern and the oxidative treatment. Additional information was subtracted from the characteristic isotopic distribution of certain molecules mass spectra containing chlorine (Cl^{35} and Cl^{37}) atoms. Table A.1.1 shows data related to the experimental and calculated masses of the protonated ions (mass to charge ratio; m/z), the error between them, the retention time, and the proposed empirical formula corresponding to the identified compounds. In all cases, the resulting accurate masses were found at an error less than 1.9 mDa or 3.4 ppm.

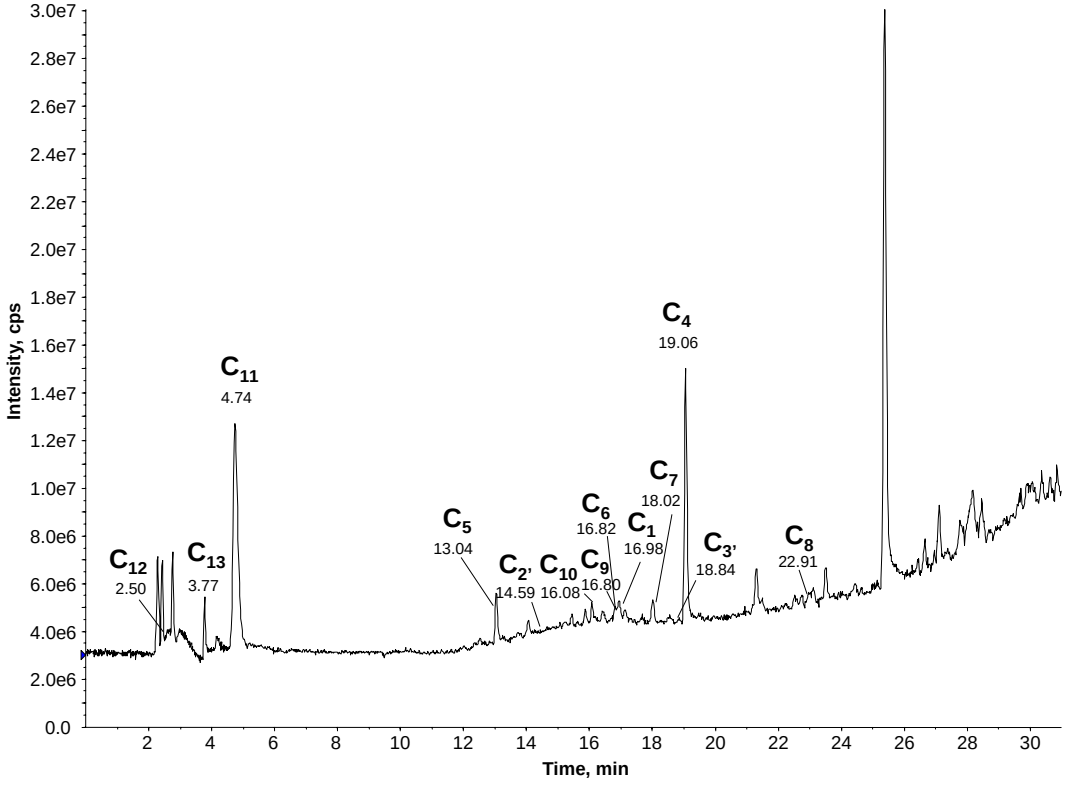

Figure A.1.3. Typical LC-(ESI)-TOF-MS full-scan chromatogram of main identified compounds after t_{30W} = 6 minutes of solar photo-Fenton treatment.

C_1, $C_{1'}$, $C_{1''}$

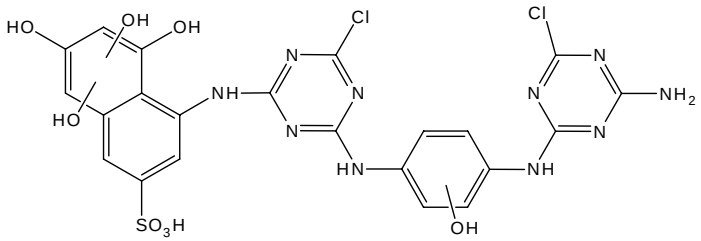

C_2, $C_{2'}$, $C_{2''}$

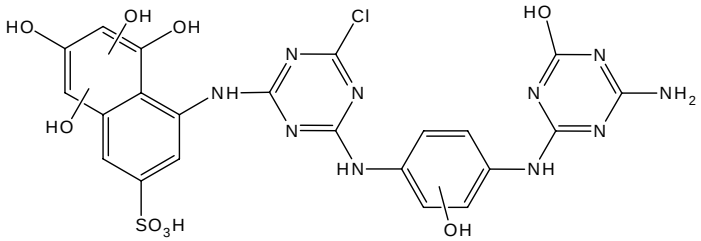

C_3, $C_{3'}$

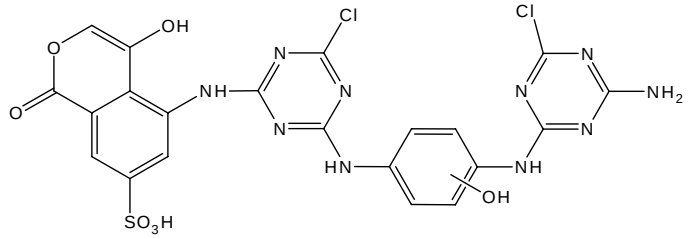

C_4

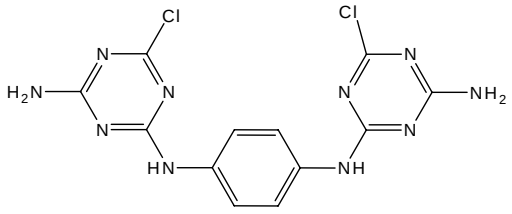

C_5

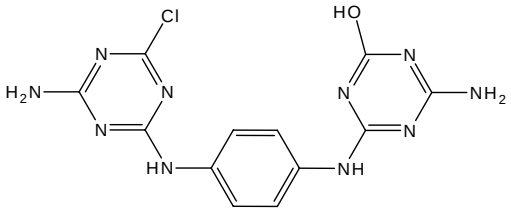

Figure A.1.4. Degradation products of Procion Red H-E7B.

C_6

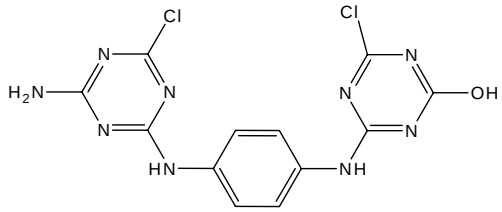

C_7

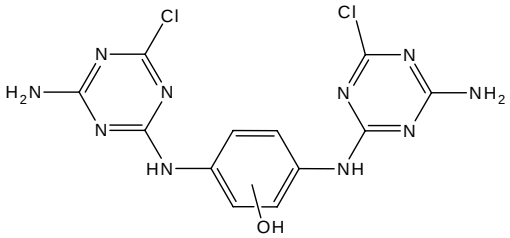

C_8

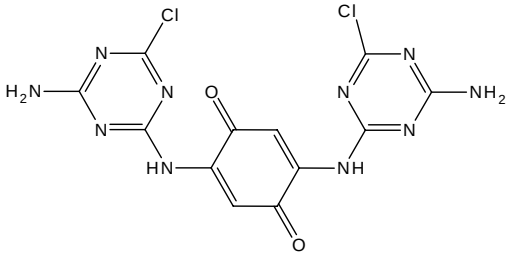

C_9

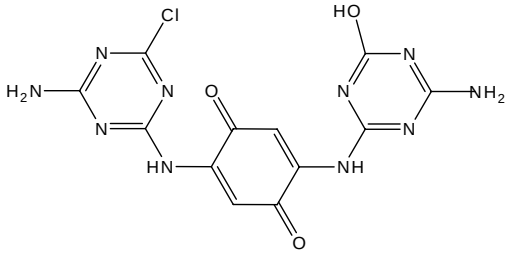

C_{10}

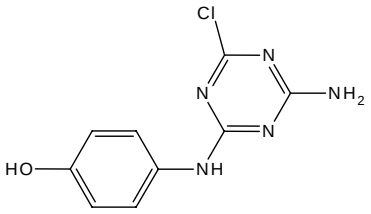

C_{11}

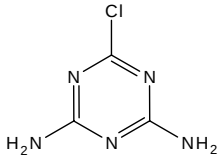

C_{12}

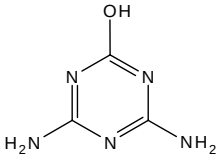

C_{13}

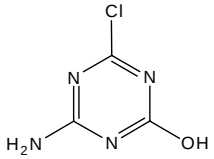

Figure A.1.4 (cont.). Degradation products of Procion Red H-E7B.

Table A.1.1. Accurate mass measurements obtained from the LC-(ESI)-TOF-MS spectra of Procion Red H-E7B degradation products (see spectra in Section A.2.1).

Compound	Formula	Retention time min	Detected m/z	Calculated m/z	Error mDa	Error ppm
C_1		16.98	651.0322		-0.1	-0.2
$C_{1'}$	$C_{22}H_{17}Cl_2N_{10}O_8S^+$	18.60	651.0312	651.0323	-1.1	-1.7
$C_{1''}$		19.34	651.0308		-1.5	-2.3
C_2		14.28	633.0676		1.4	2.2
$C_{2'}$	$C_{22}H_{18}ClN_{10}O_9S^+$	14.59	633.0642	633.0661	1.9	-3.2
$C_{2''}$		14.82	633.0664		0.2	-0.3
C_3	$C_{21}H_{15}Cl_2N_{10}O_7S^+$	16.77	621.0231	621.0217	1.4	2.2
$C_{3'}$		18.84	621.0220		0.2	0.4
C_4	$C_{12}H_{11}Cl_2N_{10}^+$	19.06	365.0551	365.0539	1.1	3.1
C_5	$C_{12}H_{12}ClN_{10}O^+$	13.04	347.0880	347.0878	0.1	0.4
C_6	$C_{12}H_{10}Cl_2N_9O^+$	16.82	366.0382	366.0379	0.2	0.6
C_7	$C_{12}H_{11}Cl_2N_{10}O^+$	18.02	381.0491	381.0488	0.2	0.6
C_8	$C_{12}H_9Cl_2N_{10}O_2^+$	22.91	395.0280	395.0281	-0.2	-0.4
C_9	$C_{12}H_{10}ClN_{10}O_3^+$	16.80	377.0619	377.0620	-0.1	-0.4
C_{10}	$C_9H_9ClN_5O^+$	16.08	238.0489	238.0490	-0.1	-0.5
C_{11}	$C_3H_5ClN_5^+$	4.74	146.0233	146.0227	0.5	3.4
C_{12}	$C_3H_6N_5O^+$	2.50	128.0571	128.0566	0.4	3.2
C_{13}	$C_3H_4ClN_4O^+$	3.77	147.0073	147.0068	0.3	1.9

Among the 18 identified by-products, C_1, $C_{1'}$ and $C_{1''}$, C_2, $C_{2'}$ and $C_{2''}$, and C_3 and $C_{3'}$ shared the same accurate mass, and consequently the same empirical formula. Nevertheless, their different retention times evidence their different molecular structures, probably by the distinct location of the –OH groups in aromatic rings (they may be indistinctly linked to either the benzene or naphthalene ring). Additionally, possible different isomers just varying the location of lactone in C_3 and $C_{3'}$ naphthalene structure, as well as the remaining sulphonic and/or chlorine substituent groups in C_1, $C_{1'}$, $C_{1''}$, C_2, $C_{2'}$, $C_{2''}$, C_3, $C_{3'}$ and C_9 by-products must also be taken into consideration.

With the information handled here, it is not possible to exactly know their molecular structures and the differences between them. In this sense, it should be noted that just one structure among the several possible isomers has been drawn in Figure

A.1.4. To reveal the exact structures, more work on degradation products analysis and identification –e.g., comparison with commercial standards (if available), Nuclear Magnetic Resonance (NMR) and/or further tandem Mass Spectrometry (MS/MS) detection– is necessary.

A.1.2.2. Procion Red H-E7B by-products evolution over time

Identified Procion Red H-E7B reactive dyes intermediates appear neither in all collected samples nor with the same profile. Figures A.1.5-A.1.8 monitor the transient kinetics of each compound in relation to t_{30W} irradiation time.

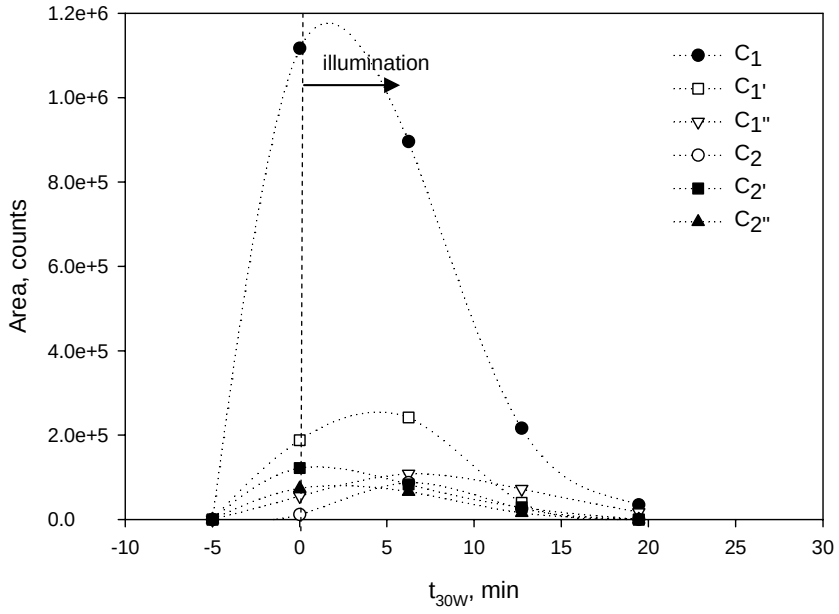

Figure A.1.5. Evolution over time of C_1, $C_{1'}$, $C_{1''}$, C_2, $C_{2'}$ and $C_{2''}$ Procion Red H-E7B degradation products.

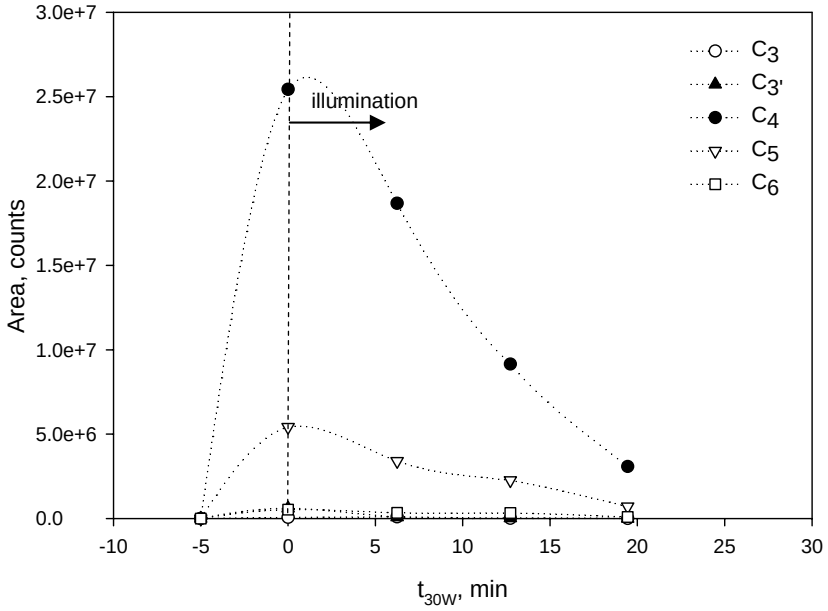

Figure A.1.6. Evolution over time of C_3, $C_{3'}$, C_4, C_5 and C_6 Procion Red H-E7B degradation products.

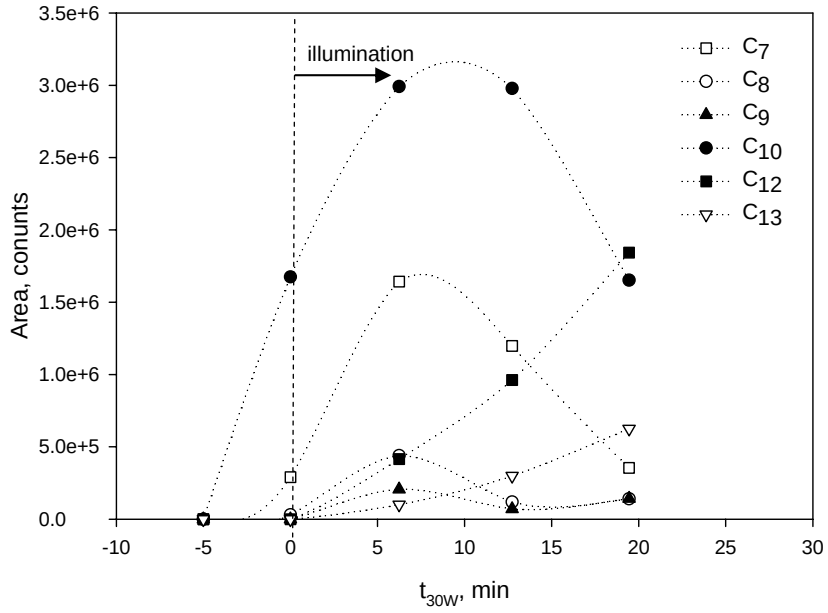

Figure A.1.7. Evolution over time of C_7, C_8, C_9, C_{10}, C_{12} and C_{13} Procion Red H-E7B degradation products.

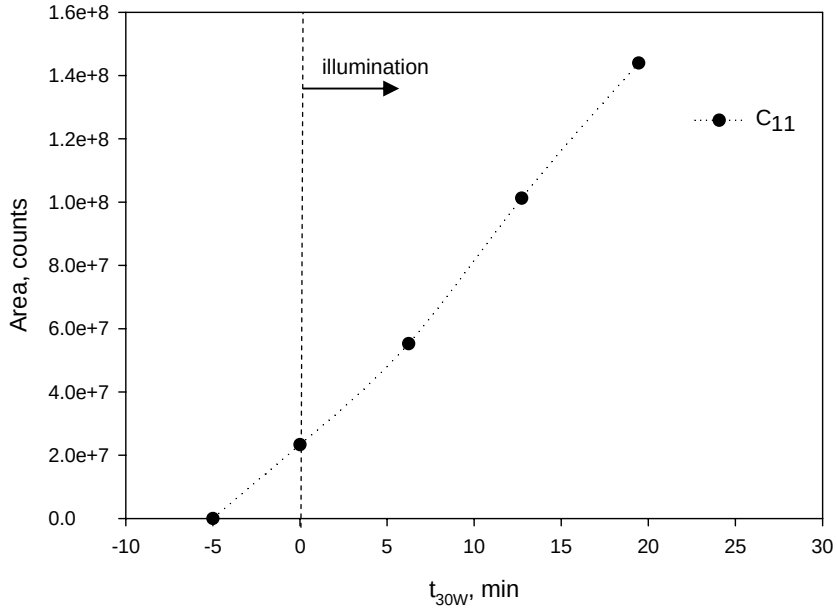

Figure A.1.8. Evolution over time of C_{11} Procion Red H-E7B degradation product.

Figures A.1.5 and A.1.6 show the early appearance of the largest C_1, $C_{1'}$, $C_{1''}$, C_2, $C_{2'}$, $C_{2''}$, C_3 and $C_{3'}$ compounds, with a maximum abundance among t_{30W} = 0 and 6 minutes. Smaller C_4, C_5 and C_6 compounds presented a similar chronological distribution, with maxima located at t_{30W} ~ 0 minutes (Figure A.1.6). C_7, C_8, C_9 and C_{10} compounds were detected later, displacing their maximum abundance at t_{30W} between 6 and 13 minutes (Figure A.1.7).

It is worth to note that once attained their maximum value, all the above compound signals decreased until complete disappearance. This decrease occurred simultaneously with the appearance and increase of the last and smallest C_{11}, C_{12} and C_{13} compounds (Figures A.1.7 and A.1.8), whose presence continuously increased along the analysed time. C_{11} is plotted in a separate graph due to its large signal.

The order of appearance of these by-products is a key issue to elucidate Procion Red H-E7B photodegradation mechanism.

A.1.2.3. Photodegradation pathways

Hydroxyl radicals, the main and best-known oxidant species involved in photo-Fenton process, are strong electrophilic oxidants. Consequently, Procion Red H-E7B reactive azo dye degradation may be initiated by the attack of HO· upon an electron-rich site; i.e., near the azo nitrogen atoms or near the amino groups [2].

In view of this, the fast full decolourisation of the dye solution appears to suggest a sequenced oxidation mechanism in which hydroxyl radical preferably attacks the chromophore centre of dye molecules (i.e., the azo groups, -N=N-) cleaving them in three parts: the two lateral substituted naphthalene rings and the central body. The non detection of reactive dye intermediates containing the original azo groups also points to this direction.

Azo groups may be mainly attacked at two positions [3, 4]. The first would be at C-N single bond between the azo group and naphthalene ring, generating N_2 gas according to Equations A.1.2 and A.1.3 [5]. This mechanism represents the environmentally more appealing pathway for the elimination of nitrogen from N-containing pollutants [5-7].

$$R_1\text{-}N{=}N\text{-}R_2 + HO^{\cdot} \rightarrow R_1\text{-}N{=}N^{\cdot} + R_2\text{-}OH \qquad \text{(A.1.2)}$$

$$R_1\text{-}N{=}N^{\cdot} \rightarrow R_1^{\cdot} + N{\equiv}N \qquad \text{(A.1.3)}$$

The second possibility of HO· reaction would be at the chromophore double bond, resulting in the formation of primary aromatic amines. By further degradation, the amino group would be finally released as NH_4^+ into aqueous solution.

The secondary amino group placed between naphthalene or benzene and the triazine rings would be subsequently attacked. The rupture between N and naphthalene or benzene rings is easier than that between N and triazine [8]. In this way, the amino groups degradation by HO· would generate a primary amine linked to the triazine ring. A simplified scheme of this reaction would be as follows (Equation A.1.4):

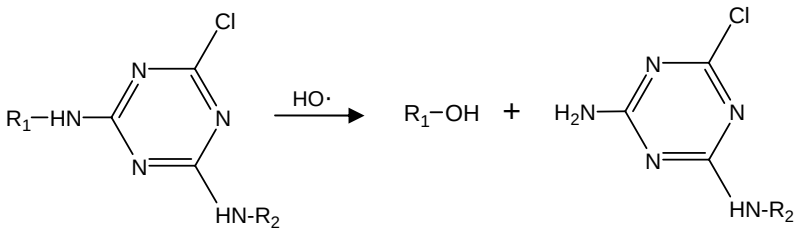

(A.1.4)

The initial apparition of C_1, $C_{1'}$, $C_{1''}$, C_2, $C_{2'}$, $C_{2''}$, C_3, $C_{3'}$, C_4 and C_5 compounds indicates that both above described decomposition pathways (azo and amino groups attack by HO•) were initially involved. However, the molecular structures of some of these compounds show that additional HO• degradation mechanisms had also taken place. C_3 and $C_{3'}$ by-products would have been originated from further C_1, $C_{1'}$ and $C_{1''}$ compounds degradation via a series of complex reactions that can not be described in detail. On the other hand, from C_1, $C_{1'}$, $C_{1''}$, C_2, $C_{2'}$, $C_{2''}$, C_3 and $C_{3'}$ structures, the addition of HO• to one of the carbon atoms bearing the sulphonic groups and the release of sulphate anion can be envisaged (Equations A.1.5 and A.1.6) [6].

$$R\text{-}SO_3^- + HO^\bullet \rightarrow R\text{-}OH + SO_3^{\bullet -} \quad \text{(A.1.5)}$$

$$SO_3^{\bullet -} + HO^- \rightarrow SO_4^{2-} + H^\bullet \quad \text{(A.1.6)}$$

The identification of such structures, jointly with the degradation mechanism proposed in Equations A.1.5 and A.1.6, is consistent with the kinetics of inorganic SO_4^{2-} appearance with irradiation time (Figure A.1.9). As reported in Section A.1.1, desulphuration gradually occurred being possible to detect up to 92% of the theoretically expected sulphur (Equation A.1.1).

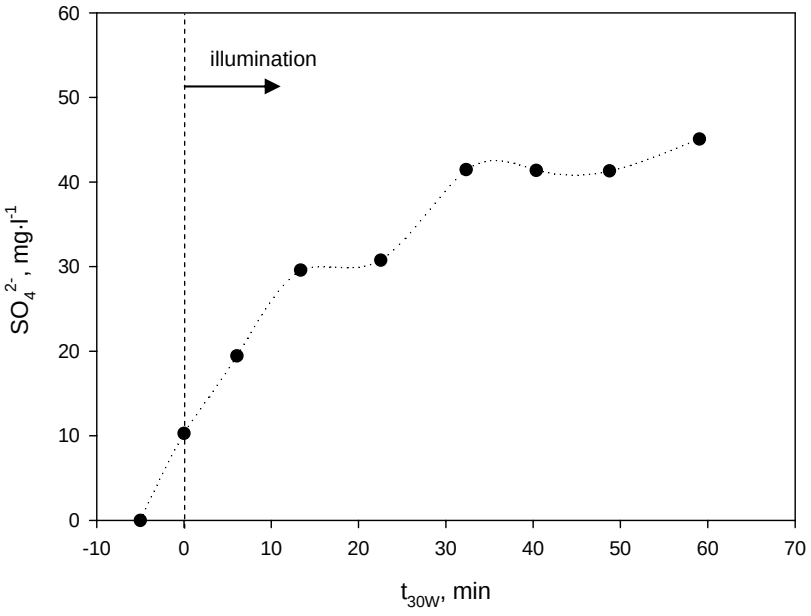

Figure A.1.9. Sulphate ion concentration *versus* t_{30W} for 250 mg·l^{-1} hydrolysed Procion Red H-E7B; photo-Fenton conditions: 2 mg·l^{-1} Fe (II), 250 mg·l^{-1} H_2O_2, pH = 2.8.

Apart from sulphonic acid groups substitution by HO·, part of the chlorine substituent groups were analogously replaced along photodegradation (it should be noted that chlorine atoms linked to the triazine groups of Procion Red H-E7B corresponded to the non hydrolysed fraction of the original dye, which is always present in spite of the hydrolysis process carried out prior photodegradation). Figure A.1.10 depicts the Cl^- formation over reaction time. The maximum attained value corresponds to 45% of the total (before hydrolysis) (Equation A.1.1), whereas the left fraction would have been released during hydrolysis process or would remain still linked to triazine moiety. In agreement with this, the stable nature of chlorine atoms bonded to triazine rings had already been observed by other authors [3].

According to the above conclusions, hydroxyl groups linked to the triazine rings of identified intermediates may be derived from either hydrolysis or oxidation processes.

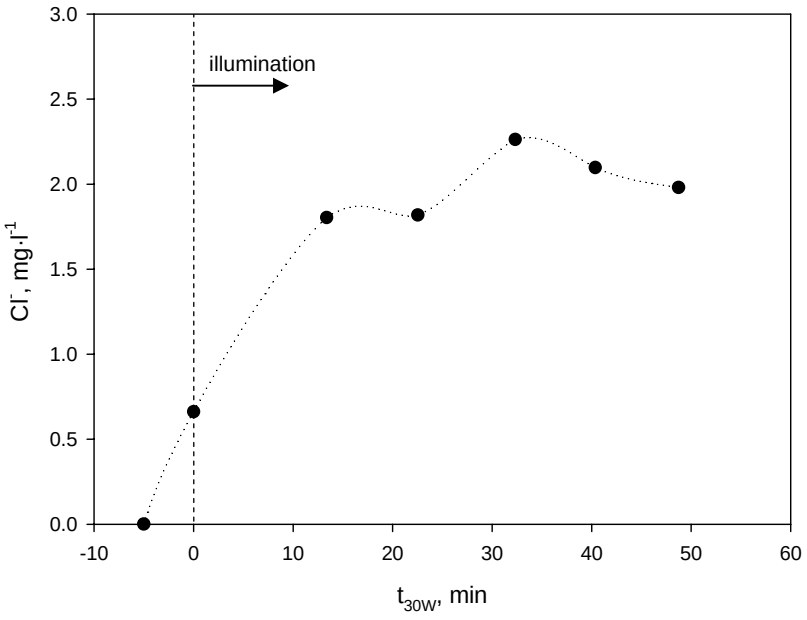

Figure A.1.10. Chloride ion concentration *versus* t_{30W} for 250 mg·l^{-1} hydrolysed Procion Red H-E7B; photo-Fenton conditions: 2 mg·l^{-1} Fe (II), 250 mg·l^{-1} H_2O_2, pH = 2.8.

On the other hand, C_1, $C_{1'}$, $C_{1''}$, C_2, $C_{2'}$, $C_{2''}$, C_3, $C_{3'}$ and C_7 by-products evidence the direct addition of HO$^{\bullet}$ to unsaturated bonds of naphthalene and/or benzene structures, giving place to the formation of mono- or poly-hydroxylated derivatives. A further oxidation would conduct to degradation intermediates containing quinone-like structures, like C_8 and C_9. These compounds are of special interest in Fenton processes chemistry since they may take part in the complex mechanism of Fe (II) regeneration (see Section 1.4.1.1).

As it is stated in the literature, the following degradation step of benzenic and naphtalenic skeletons would be the ring opening to form short chain carboxylic acids [5, 9, 10]. In conformity with this, Figure A.1.11 displays the transient concentration of formic, acetic, oxalic and maleic acids.

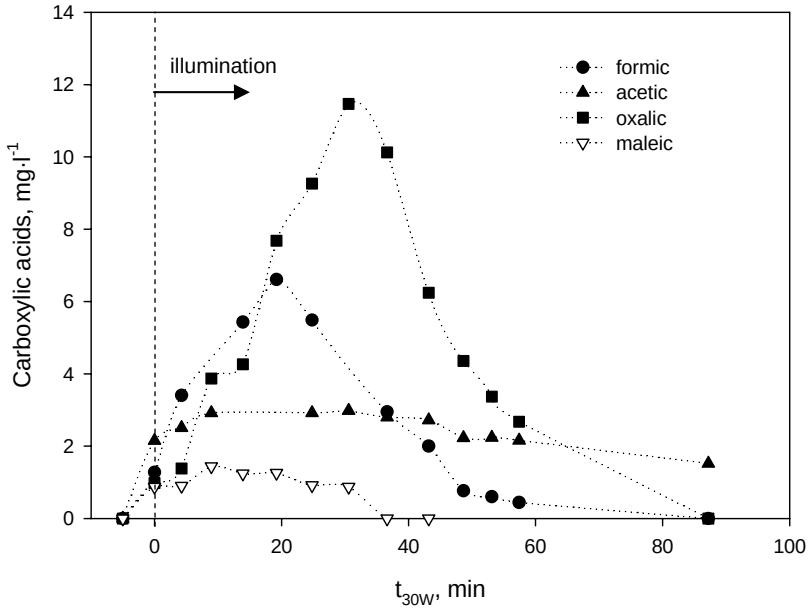

Figure A.1.11. Carboxylic acids concentration *versus* t_{30W} for 250 mg·l^{-1} Procion Red H-E7B; photo-Fenton conditions: 2 mg·l^{-1} Fe (II), 250 mg·l^{-1} H_2O_2, pH = 2.8.

The Figure reveals that all carboxylic acids appeared at the outset of photo-Fenton process. In fact, their presence was evident even before the beginning of solar irradiation (t_{30W} = 0 minutes). This behaviour is indicative of the fast and easy naphthalene and/or benzene rings breaking, which may even directly release the smallest aliphatic carboxylic acids. Other studies have already reported the generation of formic acid as an initial intermediate [5].

Although they were present so early in solution, their concentration reached a maximum around t_{30W} = 30 minutes. At this point, C_1, $C_{1'}$, $C_{1''}$, C_2, $C_{2'}$, $C_{2''}$, C_3, C_4, C_5, C_6, C_7, C_8 and C_9 compounds had disappeared (Figures A.1.5-A.1.7) and free sulphate and chloride anions had attained their maximum concentration (Figures A.1.9 and A.1.10).

To achieve complete mineralisation, the largest acids would be later degraded following the tentative mechanism reported in Scheme A.1.1, slowly yielding CO_2 and water [5]. As previously known [5], acetic acid required longer reaction times (Figure A.1.11).

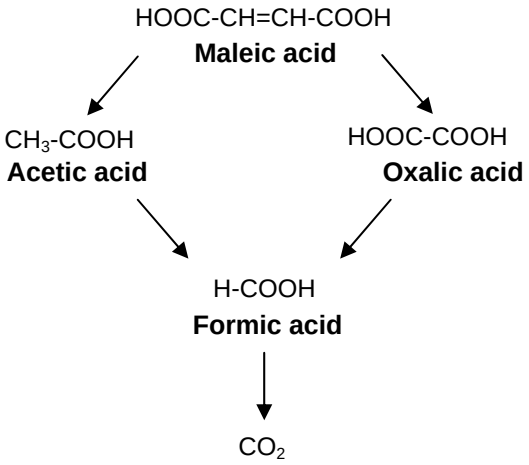

Scheme A.1.1. Mechanism of carboxylic acids degradation.

The fate of Procion Red H-E7B triazine groups was quite different. The amino groups degradation mechanism illustrated in Equation A.1.4 would gradually transform large intermediates to smaller structures, like C_{10}, C_{11}, C_{12} and C_{13}.

As commented in Section A.1.2.2, the C_{11}, C_{12} and C_{13} by-products continuously increased their concentration throughout reaction. This profile points to their accumulation and permanence in the final phototreated solution, a fact that would be in accordance with other studies about the difficulty of mineralisation of the triazine moiety by photo-Fenton and other AOPs treatments [3, 4, 7, 11-14]. In those previous studies, cyanuric acid (Figure A.1.12) is described as the final degradation product, thought it has not been detected in the analysis carried out within the present work.

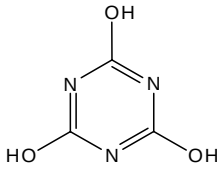

Figure A.1.12. Chemical structure of cyanuric acid.

The degradation of C_{11}, C_{12} and C_{13} by-products to cyanuric acid would involve the hydroxylation of the carbon atoms holding both chlorine and primary amino group. It is worth to note that, analogously to Cl^- release, the substitution of primary amino groups linked to triazine rings by $HO^{\bullet}$ is a particularly slow process [13]. Additionally, it would be directly transformed into NO_3^- rather than NH_4^+ [3]. Among the identified intermediates, C_{13} and the larger C_6 could undergo such amino group degradation mechanism.

Finally, Figure A.1.13 shows the total nitrogen concentration corresponding to NH_4^+ and NO_3^- ions arising from Procion Red H-E7B mineralisation. As reported in Section A.1.1, the complete balance of N was not obtained, scarcely attaining 9% of the expected stoichiometric quantity (Equation A.1.1).

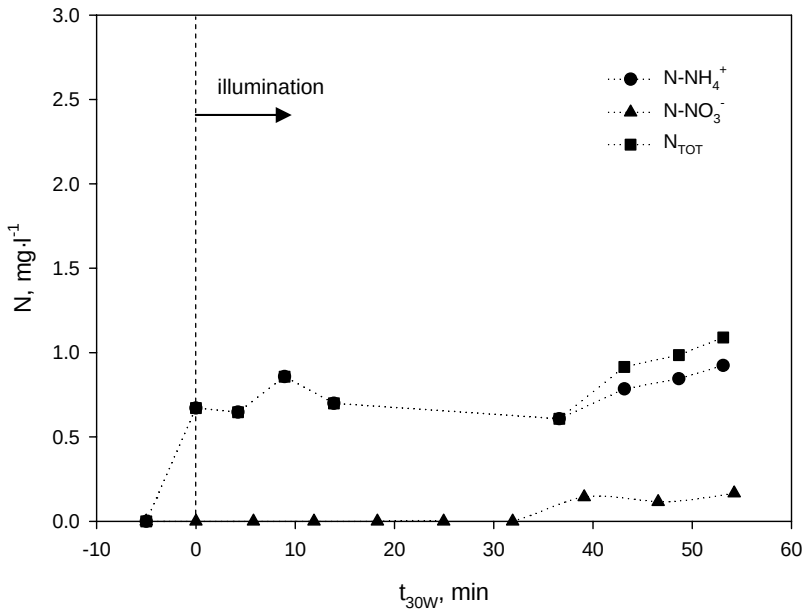

Figure A.1.13. Inorganic nitrogen release *versus* t_{30W} for 250 mg·l^{-1} Procion Red H-E7B; photo-Fenton conditions: 2 mg·l^{-1} Fe (II), 250 mg·l^{-1} H_2O_2, pH = 2.8.

Summarising the earlier discussions, the detected ammonium may be generated from either azo bonds or amino groups degradation. On the other hand, the quantified nitrate concentration would correspond to both the direct transformation of amino groups into NO_3^- and the oxidation of NH_4^+. Nonetheless, it should be remarked that

ammonium intermediate oxidation is not a favourable process in acid media, taking place slowly [15]. The presence of triazine derivatives in final solution (e.g., C_{11}, C_{12}, C_{13}, which may even contain 5 nitrogen atoms in their structure), in addition with N_2 gas generation as a result of azo group attack by $HO^{\bullet}$, would justify the incomplete nitrogen mass balance. On the other hand, the long-living triazine species would also give explanation for the remaining DOC observed at the end of photo-Fenton process (Figure A.1.2).

The knowledge of the reaction pathways is a key issue from a practical point of view, especially in cases where the chemical treatment precedes a biological process; a relationship between generated by-products and biocompatibility may be established. As reported in Section A.1.1, 2 $mg \cdot l^{-1}$ Fe (II) and 65 $mg \cdot l^{-1}$ H_2O_2 concentrations generated biodegradable Procion Red H-E7B solutions with 20% DOC removal. This mineralisation percentage corresponded to t_{30W} = 19 minutes (see Figure A.1.2), just when C_{11}, C_{12}, C_{13} and carboxylic acids intermediates were gaining importance and the large compounds had nearly completely disappeared (see Figures A.1.5-A.1.8 and A.1.11). Such results evidence the higher biodegradability degree of the smallest triazine-like species with regard to their precursors. In fact, cyanuric acid –their last degradation product– is reported to be biodegradable and non toxic [16]. On the other hand, short chain carboxylic acids are well known to be of biodegradable nature.

Overall, the whole Procion Red H-E7B solar photo-Fenton degradation process can be described by a series of consecutive steps, schematically depicted in Scheme A.1.2. In order to complete the degradation pathways, which are composed of a multiple and complex set of simultaneous reactions (none of them exclusive), further experimentation making use of complementary analytical tools is necessary.

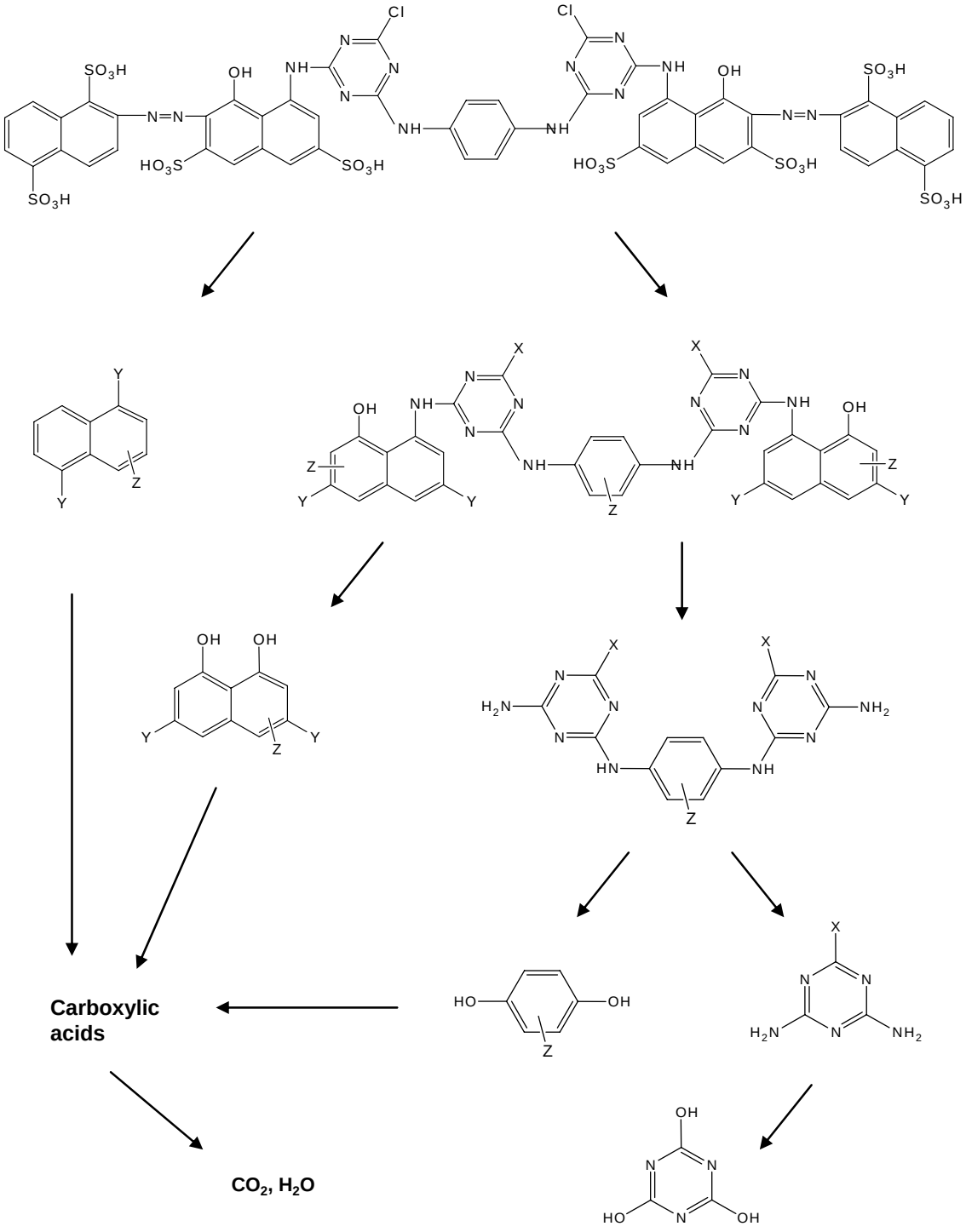

Scheme A.1.2. Proposed reaction pathways for Procion Red H-E7B degradation; **X**: Cl or OH, **Y**: SO_3H or OH, **Z**: possible mono- or poly-hydroxylations of naphthalene or benzene rings.

A.1.2.4. References

[1] Pérez-Estrada L., Malato S., Gernjak W., Agüera A., Thurman E.M., Ferrer I., Fernández-Alba A.R. (2005). Photo-Fenton degradation of Diclofenac: main intermediates and degradation pathway. *Environ. Sci. Technol*., 39, 8300-8306.

[2] Galindo C., Jacques P., Kalt A. (2000). Photodegradation of the aminoazobenzene acid orange 52 by three advanced oxidation processes: UV/H_2O_2, UV/TiO_2 and VIS/TiO_2. Comparative mechanistic and kinetic investigations. *J. Photoch. Photobio. A*, 130, 35-47.

[3] Hu C., Yu J.C., Hao Z., Wong P.K. (2003). Photocatalytic degradation of triazine-containing azo dyes in aqueous TiO_2 suspensions. *Appl. Catal. B: Environ.*, 42, 47-55.

[4] Hu C., Yizhong W., Hongxiao T. (2001). Influence of adsorption on the photodegradation of various dyes using surface-bond-conjugated TiO_2/SiO_2 photocatalyst. *Appl. Catal. B: Environ*., 35, 95-105.

[5] Karkmaz M., Puzenat E., Guillard C., J.M. Herrmann (2004). Photocatalytic degradation of the alimentary azo dye amaranth. Mineralization of the azo group to nitrogen. *Appl. Catal. B: Environ*., 51, 183-194.

[6] Lachheb H., Puzenat E., Houas A., Ksibi M., Elaloui E., Guillard C., Herrmann J.M. (2002). Photocatalytic degradation of various types of dyes (Alizarin S, Crocein Orange G, Methyl Red, Congo Red, Methylene blue) in water by UV-irradiated titania. *Appl. Catal. B: Environ*., 39, 75-90.

[7] Calza P., Pelizzeti E., Minero C. (2005). The fate of organic nitrogen in photocatalysis: an overview. *J. Appl. Electrochem*., 35, 665-673.

[8] Bui T.H., Guillard C., Perol N., Herrmann J.M. (2004). Influence of the presence of a triazinic ring on the fate of nitrogen from amino groups of dyes during their photocatalytic degradation. *3rd European Meeting on Solar Chemistry and Photocatalysis: Environmental applications (SPEA3)*, Barcelona, Spain.

[9] Brillas E., Mur E., Sauleda R., Sanchez L., Peral J., Domènech X., Casado J. (1998). Aniline mineralization by AOP's: anodic oxidation, photocatalysis, electro-Fenton and photo-electroFenton processes. *Appl. Catal. B: Environ*., 16, 31-42.

[10] Stylidi M., Kondarides D.I., Verykios X.E. (2003). Pathways of solar light-induced photocatalytic degradation of azo dyes in aqueous TiO_2 suspensions. *Appl. Catal. B: Environ.*, 40, *271-286.*

[11] Pelizzeti E., Carlin V., Minero C., Pramauro E., Vincenti M. (1992). Degradation pathways of atrazine under solar light and in the presence of titanium oxide colloidal particles. *Sci. Total. Environ*., 161, 123-124.

[12] Huston P.L., Pignatello J. (1999). Degradation of selected pesticide active ingredients and commercial formulations in water by the photo-assisted Fenton reaction. *Water Res*., 33, 1238-1246.

[13] Pérez M.H., Peñuela G., Maldonado M.I., Malato O., Fernández-Ibáñez P., Oller I., Gernjak W., Malato S. (2006). Degradation of pesticides in water using solar advanced oxidation processes. *Appl. Catal. B: Environ*., 64, 272-281.

[14] Zhang F., Yediler A., Liang X. (2007). Decomposition pahtways and reaction intermediate formation of the purified, hydrolyzed azo reactive dye C.I. Reactive Red 120 during ozonation. *Chemosphere*, 67, 712-717.

[15] Bravo A., García J., Domènech X., Peral J. (1993). Some aspects of the photocatalytic oxidation of ammonium ion by titanium dioxide. *J. Chem. Research*, 376-377.

[16] Lapertot M., Pulgarín C., Fernández-Ibáñez P., Maldonado M.I., Pérez-Estrada L., Oller I., Gernjak W., Malato S. (2006). Enhancing biodegradability of priority substances (pesticides) by solar photo-Fenton. *Water Res*., 40, 1086-1094.

A.1.3. The testing of several biological and chemical coupled treatments for Cibacron Red FN-R azo dye removal

Julia García-Montaño[a], Xavier Domènech[a], José A. García-Hortal[b], José Peral[a], Francesc Torrades [c*]

[a]*Departament de Química, Edifici Cn, Universitat Autònoma de Barcelona, E-08193 Bellaterra (Barcelona), Spain*

[b]*Departament d'Enginyeria Tèxtil i Paperera. ETSEIA de Terrassa (UPC), C/Colom, 11, E-08222 Terrassa (Barcelona), Spain*

[c]*Departament d'Enginyeria Química. ETSEIA de Terrassa (UPC), C/Colom, 11, E-08222 Terrassa (Barcelona), Spain*

Submitted for publication

*Corresponding author

F. Torrades: francesc.torrades@upc.edu

Abstract

Several biological and chemical coupled treatments for Cibacron Red FN-R reactive azo dye degradation have been evaluated. Initially, a two-stage anaerobic-aerobic biotreatment has been assessed for different dye concentrations (250, 1250 and 3135 $mg \cdot l^{-1}$). 92-97% decolourisation was attained during anaerobic digestion operating in batch mode. However, no Dissolved Organic Carbon (DOC) removal neither biogas production was observed from dye metabolites, indicating that no methanogenesis occurred. Additionally, according to Biotox® and Zahn-Wellens assays, anaerobically generated colourless solutions (presumably containing the resulting aromatic amines from azo bond cleavage) were found to be more toxic than the initial dye as well as aerobically non biodegradable, impeding the anaerobic-aerobic biological treatment. In a second part, the application of Advanced Oxidation Processes (AOPs) like photo-Fenton or ozonation as chemical post-treatments of the anaerobic process has been considered for the complete dye by-products mineralisation. The best results were obtained by means of ozonation at pH = 10.5, achieving 83% mineralisation and giving place to a final harmless effluent. In contrast, the tested photo-Fenton conditions were not efficient enough to complete oxidation.

Keywords: Aerobic biodegradation; Anaerobic digestion; AOPs post-treatment; Colour removal; DOC removal; Reactive azo dye

1. Introduction

Azo dyes are the class of dyes most widely used industrially, constituting 60-70% of all dyestuffs produced [1]. During the dyeing process, the degree of fixation of dyes is never complete resulting in dye-containing effluents [2]. Not only aesthetic problems occur, but also biotoxicity and the possible mutagenic and carcinogenic effects of azo dyes have been reported [3]. Their degradation by conventional wastewater treatment technologies is difficult due to their complex structure and synthetic nature; they are non biodegradable by standard aerobic activated sludge methods, and systems based on physical and chemical methods are quite inefficient and require further treatment or disposal of the pollutant. Therefore, the development of effective and economic methods for textile wastewater treatment should deserve particular attention. Not only colour removal but also organic degradation of dyes and their metabolites must be the pursued goals.

Among the emerging technologies for wastewater decontamination, Advanced Oxidation Processes (AOPs) are capable to mineralise almost all toxic and non biodegradable organic compounds [4]. These processes are principally based on the *in situ* generation of highly reactive hydroxyl radicals ($HO^{\bullet}$, E^{o} = 2.8 V vs NHE). The most widely studied AOPs include: heterogeneous photocatalytic oxidation with TiO_2 [5, 6], treatment with ozone (often combined with H_2O_2 and/or UV) [7, 8], UV/H_2O_2 systems [9], and Fenton and photo-Fenton type reactions [10-12], which generate $HO^{\bullet}$ by interaction of H_2O_2 with ferrous salt in aqueous media. Nevertheless, the operational costs associated are a common problem of all AOPs and they often are too expensive to be applied as exclusive treatment. In this sense, several earlier studies focus on the combination of an AOP with conventional aerobic biological treatment in an attempt to avoid the drawbacks of each of them. A minimum oxidation is performed as a pre-treatment to just increase the biodegradability and generate a new effluent more amenable to biodegradation [13-15].

On the other hand, since azo dyes are potentially reduced under anaerobic conditions, and biological processes are the preferred choice for wastewater treatment, biotreatments based on anaerobic-aerobic sequences are currently under investigation

[1, 16-18]. Azo bonds (R_1-N=N-R_2) can be anaerobically reduced basically leading to the corresponding aromatic amines (dye solution decolourisation), compounds that are recalcitrant and toxic under reducing atmosphere but theoretically susceptible to further aerobic biodegradation [19].

In a previous work, the coupling of photo-Fenton reaction and an aerobic biological process for the degradation of a representative reactive azo dye employed for cellulosic fibres dyeing (250 $mg \cdot l^{-1}$ hydrolysed Cibacron Red FN-R, DOC = 79.5 $mg \cdot l^{-1}$ C) was carried out [15]. At the studied concentration, the dye was neither aerobically biodegradable nor toxic (EC_{50} > 79.5 $mg \cdot l^{-1}$ C) as seen by Zahn-Wellens and Biotox® assays, respectively. With the application of photo-Fenton catalytic process as a biological pre-treatment, a complete decolourisation and 80% mineralisation was accomplished in the combined oxidation system.

In this paper, several biological and chemical coupled treatments for Cibacron Red FN-R azo dye removal were evaluated as alternatives to the chemical-biological (aerobic) strategy. In a first part, the possibility of Cibacron Red FN-R anaerobic digestion coupled to an ensuing aerobic degradation was tested. Anaerobic assays were carried out in batch mode. Biogas production, % decolourisation, DOC reduction and toxicity evolution after digestion were monitored in order to evaluate the success of the anaerobic stage. The Zahn-Wellens test was carried out for the aerobic biodegradability assessment of the resulting anaerobic effluent. In a second part, the application of an AOP as a chemical post-treatment of the anaerobic process has also been considered to complete reactive azo dye and by-products mineralisation. Ozonation and photo-Fenton processes have been chosen to play this role.

2. Materials and methods

2.1. Synthetic dye solution

A commercial azo dye, Cibacron Red FN-R bireactive vinylsulphone fluorotriazine dye (CI Reactive Red 238, empirical formula $C_{29}H_{15}O_{13}S_4ClFN_7Na_4$, 944.2 $g \cdot mol^{-1}$) was purchased from CIBA and used as received without further purification (80% purity

approx.). Its chemical structure was not disclosed by the manufacturer. The different Cibacron Red FN-R concentrations were prepared by diluting an initial concentrated stock solution of 4180 $mg \cdot l^{-1}$ (DOC = 1213 $mg \cdot l^{-1}$ C; Chemical Oxygen Demand (COD) = 3433 $mg \cdot l^{-1}$ O_2). The initial solution of Cibacron Red FN-R was hydrolysed to convert it to the form in which it is normally found in industrial effluents. The hydrolysis was done by adjusting the pH to 10.6, followed by heating to 60 ºC for 1 hour. Finally, the pH of the hydrolysed stock solution was adjusted to 7.0 ± 0.2 before storage at 4 ºC.

2.2. Anaerobic biodegradation set-up and operation conditions

The anaerobic experiments were conducted in batch mode and under static conditions in 600 ml thermostated aluminium bottles. The test sample volume was 500 ml and the headspace 100 ml. Anaerobic seed sludge was a methanogenic culture obtained from a mesophilic municipal anaerobic digester (Manresa, Spain), containing an initial Total Suspended Solids (TSS) and a Volatile Suspended Solids (VSS) content of 30 and 12 $g \cdot l^{-1}$, respectively. All bottles were seeded with the same volume of original sludge to finally obtain an initial 1.5 $g \cdot l^{-1}$ VSS and 3.8 $g \cdot l^{-1}$ TSS concentration.

0.2 g of yeast extract and 2 ml of the following solutions were added per litter of sample [20]: 100 $mg \cdot l^{-1}$ $Na_2S \cdot 9H_2O$ solution; a macronutrients solution composed of 170 $g \cdot l^{-1}$ NH_4Cl, 37 $g \cdot l^{-1}$ KH_2PO_4, 8 $g \cdot l^{-1}$ $CaCl_2 \cdot 2H_2O$ and 9 $g \cdot l^{-1}$ $MgSO_4 \cdot 4H_2O$; a micronutrients solution composed of 2000 $mg \cdot l^{-1}$ $FeCl_3 \cdot 4H_2O$, 2000 $mg \cdot l^{-1}$ $CoCl_2 \cdot 6H_2O$, 500 $mg \cdot l^{-1}$ $MnCl_2 \cdot 4H_2O$, 30 $mg \cdot l^{-1}$ $CuCl_2 \cdot 2H_2O$, 50 $mg \cdot l^{-1}$ $ZnCl_2$, 50 $mg \cdot l^{-1}$ H_3BO_3, 90 $mg \cdot l^{-1}$ $(NH_4)_6Mo_7O_{24} \cdot 4H_2O$, 100 $mg \cdot l^{-1}$ $Na_2SeO_3 \cdot 5H_2O$, 50 $mg \cdot l^{-1}$ $NiCl_2 \cdot 6H_2O$, 1000 $mg \cdot l^{-1}$ EDTA, 1$ml \cdot l^{-1}$ HCl 36% and 500 $mg \cdot l^{-1}$ resazurin. Additionally, 1g of $NaHCO_3$ per g COD was added to solution in order to maintain the pH and reduce the negative effects to methanogenesis due to the possible acidification caused by Volatile Fatty Acids (VFA) production. Before incubation, nitrogen gas was bubbled into the bottles to ensure anaerobic conditions during the biodegradation process. Temperature was maintained under mesophilic conditions at 37 ± 1 ºC.

Biogas production was measured at regular intervals from bottles headspace by means of a digital manometer (SMC Pressure Switch 10 bars) connected to the bottles

by a valve. Biogas was sampled through an outlet located at the valve that could be opened or closed with a regulator key. The % methane composition was determined using a HP 5890 gas chromatograph equipped with a thermal conductivity detector and a Porapak Q, 3 m x 1/8" column (Supelco). The temperature of the injector was 130 ºC. The oven temperature was initially maintained at 30 ºC for 3 minutes. Then, it was increased to 70 ºC at a 10 ºC·min^{-1} rate and finally maintained at 70 ºC for 5 minutes. The temperature of the detector was 180 ºC.

To analyse dye solutions, samples were centrifuged and the supernatant was filtered through 0.45 μm pore size. Prior toxicity testing, sample was gassed with nitrogen to strip out any possible remaining H_2S. Every assay was performed at least twice.

2.3. Adsorption assay

Adsorption experiments were conducted in 100 ml closed thermostated flasks at 37 ± 1 ºC containing 1.5 g·l^{-1} VSS and 3.8 g·l^{-1} TSS of anaerobic sludge and 30 ml of dye solutions with 85, 250, 425, 850, 1275, 1700, 2550 and 3000 mg·l^{-1} concentrations. Neither nutrients nor trace elements were added into the media. The contact time was set at 24 hours and pH = 7.0 ± 0.2. One flask with biomass suspended in deionised water was used as control. Hand shaking was occasionally conducted. Every concentration was performed by duplicated.

2.4. Photo-Fenton and ozonation set-up

Photo-Fenton and ozonation processes were conducted in a thermostated (T = 23 ± 1 ºC) well stirred cylindrical Pyrex cell of 300 ml of capacity. The solution volume was 200 ml. In photo-Fenton process, analytical grade hydrogen peroxide (33% w/v, Panreac) and $FeSO_4 \cdot 7H_2O$ (99.5%, Merck) were used as received to generate hydroxyl radical ($HO^{\bullet}$) in aqueous solution. A 6 W Philips black light fluorescent lamp was used as artificial light source. The intensity of the incident UVA light, measured employing a luminometer, was 0.6 mW·cm^{-2}. Ozone was generated by an Erwin Sander 301.7 model

equipment fed with a pure oxygen stream. To ensure saturation of the system the input in the solution was 1.75 $g \cdot h^{-1}$ O_3 as determined by iodometric titration [21]. Unreacted ozone was measured by means of an Erwin Sander Quantozone-1 ozone-meter and finally destroyed with a KI trap. Prior toxicity testing, solutions were gassed with nitrogen to strip out the remaining dissolved O_3 gas.

2.5. Chemical analysis

UV/Vis-absorption spectra were recorded by using a Shimatzu UV-1603 double beam spectrophotometer in the 200-700 nm range. All colour data were reported as the absorbance at the maximum absorption in the visible region (λ_{max} = 542.5 nm), and were taken as an estimation of the dye presence in solution. Samples were diluted prior to measurements if necessary. DOC was determined with a Shimadzu TOC-V_{CSH} analyser. COD was assessed by the closed reflux colorimetric method [22] with a HACH DR/2000 spectrophotometer. Determination of TSS and VSS was carried out following Standard Methods [22].

2.6. Biological assays

Non acclimated activated sludge coming from a wastewater treatment plant (Manresa, Spain) was used to perform the Zahn-Wellens test [23]. Acute toxicity was assessed using the Biotox® bacterial bioluminescence assay [24], by determination of the inhibitory effect that the sample has on the marine photobacteria *Vibrio fischeri.* The toxicity effect was quantified as the EC_{50} parameter (the concentration of toxicant that causes 50% decrease of light emission after 30 minutes of exposure) and was expressed in DOC units ($mg \cdot l^{-1}$ C). When the DOC of the sample was lower than the EC_{50}, it was assumed to be non toxic and toxicity values were given as $EC_{50} > 100\%$. Phenol and glucose solutions were used as standard toxic and non toxic samples to check the technique suitability. Colour correction was applied in toxicity determinations of coloured solutions.

3. Results and discussion

3.1. Adsorption study

Since biological dye removal from wastewaters may involve both adsorption and biodegradation by bacteria [17], an adsorption test was conducted in order to investigate the potential of Cibacron Red FN-R adsorption onto the anaerobic sludge. DOC and colour ($Abs_{542.5}$) parameters were used as indicators. After 24 hours of contact time, neither significant DOC nor colour reduction was observed for any concentration tested, discarding a possible biosorption mechanism for colour and organic removal during anaerobic digestion. The repulsive electrostatic interaction between Cibacron Red FN-R reactive azo dye (of anionic nature) and the negative charges of anaerobic sludge might be responsible for the of lack of biosorption observed [25].

3.2. Cibacron Red FN-R anaerobic digestion

The methanogenic activity of the anaerobic sludge was firstly ensured by the assessment of the Specific Methanogenic Activity (SMA) of a VFA standard solution composed of acetic, propionic and butyric acids (73:21:4 weight proportion, total COD = 4500 $mg \cdot l^{-1}$ O_2) [20]. From the maximum biogas generation slope (60-70% in CH_4), a SMA value of 0.084 $gCOD_{CH4} \cdot g^{-1}VSS \cdot day^{-1}$ was obtained (Figure 1) (typical SMA values of anaerobic biomass from a municipal anaerobic digester range between 0.02 and 0.2 $gCOD_{CH4} \cdot g^{-1}VSS \cdot day^{-1}$ [20]). Afterwards, once guaranteed the methanogenic potential of biomass, Cibacron Red FN-R was submitted to anaerobic digestion. Three different concentrations were tested in order to assess the anaerobic sludge response to azo dye dosage: 250, 1250 and 3135 $mg \cdot l^{-1}$ (bottles 1, 2 and 3). High dye concentrations were employed to allow better biogas determination sensitivity. On the other hand, to obtain information about Cibacron Red FN-R anaerobic degradation in presence of an auxiliary substrate –which may be required for generation of reducing equivalents consumed during azo bond cleavage [1]–, 2500 $mg \cdot l^{-1}$ of yeast extract was added to another 1250 $mg \cdot l^{-1}$ dye solution (bottle 4). As a basis for comparison, a control bottle just containing anaerobic biomass with the corresponding nutrients and trace elements

(control I), and another also containing 2500 mg·l^{-1} yeast extract (control II) were run in parallel. Each batch experiment was extended to 50 days.

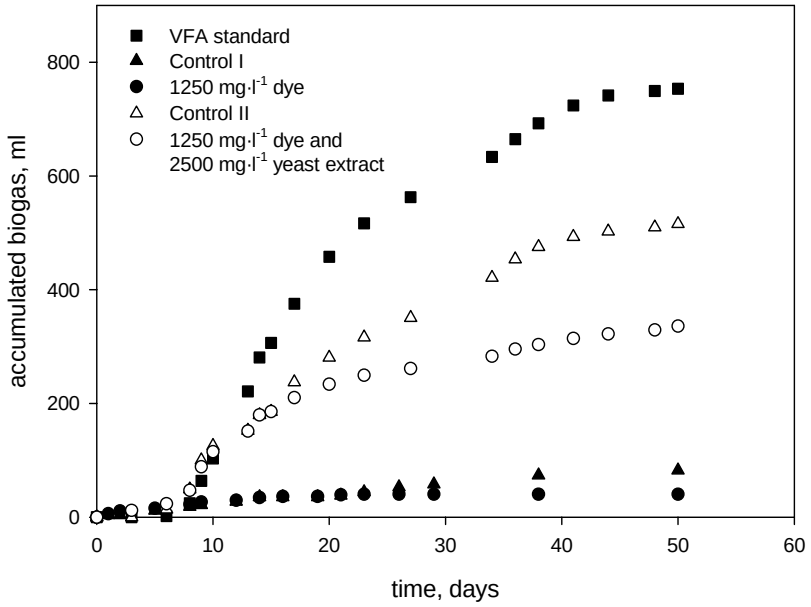

Figure 1. Accumulated biogas production (1 atm, 37 ºC) of the VFA standard and 1250 mg·l^{-1} Cibacron Red FN-R solution in presence and absence of 2500 mg·l^{-1} yeast extract.

The parameters employed to evaluate the biodegradation efficiency were the maximum methane generation slope per unit of weight of biomass ($gCOD_{CH4}$·g^{-1} VSS·day^{-1}, determined in the same way than SMA [20]), the accumulated biogas production within the 50 days of assay (1 atm, 37 ºC), as well as the % decolourisation ($Abs_{542.5}$ determination) and DOC reduction after the 50 days of experiment (Table 1).

From Table 1, it is noteworthy that nearly complete decolourisation had taken place after digestion of all substrate types (even when no additional yeast extract was present). The visible band at 542.5 nm, characteristic of azo bonds and responsible for the red colour of the solution [26], disappeared within the anaerobic treatment with 92-97% effectiveness. However, DOC data evidence that no methanogenesis from dye by-products had taken place during the anaerobic stage. When comparing the control experiments with the dye containing experiments (the DOC content of control I is due to biodegradable organic nutrients supplied to all the bottles (see section 2.2)), none of

the dye concentrations showed higher DOC removal that the attained by the control experiments. DOC reduction was almost the same for the 250 $mg \cdot l^{-1}$ Cibacron Red FN-R solution and control I experiment, and even lower for higher dye dosages (Table 1), evidencing a possible toxic/inhibitory effect to anaerobic biomass. The DOC removal of 1250 $mg \cdot l^{-1}$ dye plus 2500 $mg \cdot l^{-1}$ yeast extract sample was also lower than control II experiment.

Table 1. Summary of experimental results for different Cibacron Red FN-R and control solutions after 50 days of anaerobic digestion.

Bottle	Substrate type	% decolourisation ($Abs_{542.5}$)	DOC $mg \cdot l^{-1}$ C			$gCOD_{CH4} \cdot g^{-1}$ $VSS \cdot day^{-1}$	Accumulated biogas ratio
			Initial	Residual	Removed		
Control I	-	-	105[a]	29	76	0.005	1
1	250 $mg \cdot l^{-1}$ dye	92	176	96	80	0.004	0.89
2	1250 $mg \cdot l^{-1}$ dye	96	467	416	51	0.005	0.49
3	3135 $mg \cdot l^{-1}$ dye	97	1013	979	34	0.005	0.38
Control II	2500 $mg \cdot l^{-1}$ yeast extract	-	1107	43	1064	0.042	1
4	2500 $mg \cdot l^{-1}$ yeast extract 1250 $mg \cdot l^{-1}$ dye	93	1471	609	862	0.038	0.65

[a] DOC corresponding to organic nutrients supplied to all the bottles

Biogas measurements show similar results. Regarding the maximum methane generation slope, it is noteworthy that none of the dye samples provided larger values than the corresponding to control I and II activities, which showed 0.005 and 0.042 $gCOD_{CH4} \cdot g^{-1}VSS \cdot day^{-1}$ values, respectively. On the other hand, when comparing the accumulated biogas production of dye solutions with the accumulated control bottles values for a period of 50 days (data expressed as accumulated biogas ratio in Table 1), they were never higher than control (ratio values lower than unity) and they decreased when dye concentration was increased. From these results, a possible toxic/inhibitory effect of solutions on anaerobic biomass is also deducible. As an example, Figure 1

shows the accumulated biogas evolution during both 1250 $mg \cdot l^{-1}$ Cibacron Red FN-R solutions degradation and their corresponding control bottles. At first, it is noticeable a lag phase with no biogas production in which the inocullum is adapted to both wastewater and operational conditions. Subsequently, anaerobic degradation begins with a continuous 60-70% methane generation at the maximum biogas generation slope (from where $gCOD_{CH4} \cdot g^{-1}$ $VSS \cdot day^{-1}$ data were calculated). Finally, compared with control experiments, total biogas and methane production of dye containing bottles dropped off. This phenomenon is markedly observed with the 1250 $mg \cdot l^{-1}$ dye plus 2500 $mg \cdot l^{-1}$ yeast extract sample.

Some conclusions can be extracted from the above results. In absence of a dye biosorption mechanism (section 3.1), and in agreement with the bibliography previously reported, Cibacron Red FN-R reactive azo dye decolourisation would be attributable to the reductive cleavage of azo bonds (dye chromophore) giving place to the resultant biorecalcitrant aromatic amines. Their biorecalcitrant nature would induce the negligible dye DOC removal and the lack of methanogenesis observed. In this frame, Biotox® bioluminescence assay was performed to the 250 $mg \cdot l^{-1}$ anaerobically degraded solution to assess the acute toxicity of Cibacron Red FN-R metabolites. The EC_{50} parameter was found to be 43.8 $mg \cdot l^{-1}$ C (degraded control I bottle presented no toxicity), manifesting a significant toxicity increase in relation to the actual dye (with $EC_{50} > 79.5$ $mg \cdot l^{-1}$ C). These results would match with the suggested toxic/inhibitory effect to anaerobic biomass and, consequently, with the harmful amines generation hypothesis. Therefore, since the final aim when treating dye containing wastewaters is not only decolourisation but also by-products degradation, it is clear from the above results that resulting textile effluents from anaerobic digestion require further post-treatment.

3.3. Aerobic biodegradation post-treatment

250, 1250 and 3135 $mg \cdot l^{-1}$ Cibacron Red FN-R metabolites were submitted to Zahn-Wellens assay to investigate the potential of standard aerobic biodegradation as a post-treatment of the anaerobic process. The 1250 $mg \cdot l^{-1}$ dye plus 2500 $mg \cdot l^{-1}$ yeast extract biodegraded solution (bottle 4) was not considered since the goal was to determine only the azo dye by-products mineralisation. Figure 2 exhibits that aerobic biomass did not

remove substantial DOC within the 28 days of contact (being the biodegradation lower than 9% in all case), with no sign of cells adaptation. On the contrary, the experiment performed with ethylene glycol, a completely biodegradable standard, achieved 94% biodegradation under the same conditions in just 3 days. The obtained results let us to conclude that Cibacron Red FN-R metabolites after anaerobic digestion (aromatic amines) are of non biodegradable nature and no further chemical transformation should be expected after aerobic treatment. In agreement with this, Figure 3 illustrates the similarity between the absorption spectra of the anaerobic and the anaerobic-aerobically degraded 250 $mg \cdot l^{-1}$ Cibacron Red FN-R azo dye solution in comparison with the untreated one. Moreover, the EC_{50} parameter was maintained at 41.9 $mg \cdot l^{-1}$ C after the aerobic process providing indirect evidence of no aromatic amines removal. The resistance of some aromatic amines from anaerobic cleavage of azo dyes regarding their aerobic treatment has already been reported [16].

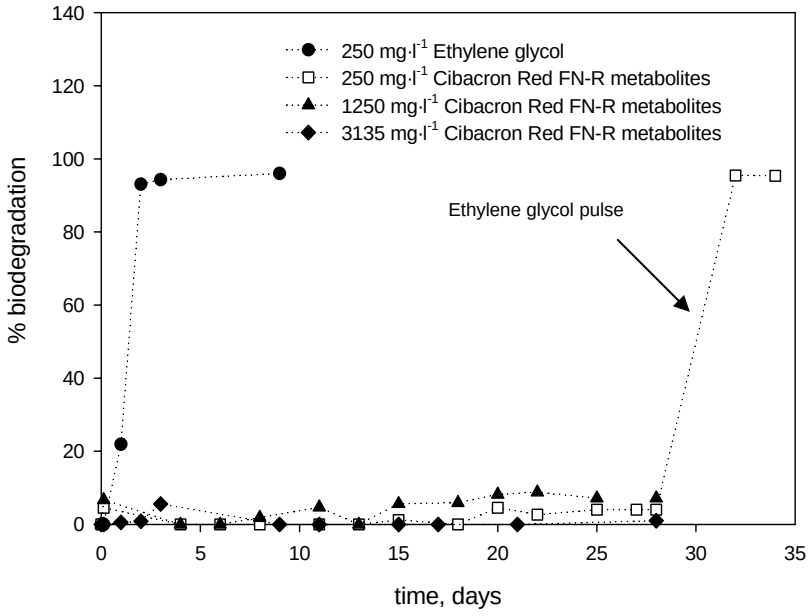

Figure 2. Zahn-Wellens assay; % biodegradability evolution of 250, 1250 and 3135 $mg \cdot l^{-1}$ Cibacron Red FN-R anaerobically treated solutions and the 250 $mg \cdot l^{-1}$ standard ethylene glycol.

Once the 28 days period was completed, a pulse of ethylene glycol was added to the 250 $mg \cdot l^{-1}$dye metabolites solution in order to detect a possible aerobic biomass

inhibition caused by the sample (Figure 2). In spite of the increased inhibition of luminescence bacteria manifested after the anaerobic process, the standard was consumed in few days demonstrating that the activated sludge was still active or not inhibited. These results evidence how Biotox® bacteria are more sensitive than activated sludge [27].

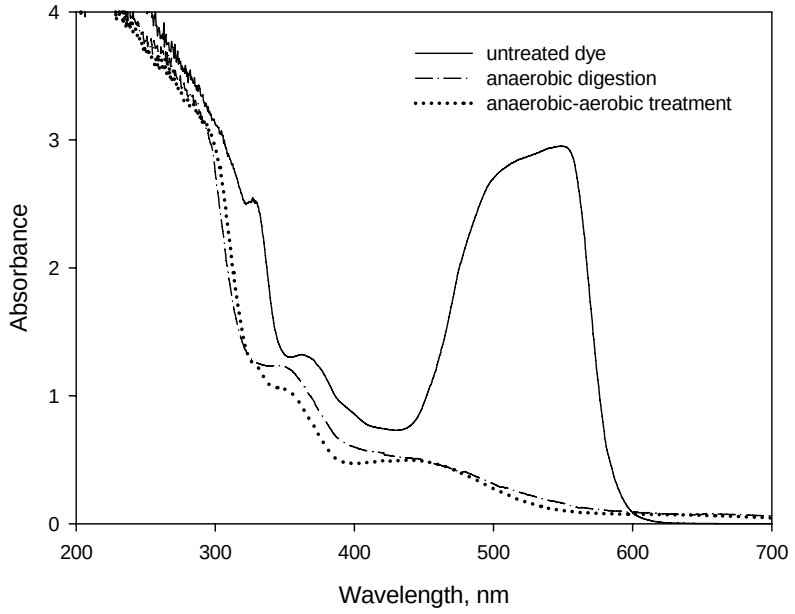

Figure 3. Absorption spectra of untreated, anaerobic and later aerobically degraded 250 $mg \cdot l^{-1}$ Cibacron Red FN-R; pH = 7.0.

3.4. Photo-Fenton and ozonation post-treatments

The solution coming from the anaerobic treatment was submitted to subsequent chemical oxidation by way of photo-Fenton and ozonation processes. The process should eliminate the DOC that could not be removed in the biological unit. The 250 $mg \cdot l^{-1}$ Cibacron Red FN-R solution was chosen for these experiments. Anaerobic digestion was repeated as many times as necessary to obtain the required volume to perform them.

For photo-Fenton reaction, the following Fenton reagent combinations were added to aqueous media: 10 $mg \cdot l^{-1}$ Fe (II)/250 $mg \cdot l^{-1}$ H_2O_2, 20 $mg \cdot l^{-1}$ Fe (II)/500 $mg \cdot l^{-1}$ H_2O_2

and 100 mg·l^{-1} Fe (II)/2500 mg·l^{-1} H_2O_2. The pH of the solutions was previously adjusted to 2.8-3.0. The evolution of DOC removal percentage *versus* time is shown in Figure 4. Results indicate that % DOC removal increased while increasing both Fe (II) and H_2O_2, although none tested dosages were efficient enough to remove dye metabolites in a reasonable treatment time. In addition, when varying the Fe (II) dosage from 10 to 100 mg·l^{-1}, an increasing DOC removal is first seen (the maximum attained value was 59% with the higher Fenton reagent dosage) followed by a plateau in which no significant DOC evolution was observed. This phenomenon is attributable to a DOC removal process by coagulation since it was accompanied with the appearance of a slight turbidity. The phosphate ion added as a macronutrient during anaerobic stage, which forms insoluble complexes with Fe (III), may be the main cause of iron precipitation. Coagulation was favoured by the high salinity content of the anaerobic effluent. It should be also pointed out that, apart from the photo-Fenton catalyst precipitation, the high salinity content of anaerobic effluent would also cause a HO· scavenging effect reducing the effectiveness of oxidation. Therefore, to effectively apply the photo-Fenton process, the complex matrix of the resulting anaerobic solution makes necessary a pre-treatment (i.e., phosphate ion removal) or higher Fenton reagent requirements.

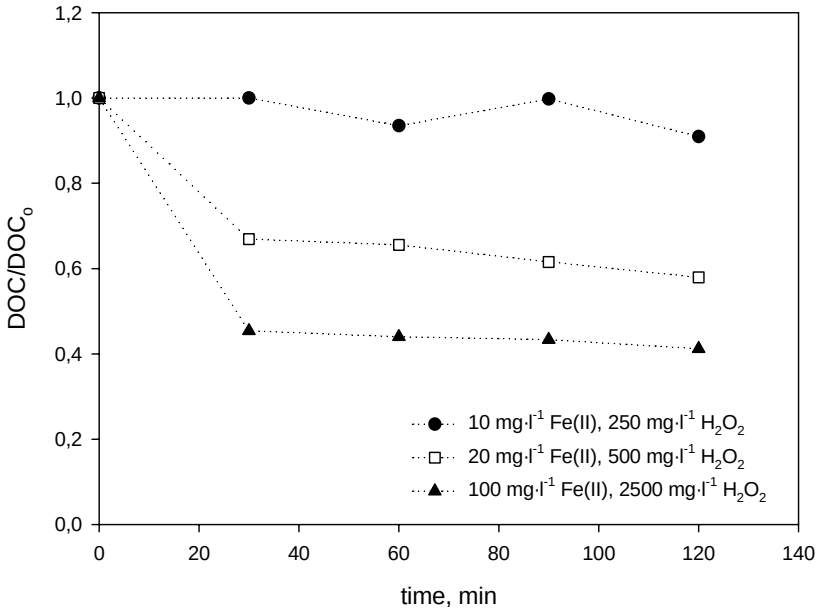

Figure 4. DOC/DOC$_o$ evolution *versus* irradiation time at different Fenton reagent doses for 250 mg·l^{-1} anaerobically treated Cibacron Red FN-R; pH = 3.0 and T = 23 ºC.

Different pH conditions were tested for dye metabolites degradation with ozone: pH = 3.0, 7.0, 10.0 and 10.5 (Figure 5). In each case, the final pH were 2.6, 3.1, 5.1 and 9.8, respectively. The best results were attained at alkaline pH, especially at 10.5, which gave a substantial 83% mineralisation in 150 minutes. Both neutral and acid conditions presented the same low 48% degradability. Obtained results are attributable to a different oxidation mechanism depending on pH conditions [28]: for acid or neutral values, the oxidising agent is the molecular ozone in a direct and highly selective attack to aromatic compounds. At alkaline pH, a reaction between ozone and the hydroxide ion gives rise to the formation of the HO· radical, which reacts non selectively with most organic compounds. According to this behaviour, only with an initial 10.5 value the pH remains alkaline through the whole experiment, favouring the free radical mechanism. Therefore, not just aromatic but aliphatic compounds generated at the final stage of the process are degraded. Finally, acute toxicity of the resulting solution was determined and EC_{50} was found to be higher than DOC concentration present in solution (EC_{50} > 100%). Therefore, in addition to Cibacron Red FN-R intermediates degradation, ozone AOP has been capable of transforming such compounds into harmless end products.

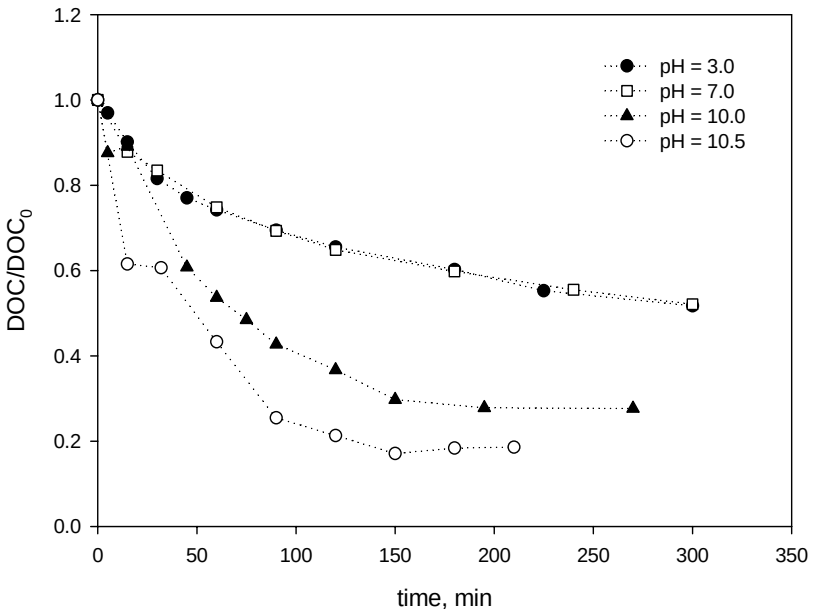

Figure 5. DOC/DOC_o evolution *versus* time for 250 mg·l^{-1} anaerobically treated Cibacron Red FN-R degradation with ozone at different pH conditions. T = 23 ºC.

4. Conclusions

The sequenced anaerobic-aerobic biological treatment was not a plausible alternative for Cibacron Red FN-R reactive azo dye and its metabolites removal. Three different dye concentrations were tested: 250, 1250 and 3135 $mg \cdot l^{-1}$. A complete decolourisation took place during the anaerobic stage for all concentrations with 92-97% effectiveness. However, the resistance of dye metabolites (presumably hazardous aromatic amines resulting from reductive cleavage of azo bonds), in addition with the lack of biogas production, evidenced that no methanogenesis occurred under reducing conditions. A possible toxic/inhibitory effect of solutions to anaerobic biomass while increasing dye concentration was observed. Moreover, according to Biotox® and Zahn-Wellens assays, the obtained anaerobic colourless solutions were found to be more toxic than the original dye solution and aerobically non biodegradable (being the % biodegradation lower than 9 in all case), impeding the biological two-stage treatment to complete degradation.

When applying photo-Fenton and ozonation processes as anaerobic digestion chemical post-treatments, the best results were obtained by means of ozonation at pH = 10.5, achieving 83% mineralisation and giving place to a final harmless effluent. In contrast, the photo-Fenton catalytic process was not efficient enough to completely oxidise the effluent. Just 59% of DOC removal of the anaerobically treated solution was attained under 100 $mg \cdot l^{-1}$ Fe (II)/2500 $mg \cdot l^{-1}$ H_2O_2 photo-Fenton conditions, mostly attributable to a non oxidative process based on iron coagulation.

In summary, complete Cibacron Red FN-R decolourisation was attained when applying anaerobic digestion though further non biological processes are required for effective by-products elimination. The % mineralisation achieved by coupling both processes was similar than the obtained in the previously reported photo-Fenton-aerobic biological treatment, which was 80% [15]. These results open the possibility of an anaerobic-chemical sequenced treatment for aerobically non biodegradable azo dyes removal, being of special interest for real textile wastewater applications.

Acknowledgements

The authors wish to thank Teresa Vicent (Departament d'Enginyeria Química, Universitat Autònoma de Barcelona) for technical assistance and also to the Ministerio de Educación y Ciencia (project CTQ 2005-02808) for financial support.

References

[1] O'Neill C, Hawkes FR, Hawkes DL, Esteves S, Willcox SJ. Anaerobic-aerobic biotreatment of simulated textile effluent containing varied ratios of starch and azo dye. Water Res 2000; 34 (8): 2355-2361.

[2] O'Neill C, Hawkes FR, Hawkes DL, Lourenço ND, Pinheiro HM, Delée W. Colour in textile effluents-sources, measurement, discharge consents and simulation: a review. J Chem Technol Biot 1999; 74(11): 1009-1018.

[3] Chang J, Chou C, Lin Y, Lin P, Ho J, Hu TL. Kinetic characteristics of bacterial azo-dye decolorization by Pseudomonas luteola. Water Res 2001; 35: 2841-2850.

[4] Andreozzi R, Caprio V, Insola A, Marotta R. Advanced oxidation processes (AOP) for water purification and recovery. Catal Today 1999; 53: 51-59.

[5] Herrmann JM. Heterogeneous photocatalysis: state of the art and present applications. Top Catal 2005; 34(1-4): 49-65.

[6] Konstantinou IK, Albanis TA. TiO_2-assisted photocatalytic degradation of azo dyes in aqueous solution: kinetic and mechanistic investigations: A review. Appl Catal B-Environ 2004; 49: 1-14.

[7] Urs von Gunten. Ozonisation of drinking water: Part I. Oxidation kinetics and product formation. Water Res 2003; 37: 1443-1467.

[8] Gogate PR, Pandit AB. A review of imperative technologies for wastewater treatment II: hybrid methods. Adv Environ Res 2004; 8: 553-597.

[9] Legrini O, Oliveros E, Braun AM. Photochemical processes for water treatment. Chem Rev 1993; 93: 671-698.

[10] Pérez M, Torrades F, Domènech X, Peral J. Fenton and photo-Fenton oxidation of textile effluents. Water Res 2002; 36: 2703-2710.

[11] Pignatello J, Oliveros E, MacKay A. Advanced Oxidation processes for organic contaminant destruction based on the Fenton reaction and related chemistry. Crit Rev Env Sci Tec 2006; 36: 1-84.

[12] Kiwi J, Pulgarin C, Peringer P. Effect of Fenton and photo-Fenton reactions on the degradation and biodegradability of 2 and 4-nitrophenols in water treatment. Appl Cat B-Environ 1994; 3: 335-350.

[13] Sarria V, Kenfack S, Guillod O, Pulgarín C. An innovative coupled solar-biological system at field pilot scale for the treatment of biorecalcitrant pollutants. J Photoch Photobio A 2003; 159: 89-99.

[14] Farré MJ, Domènech X, Peral J. Assessment of photo-Fenton and biological treatment coupling for Diuron and Linuron removal from water. Water Res 2006; 40: 2533-2540.

[15] García-Montaño J, Torrades F, García-Hortal JA, Domènech X, Peral J. Combining photo-Fenton process with aerobic sequencing batch reactor for commercial hetero-bireactive dye removal. Appl Catal B-Environ 2006; 67: 86-92.

[16] Frank P van der Zee, Villaverde S. Combined anaerobic-aerobic treatment of azo dyes-A short review of bioreactor studies. Water Res 2005; 39: 1425-1440.

[17] Soon-An Ong, Toorisaka E, Hirata M, Hano T. Treatment of azo dye Orange II in aerobic and anaerobic-SBR systems. Process Biochem 2005; 40: 2907-2914.

[18] Shaw CB, Carliell CM, Weatley AD. Anaerobic/aerobic treatment of coloured textile effluents using sequencing batch reactors. Water Res 2002; 36: 1993-2001.

[19] Carliell CM, Barclay SJ, Buckley CA. Treatment of exhausted reactive dyebath effluent using anaerobic digestion: Laboratory and full-scale trials. Water S.A 1996; 22: 225-233.

[20] Field J, Alvarez RS, Lettinga G. Ensayos anaerobios. Proc. of 4th Symp. on Wastewater Anaerobic Treatment. Valladolid, Spain; 1988. p. 52.

[21] Beyer M, Walter W. Manual de Química Orgánica. Ed. Reverté S.A. Barcelona, Spain; 1987.

[22] APHA-AWWA-WEF. Standard Methods for the Examination of Water and Wastewater. 18th ed. Washington, DC; 1992.

[23] ECD Guidelines for Testing of Chemicals. Test 302B. Vol 2. Paris, France; 1996.

[24] ISO 11348-3. Determination of the Inhibitory Effect of Water Samples on The Light Emission of Vibrio fischeri (Luminescent bacteria test); 1998.

[25] Wang Y, Mu Y, Zhao Q-B, Yu H-Q. Isotherms, kinetics and thermodynamics of dye biosorption by anaerobic sludge. Sep Purif Technol 2006; 50: 1-7.

[26] Silverstein RMC, Bassler GC, Morril TC. Spectrophotometric Identification of organic compounds. New York: Wiley; 1991.

[27] Farré M, Barceló D. Toxicity testing of wastewater and sewage sludge by biosensors, bioassays and chemical assays. Trends Anal Chem 2003; 22(5): 299-310.

[28] Hoigné J, Bader H. The role of hydroxyl radical reactions in ozonation process in aqueous solutions. Water Res 1976; 10: 377-386.

Annexe 2

Supporting Information

A.2.1. LC-(ESI)-TOF-MS spectra

The following Figures show the LC-(ESI)-TOF-MS spectra of Procion Red H-E7B degradation products after t_{30W} = 6 minutes of solar photo-Fenton treatment:

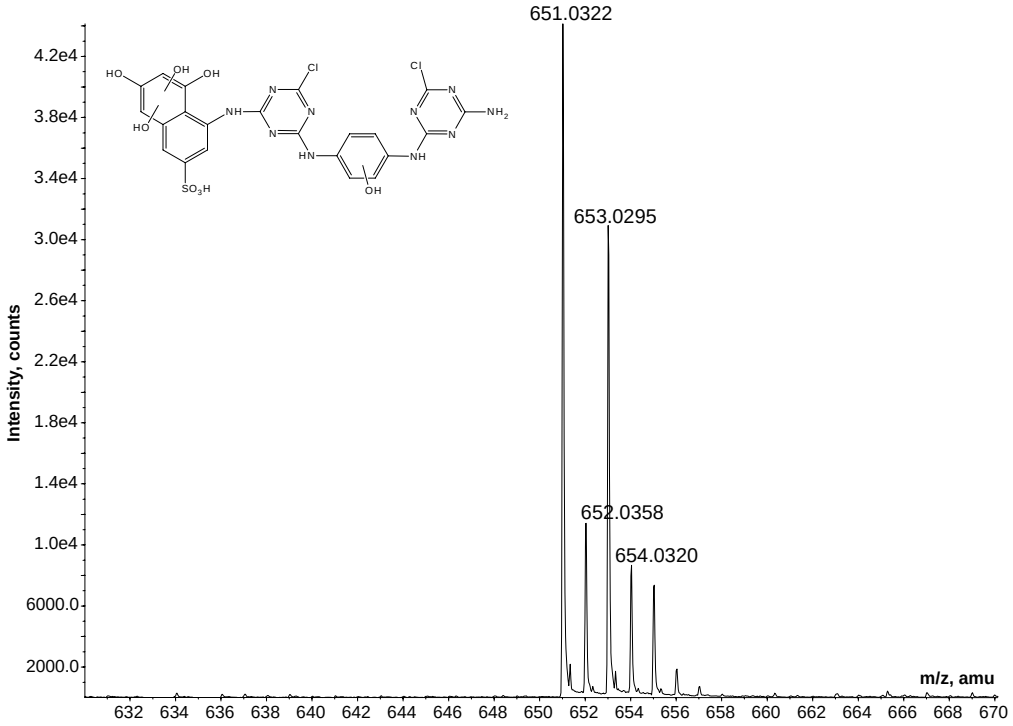

Figure A.2.1. MS spectrum of C_1.

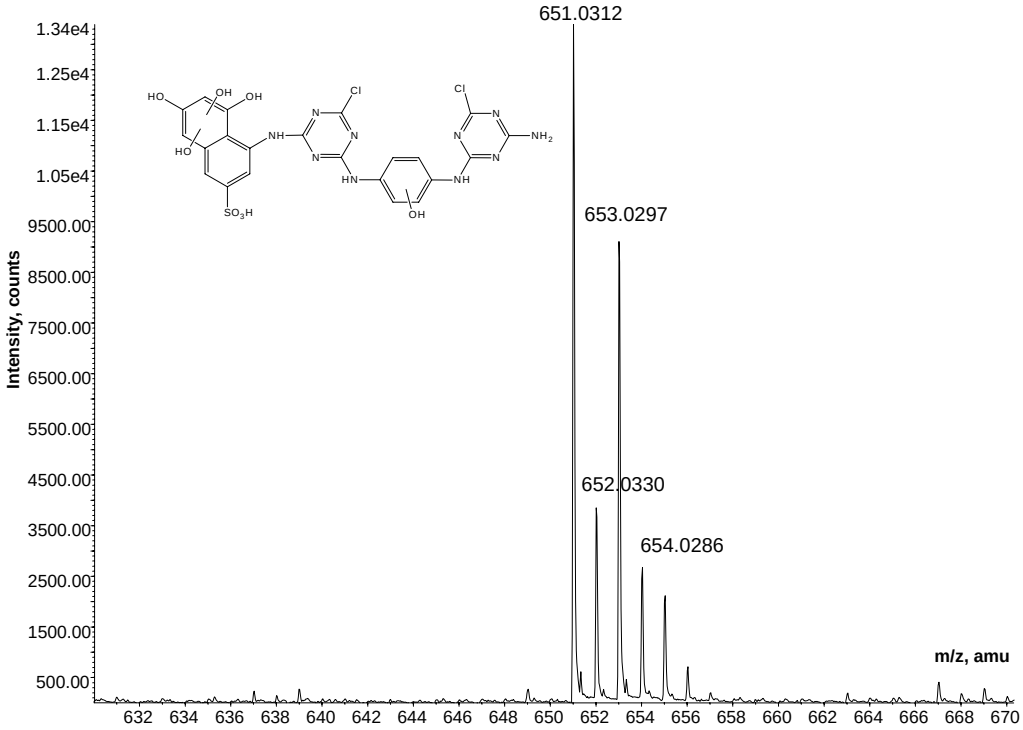

Figure A.2.2. MS spectrum of $C_{1'}$.

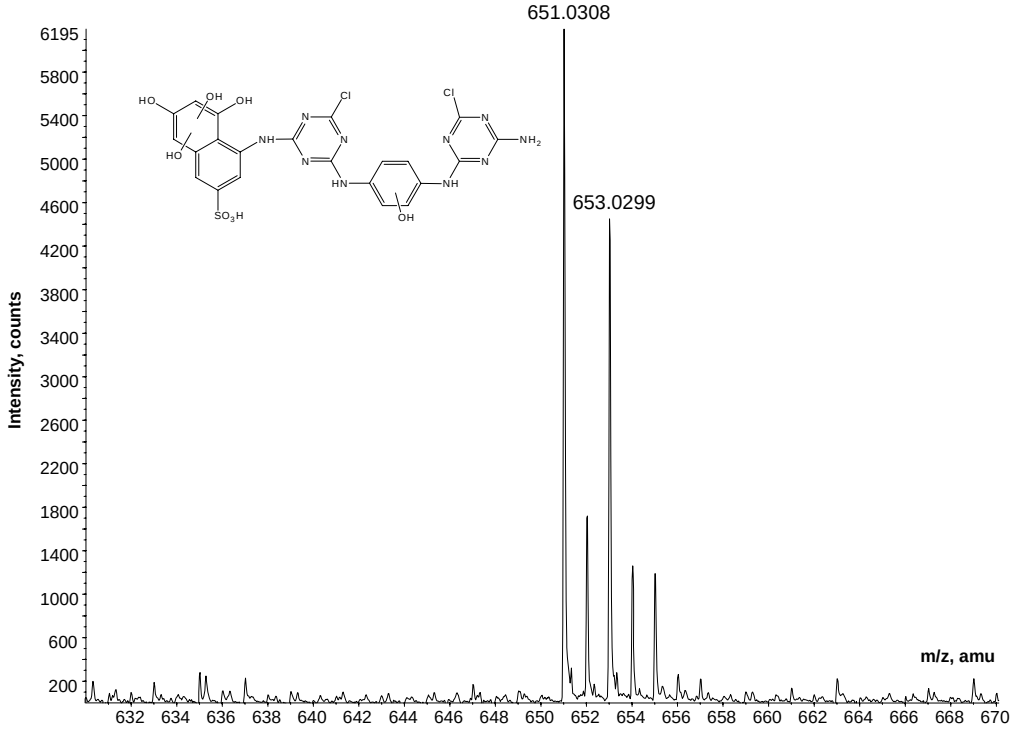

Figure A.2.3. MS spectrum of $C_{1''}$.

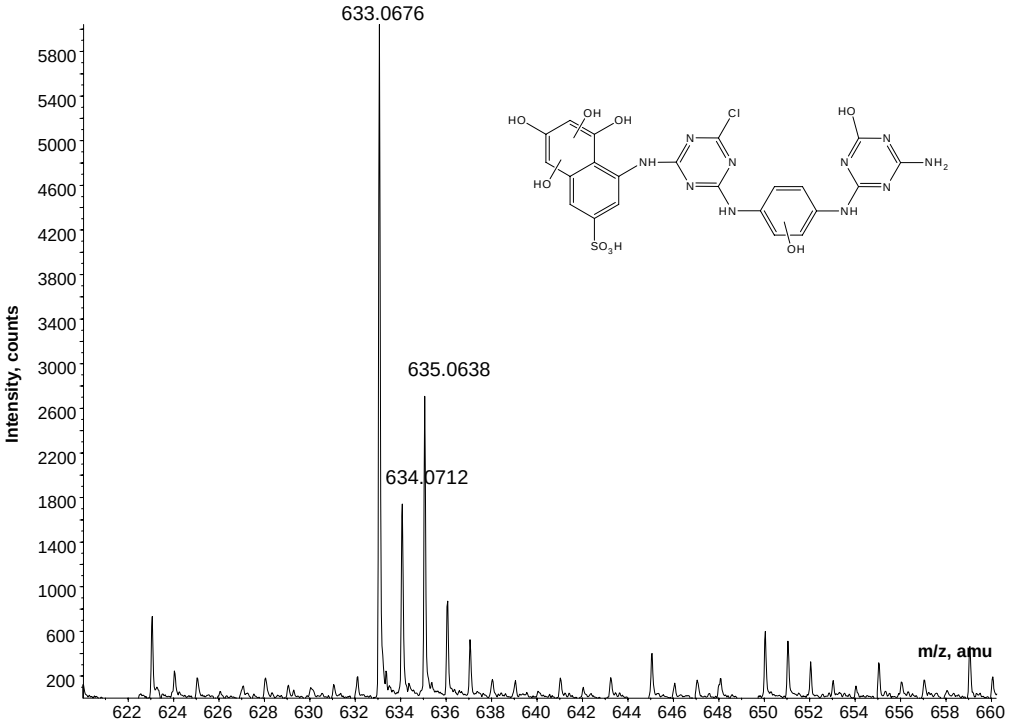

Figure A.2.4. MS spectrum of C_2.

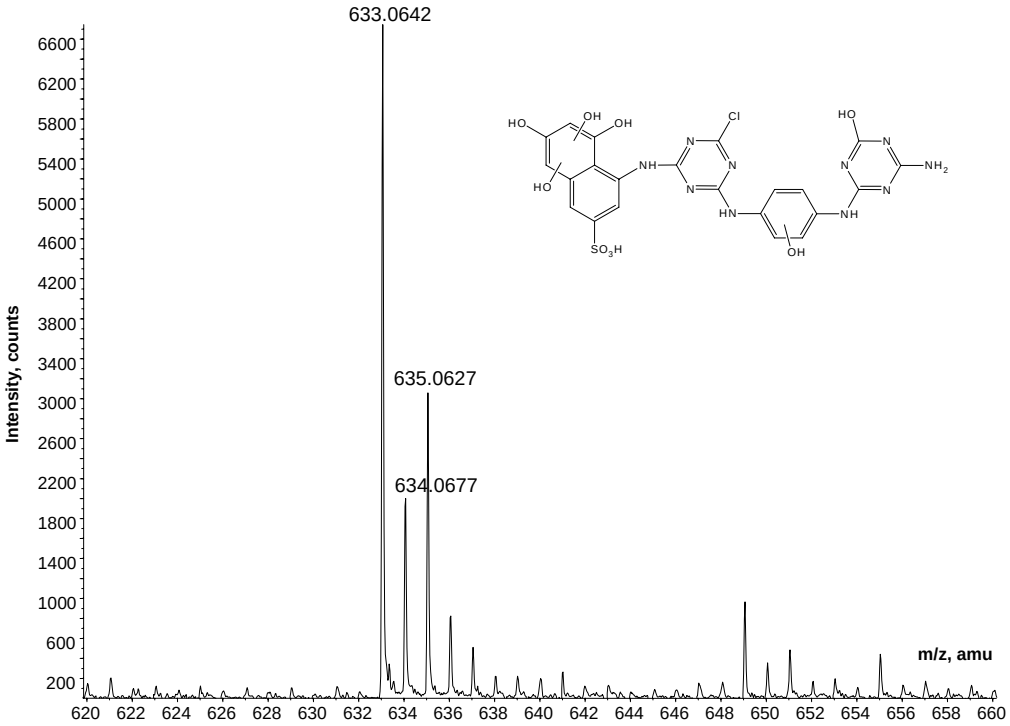

Figure A.2.5. MS spectrum of $C_{2'}$.

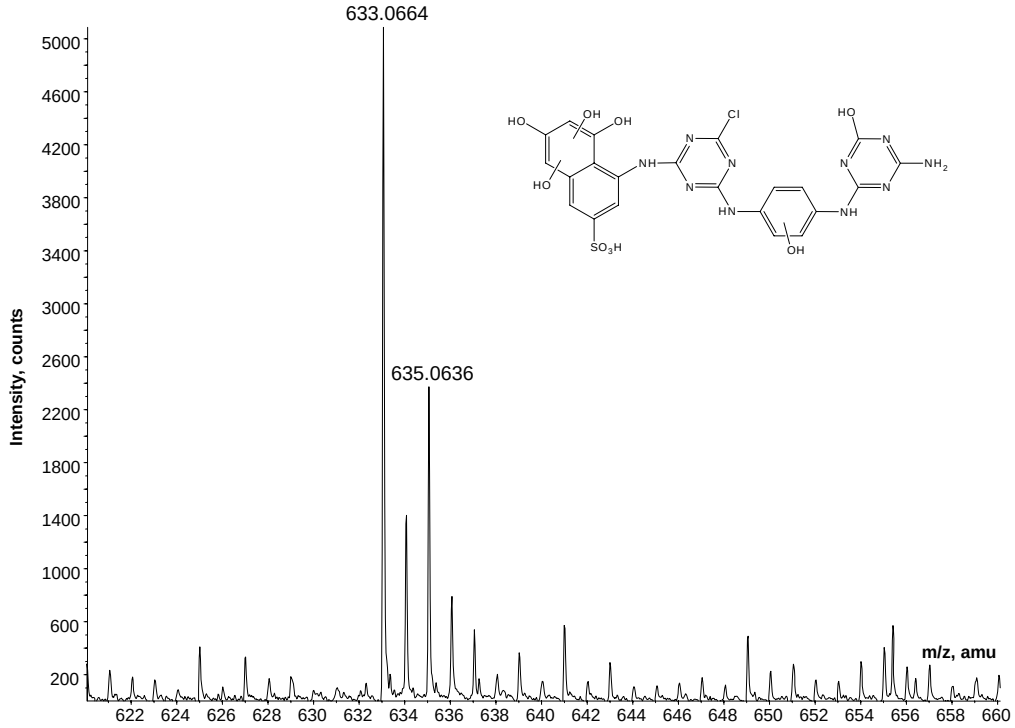

Figure A.2.6. MS spectrum of C_{2}''.

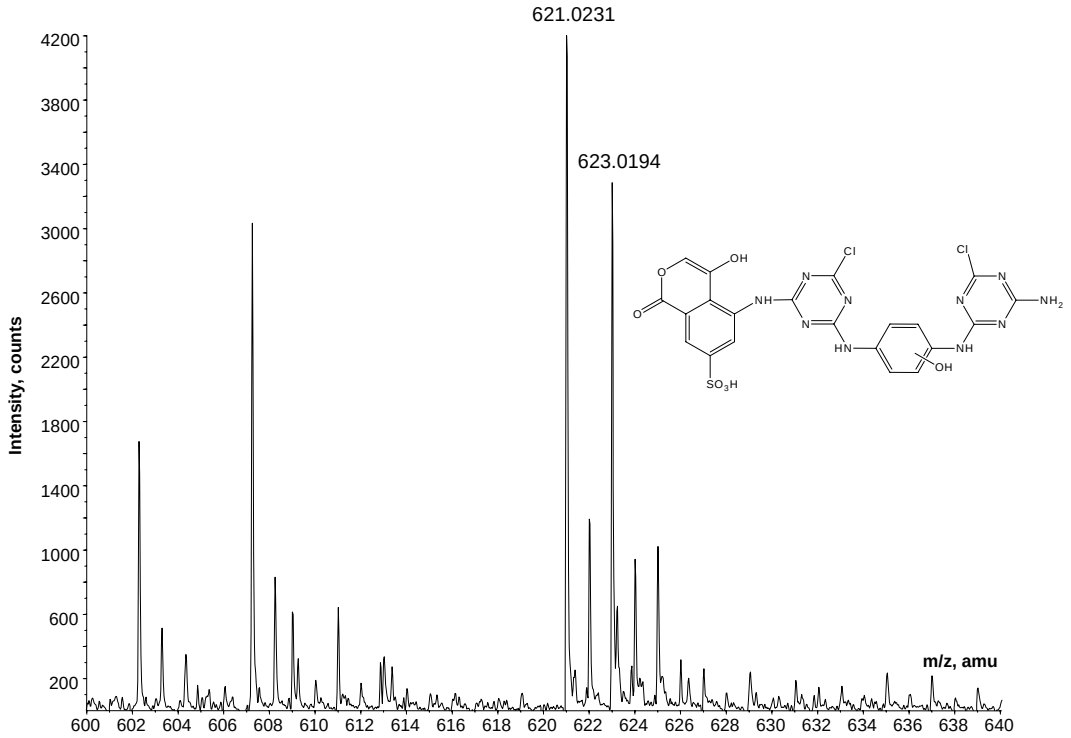

Figure A.2.7. MS spectrum of C_{3}.

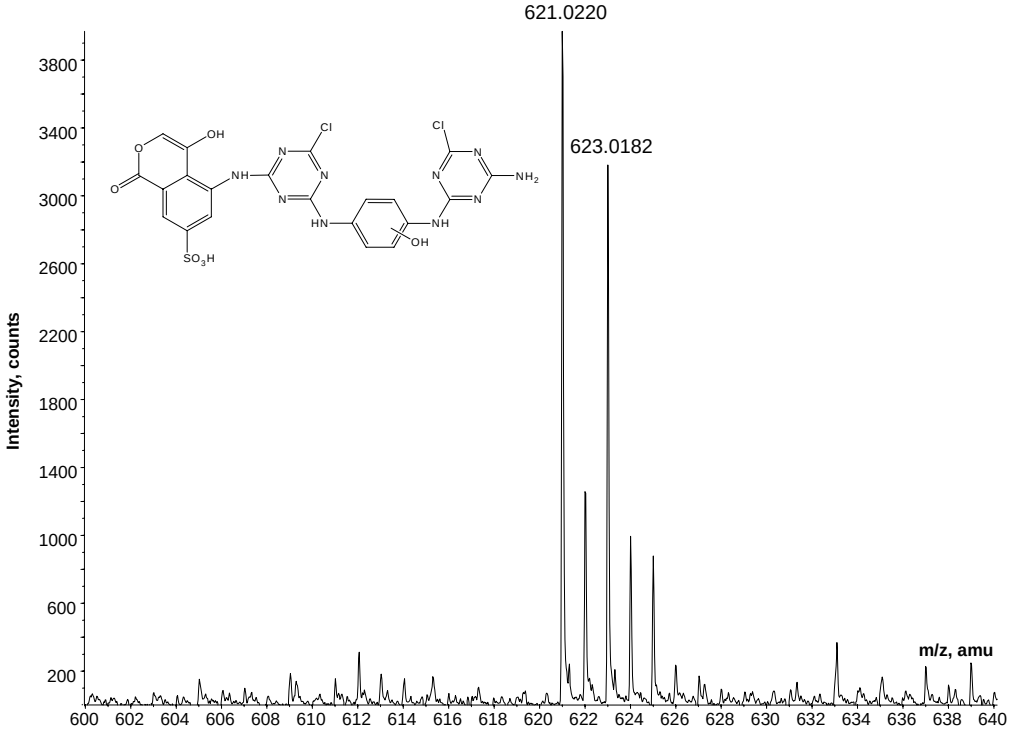

Figure A.2.8. MS spectrum of $C_{3'}$.

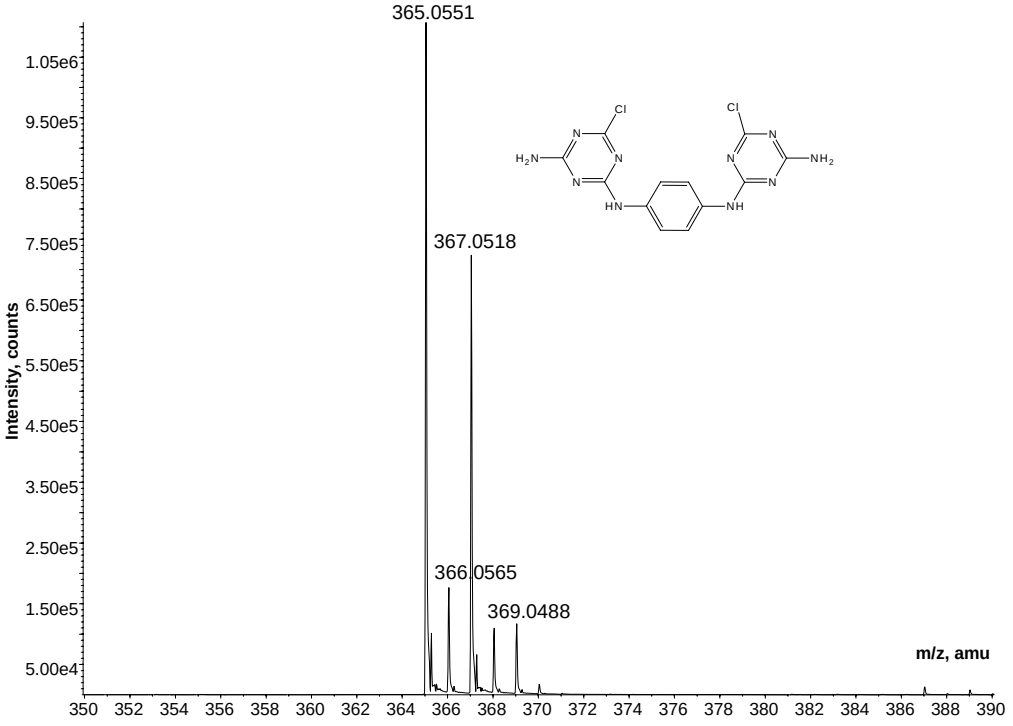

Figure A.2.9. MS spectrum of C_4.

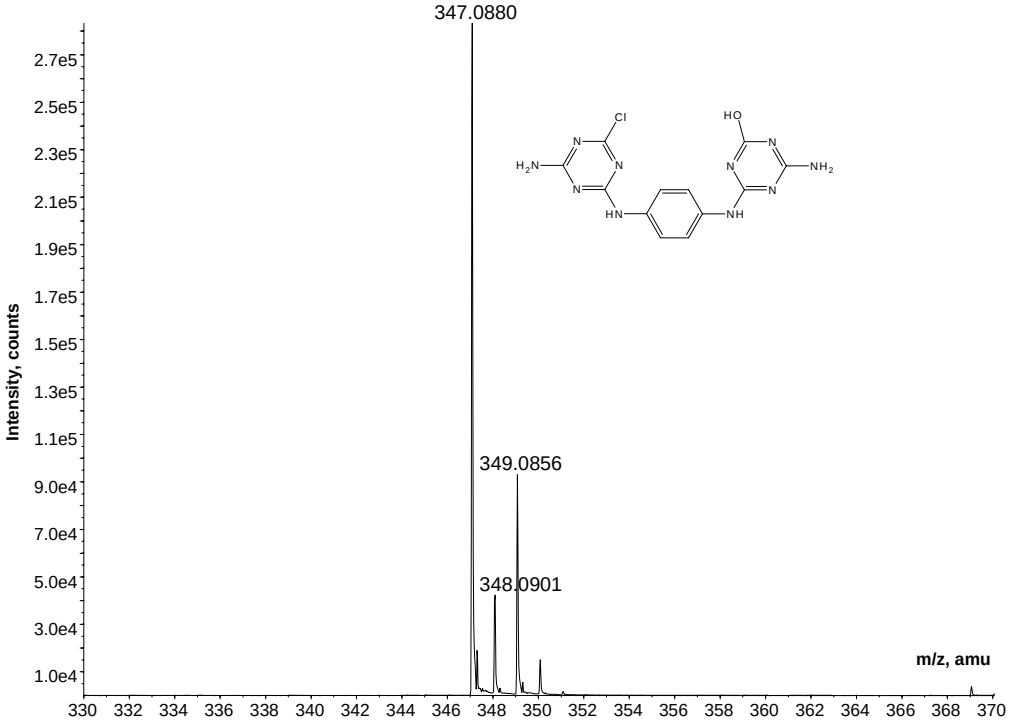

Figure A.2.10. MS spectrum of C_5.

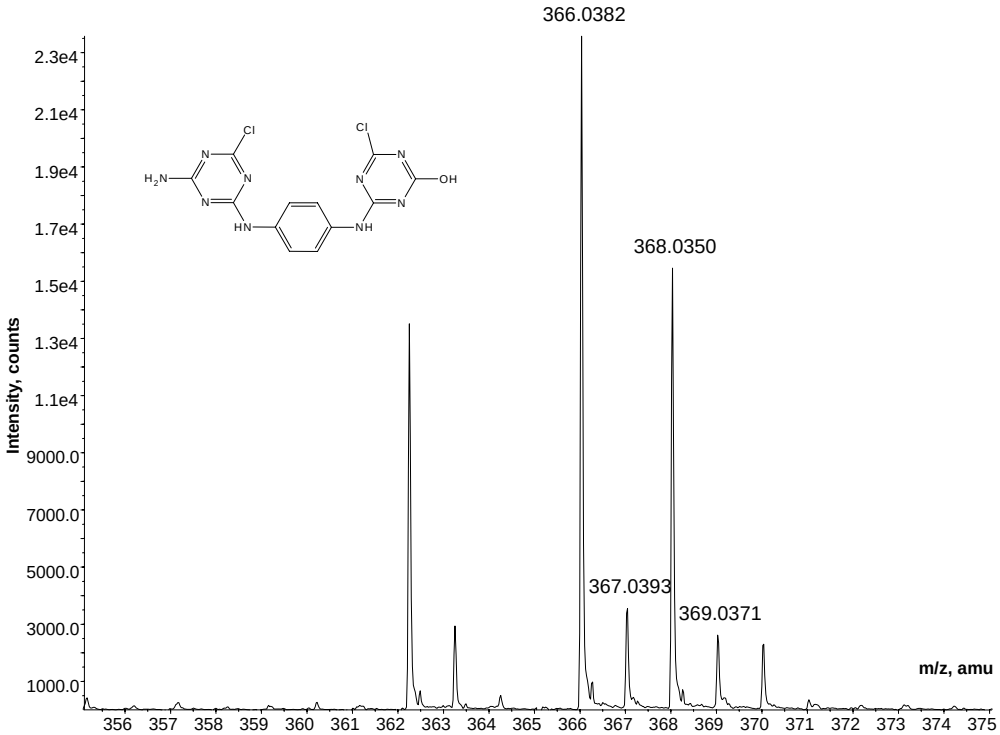

Figure A.2.11. MS spectrum of C_6.

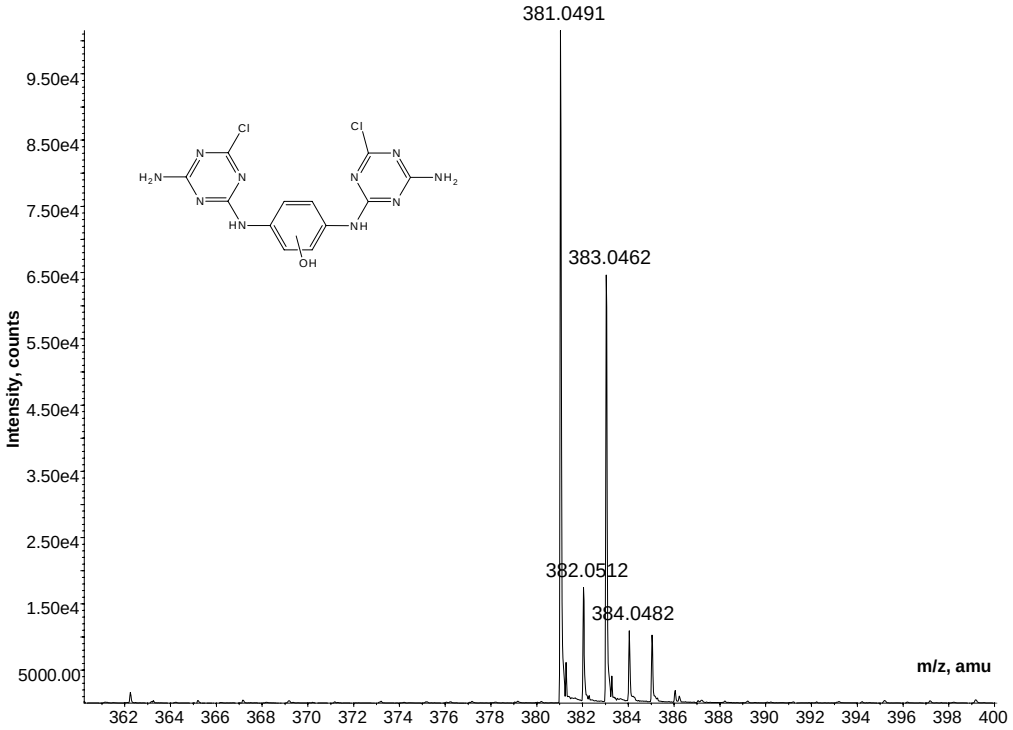

Figure A.2.12. MS spectrum of C_7.

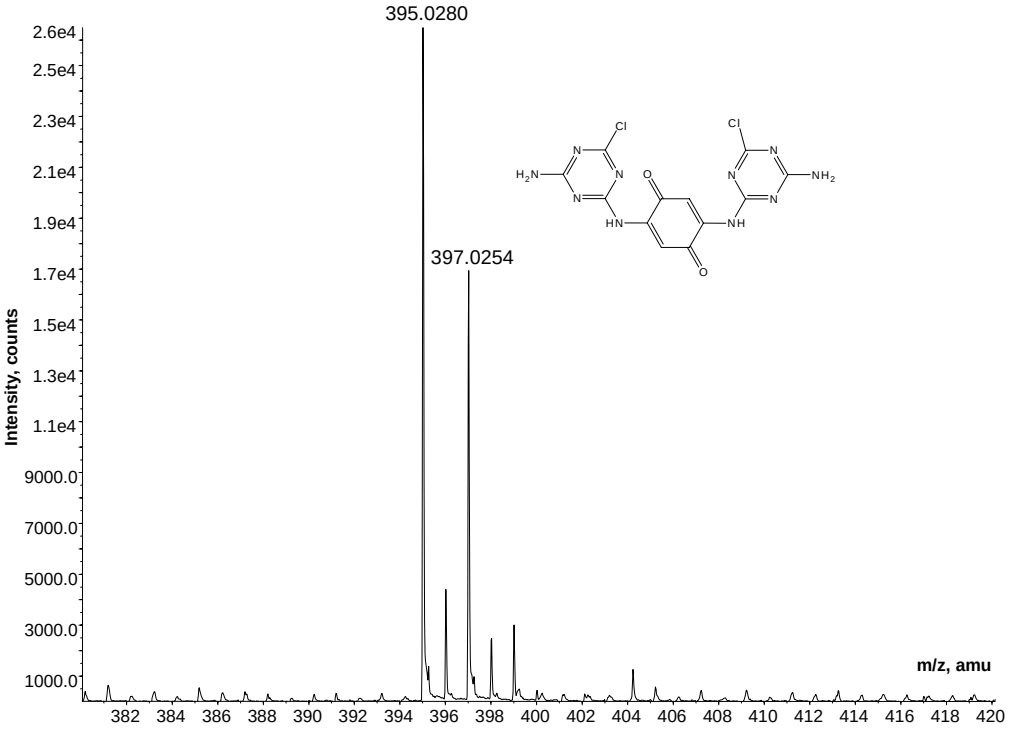

Figure A.2.13. MS spectrum of C_8.

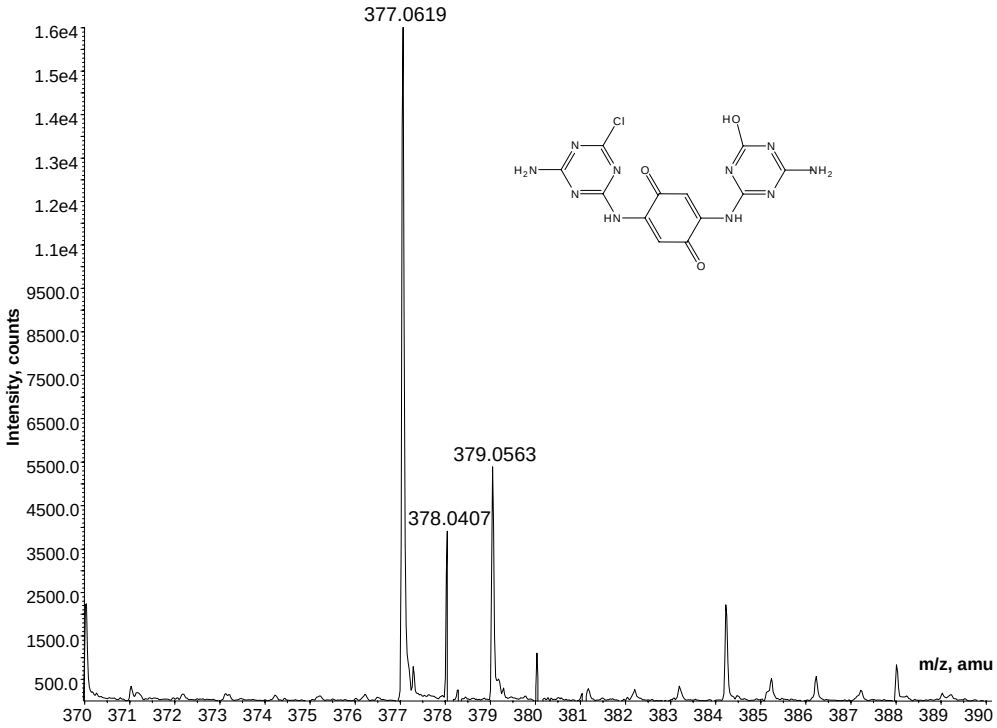

Figure A.2.14. MS spectrum of C_9.

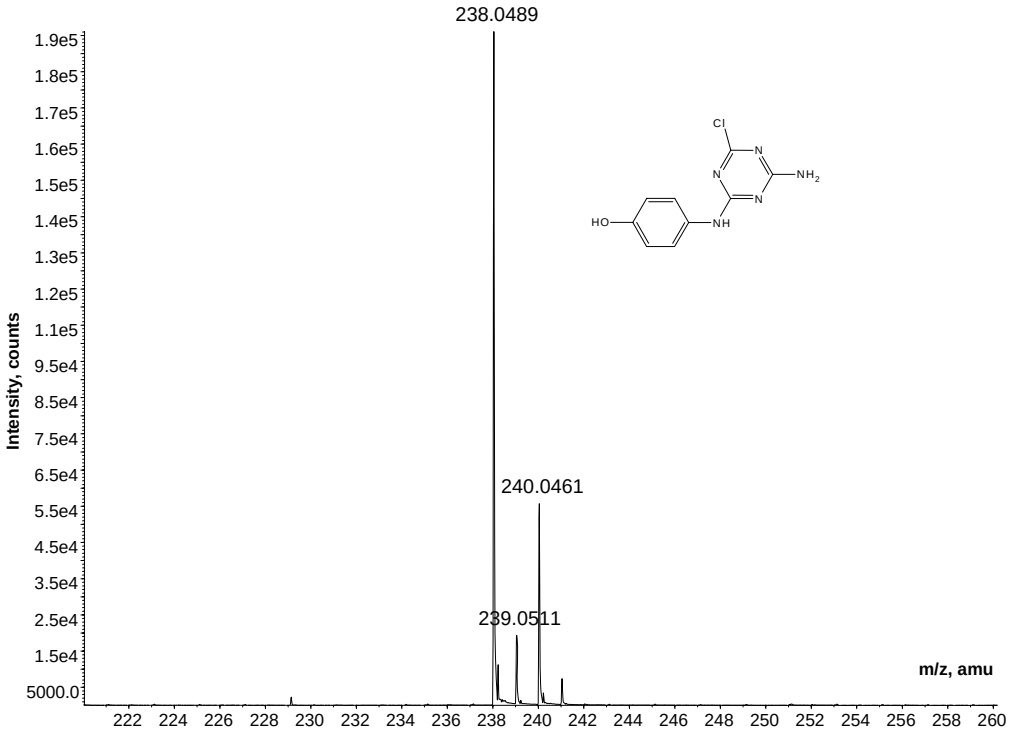

Figure A.2.15. MS spectrum of C_{10}.

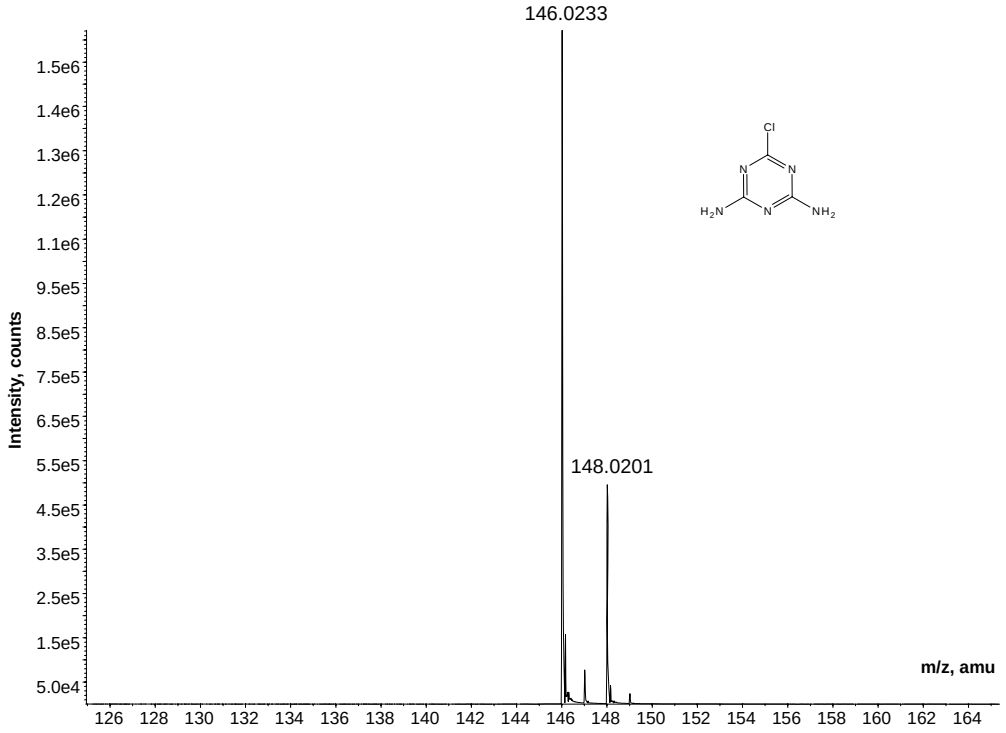

Figure A.2.16. MS spectrum of C_{11}.

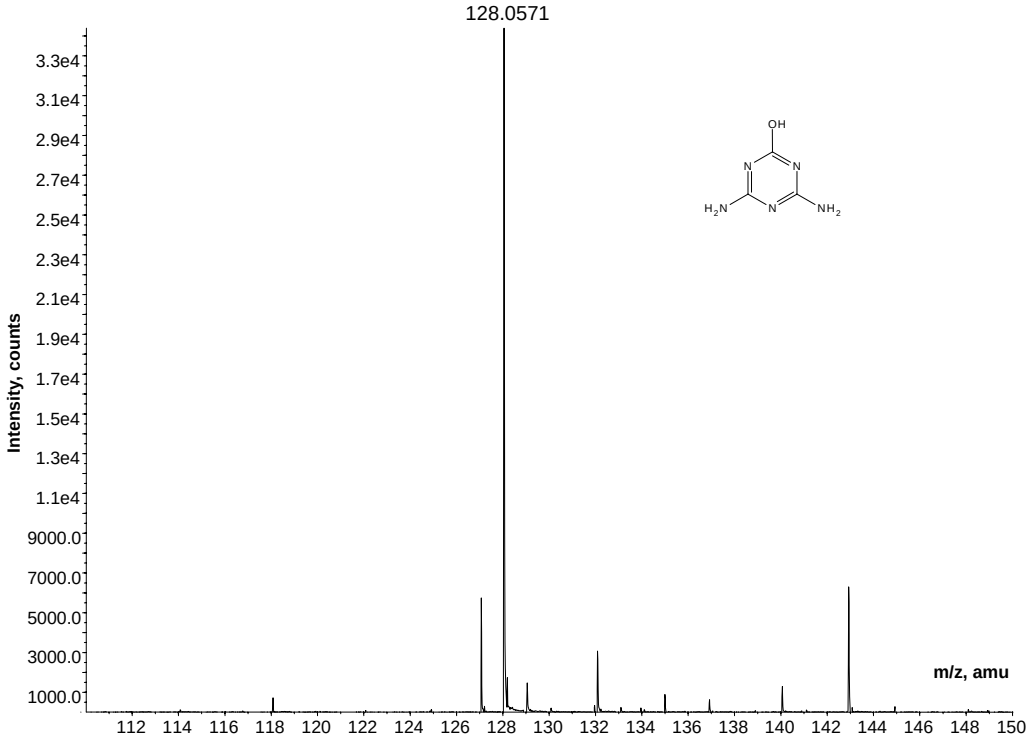

Figure A.2.17. MS spectrum of C_{12}.

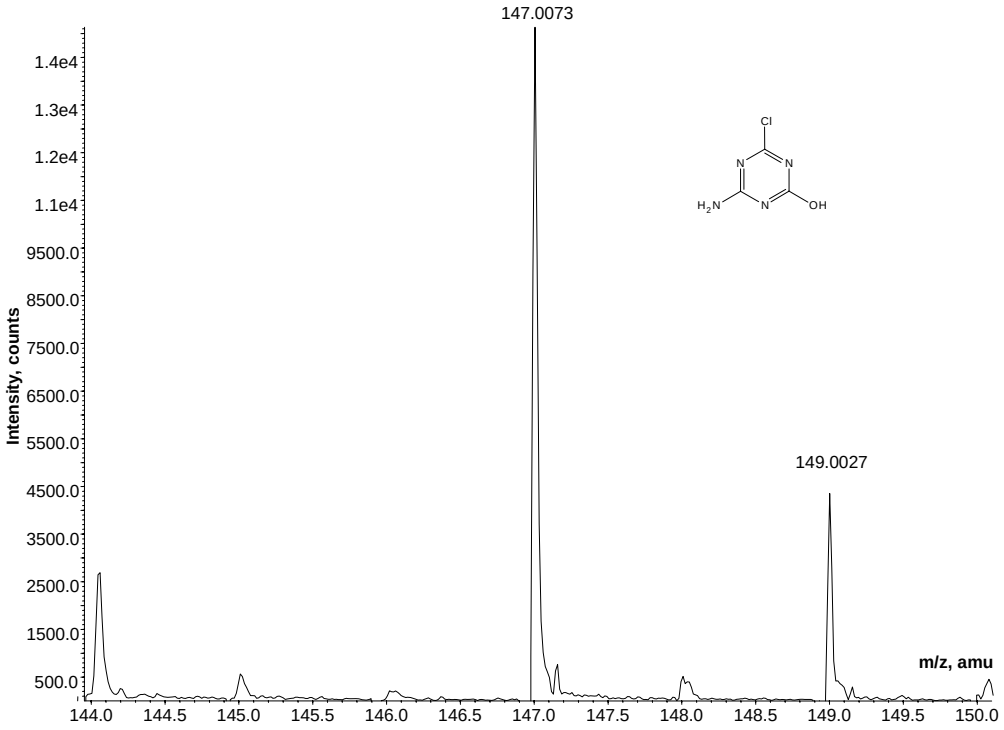

Figure A.2.18. MS spectrum of C_{13}.

A.2.2. LCA characterisation tables

The following Tables show, for each wastewater treatment, the characterisation results disaggregated by sub-systems:

Table A.2.1. Characterisation results for artificial light photo-Fenton process.

Category	Unit	Hydrogen peroxide 50%	Iron sulphate	Grid electricity	Transports	Emissions
ARD	kg Sb	$5.4 \cdot 10^{-6}$	$6.6 \cdot 10^{-8}$	$2.4 \cdot 10^{-6}$	$1.4 \cdot 10^{-7}$	0
GPW	kg CO_2	$6.6 \cdot 10^{-4}$	$9.2 \cdot 10^{-6}$	$3.4 \cdot 10^{-4}$	$2.0 \cdot 10^{-5}$	$2.9 \cdot 10^{-4}$
ODP	kg CFC 11	$6.1 \cdot 10^{-11}$	$4.2 \cdot 10^{-13}$	$1.4 \cdot 10^{-11}$	$3.2 \cdot 10^{-12}$	0
HTP	kg 1,4-D[a]	$2.2 \cdot 10^{-3}$	$1.5 \cdot 10^{-5}$	$1.7 \cdot 10^{-4}$	$1.1 \cdot 10^{-5}$	0
FATP	kg 1,4-D[a]	$1.4 \cdot 10^{-4}$	$2.3 \cdot 10^{-6}$	$2.2 \cdot 10^{-5}$	$1.3 \cdot 10^{-6}$	0
MAEP	kg 1,4-D[a]	$2.6 \cdot 10^{-1}$	$7.0 \cdot 10^{-3}$	$2.2 \cdot 10^{-1}$	$2.5 \cdot 10^{-3}$	0
TEP	kg 1,4-D[a]	$4.6 \cdot 10^{-6}$	$6.3 \cdot 10^{-8}$	$6.4 \cdot 10^{-6}$	$3.9 \cdot 10^{-8}$	0
POP	kg C_2H_4	$9.9 \cdot 10^{-8}$	$2.2 \cdot 10^{-9}$	$7.5 \cdot 10^{-8}$	$4.0 \cdot 10^{-9}$	0
AP	kg SO_2	$2.2 \cdot 10^{-6}$	$5.3 \cdot 10^{-8}$	$1.9 \cdot 10^{-6}$	$1.2 \cdot 10^{-7}$	0
AEP	kg PO_4^{3-}	$2.2 \cdot 10^{-7}$	$3.5 \cdot 10^{-9}$	$9.4 \cdot 10^{-8}$	$2.5 \cdot 10^{-8}$	$3.4 \cdot 10^{-6}$

[a] 1,4- Dichlorobenzene

Table A.2.2. Characterisation results for solar driven photo-Fenton process.

Category	Unit	Hydrogen peroxide 50%	Iron sulphate	Transports	Emissions
ARD	kg Sb	$5.4 \cdot 10^{-6}$	$6.6 \cdot 10^{-8}$	$1.4 \cdot 10^{-7}$	0
GPW	kg CO_2	$6.6 \cdot 10^{-4}$	$9.2 \cdot 10^{-6}$	$2.0 \cdot 10^{-5}$	$2.8 \cdot 10^{-4}$
ODP	kg CFC 11	$6.1 \cdot 10^{-11}$	$4.2 \cdot 10^{-13}$	$3.2 \cdot 10^{-12}$	0
HTP	kg 1,4-D[a]	$2.2 \cdot 10^{-3}$	$1.5 \cdot 10^{-5}$	$1.1 \cdot 10^{-5}$	0
FATP	kg 1,4-D[a]	$1.4 \cdot 10^{-4}$	$2.3 \cdot 10^{-6}$	$1.3 \cdot 10^{-6}$	0
MAEP	kg 1,4-D[a]	$2.6 \cdot 10^{-1}$	$7.0 \cdot 10^{-3}$	$2.5 \cdot 10^{-3}$	0
TEP	kg 1,4-D[a]	$4.6 \cdot 10^{-6}$	$6.3 \cdot 10^{-8}$	$3.9 \cdot 10^{-8}$	0
POP	kg C_2H_4	$9.9 \cdot 10^{-8}$	$2.2 \cdot 10^{-9}$	$4.0 \cdot 10^{-9}$	0
AP	kg SO_2	$2.2 \cdot 10^{-6}$	$5.3 \cdot 10^{-8}$	$1.2 \cdot 10^{-7}$	0
AEP	kg PO_4^{3-}	$2.2 \cdot 10^{-7}$	$3.5 \cdot 10^{-9}$	$2.5 \cdot 10^{-8}$	$2.5 \cdot 10^{-6}$

[a] 1,4- Dichlorobenzene

Table A.2.3. Characterisation results for artificial light photo-Fenton process coupled to a biological treatment.

Category	Unit	Hydrogen peroxide 50%	Iron sulphate	Grid electricity	Transports	Emissions	Biological treatment
ARD	kg Sb	$2.7 \cdot 10^{-6}$	$6.6 \cdot 10^{-8}$	$1.5 \cdot 10^{-6}$	$7.4 \cdot 10^{-8}$	0	$6.3 \cdot 10^{-8}$
GPW	kg CO_2	$3.3 \cdot 10^{-4}$	$9.2 \cdot 10^{-6}$	$2.0 \cdot 10^{-4}$	$1.0 \cdot 10^{-5}$	$1.7 \cdot 10^{-4}$	$9.9 \cdot 10^{-5}$
ODP	kg CFC 11	$3.1 \cdot 10^{-11}$	$4.2 \cdot 10^{-13}$	$8.4 \cdot 10^{-12}$	$1.7 \cdot 10^{-12}$	0	$1.2 \cdot 10^{-12}$
HTP	kg 1,4-D[a]	$1.1 \cdot 10^{-3}$	$1.5 \cdot 10^{-5}$	$9.9 \cdot 10^{-5}$	$5.8 \cdot 10^{-6}$	0	$3.4 \cdot 10^{-6}$
FATP	kg 1,4-D[a]	$7.2 \cdot 10^{-5}$	$2.3 \cdot 10^{-6}$	$1.3 \cdot 10^{-5}$	$7.0 \cdot 10^{-7}$	0	$4.1 \cdot 10^{-7}$
MAEP	kg 1,4-D[a]	$1.3 \cdot 10^{-1}$	$7.0 \cdot 10^{-3}$	$1.3 \cdot 10^{-5}$	$1.3 \cdot 10^{-3}$	0	$2.9 \cdot 10^{-3}$
TEP	kg 1,4-D[a]	$2.3 \cdot 10^{-6}$	$6.3 \cdot 10^{-8}$	$3.8 \cdot 10^{-6}$	$2.0 \cdot 10^{-8}$	0	$8.0 \cdot 10^{-8}$
POP	kg C_2H_4	$5.0 \cdot 10^{-8}$	$2.2 \cdot 10^{-9}$	$4.5 \cdot 10^{-8}$	$2.1 \cdot 10^{-9}$	0	$1.9 \cdot 10^{-8}$
AP	kg SO_2	$1.1 \cdot 10^{-6}$	$5.3 \cdot 10^{-8}$	$1.1 \cdot 10^{-6}$	$6.2 \cdot 10^{-8}$	0	$1.2 \cdot 10^{-7}$
AEP	kg PO_4^{3-}	$1.1 \cdot 10^{-7}$	$3.5 \cdot 10^{-9}$	$5.7 \cdot 10^{-8}$	$1.3 \cdot 10^{-8}$	$2.2 \cdot 10^{-6}$	$3.8 \cdot 10^{-7}$

[a] 1,4- Dichlorobenzene